DEVELOPMENT OF RELIABLE VIBRATION-BASED CONDITION INDICATORS AND THEIR DATA FUSION FOR THE ROBUST HEALTH DIAGNOSIS OF GEARBOXES

A THESIS

SUBMITTED TO THE UNIVERSITY OF MANCHESTER

FOR THE DEGREE OF

DOCTOR OF ENGINEERING (ENGD)

IN THE FACULTY OF ENGINEERING AND PHYSICAL SCIENCES

2011

PAWEL JAKUB RZESZUCINSKI

SCHOOL OF MECHANICAL, AEROSPACE AND CIVIL ENGINEERING

CONTENTS

Total word count: 50301

LIST OF FIGURES

LIST OF TABLES

NOMENCLATURE

Notation	Description
θ	Contact angle between the balls and the races in a bearing
σ	Standard Deviation
A	Amplitude of sideband
abs	Absolute value
Bd	Rolling element ball diameter
f	Frequency
f_r	Shaft rotational frequency
f_s	Sampling frequency of the system
max	Maximum value
N	Number of samples recorded during single shaft revolution
Nb	Number of rolling element balls
P	Value of the curve on NPP plot
Pd	Bearing pitch diameter
s	Second
τ	Torque
t	Time
T	Time of one complete shaft revolution
$tacho$	Tachometer signal
x	Vibration response
$\bar{x}$	Mean value of the vibration response
X	Vibration response in frequency domain

LIST OF ABBREVIATIONS

Notation	Description
3D	3 Dimensions
AGMF	Amplitude of Gear Mesh Frequency
AI	Artificial Intelligence
ANN	Artificial Neural Network
APDF	Amplitude of Probability Density Function
AR	Autoregressive Modelling
ARMA	Autoregressive Moving Average Modelling
ASB	Amplitude of Sidebands
BPFO	Ball Pass Frequency Outer
CAA	Civil Aviation Authority
CCI	Cumulative Condition Indicator
CF	Crest Factor
CI	Condition Indicator
DFT	Discrete Fourier Transform
DND	Deviation from Normal Distribution
DOD	Department of Defense
EDM	Electrical Discharge Machine
EngD	Engineering Doctorate
EPSRC	Engineering and Physical Sciences Research Council
ER	Energy Ratio
FFT	Fast Fourier Transform
GMF	Gear Mesh Frequency
HIDS	Helicopter Integrated Diagnosis System
HM	Health Monitoring
HUMS	Health and Usage Monitoring System
Hz	Hertz
IGB	Intermediate Gearbox
JDL	Joint Directors of Laboratories

LASPI	Laboratory of Signal Analysis and Industrial Processes
MBA	Master of Business Administration
MLP	Multi Layer Perceptron
MOD	Ministry of Defence
NASA	National Aeronautics and Space Administration
NDE	Non Destructive Evaluation
N	Newton
Nm	Newton-meters
NPP	Normal Probability Plot
nRMS	Normalised RMS
NTSB	National Transportation Safety Board
ODM	Oil Debris Monitoring
PDF	Probability Density Function
PhD	Doctor of Philosophy
QQ	Quantile-Quantile
RE	Research Engineer
resRMS	Residual RMS
RMS	Root Mean Square
RPM	Revolutions Per Minute
SD	Standard Deviation
SEM	Scanning Electron Microscope
SI	Sideband Index
SLF	Sideband Level Factor
SNR	Signal-to-noise Ratio
SOAP	Spectrographic Oil Analysis Procedure
STFT	Short Time Fourier Transform
TSA	Time Synchronous Average
UK	United Kingdom
WT	Wavelet Transformation
WVD	Wigner-Ville Distribution

ABSTRACT

The University of Manchester
Pawel Jakub Rzeszucinski
Engineering Doctorate (EngD)
Development of reliable vibration-based condition indicators and their data fusion for the robust health diagnosis of gearboxes
2nd November 2011

Performing condition monitoring related tasks on any machinery is an essential element of their rational maintenance. Endeavours to detect an incipient fault within a system serve multiple purposes from increasing the safety of people responsible for operating the machines through decreasing the running and operational costs, allowing time to plan for the inevitable repairs and making sure that the downtime of the machine is kept to an absolute minimum. All these tasks gain extra importance in a case when machines are operated in dangerous conditions putting people's lives in potential jeopardy – for instance in the field of operating a helicopter.

The robust assessment of the condition of gearboxes used by helicopters has recently been given an increased attention due to a number of accidents which followed an undetected drive train component failure. The majority of the on-board mounted condition monitoring systems use vibration response signals which are specifically processed to obtain a single number which is representative of a condition of a given monitored drive train component. Those signal processing methods are called Condition Indicators (CIs). There are a number of such CIs which are already in use and they seem to adequately indicate faults in most of the cases. However in a number of instances it has been observed that the most popular parameters like Crest Factor or FM4 failed to dependably reflect the true condition of the gear causing serious accidents, some of which resulted in a number of lives being lost. For this reason the presented research is focused on investigating the limitations of the existing CIs and designing a set of improved CIs. The development process is based on overcoming the drawbacks of the techniques used in existing CIs combined with the intelligence gathered while analysing the acceleration vibration signals which contained a gear or a bearing fault. Five new CIs are proposed and the details of their design are documented. Both the existing and the proposed CIs are applied on the available, uncorrelated datasets. The results of the comparison show that the newly developed CIs are capable of indicating a gear or a bearing fault in a more robust and dependable fashion.

Each proposed CI alone may not be the most robust indicator of the actual condition of the monitored component hence the output from all proposed CIs is combined into a single indication through use of a novel data fusion model. The Combined CI created based on the data fusion model is observed to be more robust compared to each CI alone, hence it may increase the confidence level of the decision making routine and is expected to decrease the number of false alarms. The methods of the existing CIs, the proposed CIs and the data fusion techniques as well as the results of the comparison between the different approaches are present in this thesis.

DECLARATION

I hereby declare that no portion of the work referred to in the thesis has been submitted in support of an application for another degree or qualification of this or any other university or other institute of learning.

COPYRIGHT STATEMENT

ACKNOWLEDGEMENTS

I would like to express my gratitude to all those who made it possible for me to complete this thesis:

Dr Duncan Shepherd and Dr Jyoti Sinha who always had time to answer my questions and share their knowledge and experience from both academic and industrial point of view. I am thankful for the day-to-day motivation to work hard through their patience and never ending words of encouragement.

Dr Rodger Edwards, Prof Andrew Starr and Dr Brian Allen who provided regular feedback on my work and gave a lot of crucial suggestions for improvement for the whole duration of this research. Their input was much more than helpful in shaping this thesis.

QinetiQ Ltd. and EPSRC for sponsoring this project and providing all the necessary facilities and resources needed to comfortably carry out all the research activities.

Dr David Stanley and whole EngD centre at The University of Manchester for all the understanding and extreme support I have received for the past 4 years.

I wish that all future researchers had a chance to get the quality of support that I had a chance to experience.

DEDICATION

I dedicate this work to my family for their never ending support and love.

CHAPTER 1

INTRODUCTION

1.1 Introduction

A helicopter, also called a rotary-wing aircraft, may be defined as any flying machine that uses rotating wings to provide lift, propulsion and control forces to rise and hover above the ground [1]. Helicopters are the most versatile flying machines ever invented [2]. Their unique properties of speed, precision and manoeuvrability are utilised in an astonishing number of different circumstances including support of military conflict operations, mountain rescue operations, forest fire fighting, transport of heavy goods and food supply for inaccessible places (for example during flooding), crop fertilization or oil rig and land transportation. The diversity of occasions in which helicopters find utilisation often makes them the only and irreplaceable means of air operations.

The way helicopters work can be simply explained as follows: a rotating set of wings (blades) rotate around a shaft generating thrust (lift) that enables the helicopter to take off vertically. The pilot is capable of steering the machine by varying the pitch or the angle of the rotor as they move through the air. All modern petroleum-fuelled helicopters consist of at least one turbine engine that provides the power to propel the drive-train which, in general, consists of a number of connected shafts, gears and supporting bearings [1].

The techniques used by helicopters to create lift makes them much more complex and difficult to operate compared to, for example, fixed wing aircraft (airplanes). The later rely on the airflow over the wing surface for lift. The special structure and shape of the wings allows them to glide. This, in turn, allows the use of much fewer movable components that must be coordinated and adjusted to take off and maintain the flight.

At the same time helicopters are much smaller and their drive trains are extremely compact which makes the task of performing proper in-flight condition monitoring very difficult. Travelling by a fixed-wing aircraft is considered to be much safer since the helicopter accident rate is about an order of magnitude greater than the fixed wing aircraft accident rate [3]. In a comprehensive analysis of the cause of helicopter accidents [4] NASA investigated that the drive trains to the main and to the tail rotors were implicated in 38% of all accidents for single piston engine helicopters, out of which 27% were directly caused by the main or the tail rotor gearbox failure, where the direct source of the failure was dominated by gear failures.

In addition to that, when the NTSB established 21 main causes of helicopter accidents, 4 of them were related to mechanical failure and one of them was directly stated as ‘gear collapse’ [4].

The fact that helicopters are utilised in so many different circumstances, often operating at the limits of their recommended loading and constantly changing operating regimes, makes them prone to many different types of drive train failures. Those malfunctions often occur when the transmission system required to drive the helicopter rotor(s) introduces a number of single point, difficult to detect failures into the system. Those single point failures have the potential to cause some severe defects within the drive train over time and, as a result, can potentially lead to some serious consequences including loss of helicopters and fatalities.

A particularly strong understanding of a need to work on improvements to the existing Helicopter Health Monitoring Systems came in 1986 when a civil Chinook helicopter performing its routine transportation operations between land and an oil rig crashed into the North Sea causing the death of 45 people. The cause of the crash was identified as a failure of the gear wheel within the forward gearbox which caused the rotors to desynchronise and collide [5]. At that time the only way of assessing the condition of the gearboxes was by analysing the wear debris within the oil which could only be performed when the helicopter was stationary on the ground. This approach, however, could only indicate wear of the components, not their fatigue. The situation prompted the UK Civil Aviation Authority (CAA) to launch a number of extensive research programs aimed at developing the in-flight vibration analysis tools capable of giving a much earlier indication (up to 20 flight hours) about the similar types of failure that caused the Chinook to crash [6].

Years of extensive funding and a number of research projects lead to development of helicopter-specific condition monitoring systems. One of the most widely used systems these days is the Health and Usage Monitoring System (HUMS) which has been specifically designed to monitor the condition of all safety-critical components operating in the helicopter through calculation of the so called Condition Indicators (CIs) – signal processing routines designed to output a single number representing the condition of a given monitored component. The purpose of constantly improving HUMS is to provide more accurate information regarding the condition of various flight critical components [7]. HUMS is discussed in more detail in Chapter 5. The introduction of these types of systems on both civil and military platforms has undoubtedly had a very beneficial impact on the helicopter accident rates, as reported in [8]. The success of helicopter HUMS in reducing helicopter incidents associated with the transmission system failures does not, however, mean that the problem of managing those systems in service is flawless.

All current HUM systems operate on the basis of calculating a set of CIs for all monitored components, and comparing them with a bank of preset threshold values [9]. The problems arise because in some cases the relationship between the value of a given CI and the level of the damage in the system is highly inconsistent, and hence the diagnosis obtained can be rather unreliable [10].

The constant need for the research aimed at improving the existing solutions can be supported by the accident that took place more than 20 years after the 1986 Chinook crash. At the end of March 2009 the Eurocopter Super Puma crashed 11 miles north-east of Peterhead, Scotland. Although HUMS detected a metal particle on the main rotor gearbox epicyclic module, no vibration data indicated the presence of the fault. In addition the discovery of the chip led to daily inspections of the gearbox chip detector and, over the next 25 flight hours, the maintenance engineers downloaded and analysed HUMS data each time the helicopter returned to the base. As no abnormalities were discovered in the period, the checks ceased the day prior to the accident. Post-crash preliminary investigation revealed that the accident occurred following a catastrophic failure of the main rotor gearbox causing detachment of the main rotor head from the rest of the helicopter [11].

Accidents like this show that although a lot has been achieved in the field of improving helicopter safety, there is still a need for developing more reliable and effective ways of performing the drive-train condition monitoring tasks.

1.2 Project objectives

1) Reviewing the most widely used helicopter drive train CIs and examining their performance using experimental data.

   Developing profound understanding of the structure of the existing CIs and understanding their weaknesses and strengths is of paramount importance when trying to improve their weak sides without losing sight of what is useful and what could be used in development of improved methods.

2) Defining new CIs based on the performance assessment of the existing methods supported by additional ideas for improvement.

   Detailed documentation and careful explanation of the proposed Condition Indicators needs to be clear and unambiguous down to the smallest detail in order to allow a thorough understanding of the suggested parameters.

3) Presenting the advantages of the proposed CIs over the existing CIs.

   Comparing the results achieved by the existing methods with the results obtained using the proposed techniques is the essential step on the way to presenting the advantages of the suggested solutions. Performing the comparison on the same set of uncorrelated data guarantees generation of unbiased results and allows meaningful conclusions to be drawn.

4) Defining the data fusion approach to strengthen the robustness of the proposed CIs.

   It has been reported many times that combining information from different sources has the potential to give better results when compared with single source of information (elaborated in Chapter 3). Performing data fusion on the proposed CIs will strengthen the ability to detect the faults and reduce the level of undesired false alarms of the proposed solutions.

1.3 Thesis layout

Chapter 2 contains a description of the Engineering Doctorate (EngD) programme. It clearly defines the difference between the traditional Doctor of Philosophy (PhD) course and the EngD as an alternative, pro-industrial approach. It outlines the EngD's structure and the Personal Development programme that takes place in addition to the research activities. This chapter also gives an overview of the project sponsor company - QinetiQ Ltd and presents some preliminary mini-projects that were carried out at the beginning stages of this research.

Chapter 3 defines the state-of-the-art in the field of gear and bearing condition monitoring. It looks at the up-to-date solutions, showing different techniques used to perform the proper assessment of the condition of gears and bearings during their operation.

Chapter 4 describes the experimental datasets used in this text. It provides information about the source of the data and the technical details about the recorded vibration signals.

Chapter 5 gives a short introduction to gearboxes, the concept of the Time Synchronous Averaging and the description of the existing CIs.
Chapter 6 examines the performance of the existing CIs on the experimental datasets. The parameters' robustness is tested and a number of conclusions are drawn about their performance.
Chapters 7 - 10 define the proposed CIs and examine their performance when applied on the experimental data.
Chapter 11 explains the data fusion approach and shows the results of applying it on the experimental data.
Chapter 12 draws conclusions based on the outcomes of this research and suggests steps to be taken in future work.

1.4 Scientific contribution

- The performance of five widely used Condition Indicators (CIs) has been tested on three uncorrelated datasets. The performance outcome for each CI has been subject to a critical evaluation. Every performance assessment has been concluded with a detailed explanation as to why given CI performs in a certain way and why it fails to deliver in some other circumstances. The critical analysis of the indications given by the CIs may be viewed as a contribution to the existing knowledge,
- An in-depth study of the nature of the vibration response generated during the gear fault onset has been performed. It helped to explain the behaviour of the existing CIs and to define a set of novel CIs. The description of the gear fault deterioration process and associated changes in the vibration response, evaluated based on three datasets, may be considered as a valuable input to the existing knowledge in the field,
- Five new CIs have been proposed, each designed as either an improved version of an existing CI or as a new approach to the vibration-based condition monitoring of geared systems. Detailed explanations of the reasoning behind the development of each CI as well as step-by-step instructions on the computational approach have been provided. The development of five new CIs for geared systems is considered as new scientific contribution,

- A novel decision making routine based on fusing data from a number of different CIs has been proposed. Its performance and associated properties have been evaluated based on both the existing and the newly proposed CIs. Detailed explanation of the design process accompanied by a flow chart outlining the decision making process has also been provided. Defining the new robust decision making routine may be considered as a novel contribution to the field of data fusion-related subjects.

CHAPTER 2

EngD PROGRAMME AND PROJECT SPONSOR COMPANY OVERVIEW

2.1 EngD programme

Engineering Doctorate (EngD) is a relatively new British academic degree awarded for the first time in 1992 [12]. The main difference between the EngD and the Doctor of Philosophy (PhD) programmes is that an EngD student, referred to as a Research Engineer (RE), apart from performing a set of comprehensive research-related activities in his field, completes a number of week-long business-oriented modules focused around enterprise management. After two years, an EngD student is awarded a Master of Business Administration (MBA) degree or its equivalent (Postgraduate Diploma in Enterprise Management in the case of The University of Manchester [13]). For this reason an EngD project lasts 4 years, as opposed to the theoretical 3 years provided for a PhD project.

In addition to that, the RE is expected to spend at least 75% of his time conducting research in the collaborating company, which – in partnership with the University – supervise the studentship. This gives the RE the opportunity to gather experience in working with real-world data, learn from more experienced engineers by closely working with them, build up contact networks and learn about the way organisations work from the managerial point of view. Because of this unique opportunity, the EngD programme primarily attracts people who want to continue their carriers in the industry and progress rapidly to positions at the senior management or the chief executive level [14].

The programme is operated by the Engineering and Physical Sciences Research Council (EPSRC) and was created as a direct suggestion from the EPSRC who, in 1990, recognised that there was a constantly rising number of enquiries from many industrial sectors for graduates with analytic skills who appreciate the specific needs of the industry and who are capable of integrating into it with ease [15].

2.1.1 EngD programme at The University of Manchester

The whole duration of the EngD course held at The University of Manchester can be divided into three distinct parts: Research Project, Diploma in Enterprise Management and Personal Development Programme. Each part of the EngD course is mandatory and failing to attend and/or pass any of them may result in serious difficulties in successfully completing the whole course.

The first and the most important part of the course is the Research Project (RP) where all the actual research work is carried out. The first year of the RP is devoted to the acclimatisation of the Research Engineer in the sponsor company and to the development of the project research strategy. The first and the second years are typically spent on developing an understanding of the basic concepts comprising the foundations of the RP as well as researching the state of the art in the given field. Year three is typically oriented on shaping and fulfilling the project objectives and the final year is mostly devoted to the preparation and submission of the thesis.

Diploma in Enterprise Management (DEM) is a part of the project that runs during the first two years of the project. It is designed to raise an RE's awareness of all the major mechanisms operating on the business site of every enterprise. Presenting researchers with an inside into the decision making apparatus related with every project helps them appreciate which requirements need to be satisfied from both technical and business points of view in order to develop and successfully run a project. This part of the project comprises 8 week-long modules during which REs are presented with theoretical foundations and take part in a number of hands-on mini-projects. Each module finishes with a written assignment which is later assessed by the lecturer. Upon successful completion of all 8 modules an RE is awarded the Postgraduate Diploma in Enterprise Management.

Personal Development Programme (PDP) is a part of the EngD course that runs, along with the RP, for 4 years and is composed of a series of 2 or 3 day-long modules aimed at developing and strengthening the, so called, soft skills of every RE. Each module is designed to give every participant the chance to test his/hers skills in various scenarios. Based on the outcomes the course suggests ways of improving the soft skills. In such a way the RE becomes more accustomed and prepared for real-world situations.

Table 2.1 gives the outline of the EngD programme run at The University of Manchester with all the activities divided to the three groups mentioned above.

Table 2.1 The University of Manchester EngD Programme Outline

Year	Research Project	Diploma in Enterprise Management	Personal Development Programme
One	· Induction in Company · Development of Project Research Strategy · First Year Presentation · First Year Progression Report · Summary Report	· New Product Innovation · Marketing · External Opportunities and Threats · Business Operations	· Introduction to Research for EngDs · Leadership and Team Development
Two	· Project Presentation · Summary Report	· Human Resource · Management · Financial Planning and Monitoring · Effective Production · Improving Quality	· Report Writing and Presentation Skills · Management of Projects · Effective Communication
Three	· Project Presentation · Summary Report	-	· Negotiating Skills · Managing Meetings · Industrial Law
Four	· Prepare and Submit Thesis · VIVA Interview	-	· Thesis Writing and Exit Strategy

2.1.2 EngD programme in QinetiQ Ltd.

The first two years of the project, apart from attending a series of DEM and PDP modules, were spent on completing a couple of technical mini-projects run and supervised by the industrial supervisor at QinetiQ Ltd. The major reason for carrying out those projects was solely training related. Building confidence and increasing experience in processing digital signals generated by real-world machinery proved invaluable in the later stages of the project. Even though the tangible outcome of each project was of insignificant importance to the project and did not carry any contribution to knowledge, the opportunity of analysing a non-artificial set of data created a great chance to, among others, understand the practical aspects of the digital signal processing and analysis, appreciate the operating principles of the most widely used Condition Indicators and increased the ability of drawing conclusions from the findings.

Mini-project 1: 4-ball bearing

4-ball bearing is a structure where one ball, attached to a shaft, is put against three fixed balls, which are placed in a casing and plunged into a special type of lubricant. The test is run under specific, sometimes smoothly altering conditions like shaft speed, temperature or load. This construction is typically used to test properties of lubricants, however sometimes it finds other utilisation for example for testing characteristics of different materials. The ball arrangement in a typical 4-ball bearing is shown in Figure 2.1.

During the tests performed by QinetiQ Fuels and Lubricants Department vibration response and Acoustic Emission (AE) signals were recorded. These signals were the basis for a training-oriented analysis in this mini-project. The four-ball test rig used to collect the data along with the location of the accelerometers is shown in Figure 2.2. The two low frequency accelerometers were operating in the frequency range up to 10 kHz, whereas the high frequency accelerometers' range was up to 1MHz. Sampling frequency during the test was set to 3.3MHz.

All the tests were run until failure. Simulation outcome was classified as a 'failure' when a pitting of the upper ball occurred. The pitting was identified by a safety sensor (piezoelectric accelerometer with adjustable threshold sensitivity) placed on the machine. When the ball started to pit, the vibration levels increased greatly. After a critical threshold value of the vibrations was crossed, the machine automatically switched off, finishing the test.

Two different types of events could be distinguished in the time domain signals as is shown in Figure 2.3. The higher amplitude event (with much shorter duration) appeared periodically at a frequency of 100Hz, whereas the weaker yet longer event, that showed logarithmic amplitude decay, repeated at a frequency of 37Hz. The analysis combined with the theoretical calculations suggested that the peaks occurring at a frequency of 37Hz were the AE events caused by some destructive changes occurring inside the ball as the fault was developing. The peaks appearing periodically at 100Hz were attributed to the operation of the motor occurring at twice the supply frequency in the case of an asynchronous AC motors. Figure 2.4 shows a zoomed spectrum of the signal from Figure 2.3 with a clear presence of the 37Hz and 100Hz components.

Apart from the visual investigations, a series of Condition Indicators were applied to the vibration signals. Also the changes in the number of the AE events were tracked as the fault was progressing. The AE events were partially calculated based on the advice that suggested selecting a threshold level at or above 30% of the maximum background amplitude for the lowest speed and load operating condition [16]. Because of the fact, that the pure background signal was not provided with the data, the threshold was found by determining the maximum amplitude from all the runs for each particular test and calculating the 30% of the maximum value. Apart from a clearly visible proportional relationship between the increase in the number of AE events present in the signal and the increase in the value of RMS as the fault was progressing, no other meaningful results were obtained.

The outcomes of the mini-project included:

- learning about the required instrumentation and the appropriate way of setting up the data acquisition system,
- gathering experience in dealing with large matrices of data;,
- distinguishing between different events appearing in the time domain of the signal,
- applying some of the most popular Condition Indicators and analysing the results generated by them.

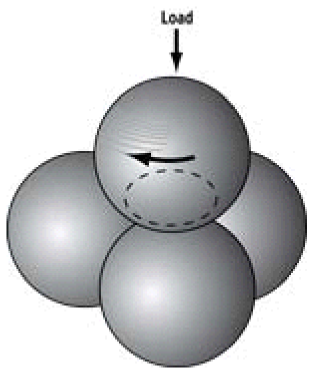

Figure 2.1 The arrangement of balls in a typical 4-ball bearing [17]

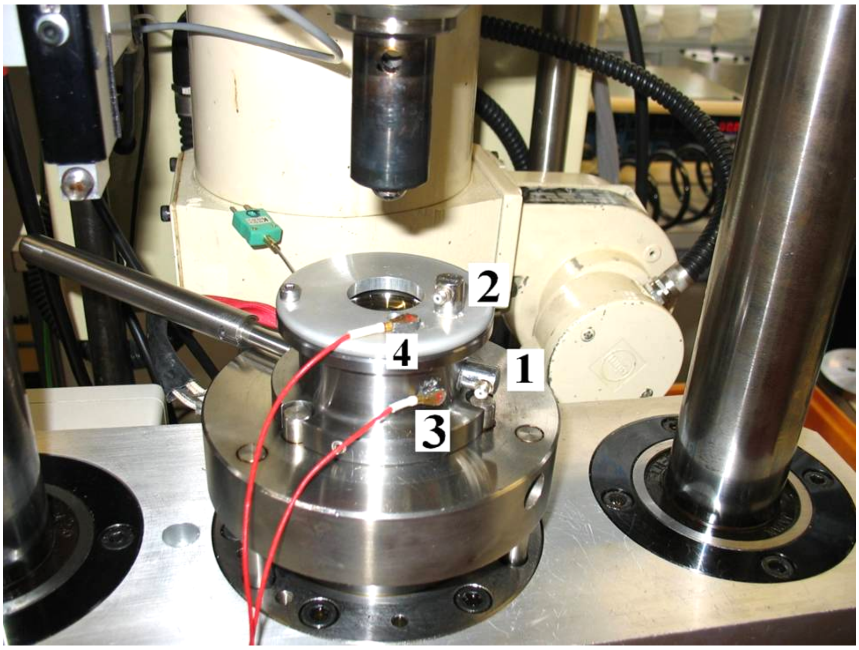

Figure 2.2 The four-ball test rig instrumented in high frequency accelerometers (1 and 2) and low frequency accelerometers (3 and 4)

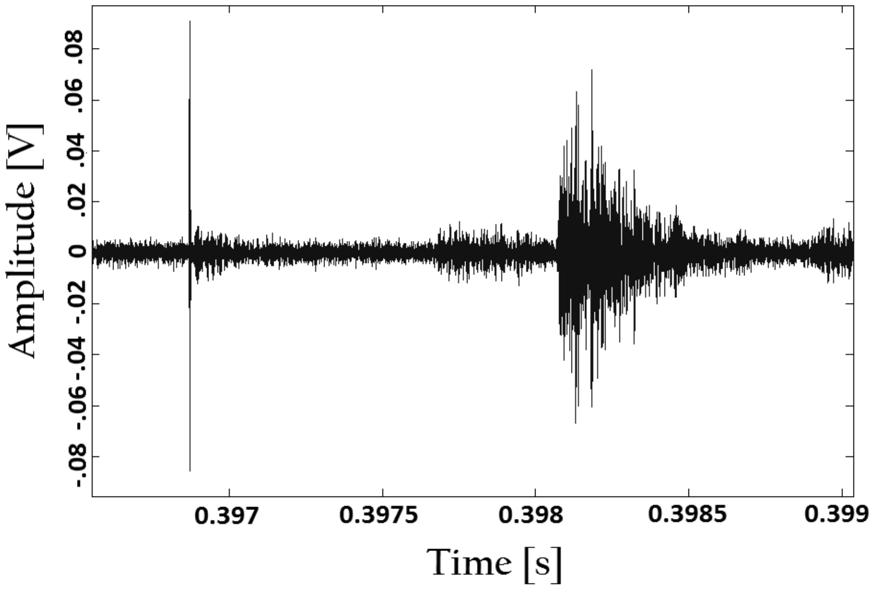

Figure 2.3 Two types of peaks present in the time domain: the '100Hz peak' (left) and the '37Hz peak' (right)

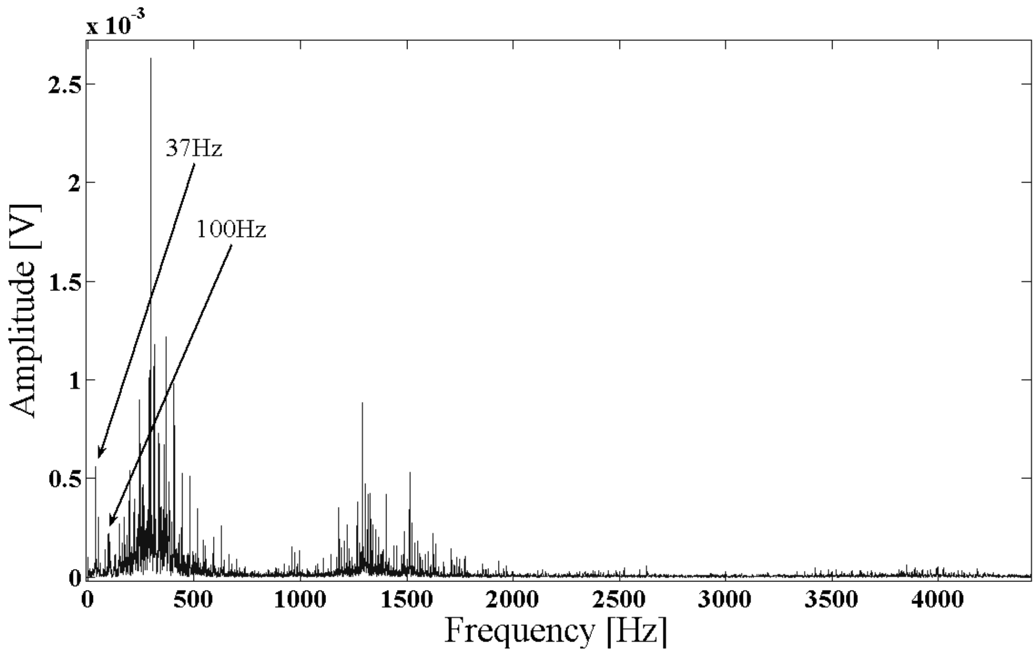

Figure 2.4 A magnified spectrum of the signal from Figure 2.3

Mini-project 2: Planetary gearing

The planetary gearing mini-project was centered around analysing data generated by the Defence, Science and Technology Organisation (DSTO) – a part of Australia's Department of Defence. The data was made available by QinetiQ Ltd. Data were generated on a test rig shown in Figure 2.5. The test rig drive train contained a bevel gear type of input and planetary gearing type of output. The whole structure was instrumented with four accelerometers (of unknown characteristics) (Figure 2.4).

The documentation attached with the dataset stated that the acceleration data contained signatures of a fault in one of the rolling element bearings. The exact type of the fault was not specified. The two main exercises of this mini-project were related: attempt to implement the McFadden separation algorithm (that allows the vibration signals generated by each planet alone to be monitored) and application of bearing related condition monitoring techniques in order to try to detect and characterise the bearing fault.

McFadden separation algorithm: Because of the way the gears are arranged in the planetary gearing, the periodic movement of the planet gears towards and away from the fixed accelerometer causes the measured vibration to be modulated at the, so called, planet pass frequency [18]. In order to perform meaningful condition monitoring of each planet gear, a special approach needs to be incorporated that would allow the required vibration traces to be separated from the rest of the vibration response.

One of the most widely used techniques that allow such a separation to be performed has been proposed by McFadden [19]. In order to verify its robustness, the algorithm was applied on the dataset under investigation. Unfortunately the obtained results did not match expectations. Implementation of the algorithm was not successful due to phase mismatch between corresponding parts of the vibration signal. The exact reason for that behavior was not fully understood. Each planet carrier rotation was indicated by a signal generated by a tachometer. This signal was used to extract vibration data generated by each planet carrier rotation from the continuous waveform. The final stage involved resampling each data segment, to account for shaft speed fluctuations. Nevertheless when constructing the final average, signals remained mismatched in phase.

Bearing fault detection: The first step on the way to detect the bearing fault involved calculating a bearing-specific Condition Indicator – M6 – in a number of different frequency bands located in the upper part of the spectrum. More information regarding signal analysis when performing condition monitoring of bearings is contained in Section 4.5. M6, in turn, is presented in Section 3.3.2. The filtering band that gave the best results was determined by observing where the highest readings and the clearest rising trend of M6 could be observed. Once the bearing fault had been localized the last step involved determining what type of fault occurred in the bearing. Theoretical evaluation of the bearing defect frequencies was made. Next the filtered vibration signal was demodulated, and the spectrum of the resultant envelope was obtained. Monitoring changes in the amplitudes of all potential bearing fault frequencies showed an increase in the components related with the Inner Race Ball Pass Frequency.

The major learning outcomes of this mini-project included:

- appreciation of the special character of the vibration signals generated by the planetary gearing, when compared with a typical vibration response of non-coaxial shafts gearing arrangements,
- understanding the principle of the separation algorithm and difficulties that one may come across when applying the theory in practice,
- increase in confidence in applying filters to vibration signals,
- appreciation of the design of a bearing and its different failure modes.,
- the use of M6 Condition Indicator in detecting bearing faults.

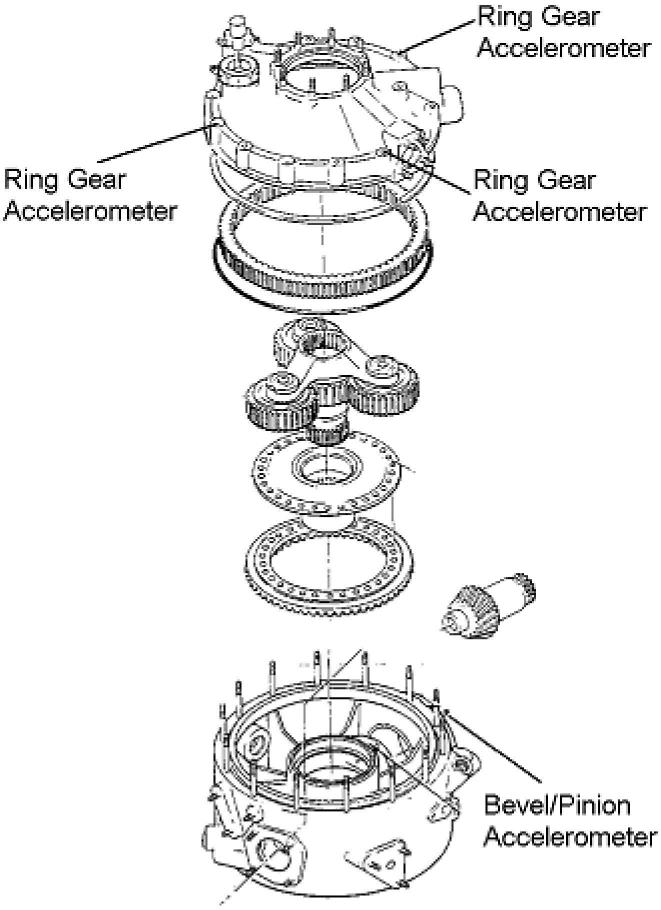

Figure 2.5 Test rig configuration

2.2 Sponsor company

QinetiQ

QinetiQ Group Plc (QinetiQ) supplies technology-based solutions and products and provides technology rich support services for government defence and security organisations, such as the UK MOD or the US DOD, and for commercial customers around the world. It employs more than 13000 people in Europe, USA and Australia [20]. The three core markets of QinetiQ's business are: Defence, Energy & Environment and Security [21].

Defence

Within the Defence market QinetiQ provides solutions in a number of domains. The most important include Aerospace, Land, Sea, Command and Intelligence or Advanced Signal and Image Processing. In addition QinetiQ offers a range of services and consulting advices in areas related to defence.

Talon® [22]

Talon® is one of the defence products that have made a major impact in the field of combat mission security. It is a remotely operated robot designed to deal with situations like explosive ordnance disposal, reconnaissance, sensing or communication [23]. It has been bought by, among others, Australian Department of Defence [24] and U.S. Army [25].

Energy & Environment

The Energy & Environment part of the company operates in a number of different fields. The most important include: wind energy, wave and tidal energy, oil and gas, civil aviation, vehicles or energy from waste.

Corlan™ [26]

One of the most innovative products developed by this branch of the company is Corlan™, a wireless pipeline monitoring system. It has been designed to detect corrosion and erosion and can be mounted in virtually any location along the pipeline [26].

Security

The Security market's major focus is around critical infrastructure protection (transport systems, energy supplies), enterprise security (secure business intelligence sharing) and government and law enforcement (secure communication between the two agencies, protection of crowded places).

X-Net® [27]

X-Net® is a QinetiQ innovative system which brings any vehicle into full stop in seconds by piercing the front tires and enveloping them with a super-strong net [27]. U.S. military invested in the design signing a 5 year production contract [28].

2.2.1 Non Destructive Evaluation (NDE) and Health Monitoring (HM) Group

The current EngD project was carried out within the Non Destructive Evaluation and Health Monitoring group which forms part of the Air Engineering Division at QinetiQ headquarters in Farnborough, UK.

The NDE part of the operation has evolved over many years developing techniques and capabilities to meet specific demanding challenges primarily within the aircraft industry. The expertise includes ultrasound, pulsed eddy current and x-radiography and is deployed where routine NDE techniques are unsatisfactory. QinetiQ have developed pulsed eddy current technology which is used in applications where direct contact with the structure is not available. The new development allows measurements to be taken on coated structures or even structures with fasteners that incorporate domed heads. The ultrasound technology can use full waveform capture allowing detailed analysis of defects within a structure and has recently been developed for composite materials. QinetiQ are now able to provide software which reveals individual ply wrinkling, both in and out of plane and porous or resin rich areas.

The Health Monitoring aspect of the group covers both hardware structural health monitoring and application of algorithms for the monitoring of the health of physical systems. The work within this thesis was carried out as a part of the algorithm application area and has focussed upon helicopter systems but other work is carried out in a number of different areas such as wind turbines, landing gear, actuators or electric generators.

The Structural Health Monitoring techniques are primarily based upon a unique QinetiQ inter-digital sensor system which allows the detection of cracks and defects within the area of structure under investigation. The system is designed to be deployed in specific areas which have been identified as having a high risk of failure which are also difficult to inspect and potentially costly and a significant impediment to aircraft availability. The system is usually inoperative and only activated with the aircraft on the ground thus avoiding interfering noise from other sources providing a robust solution to structural health monitoring.

Members of the group chair national technical committees and professional bodies within the relevant fields.

CHAPTER 3

LITERATURE REVIEW

3.1 Introduction

Gearboxes are one of the most extensively studied elements as far as machinery condition evaluation is concerned. Historically all of the vibration-based gear transmission damage detection techniques were based on some sort of statistical property of the raw vibration signal. For example, it has been observed that the Root Mean Square (RMS) of the vibration signal changes in the presence of damage [29]. The monitoring of the condition of geared systems based solely on the raw vibration signals is not trivial. Vibrations are generated by all the components operating in a given machine, often leading to very complex and difficult-to-analyse waveforms. The majority of those component signals do not hold any useful diagnostic information and simply contribute to the level of the background noise. This leads to a situation where weak signatures of an incipient failure are masked by much stronger, ambient noise. However, intensive funding of research projects has led to development of a number of very important advancements in the field of condition monitoring of geared systems.

One of the breakthroughs was Stewart's definition of residual and difference signals in the mid 1970s. The author proposed removing all the known components from the vibration signal (shaft and gear mesh related frequencies) in order to get a quicker and clearer indication of an incipient gear fault [30]. The residual signal is discussed in more detail in Chapter 5.

Condition monitoring techniques became much more efficient and gained much more attention. Maintenance engineers started to realise the potential benefits of a system that could help to prevent unexpected downtime of the production processes. They also realised that incorporating machine condition monitoring consumed relatively small costs compared with costs occurring when a machinery failure occurred. At the same time the advent of dedicated condition monitoring hardware and greater computational capabilities stimulated the development of new ways of approaching vibration analysis tasks. Furthermore the development of new signal processing techniques combined with constantly decreasing size and increasing hardware capabilities enabled condition monitoring to be performed in real time.

Most of the current research into condition monitoring is focused on the development of on-line condition monitoring systems mounted onboard. The aim is to substantially increase the machine/vehicle's efficiency (reduce off-line inspections time) and increase its operational safety. New ideas are constantly being tested whilst the existing and well proven techniques are constantly used to make sure the condition of the machinery is under control and that the incipient damage is detected and dealt with accordingly.

The most popular approaches currently used to monitor the condition of geared systems can be divided into two groups. The first group makes use of the oil debris particles produced during the wear process of the machine elements, whereas the second group uses the vibration signals generated by those components [31].

Oil debris analysis involves collecting and analysing small debris particles present in the lubricating oils. Those particles can be produced by rotating elements like gears or bearings and can provide an early warning of the potential wear modes and, therefore, indicate the condition of the machine [32]. This approach is briefly discussed in Section 3.2 as one of the condition monitoring techniques.

Vibration-based methods operate on vibration data recorded during machinery operations. The use of the appropriate signal analysis methods depends on the exact machinery component being monitored and the nature of the fault to be detected [33]. Vibration signals can be analysed in the time domain, the frequency domain or by combining both domains in a time-frequency analysis.

There are many different vibration-based signal processing techniques. The most widely used techniques are listed below and described in more details in Section 3.3. Frequency spectra analysis transforms a vibration signal into the frequency domain and examines the resultant spectrum for the presence of fault-specific frequency components. Statistics-based analysis determines the condition of the monitored component with the use of statistical algorithms. Time-frequency analysis allows the analysis of a vibration signal to be performed in both the time and the frequency domain. Such a representation of a signal gives a chance to indicate the exact location of a particular event in time. Time series modelling is an approach where a mathematical model of the analysed system is created and used to predict the future behaviour of the system based on both the historical data and the model simulation output.

After analysing the vibration signal and extracting a set of diagnostics features, the next level of the condition monitoring system may perform fusion of the gathered intelligence. Combining data from different sources has been identified as capable of improving the accuracy of machinery fault diagnosis in a number of different occasions [34]. Depending on the exact structure of the data fusion process, a number of different techniques can be used.

Those techniques can be divided into two groups (elaborated in Section 3.4): pattern recognition and Artificial Intelligence (AI) probabilistic methods. The most widely described methods from the first group comprise:

- parametric templates where the predefined sets of characteristic features are compared against the actual observations,
- physical models where the observations are compared against the outputs of models that were specifically designed to simulate expected result,
- neural networks were inspired by the way human brain is structured and so the decisions are made based on many input arguments that are fed to the system with appropriate weights and each weight represents the diagnosis confidence or relative importance of a given indication,
- clustering detects patterns in the data by dividing any regularities present in the signal into different pattern groups,
- knowledge-based systems utilise Artificial Intelligence techniques in recognising patterns. In doing so, knowledge-based systems are combining expert knowledge stored in a form of databases,
- fuzzy logic makes use of some non-Boolean inputs fed into the system and reaches a conclusion based on the output of one of many different decision making functions.

Those techniques are described in more details in Section 3.4.3.

The most widely used methods that comprise probabilistic Artificial Intelligence include: Classical Inference where the proposed assumption is tested with the use of some empirical (experimentally determined) probability methods which require a high number of repetitive samples in order to be validated; Bayesian Inference which is an extended approach compared to Classical Inference and can be supplemented by the use of *a priori* (based on history) knowledge about the process; Heuristic methods that attempt to perform data fusion using experience-based rules designed specifically for reaching a multi-input single-output conclusions. Wider description of these techniques is made in Section 3.4.4.

3.2 Oil debris analysis

Aircraft bearings and gears work under very harsh conditions of varying load, temperature, shaft speed and oil temperature. In some cases, especially in very noisy environments, damage can progress undetected even until complete failure. That is why diagnosis based on vibration analysis is often supported by information provided by analysis of wear debris that is present in the lubricant.

Oil debris analysis is a common method used for detecting gears/bearing failures. It was introduced in the late 1950s and quickly found utilisation in a number of different mechanical systems [35]. The main reasoning behind oil debris analysis is that the failing element (ususally a gear or bearing) generates metallic debris, which falls into the lubricating oil [36]. The oil debris analysis approach examines all metal particles contained in the lubricating oil. Different techniques are used to count the number of particles, examine their shape and size and monitor their progression over time. Those parameters are then used to determine what kind of failure is occurring. Many authors have reported successful detection of gear and bearing faults based on the wear debris analysis, for example [37 - 41]. Combining outcomes from the oil debris analysis with the results obtained from the vibration signal analysis might constitute a very powerful condition monitoring tool.

There are a number of different oil debris analysis techniques among which the most widely used are: Scanning Electron Microscopy (SEM), In-Line Oil Debris Monitoring, Optical Oil Debris Monitoring and Spectrographic Oil Analysis Procedure (SOAP).

3.2.1 Scanning Electron Microscopy (SEM)

This technique is based on the use of a Scanning Electron Microscope. In this microscope electrons in a vacuum are accelerated until they reach a wavelength which is equal to one hundred thousandth of the white light wavelength. Beams of such electrons are projected onto the sample material. As the electron beam hits each spot on the sample, secondary electrons are knocked loose from its surface. A detector counts those electrons and sends relevant signals to an amplifier. Proper processing of the results gives a 3D image [36]. The resulting image allows particles to be observed with a magnification 250 times greater than the best optical microscopes, reaching detail levels of nanometres and leading to generation of images having very high depth-of-field. This allows for a very precise description of the particles, hence better debris type identification. A major disadvantage of this approach lies in the fact that SEM is usually performed off-line due to the size of the instrument. Therefore it can not be used in small spaces like, for example, helicopter gearboxes.

3.2.2 In-Line Oil Debris Monitoring (ODM)

A different approach was used by Miller and Kitalievich [42]. An In-Line Oil Debris Monitoring (ODM) Sensor can be used on-line due to its relatively small size allowing real-time analysis of the particles. The presented sensor relies upon sensing changes of an electromagnetic field caused by metallic particles passing the sensing coil assembly. The amplitude of the generated signal is proportional either to the mass of the particle of ferromagnetic metals, or to the surface size of non-ferromagnetic metals. The distinction between the two is as follows: in general, as the ferromagnetic particle passes through the magnetic field generated by the coil, it increases the magnetic field (and corresponding coil inductance), whereas non-ferromagnetic material decreases the magnetic field (and coil inductance). As a result the effect on the magnetic field generated by ferromagnetic metals is opposite to that of non-ferromagnetic metals which manifest itself by 180 degrees phase shift in the output of the monitoring system. Detailed discussion on this phenomenon can be found in [43]. Several size-based threshold levels can be defined to allow easier classification of different debris sizes. ODM is capable of detecting spherical ferromagnetic particles of up to 125 micrometers.

The main disadvantage of this approach is that it does not analyse the shapes of the particles making it very difficult to automatically determine the type of wear occurring within the machine.

3.2.3 Optical Oil Debris Monitor

Another approach to oil debris analysis – particle size analyser - was presented by Tucker et al. [44]. The main idea is to use a flowing fluid column which is back illuminated by a laser pulse. The light transmitted through the fluid is magnified and imaged by a digital camera and later analysed by an image processor. Each laser pulse provides a single image frame and the result of multiple frames is a complete record of the flowing fluid. The system analyses the objects for the size and a number of shape characteristics to diagnose the fault type. This kind of system can be used both off- and on-line. Particle size which can be analysed varies between 5 and 100 micrometers.

3.2.4 Spectrographic Oil Analysis Procedure (SOAP)

SOAP operates on the basis of sampling the lubricant at regular intervals and determining its properties with the use of the spectrographic chemical analysis [45]. It provides quantitative information about the number of different chemical particles present in the lubricating oil of the monitored component. SOAP is performed by measuring the wavelength and the spectral line intensity of the particles after they are excited by a radiation source such as infrared or X-ray. By monitoring the changes in the level of the metal particles in the oil, the presence of wear debris or corrosion may be determined [46]. The disadvantage of SOAP is that it is incapable of indicating particle size and cannot analyse particles greater than 10 micrometers [47].

Oil debris analysis is a well established approach in the field of condition monitoring however this study focuses on the vibration analysis aspects of performing health assessment of the monitored components. Oil debris is often used only as a supplementary technique to vibration analysis [48]. Because of that the additional investment required to install the oil debris monitoring system is not always accepted. Also installation of the oil debris analysis tools often requires a shutdown of the machine in order to be properly installed. This is a clear disadvantage compared to accelerometers which can be installed under virtually any machine operating condition.

As oil debris analysis is out of scope of this text, not all existing solutions are presented. This condition monitoring technique is included in this review for completeness of the list of the existing condition monitoring approaches.

3.3 Vibration-based condition monitoring techniques

One of the most widely utilised approaches in monitoring the condition of the machinery drive train components makes use of information contained in the statistical properties of the signal. In general, statistical techniques are based on applying signal processing algorithms to a vibration signal that has been pre-processed in a specific, case-dependent way.

3.3.1 Frequency spectra analysis

Analysing vibration signals in the frequency domain gives the advantage of clearly displaying the periodic content of the signal, stating at which frequency it occurs and what its contribution to the signal is. Vibration signals are typically transformed into the frequency domain by means of a Fast Fourier Transform (FFT).

The output of the FFT is called a spectrum and it presents the amplitude versus the frequency of the signal components. Analysing complex vibration signals in the time domain is often a very difficult task, since all frequency components generated by different sources are displayed as a sum of a large number of sinusoids. Specific types of faults occurring in a system have the tendency to produce characteristic frequency components. Figures 3.5 and 3.6 show typical spectra generated under the condition of outer race bearing fault and gear fault respectively.

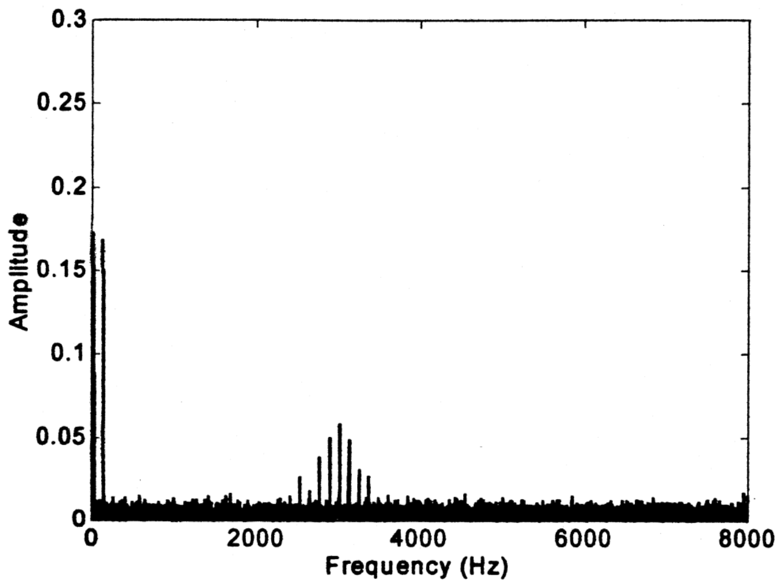

Figure 3.5 Spectrum containing typical fault signatures of an outer race bearing [49]

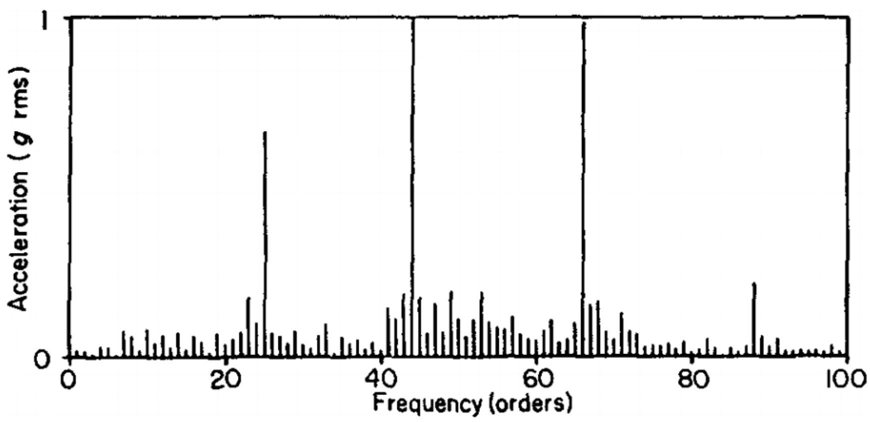

Figure 3.6 Spectrum containing typical fault signatures of a gear [50]

Years of spectral analysis allowed a long list of characteristic frequency features that occur when a specific fault takes place to be composed. Some failure modes, which are relatively easy to detect in the frequency domain, are much more difficult to detect when analysing the signal in the time domain alone. A number of different possible defects like unbalance, bent shaft, misalignment, gear defect, bearing defect, eccentricity all generate characteristic sets of frequencies which have been documented in many sources over the years, for example [51].

The fact that FFT creates its output based on the whole signal is the source of its shortcomings – the frequency content of the whole vibration record is averaged, hence the information that could be used to determine when exactly in time a given transient signal was generated gets lost. In addition to that performing the analysis based solely on signal's spectrum requires some expert knowledge in order to properly detect the characteristic features of a given fault.

Because of that the spectrum analysis alone can not be used as a tool for a quick condition assessment when performed by a non-expert in the field and some dedicated, pre-defined algorithms are required that are capable of determining the condition of the monitored component automatically.

3.3.2 Statistical techniques in time domain

Techniques presented in this subsection are performed on the raw vibration data in the time domain.

(a) Root Mean Square (RMS)

The most popular indicator giving an overall view of the signal condition is the Root Mean Square. It is the square root of the arithmetic mean of the sum of the squared signal samples [52]. In mathematical terms RMS can be expressed as follows [53]:

$$RMS = \sqrt{\frac{\sum_{i=1}^{N} {x_i}^2}{N}} \tag{3.1}$$

where x_i is the signal's amplitude at the *i*-th sample, *N* is the total number of samples in signal x.

This metric provides information about the energy level of the measured signal. RMS value follows any change of the energy level occurring in the signal, which gives a very simple, yet robust indicator, provided it can be properly interpreted. The disadvantage of this approach is that it is sensitive to changes within the signal caused by varying load or speed. The RMS has also been reported to be insensitive to the incipient tooth failures [53].

Note: Due to its wide application within the field, the RMS properties are further studied in the current research.

(b) Standard Deviation (SD)

Another simple, but not so widely used technique is the Standard Deviation. It is described as the RMS of the deviation of the signal from its mean value. SD can be defined as follows [54]:

$$SD = \sqrt{\frac{\sum_{i=1}^{N}(x_i - \bar{x})^2}{N-1}} \tag{3.2}$$

where $\bar{x}$ is the mean value of signal x.

This parameter is designed to indicate how far the signal fluctuates from its mean value [56]. Zakrajsek et. al. [55] tested a number of gear fault detection techniques on a spiral bevel fatigue rig. The tests were run until a significant piece of tooth broke off. The standard deviations of instantaneous phase and frequency proved to be good indicators of pitting, but only after it was well established in the gear. This highlights the disadvantage of this technique which is late indication of the gear fault development.

(c) Crest Factor (CF)

Crest Factor is a ratio of the maximum value (peak) present in the signal and the RMS of the signal. Formula describing the CF is as follows [57]:

$$CF = \frac{\max|x|}{RMS} \tag{3.3}$$

where $\max|x|$ is the maximum absolute value present in signal x.

The purpose of the CF calculation is to give the analyst a quick overview of how much impacting is occurring within a waveform. This information can be one of the symptoms of a tooth damage [58]. This parameter is used in detecting damage in its early stages – if only one tooth of the gear develops an early fault the RMS value does not increase greatly, whereas the peak value will be higher then normal. As damage progresses, the values of the RMS will start to increase making the CF parameter decrease [53].

Note: Due to extensive usage of this parameter in the industry, its properties are further studied in the current research.

(d) Kurtosis

Kurtosis has proven over the years to be a very good indicator of damage in gears. It is defined as the fourth normalised moment of the signal [53]. Moments often find utilisation when describing general parameters of a signal's distribution. They provide information about the shape of the distribution without the need for any information about the signal’s probability density function [59]. Moments may indicate how spread-out a given signal is according to the rule that the higher the moment, the more sensitive it is to the extreme points (tails) in the distribution [60]. Moments are often normalised in order to allow for easier comparison between different signals. Kurtosis, being the fourth normalised moment is defined as [53]:

$$kurtosis = \frac{N \cdot \sum_{i=1}^{N} (x_i - \bar{x})^4}{\left(\sum_{i=1}^{N} (x_i - \bar{x})^2 \right)^2} \tag{3.4}$$

In many publications (for example [29]) kurtosis is described as a measure of the amplitude distribution peakedness. Kurtosis is used as an indicator of major peaks in a set of data. As the gear wears and breaks, the vibration levels increase. Therefore kurtosis, due to changes in vibration signal level, should indicate an error [61]. The disadvantage of kurtosis is that as the gear condition deteriorates, more energy is concentrated in the tails of the distribution of the vibration signal decreasing the extent of its peakedness, hence lowering the kurtosis value [29].

Note: Kurtosis was found to be a reliable measure of a gear crack in a number of publications as reported in [50], therefore its behaviour is studied in more details in the present research.

Decker [62] used RMS, Crest Factor and kurtosis to detect a gear crack. The crack was simulated on a spur gear fatigue test stand by introducing a notch in the root area of the gear, which allowed a crack to be initiated. Based on the results and the previous experiments it was emphasized that none of the three techniques was clearly better than the other two for gear crack detection and they should be used together in order to increase the crack detection rate.

3.3.3 Statistical techniques in combined time and frequency domain

The approach used in the techniques presented in this Section is similar to the ones described in Section 3.3.2. However because of the way they were designed their proper implementation requires various modifications of the signal in both the time and the frequency domain.

Analysing raw vibration signals in the frequency domain alone may not be a very efficient tool for detecting gear faults because of the fact, that the whole spectrum is dominated by the gear mesh frequencies, making the analysis of other important frequencies, difficult. Taylor [63] experimentally tested a two-stage planetary gearbox and a single-stage parallel shaft gearbox aiming to detect a looseness fault solely in the frequency domain. Despite being able to detect the problem, he concluded that the frequency domain analysis alone was insufficient to diagnose this type of fault. Besides, localised faults (for example gear teeth cracks) excite transients into the background vibrations, resulting in a sequence of sideband components in the spectrum. Often it may be troublesome to detect such weak vibration components, as they are distributed in broad frequency bands and very often overlap with other components [64].

On the other hand, some condition monitoring techniques operating solely in the frequency domain are often used in the field of bearing condition monitoring. This is due to the fact that the bearing defect frequency components and their harmonics constitute very characteristic features that appear in the spectrum only as the bearing fault develops. Hence changes in the amplitudes of those frequencies can be utilised to indicate bearing degradation [65].

In order to take full advantage of the diagnostic information both in the time and the frequency domain, most of the vibration-based gear condition monitoring techniques use the, so called, residual and difference vibration signals, suggested for the first time by Stewart [30]. There are various, non-standardized definitions of these two signals present in the literature. However, the most widely used is the one given by Zakrajsek [55]: the residual signal is constructed by removing the regular meshing components from the raw signal (that is the shaft, gear mesh and their harmonic frequencies). The difference signal is created by removing the regular meshing components and their first order sidebands from the raw signal.

The techniques outlined in this section perform operations on signals in both the time and frequency domains, but not simultaneously. If necessary, filtering is first applied in the frequency domain to obtain the residual/difference signal and this is followed by calculation of the Condition Indicator function in the time domain. The reason for creating the residual/differential signal is to remove the known frequencies that dominate the whole vibration signal and possibly mask some important diagnostic information.

Stewart [30] proposed a number of Condition Indicators able to detect several different defects types related to gears. They are non-dimensional numbers referred to as 'Figures of Merit' (FM). CIs proposed by Stewart are described below.

(a) FM0

FM0 was designed to detect changes in the signal's Time Synchronous Average (TSA) (described in Section 5.2). It is defined as the peak-to-peak value of the signal's TSA divided by the sum of the RMS of the meshing frequency harmonics [66]. In mathematical terms it is described as [53]:

$$FM0 = \frac{S_{peak-peak}}{\sum_{i=1}^{N} A(i)} \tag{3.5}$$

where $S_{peak-peak}$ is the peak-to-peak value of the TSA vibration signal in the time domain, $A(i)$ is the RMS amplitude of the i-th mesh frequency harmonic.

FM0 was not designed to detect one particular failure type, and it works well in detecting several of them including tooth breakage, heavy wear, bearing instability or misalignment. Once a potential fault has been detected, other techniques can be applied to specify the type of failure in detail. Since FM0 operates on a similar basis as Crest Factor, and hence has similar disadvantages, it will not be further studied in the current research.

(b) FM4

FM4 is defined as kurtosis (as per Eq. 3.4) calculated on a residual signal [30]. It is based on the concept that the typical vibration of an ideal gear will only contain the shaft-order harmonics evenly distributed within the average. In reality many different components appear in the signal due to the manufacturing imperfections and inaccurate assembling processes. Therefore, by reconstructing the 'ideal' TSA one can subtract it from the original one and track any unexpected components that appear.

Hochmann et al. [67] describe a test where a notch was machined into a helicopter Intermediate Gearbox (IGB) pinion root. FM4 is presented as a good detector of transients generated by the weakening of the gear tooth.

FM4 is usually applied on the residual signal which, for a gear in a good condition, would primarily contain noise with a Gaussian amplitude distribution. The output of FM4 applied on such a signal would typically give a value of around 3 [67]. FM4 is supposed to be sensitive to localised pitting and cracks. FM4 is generally capable of properly detecting the fault in its early stages, but its values continue to rise only as long as the fault remains localised. It has been observed that as the fault starts to broaden, interacting with the adjacent gears, the values of kurtosis (and therefore FM4) start to decrease [69 - 71].

Note: Because FM4 has been well adopted in the industry, its properties are evaluated in more detail in the present research.

(c) NA4

NA4 is a modified version of FM4 designed not only to detect the onset of damage, but also to continue to increase in value along with the growth of the fault [30]. It uses an average value of variance in the normalisation step. However due to the modification NA4 became load sensitive which is a major disadvantage of this technique. NA4 can be expressed as follows [53]:

$$NA4 = \frac{N \cdot \sum_{i=1}^{N} (r_i - \bar{r})^4}{\left(\frac{1}{M} \cdot \sum_{j=1}^{M} \left(\sum_{i=1}^{N} (r_{ij} - \bar{r}_j)^2 \right) \right)^2} \tag{3.6}$$

where r_i is the i-th point in the time record of the residual signal, $\bar{r}_j$ is the mean value of the residual signal, r_{ij} is the i-th point in the j-th time record of the residual signal, j is the current time record, i is the data point number per reading, M is the current time record in the run ensemble, N is the number of points in the time record.

(d) NA4 Reset

Dempsey [72] suggested a change to the calculation of NA4 that allows minimises the negative effect of load changes. This technique, however, requires additional information about the level of applied load which, in turn, requires additional instrumentation. This increases the cost and complexity of the measurements.

(e) NB4

NB4 is derived in the same way as NA4, however instead of using the residual signal, the signal's envelope is used in the calculations [67] as per Eq. 3.6. NB4 was created based on the assumption that few damaged teeth will cause transient load fluctuations which are not present in the case of the normal tooth load fluctuations. The transient variations in the loading lead to amplitude modulation of the signal [73] which is typically observed in the envelope of the signal. The disadvantage of this approach is that in order to properly implement it, the vibration signal under consideration has to be filtered in a specific frequency band. However there is no unified guidance as to what filtering band should be used, hence different authors use different approaches [53]. This makes the implementation of NB4 ambiguous and case dependent.

(f) M6

M6 is the sixth centralised moment of the residual signal, normalised by the cube of the signal's variance [29]. This can be mathematically expressed as:

$$M6 = \frac{N \cdot \sum_{i=1}^{N} (r_i - \bar{r})^6}{\left(\sum_{i=1}^{N} (r_i - \bar{r})^2 \right)^3} \tag{3.7}$$

The underlying theory is the same as in the case of FM4, however because of the way M6 was designed it is expected to be more sensitive to the presence of peaks within the signal. Therefore M6 is widely used as a surface damage detector, especially in the context of bearing defects.

(g) NA4*, NB4*

In order to account for the poor ability to properly indicate the advanced stages of the gear fault the denominators of NA4 and NB4 have been statistically modified. When the variance of the residual signal exceeds a certain threshold value, the variance averaging stops and the denominator value becomes fixed. This alteration was based on the observation that as the gear tooth damage progress from being localised to more distributed the variance of the signal increases significantly. In the previous versions of the parameters this causes the undesired effect of the parameter values settling back to their nominal values, despite the correct initial indication of the fault advent. By normalising the fourth moment by the variance of a signal generated by the transmission operating under nominal conditions, the three parameters are provided with enhanced trend capabilities [29].

Decker et al. [74] used a Helicopter Transmission Test Rig to test several of the mentioned gear fault detection techniques. Tests were run on an OH-58 helicopter gearbox and the goal was to initiate a crack in the pinion at lowest possible torque. NB4 turned out to be very effective in detecting the damage despite torque fluctuations.

Choy et. al have put some of the described Figures of Merit into the test [75]. The study was based on experimental data generated on a spiral bevel gear fatigue test rig at NASA Lewis Research Centre. During the test the fatigue progressed from a small pit to severe pitting and, eventually, a tooth fracture. All tested Figures of Merit: FM0, FM4, $NA4^*$ and $NB4^*$ reacted to the start of the pitting process, however the last two parameters were much more efficient in indicating the progress of the damage. It has also been reported that both $NA4^*$ and $NB4^*$ are good indicators of initial pitting, reacting to gear surface damage in its early stages. The response from both metrics was also good when the surface pitting increases, showing general capabilities of the parameters for indicating gear tooth damage progression [55, 76].

(h) Energy Ratio (ER)

Energy Ratio is designed as the ratio of the RMS of the difference signal (raw vibration signal without the known components, that is gear mesh frequency, shaft speed frequency, their harmonics and first order sidebands) and the RMS of a signal that contains only the regular gear meshing components (gear mesh frequency and its harmonics) [29]. ER can be expressed as [53]:

$$ER = \frac{\sigma(d)}{\sigma(r)} \tag{3.8}$$

where $\sigma(d)$ is the standard deviation of the difference signal, $\sigma(r)$ is the standard deviation of a signal containing only the regular gear meshing frequency components.

ER has been designed to increase in the presence of heavy uniform wear. In the presence of significant wear the RMS of the difference signal increases, while the energy contained in the meshing components decrease. This parameter has been created according to the idea, that the energy will be transferred from regular meshing components to the rest of the signal as wear develops [53]. Not many publications included this parameter in further research and this approach has not been adopted by industry.

(i) RMS of residual signal

Wu et.al [78] tested the behaviour of the RMS applied on a simulated residual vibration signal that contained signatures of a gear tooth crack. Although the RMS was capable of indicating the early signatures of the gear failure, the approach used to create the residual signal was different from that suggested by Stewart (and used in this text). The proposed technique was based on subtracting a healthy signal from a signal containing a gear fault. This method is relatively easy to implement in a simulated environment, however it is very difficult to apply in practice in field applications. This is due to the very high precision and repeatability of the process that is required in order to achieve a satisfactory residual signal.

Decker [77] performed a very similar test to the one reported previously [62] however, this time he examined higher number of statistical techniques including: RMS, CF, ER, kurtosis, M6, FM0, FM4, NA4, NB4, NA4*, NB4*. Although higher number of CIs was included in the test, the conclusions were similar to the ones reported in [62]: none of the techniques showed sufficient capability and accuracy in detecting gear tooth cracks and should always be used in conjunction with other methods.

3.3.4 Time-frequency techniques

Signals whose parameters evolve in time are called non stationary signals [79]. In processing this kind of signal one is interested not only in what has happened, but also when it took place. Performing the analysis in the frequency domain might provide information about the frequency composition of the signal, but it will not inform when exactly the given event occurred. To overcome this problem a new set of techniques was developed that combine information from both the time and the frequency domain. Some of the most widely used time-frequency techniques are presented below.

(a) Short Time Fourier Transform (STFT)

Short Time Fourier Transform (also known as Windowed Fourier Transform) is a development that extends the Fourier Transform techniques to work with non-stationary data [80]. STFT is performed by dividing a given signal into a number of shorter parts and analysing each part separately with the use of FFT. The division of the signal serves to decrease the amount of information that is averaged by the traditional FFT approach.

The formula describing STFT can be outlined as follows [81]:

$$STFT(f,t) = \int_{-\infty}^{\infty} x(t+\tau) \cdot w(\tau) \cdot \exp(-t2\pi f\tau) d\tau \tag{3.8}$$

where f represents frequency, t represents time, τ represents time delay, $w(\tau)$ represents window function, $x(t+\tau)$ represents signal to be transformed, $\exp(-t2\pi f\tau)$ is the Fourier Transform kernel.

Wang and McFadden [82] used a STFT with a Gaussian window to detect an abnormal energy distribution which was produced by an early gear damage; Staszewski and Tomlinson [83] used the principle of STFT to detect a broken tooth in a spur gear, by using an appropriate window; Williams and Zalubas [84] and Loughlin et al. [85] claimed that STFT performs very well for periodic data, where strong harmonics may mask small transient events (that can be generated in the presence of incipient gear faults); Bartelmus and Zimroz [86] used STFT to distinguish characteristic vibration signals that were generated by some elements of the bucket wheel excavators.

The limitation of STFT is that fixing the window size leads to an unavoidable trade off in the resolution of the generated results – the shorter the window, the better the time resolution, but the worse frequency resolution (shown in Figure 3.7). Symmetrically – the longer the window the better the resolution in frequency, at the cost of time resolution [87].

For this reason the STFT might find utilisation only in situations where one is interested in obtaining fine results in just the time or just the frequency domain. In addition to that the need to set an appropriate window length for a given situation makes the implementation of the technique case-dependent.

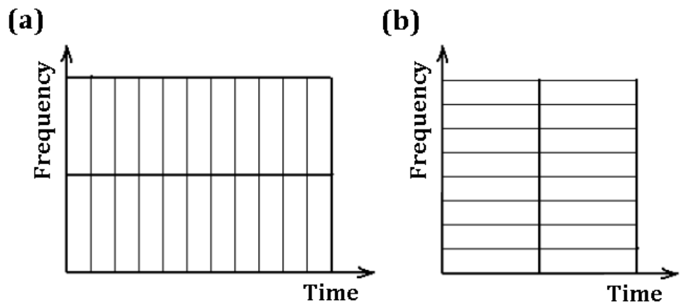

Figure 3.7 Increasing the frequency resolution shown in (a) results in a decreased resolution in the time domain as seen in (b).

(b) Wigner-Ville Distribution (WVD)

Wigner-Ville Distribution is a bilinear technique which means that the same signal must be used twice in one equation [88]. Based on that, WVD creates so called auto-terms which allow a very precise representation of instantaneous frequency. As a result WVD has a much better time-frequency resolution compared with STFT [89]. Wigner-Ville Distribution can be mathematically expressed as [90]:

$$W(t,f) = \int x^*(t-\frac{\tau}{2}) \cdot x(t+\frac{\tau}{2}) \cdot \exp(-t2\pi f\tau)d\tau \qquad (3.9)$$

where $x(t)$ is the analytical form of vibration signal, * represents the complex conjugate, f represents frequency, t represents time, τ represents time delay, $\exp(-t2\pi f\tau)$ is the transform kernel.

Choy et al. [75] showed that the Wigner-Ville Distribution gives reliable information about both the location and the severity of pitting developing within a gear. Baydar and Ball [91] analysed vibration signals coming from three different types of simulated gear failures: broken tooth, gear crack and localized wear. They concluded that the Wigner-Ville Distribution is capable of detecting the above mentioned types of gear faults in a reliable way. Staszewski et al. [92] showed that WVD was capable of detecting local tooth faults (created by partial tooth removal) generated on a test rig.

The disadvantage of the bilinear approach is the generation of so called cross-terms. They are redundant, artificial components that appear in the result of the transformation [93]. The process of creation of the auto- and cross-terms can be shown on the simple example in Figure 3.8 as follows: if one takes a signal containing a single frequency component (Case 1) and multiplies it by itself the result is a squared version of the same signal – the auto-term. No additional components appear as a result of the multiplication. However when a signal contains more than one frequency component (in this example two components – Case 2), multiplying the signal by itself leads to generation of some additional components – the cross-terms – which appear between the two auto-terms. The more frequency components appear in the signal, the higher the number of the cross-terms generated. This can cause difficulties in performing quick and reliable assessment of the condition of the monitored component.

auto-term

auto-terms

Case 1: $a \cdot a = a^2$

Case 2: $(a+b)\cdot(a-b) = a^2 - 2ab + b^2$

cross-term

Figure 3.8 Creation of auto and cross-term

(c) Wavelet Transformation (WT)

The concept of Wavelet Transform is to perform analysis using a scalable, movable window (as opposed to a fixed-size window in the case of STFT). In simple terms a wavelet is a waveform, a windowed wave, of a limited duration which is scaled and shifted during the analysis process in order to resemble signal artefacts characteristic of a given failure. In general form the continuous Wavelet Transform applied on signal $x(t)$ can be presented as [94]:

$$CWT(a,b) = \frac{1}{\sqrt{a}} \int_{-\infty}^{\infty} x(t) \cdot \Psi^* \left(\frac{t-b}{a} \right) dt \tag{3.10}$$

where *a* and *b* represent parameters used to scale and shift the wavelet, $\Psi^*(t)$ denotes the complex conjugate of wavelet function $\Psi(t)$.

Wang and McFadden [95] successfully used Wavelet Transformation to detect fatigue in a helicopter rotor gearbox. The test was run in a full-scale gearbox test facility. During the test a fatigue crack developed at the root of a tooth in the input spiral bevel pinion and subsequently started to propagate along the length of the tooth. It has been reported that the WT is capable of detecting specific features of vibration signals. Sung et. al [96] ran a series of tests on simulated and experimental data. They concluded that the WT is capable of detecting characteristic features present in vibration signal that were generated by a gear subject to pitting. Belsak and Flasker [97] analysed signals collected from a single-stage helical gear test plant. They concluded that Wavelet Transform is able to clearly indicate a crack in a gear. Lopez et al. [98] showed the high efficiency of the WT in detecting gear faults by comparing WT plots derived for a healthy gear and a gear with half a tooth cut off. Dalpiaz et al. [99] showed that even though WT does not give satisfactory results when applied on a raw vibration signal generated by a gear with a localised fault, the application of a WT on the Time Synchronous Averaged signal can reliably localise the faulty tooth. Lin et al. [100] successfully used wavelets in extracting features related to a gear tooth crack from a noisy vibration signal. Omar and Gaouda [103] successfully applied a wavelet-based technique for characteristic feature detection within a vibration signal produced by a gear with a faulty tooth.

The WT has been extensively studied in a number of publications however it has not been widely adopted in the industry for the purpose of gearbox condition monitoring. The reason for that might lie in the fact that the WT works on the basis of comparing the analysed signal with a pre-selected wavelet [80]. The more the selected wavelet resembles the shape of the feature that is to be detected, the higher the correlation between the two and the larger the wavelet output [101]. Because of that it is essential to provide some *a priori* information about the character of the signal to be analysed in order to use a wavelet of the appropriate shape. Using a wavelet of shape similar to the observed event was found to enable effective analysis of impulses in vibration signals [102]. The appropriate selection of wavelet parameters (including its shape) creates a very challenging task when trying to take full advantage of the technique [103]. The use of different wavelets leads to generation of different WT outputs. This, in turn, makes the technique case dependent.

3.3.5 Time series modelling

A time series is a collection of observations made sequentially in time (data samples collected at equal intervals of time) [104]. The idea of time series modelling is to describe a system and processes ongoing inside of it by creating a model of that system using mathematical expressions. The aim is to predict the future system values by combining its historic outputs with the model parameters. In general terms, time series analysis is performed in two stages: designing a model that tries to characterise the given time series and then using its outputs to predict the future values. If vibration data originating from a healthy source can be successfully modelled, then the model can be employed to determine if the present data show any signatures of change due to damage [29]. The majority of vibration data collected from a gearbox is stochastic (involves randomness and cannot be exactly described by mathematical equations), therefore future samples are dependent on past events only up to a certain degree - an exact forecast is not possible and must be supplemented by the assumption that future values have a probability distribution which is conditioned by a knowledge of the past values.

Two mathematical modelling techniques are often used in applications: Autoregressive modelling (AR) and Autoregressive moving average modelling (ARMA).

AR modelling uses a linear regression on itself in addition to an error represented as noise with a Gaussian amplitude distribution [104]. In mathematical terms the autoregressive model can be represented as [105]:

$$y_t = \mu + \sum_{j=1}^{p} \phi_j (y_{t-j} - \mu) + \varepsilon_t \tag{3.11}$$

where y_t is the target value of the time dependant series y, μ is the mean value of the process, p represents the order of the model (the number of the historical values to be used), ϕ represents model coefficients, ε represents normally distributed noise that is not correlated with series y.

ARMA modelling uses two processes for estimating the future values of a time series: the autoregressive (AR) process and moving average (MA) process. It not only uses historical data to predict a value but also forecasts the noise values as well. In general terms ARMA can mathematically be described as [106]:

$$y_t = \mu + \sum_{j=1}^{p} \phi_j (y_{t-j} - \mu) + \sum_{j=1}^{q} \theta \varepsilon_t \tag{3.12}$$

where q represents the order of the MA process, θ represents the coefficients of the MA process. ARMA model is designed to forecast the future value of the series y as a linear function of the historical values (AR) supplemented by the influence of the recent random noise (MA).

In a complex model design process the crucial point is to find the appropriate coefficients [104]. It is generally accepted that AR models are suited to processes that exhibit peaks in the power spectral density function, whereas ARMA are suited to processes that exhibit notches. This is due to the fact that AR models are designed as all-poles filters, whereas ARMA models additionally contain zeros which makes them capable of detecting notches in the signals [104].

Although the AR and ARMA models (separately) are able to represent a broad range of signals over an arbitrary large frequency range, the ARMA model is able to achieve this with a smaller number of parameters [107].

Rantala and Suoranta [108] used an AR model in predictive maintenance of rotating machinery. They used signals collected during nearly 500 working hours of a single-stage gearbox run under the conditions of constant speed and constant load. The test was run until failure and stopped after three teeth of the input gear were damaged. An AR model was established based on the healthy stage signals and which was followed by generation of a residual signal. This was then compared with the actual residual signal derived from the test rig. The AR model produced good results giving advanced notice of failure, although further research, performed under conditions of changing load and speed, has been suggested.

Wang and Wong [109] used AR models in the detection and diagnosis of gear faults generated under various conditions: single-stage gearbox test rig, full scale helicopter transmission test facility and in-flight vibration from a Wessex helicopter. An AR model was used as a filter to create a residual signal. The authors concluded that when the values of load are fixed, kurtosis calculated on the AR model-based residual signal is capable of detecting gear tooth crack better than traditionally derived residual kurtosis (FM4). Under low loading conditions, kurtosis based on AR model is far more sensitive to the signatures of a gear tooth crack than traditional FM4. The results of analysis done under different loads have shown that the AR model is superior to traditional methods for trending the development of faults.

Wang and Wong [110] compared three different methods: Wavelet Transform, Resonance Demodulation and Autoregressive Modeling. The research tested how the three techniques performed in detecting and diagnosing gear faults. The experiments were run on existing vibration data collected in a tooth-crack propagation test acquired at low load (40% rated load of the gears). All three techniques performed very well, however AR modeling requires less ‘expert’, *a priori,* knowledge than WT and Resonance Demodulation, which makes this approach the easiest to use.

The disadvantage of time series modelling is the complexity of proper assessment of the order of the models [111]. As a result evaluation of the validity of the model output requires expert knowledge and does not provide direct diagnosis information. Proper interpretation of the results requires experience and so AR modelling is not useful as a quick decision making tool.

3.3.6 Shock Pulse Method

The Shock Pulse Method (SPM) is a signal processing technique widely used to indicate impacts within the system and the level of noise generated during metal-to-metal interaction (for example a rolling element ball over a race surface). As two pieces of metal come into contact an initial impact in the form of a shock or a pressure wave is excited and propagates through metal. It typically occurs at around 32-36 kHz and the amplitude of the transient is related to the velocity of the impact. As the fault develops on the metal surface (for example a bearing outer race) the interaction with another metal surface (for example a rolling element ball) creates a periodic high amplitude burst of shock pulse waves that stand out of the vibration waveform. The SPM uses a special type of transducer tuned to the expected frequency of the pressure wave occurrence typically around 32-36 kHz [112 - 114]. The disadvantage of this technique is that it requires mounting of dedicated sensor and maintaining relatively high sampling frequency in order to properly detect the appearance of the components around the resonance frequency.

3.3.7 Enveloping

The spectrum of a raw vibration signal often contains little diagnostic information about bearing faults. For that reason for many years the standard signal processing operation when trying to detect bearing faults has been band pass filtering of the raw vibration signal in high frequency regions where the vibration signatures of a bearing fault (short duration impulses) are amplified by structural resonances [45]. Such a signal is free from the influence of typically the strongest components in a gearbox vibration signal: the gear mesh frequencies and the shaft speed frequencies. As the fault develops the faulty surface (for example bearing inner race) comes in contact with passing rolling elements generating an impulse. This interaction repeats periodically with a frequency equivalent to the given bearing failure mode. The periodic generation of impulses causes an amplitude modulation of the vibration signal. To separate the impulsive content from the rest of the signal, the later is subject to an enveloping procedure which allows the amplitude modulation to be extracted. Such an enveloped signal is then transformed into the frequency domain where the characteristic bearing failure mode frequencies can be more easily detected and monitored, when compared with performing detection applied directly to the raw vibration signal.

The limitation in successfully implementing the enveloping process comes from the fact that it is not always straightforward to determine the appropriate filtering band in which the desired frequency components would be present [115]. On the other hand recent developments in signal processing techniques like the max-envelope of the complex Morlet wavelet [116] or spectral kurtosis [117] have the potential to substantially simplify the selection of appropriate filtering bands.

3.4 Data fusion

Integration of data collected from different sources, information based on processing this data and knowledge achieved from studying relationships and dependencies between different sources of information is the principle of data fusion.

The assessment of the condition of any mechanical system is rarely based on the value of only one parameter [118]. It is much more likely that conclusions are made based on the values of various parameters coming from one or many sensors. Typically, gathered signals need further processing in order to derive meaningful information. Collection of data from different sources, its proper interpretation and learning internal dependencies between various parameters are the foundations of data fusion. More precise definition was given by Hall and Llinas [119]: "data fusion techniques combine data from multiple sensors and related information from associated databases, to achieve improved accuracies and more specific inferences than could be achieved by the use of a single sensor alone". On the other hand, however, in practical applications the use of multiple sensors is not always feasible – the amount of available space required for appropriate sensor location may be limited, the access to the optimal sensor placement areas may not be available and the cost related to instrumenting machines with additional sensors may be unacceptable. Therefore, in most cases a more acceptable solution might be to install smaller number of higher-quality sensors and focus on efficient signal processing that allows a more robust signal analysis. This, in turn, should result in an equally good data fusion outcome. Data fusion has found application in many different, unrelated domains of everyday life, including aerospace systems, medicine, finance, radar tracking or maintenance engineering [118].

The data fusion system has to be precisely planned and designed for each and every case. If not created with care, the results of fusing data from multiple sources might give worse results than information from each of the sources alone. Such a situation can occur when fusing good, reliable data with biased data, especially if the uncertainties or variances of the data are unknown. There are many questions that need to be addressed before setting up data fusion systems. Among others these include [119]: what algorithms or techniques are appropriate and optimal for the application; what architecture should be used; what type of sensors to use; how the measurement environment can affect the reliability of the results.

The biggest challenge and the fundamental task of data fusion system is to transform input information into a meaningful, reliable output information. This process involves many stages and, because it often combines information from different sources, it is usually a complex and challenging task.

3.4.1 Data Fusion Process Model

In the past, the lack of a standardised terminology created serious problems within the data fusion comumnity as it disabled technology transfer between different fields. This changed in 1986 when the Joint Directors of Laboratories (JDL) Data Fusion Working Group created a general process model and Data Fusion Lexicon [119]. The JDL model is a functionally oriented model of data fusion. Its purpose is to be general and therefore easily incorporated in a number of different fields and applications. The model has been widely described in literature ([118 - 124]) and the concept is presented in Figure 3.9.

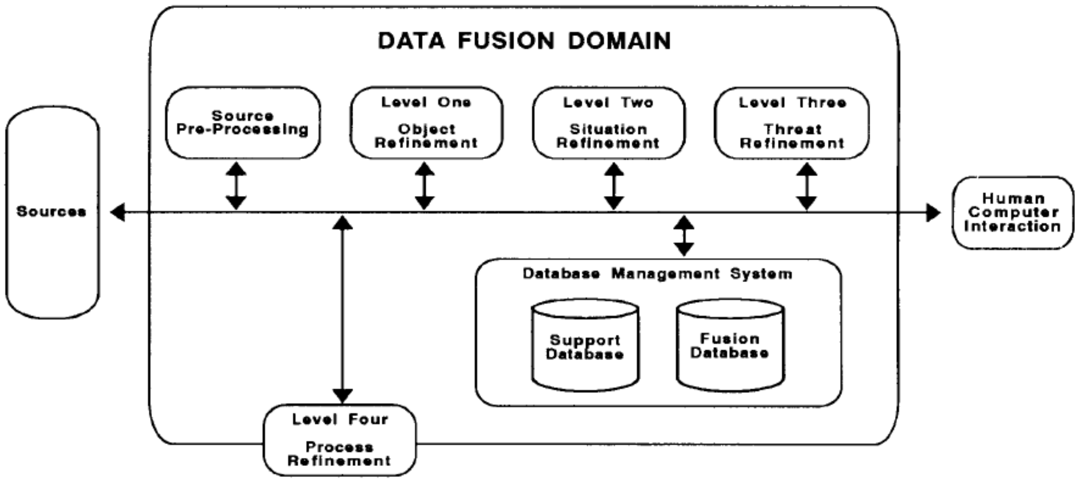

Figure 3.9 Top level data fusion process model [119]

Sources represents all the sensors that produce an output that is directly input to the model; *Human Computer Interface* provides an interface that allows efficient interaction between the operator and the system; *Source Pre-Processing* represents a phase where data from the individual sensors are extracted, signal-to-noise ratio (SNR) is improved and data is prepared for the subsequent fusion processes; *Level One – Object Refinement* tries to determine the character of the observed event (for example a gear fault type) based on a combination of information coming from different sources (for example different CIs); *Level Two – Situation Refinement* combines information about the nature of different objects (for example different drive train failures) and establishes the relationships between them in the context of a specific environment (for example if the objects refer to the same component); *Level Three – Threat Refinement* is designed to project the impact of the present objects on the future (for example how severe a given fault is in the light of the whole machinery operation) and assess the benefits and costs of performing further steps; *Level Four – Process Refinement* is an ongoing process that tries to improve the existing data fusion model by altering the performance of each level; *Database Management System* allows to store all the generated data as well as make use of the past intelligence [124].

The process of actually combining the knowledge may take place at a variety of levels in the data fusion system hierarchy, depending on the nature of the raw data. The most commonly used and widely described (for example [119 - 121]) are 'raw data fusion level', 'feature extraction fusion level' and 'decision fusion level'.

3.4.2 Raw data fusion level

If data recorded by sensors are of the same type, that is they measure the same physical parameter (for example acceleration), then fusion can be done at the raw data fusion level. In this approach raw data from all sensors are transmitted to a central point of the system where the data fusion procedure takes place. A final decision is made based on the output of the data fusion unit (Figure 3.10). At this stage the techniques that can be applied to fuse the data involve classical detection and estimation methods (since all measured information is of the same type).

The disadvantage of this approach, apart from the already mentioned limited access to the optimal sensor placement and cost related to procurement of additional sensors, is that fusing information at the raw data fusion level might mask important information contained in one of the sensors. Consider sensors installed at different locations that receive signals being transmitted thorough different paths. Fusing the raw data could lead to a situation where one sensor receives a clear indication of a fault and, at the same time, this information gets completely lost when fused with data from the other sensors. Performing data fusion at the raw data fusion level might smear that information decreasing its significance.

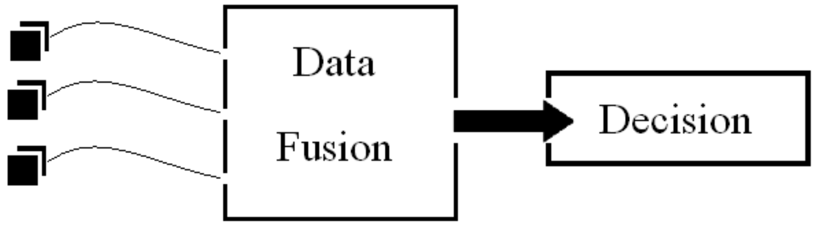

Figure 3.10 Simplified model of raw data fusion level architecture

3.4.3 Feature fusion level

If data are recorded by sensors of different types (for example accelerometers, oil debris analysis tools, thermometers), then data fusion can be done after extracting characteristic features from individual sensors (Figure 3.11). Feature fusion level begins by obtaining features from the raw data generated by every sensor. Extracted features are put together into a feature vector. This vector is then used as an input to one of the pattern recognition techniques, which is used to seek characteristic patterns present among the features. The most commonly used pattern recognition techniques include methods based on clustering algorithms, neural networks, physical models, parametric templates or knowledge-based solutions.

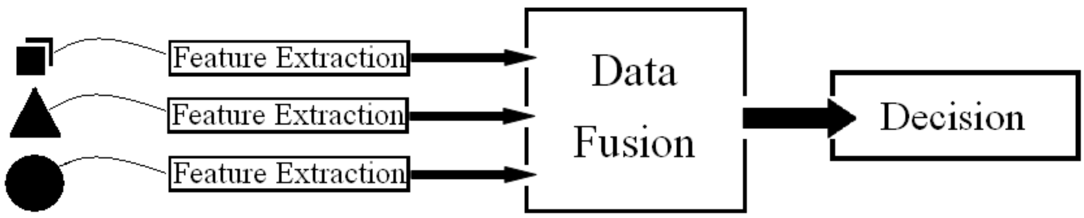

Figure 3.11 Simplified model of feature extraction fusion level architecture

Pattern recognition techniques

The concept behind pattern recognition is to assign an object or event to one of a number of categories, based on a characteristic feature [125]. In practice features are typically extracted from sensors of different types and grouped based on some *a priori* knowledge or statistical information extracted from the data. The classification is usually performed using a statistical or syntactic approach. The first one assumes that patterns are being generated by probabilistic systems and that therefore recognition is based on a statistical description of the patterns. A syntactic approach is based on structural associations between the features. A wide range of approaches and algorithms are used for pattern recognition, all of them operated in two stages: establishing relationships between feature vectors (vectors of features differentiating different objects) and recognising/classifying patterns within the feature vector. The most widely used pattern recognition techniques are described below.

a) Parametric templates

Thsi is probably the simplest method of pattern recognition based on the idea of comparing observations with *a priori* defined classes [126]. The assumption behind it is that the whole feature space (collection of single features) can be divided into distinct non-overlapping boundaries. Each of the boundaries represents one particular identity class. If features extracted from the measured data fall into one of the pre-defined feature space boundaries then the emitter of the data (for example a gear with a cracked tooth) has the same identity (condition) as the emitter of the pre-defined class (defined based on historical data). However, if it does not fall into any of the boundaries, then in the absence of other criteria, the emitter is labeled as having an unknown identity. The effectiveness of this technique depends heavily on appropriate definition of classes and may impose problems in decision making when an overlap occurs.

b) Physical models

Physical models are designed to represent specific characteristics of real systems that are being analysed [127]. They represent a direct method of pattern recognition. The idea is to compare features produced by a sensor with a set of previously prepared, desired features or with simulated features that were generated based on assumed target characteristics or physical models that try to predict the observed model. Usually the comparison method involves calculating the level of correlation between the observed and the previously gathered/modelled data. When the correlation result is greater than a pre-defined threshold value, an identity match is declared and the given data is put into one of the specific identity classes. The disadvantage of physical models is that their implementation may require operating very large software programs which, in turn, may demand high computational power [128]. For this reason physical models may require some time to reach a final decision and may not be suitable for quick decision making tasks.

c) Artificial Neural Network (ANN)

The inspiration behind ANN was the way human neural network. In the human brain the network function is determined by the connection strength between different elements. The same idea has been applied to ANN where each input to an artificial *neuron* (simple processing element working in parallel with different neurons) comes with a certain strength (weight). Each neuron receives a number of inputs (from original data or from other neurons). Based on values from all the inputs and their weights, a weighted sum is formed. If its value exceeds a certain level (activation value), a neuron *fires* data to another neuron and the cycle continues. The artificial neuron input signals are similar to the electrical impulses received by brain neurons. Because the neurons work in parallel, they are capable of performing many simultaneous operations, which decreases the working time and increases the number of probable solutions that can be reached in a given time interval. ANN works in a similar way as the human brain because it can learn new things provided sufficient data and knowledge is stored within inter-neuron connections. There are three basic learning types [129]:

Supervised learning. For each input pattern, the value of the desired output is pre-defined. In each cycle the output of the neural network is compared with the desired output. Based on this knowledge an error is computed. The error value is then fed back to the neural network, which adjusts the weights of each connection. This helps to decrease the error, bringing the actual result closer to the desired one. This learning system is appropriate when input-output mapping is already known. Because of that it is not capable of finding anything new about the data [125].

Unsupervised learning. For each input there is no desired output value therefore there is no error factor that helps to improve the work of the network. This training type is used when trying to finding a probability distribution of the input data, rather then exact signal values. This, in turn, makes it capable of performing data mining operations. It can be achieved by using the property of unsupervised learning to find hidden patterns contained in unlabeled data.

Reinforcement learning. There is no desired output data, but information is given about whether the network outputs are good or bad and the performance of the network is altered, based on the feedback information. This approach is mainly used for control applications.

The most widely used ANN structure is a Multi Layer Perceptron (MLP) network [130]. This arrangement consists of an input layer, a number of hidden layers and an output layer. Initially the values of the input variables are applied to the input units of the network, which is followed by other parts of the network being activated. If a pre-defined activation value is reached, it is passed through an activation function, which produces the output of the neuron. After all the operations are executed the outputs of the output layer acts as the output of the entire network as is shown in Figure 3.12.

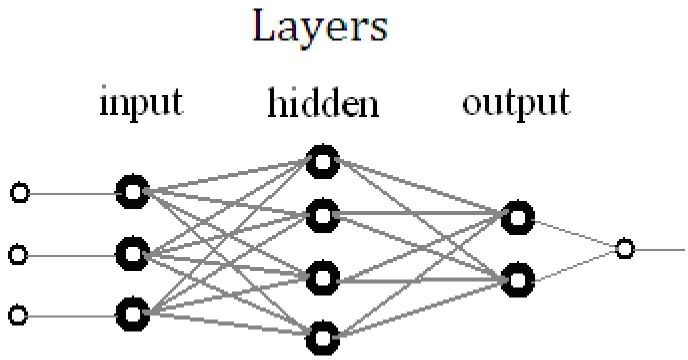

Figure 3.12 Schematic diagram of Multi Layer Perceptron

Despite being considered as the most dependable classifier (because of the small classification errors they produce), ANN has two major disadvantages that limit the usefulness of this technique to a very restricted range [131]: the first shortcoming comes from the fact that neural networks require a vast amount of training data to learn to react to a specific case, and it may be a very time demanding task to obtain this amount of data. The second drawback is that ANN does not provide explanations about why the classification is made in one and not the other way. The important details about each neural network are hidden in their structures and weights – for that reason it is often complicated to extract rules from a trained network. Sometimes the system is referred to as a black box [132]. Transparency in decision making is very important in the field of condition monitoring which makes ANN an unacceptable tool in safety-critical applications.

d) Clustering

The term ‘clustering’ is used in several research communities to describe methods for grouping unlabeled data. Cluster analysis represents a wide variety of statistical procedures designed to divide patterns present in the data into specific clusters [133]. The division is based on the degree of similarity between different features, so that patterns within one cluster are more similar to each other than they are to a pattern assigned to a different cluster, as is shown in Figure 3.13.

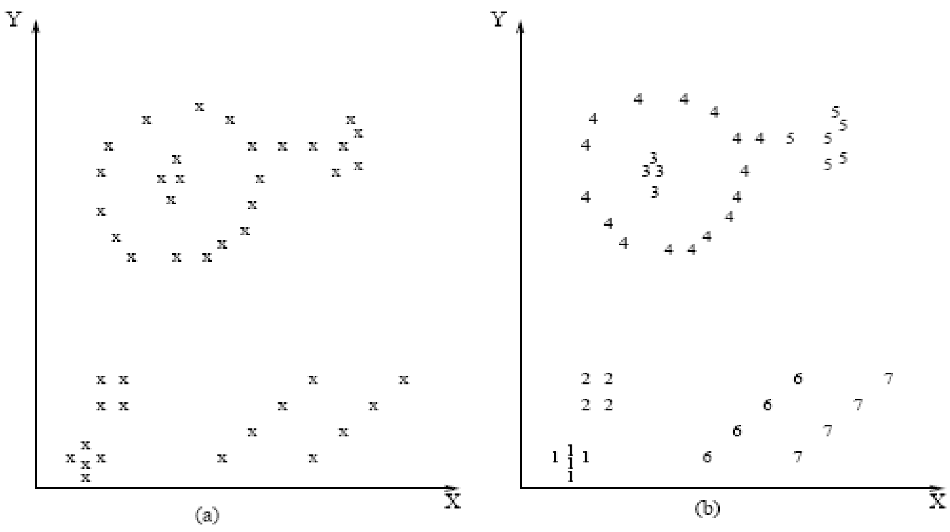

Figure 3.13 Data clustering: (a) input patterns, (b) desired clusters [134]

It is crucial to understand the basic distinction between discriminant analysis (that is supervised classification) and clustering (that is unsupervised classification). In the first one the system is provided with a set of pre-classified patterns. Based on given knowledge, the system is designed to find and classify patterns that are new to the system. In the clustering case the aim is to group the unlabeled pattern into different clusters without the *a priori* knowledge. Hesham Azzam et. al. [135] successfully used clustering in classifying data collected from a sensor monitoring a combiner bearing in a Chinook helicopter.

The disadvantage of methods used in cluster analysis is that they evolved from many different disciplines and it is crucial to understand the details of the different approaches and assumptions made before applying a given method to a given task. For this reason different clustering techniques can give different results for the same data [133]. Expert knowledge is crucial in applying the appropriate algorithms and interpreting their outputs.

e) Knowledge-based models

Knowledge-based systems are systems that use Artificial Intelligence (AI) techniques in solving problems. Such systems comprise databases that contain expert intelligence about a given subject and are equipped with dedicated utilities capable of retrieving specific information from the database in response to a specific query [136]. The main approach of knowledge-based systems is to try to follow cognitive methods used by humans to perform identity recognition. Expert systems represent one of the derivatives of the knowledge-based models. They are computer programs that use knowledge representation techniques to reach conclusions by performing appropriate analysis with the use of ‘knowledge databases’. Knowledge acquisition and analysis is performed in accordance with some dedicated knowledge modelling methodologies [137]. An interaction between the operator and the system is required so that the operator provides some facts and related information, and the model provides expertise about the given subject.

The disadvantage of knowledge-based systems is that they require *a priori* information in the form of vast databases. They contain large amounts of information about the specific behaviour of a machine. This, unfortunately, is rarely available in practice. It is also impossible to make a general model for different machines (even of the same type) as each instrument carries its own fingerprints incorporating its unique operating characteristics.

Feature fusion level, in its typical form, might suffer some of the problems that were discussed in the case of raw data fusion level - limited access to the optimal sensor placement and extra cost related to the procurement of additional sensors (especially as the sensors are of different types).

3.4.4 Decision fusion level

The third data fusion arrangement is the decision fusion level. In this approach information from each sensor is analysed to make a separate, independent assessment about entity’s location, characteristic and identity. That is followed by gathering all the information and making a final identity declaration (Figure 3.14). Techniques used at this stage involve classical inference, Bayesian inference (and its modifications), heuristic methods and fuzzy logic.

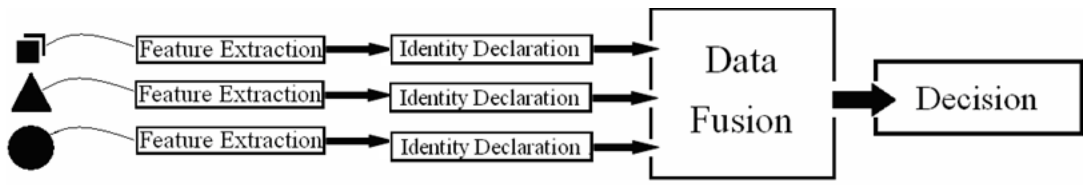

Figure 3.14 Simplified model of decision fusion level architecture

a) Classical inference

Classical Inference tries to determine the validity of a proposed assumption using empirical probabilities. Empirical probabilities see probability as the limit of long-term frequencies. For example in a coin throwing test the assumption is that the frequency distribution of the observed heads and tails will approximate the actual probability as the number of trials increases without limit. Each assumption is made against an alternative assumption. This method cannot take advantage of *a priori* knowledge about the likelihood of a given hypothesis (that is how probable a tested assumption is) [128]. The disadvantage of this approach is that empirical probabilities are only valid for repeatable processes. In addition, classical inference can only assess two hypotheses at a time (a given hypothesis or its alternative (for example STOP and GO) without intermediate stages).

b) Bayesian inference

Bayesian inference overcomes some of the inconveniences of the classical inference. It updates the known probabilities of occurrence of alternative hypotheses, based on observational evidence (previous results) [138]. The known data can come from models, historical data, statistical databases and subjective sources. New information is used as a feedback for the system and helps to update the known probability of each hypothesis. In addition, Bayesian inference can account for empirical and subjective (not requiring known probability density functions) probabilities. The disadvantages however, include difficulty in acquiring the prior probabilities, complexity of evaluating multiple hypotheses and the use of subjective probabilities that lack mathematical description. If used without care, they may have a negative influence on the functioning of the whole system [128].

c) Fuzzy logic

Fuzzy logic techniques represent another approach in trying to model the way people construct their decisions. It can be applied to parameters that are difficult to describe using just the Boolean, 'black-white' values. In addition to using the classical 0 for false and 1 for truth, fuzzy logic allows intermediate states to be used and assumes that each statement has a degree of truth ranging from 0 to 1.

This way of describing reality is more natural and closer to the way people perceive things [139]. On the other hand the lack of the *a priori* knowledge might make it difficult to properly estimate the intermediate states.

Decision fusion level seems to be the optimal solution for the purpose discussed in this work. After collecting raw vibration data, a number of Condition Indicators (features) are typically derived and their values are evaluated against a pre-set threshold. Once a decision based on the threshold-crossing criterion is derived from all the CIs, a joint decision can be reached about the condition of the monitored component. This approach minimises the number of the required sensors, yet – by the use of different CIs – derives versatile information which can be fused into a meaningful 'GO – NO GO' decision. For this reason decision fusion level will be further studied in Chapter 11.

d) Heuristic methods

Heuristic methods are based on the way people make decisions and reach consensus when operating in a group. In condition monitoring terms each sensor represents one person collecting data and making decisions. The inputs to the method include a number of observations in either hard format where only one possible identity is reported for example ‘this colour is red’ or in soft format where several possibilities occur, each with confidence ratio for example ‘this colour red (70% confidence), brown (25% confidence), orange (5% confidence)’.

Once all the input information has been gathered one of the identity fusion heuristic methods can be applied to reach a decision. The most widely used techniques include [128]:

- *voting* which utilise counting the number of the same identities and making a decision based on some fixed rules (majority or minority), usually used with the hard format observations,
- *scoring* where weighted sums of ranked identity declarations are made to reach a consensus as to which option is the most probable. The weights can be prepared as functions of distance from the source or the signal-to-noise ratio,
- *Q-sort models* – the idea is based on modelling processes similar to those by which human groups achieve consensus .

The disadvantage of this technique is that the subjective methods lack mathematical description and hence might be difficult to quantify [128].

Observations

This section examined the state-of-the-art in the field of gearbox condition monitoring. A short introduction was followed by a brief description of oil debris analysis techniques. Oil debris analysis is a popular condition monitoring technique, but most of the time it is used just as a supplementary technique to vibration analysis. Since oil debris analysis is out of scope of this text, only the most important analysis techniques were outlined. The main part of this chapter focused on examining the properties of existing vibration-based condition monitoring techniques. Many vibration analysis and signal processing techniques were presented including spectral analysis, time domain methods, methods involving signal processing in both the time and frequency domain, time-frequency techniques capable of analysing signals in time and frequency domains simultaneously, time series modelling approach and other popular methods like the Shock Pulse Method or enveloping. The philosophy behind their development and their most important properties were outlined. This was followed by a critical evaluation of their performance. Table 3.1outlines the examined techniques together with a summary of the critical evaluation.

The analysis of the properties of the existing techniques showed that time, or combined time and frequency domain techniques, are best suited for creation of Condition Indicators that would not require expert knowledge in order to be properly interpreted. All other techniques, despite showing great potential and possibly a greater insight into the nature of the vibration signals, require much bigger input from the potential operator in setting up the required parameters. Such parameters, in turn, quite often have to be re-configured on a case-to-case basis. All examined CIs operating in the time or combined time and frequency domain are routines that, by default, output just a single number. Such an indication of the condition of the monitored component is the easiest to understand by a vibration non-specialist. Outputs of such CIs can be easily fed into the cockpit of a helicopter providing a clear indication in the form of a 'GO-NO GO' message. In addition to that, designing new CIs in a similar fashion to the existing solutions makes their usage case independent and easily applicable to virtually any gearbox without the need for vast experience and expert knowledge in the field. Research work contained in this text will therefore concentrate around examining the properties of the most widely used CIs, based in the time or time-frequency domain. The intelligence gathered as a result of the investigations will be used to develop new, improved CIs, capable of indicating the condition of a given component with a single numerical output.

The second part of this chapter characterised the most widely used data fusion techniques and architectures. A critical evaluation of the methods allowed discriminating between techniques that, among other differences, require historical data (not always available) in order to work properly. The data fusion model used in this research work is discussed in detail in Chapter 11.

In addition to the specific techniques used in data fusion, three different levels at which data fusion can take place were evaluated. Raw data fusion level requires more than one sensor in order to be operational. This, in turn, requires good access to acceptable sensor mounting locations and increases the overall cost related with the condition monitoring operations. Feature fusion level works on the basis of deriving features from sensors (often of different types) and using them as inputs to the data fusion process. Fusing data at this level could be applicable even to situations when only one sensor is used for monitoring purposes. Performing feature level fusion might promote more dynamic features at the cost of features with smaller range of values. For this reason it is reasonable to generate a decision from each feature before feeding them into the data fusion model. This approach could mitigate the problem of using features with different scales and dynamic ranges. Feature fusion and decision fusion levels will be examined in more details in Chapter 11.

Table 3.1 Critical evaluation of the most widely used vibration-based condition monitoring techniques

Technique	Outcome of critical evaluation
Frequency domain analysis	
Spectral analysis	Requires expert knowledge and experience for proper detection of the characteristic features of a given fault
Time domain analysis	
Root Mean Square	Sensitive to changes in signal energy caused by varying load or speed
Standard Deviation	Late indication of the gear fault development
Crest Factor	Decrease in value when the fault changes from localised to more widely distributed
Kurtosis	Decrease in value when the fault changes from localised to more widely distributed

Combined time and frequency analysis	
FM0	Decrease in value when the fault changes from localised to more widely distributed
FM4	Decrease in value when the fault changes from localised to more widely distributed
NA4	Sensitive to changes in signal energy caused by varying load or speed
NA4 Reset	Requires additional instrumentation which increases the cost and complexity of the measurements
NB4	Filtering in appropriate frequency band required – case dependent
M6	Decrease in value when the fault changes from localised to more widely distributed
NA4*, NB4*	Historical data required
Energy Ratio	Not sensitive to incipient fault
RMS of residual signal	Requires data from the heathy gear for the construction of the residual signal
Time-frequency analysis	
Short Time Fourier Transform	Trade-off between frequency and time resolution; Requires appropriate window length for a given situation – case dependent; Requires expert knowledge and experience to interpret results
Wigner-Ville distribution	Appearance of cross-terms makes it difficult to analyse signal from complex systems; Requires expert knowledge and experience to interpret results
Wavelet Transformation	Requires proper selection of wavelet parameters and shape – case dependent; Different wavelets produce different results; Requires expert knowledge and experience to interpret results
Time series modelling	
Autoregressive model /Autoregressive Moving Average model	Complexity of proper assessment of the order of the models – case dependent
Other	
Shock Pulse Method	Requires additional instrumentation which increase the cost and complexity of the measurements; Requires high sampling frequency; May not be useful when fault progresses to advanced levels
Enveloping	Filtering in appropriate frequency band required – case dependent

Table 3.2 Critical evaluation of the most widely used data fusion techniques

Technique	Outcome of critical evaluation
Parametric template	Requires appropriate definition of classes; Potential problems in decision making when an overlap occurs
Physical model	Requires operating very large software programs - may require excessive computational power/processing time
Artificial Neural Network	Often referred to as a black box – lack of transparency of operations; Requires high volume of data to adequately train the network
Clustering	Different clustering techniques can give different result for the same data; Expert knowledge required in applying the appropriate algorithms and interpreting their outputs.
Knowledge-based model	Requires vast databases containing very large volume of information about specific behaviour of the machine; Databases not transferrable between machines
Classical Inference	Only valid for repeatable processes; Capable of assessing only two hypotheses at a time
Bayesian Inference	Difficulty in acquiring the prior probabilities; Use of subjective probabilities that lack mathematical description
Heuristic methods	Use of subjective methods that lack mathematical description
Fuzzy Logic	Potential difficulty in estimating membership functions if no *a priori* knowledge is available

CHAPTER 4

EXPERIMENTAL DATA

This chapter begins with a brief introduction to the concept of gear transmission systems. An initial explanation of the principles of gear transmission is followed by a description of the three most popular gear transmission system architectures: single-stage, multiple-stage and epicyclic gear systems. This is followed by an explanation of the working principles of the transducer used to collect vibration signals.

All datasets that have been used throughout the present research, first to test the performance of all the existing CIs (Chapter 6) and later to evaluate the newly proposed ideas (Chapters 7-11) are outlined. There are 3 datasets, 2 of which contain a gear fault signature and 1 containing a roller element bearing fault. One dataset contains helicopter operational data and the remaining 2 datasets were experimentally generated on different test rigs. The description of each dataset is summarised by characterising the nature of a typical vibration signal generated by each set up. Unfortunately, the technical specification of the accelerometers used to collect the data in the presented datasets, as well as the acceleration units in which the vibration response is shown are unknown. However, the data collection process was unchanged for the whole duration of each test. Also the time domain and the frequency domain representations were created using the same signal processing routine for every dataset analysis.

4.1 Gear types

There are numerous types of gears used in gearboxes, each having its characteristic strengths and limitations. The type of gear used in a given system depends on a number of factors such as the required decrease/increase of the shaft speed, the load being carried, the resistance to specific operational conditions or permissible noise level. Among many other types, there are three basic designs that are very popular in field applications and come with their own characteristic properties. They are outlined in the following sections.

4.1.1 Worm gear

Worm gear drives are used to transmit power between non-intersecting shafts that are typically at right angles to each other. Figure 4.1 shows a typical worm gear drive arrangement where the top gear is referred to as the worm, and the bottom gear is called the worm gear [140]. Typically, the worm is a threaded screw and the worm gear is a toothed gear. The advantages of using a worm gear drive include speed reduction, as high as 100:1 for a simple pair of worm gears, small dimensions compared with equivalent spur or helical gear drives and extremely smooth and silent operation due to almost entirely sliding motion during the gear mesh. The disadvantages of this design include low efficiency compared to other gear drives, the high cost of typically used materials (mostly phosphor bronze) and the substantial amount of heat that needs to be dissipated through the lubricating system [140].

Figure 4.1 Worm gear drive [141]

4.1.2 Bevel gear

Bevel gear drives are used to transmit power between intersecting shafts that are typically at right angles to each other. The two most common types currently in use include straight bevel gears (the teeth are lined up in straight lines converging to a common point) and spiral bevel gears (the teeth have spiral curves also converging to a common point). Both types of bevel gears are shown in Figure 4.2. The advantages of straight bevel gears include ease of design and manufacture and relatively good service when mounted on shafts properly. The disadvantage of straight bevel gears is that they create high levels of noise during high speed operation. The advantages of spiral bevel gears include quiet operation (even at high speed) due to smooth gear engagement and the capability of transmitting higher power/loading (up to 25% compared to straight bevel gears). The disadvantages of spiral bevel gears is that they apply additional axial pressure increasing wear in the shaft bearings together with complexity of design and high cost of manufacturing.

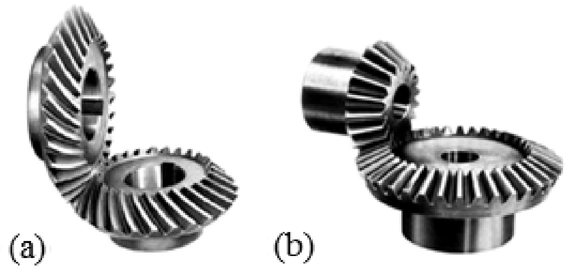

Figure 4.2 Bevel gear drive - (a) spiral bevel gears [142], (b) straight bevel gears [143]

4.1.3 Spur gear

Spur gears are mounted on shafts which are parallel to each other. They are cylindrical gears with external teeth parallel to the axis of the shaft. The line of contact between the mating teeth is always parallel to the axis of the shaft [144]. A typical spur gear setup is shown in Figure 4.3. The advantages of spur gears include low manufacturing costs, simple design and ease of maintenance. The main disadvantage of spur gears is that they have smaller load capacity and higher noise levels compared with helical gears.

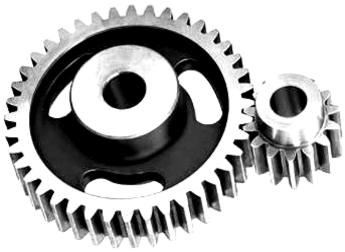

Figure 4.3 Spur gears [145]

4.1.4 Helical gear

Helical gears have teeth with lead angle relative to the axis of rotation and follow the curve of a helix across the face width of the gear [146]. The advantages of helical gears are higher load capacities and smaller noise compared with spur gears. The disadvantage of helical gears is the development of the *end thrust* – lateral force exerted on the end of the shaft. For this reason thrust bearings are often required to account for the end thrust effect [147]. Typical helical gears are shown in Figure 4.4.

Figure 4.4 Helical gears [148]

The difference between helical gear and spur gear drives is that in the helical arrangement, the transmitted load is distributed through a higher number of teeth pairs. In addition, the load is transmitted much more smoothly between the teeth. Therefore helical gear drives are capable of carrying more load, running more smoothly and generating less vibrations than spur gear drives. The difference in transmission error – one of the main components of vibration generated by gears - between the two types of gears is shown in Figure 4.5.

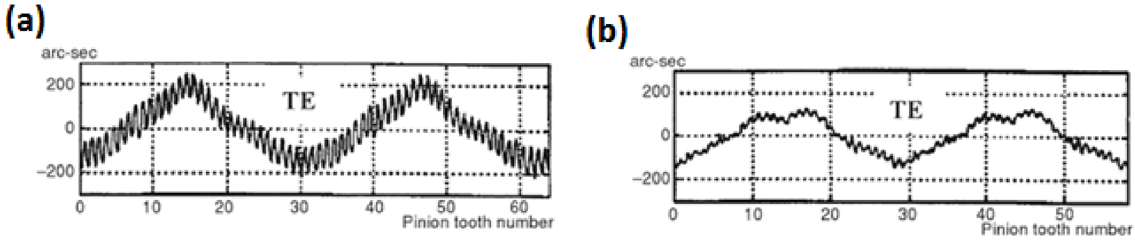

Figure 4.5 Transmission error for gears with 1:1 ratio: (a) spur gear, (b) helical gear [45]

4.2 Gear Transmission Systems

Gear transmission systems are mechanical systems designed to convert or transmit speed and torque from the driving to the driven equipment [149]. At the same time they are capable of changing the direction of rotation of the driven shafts [150]. Speed refers to the rotational speed of the shaft - the rate of change of shaft angular displacement (typically expressed in radians per second or revolutions per minute (RPM)) measured in a given time window [151]. Rotational speed V_r can be obtained as per Eq. 4.1.

$$V_r = \frac{\alpha}{t} \tag{4.1}$$

where α represents the angular displacement, t represents time.

Torque is the tangential of force applied to a shaft multiplied by the radial distance (radius) to the point of application of the force – in gear systems torque is derived as the distance between the centre of the gear and the part of its teeth where the load is applied (called the radius) multiplied by the tangential force being applied by the teeth. Torque is measured in Newton-meters (Nm) in metric system [150]. In mathematical terms torque τ can be described as [151]:

$$\tau = r \cdot F \tag{4.2}$$

where r represents the radial distance to the point of application of the force and F represents the tangential force.

The torque transmitted through a gear transmission system depends on the gear transmission system's design. In a basic arrangement this operation is performed through an interaction of at least one set of gears. If unchanged transmission of torque is required, the number of teeth on both meshing gears should be the same. Otherwise by making the number of teeth on the gears non-identical the input parameters are transformed and the degree of the change depends on the exact design of the meshing gears.

There are many different gear transmission systems and their design is dependent on the specific requirement of the system. However, among the different types one can distinguish three main gear transmission system arrangements that are the most widely used.

4.2.1 Single-stage transmission system

This is the simplest construction of the three, based on the arrangement shown in Figure 4.6. It consists of one input from the driving device, for example a motor which is connected to the drive gear. The drive gear meshes with the driven gear and the later drives the output shaft, which is connected to the input end of the system, for example a generator. This system is used when a simple, one-stage speed/torque conversion or a directional change is required, for example in a helicopter tail rotor drive shaft or in a wind turbine that uses the Multibrid technology. Multibrid technology is based on the concept of using lower speed generators (compared to the traditional 1500 RPM generators), hence a much smaller speed increase is needed between the tubine shaft and the generator [152]. The advantage of using this transmission system is its simplicity and relatively small size. The disadvantage, however, is that there is a practical limit to the gear ratio that can be used, and hence limited torque/speed conversion can be achieved [153].

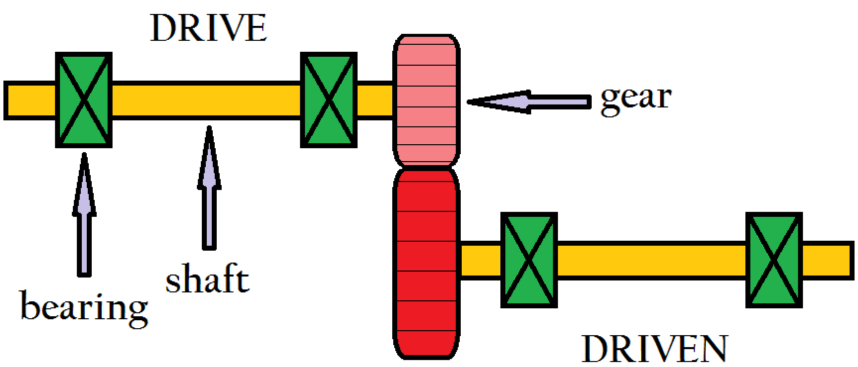

Figure 4.6 Simplified single-stage gear transmission system

4.2.2 Multi-stage transmission system

Multistage gear transmission systems are similar to the single-stage arrangements with the difference that they contain more pairs of meshing gears. This makes them capable of accommodating larger speed/torque conversions and allows much higher gear ratio values to be reached. This arrangement finds utilisation in, for example, open cast mining machinery where the size of the gearbox is not the main concern to the machine designers and a high degree of speed/torque conversion is required [154]. Figure 4.7 shows an example of a three-stage gearbox (three pairs of meshing gears).

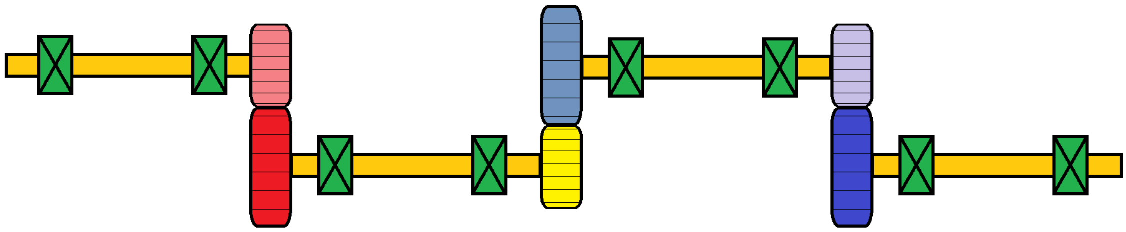

Figure 4.7 Simplified multi-stage gear transmission system

4.2.3 Epicyclic transmission systems

Epicyclic (or planetary) configuration is a slightly different approach to the single or multi-stage gear systems. In typical arrangement it consists of three or more gears (planets) revolving between a centrally located gear (sun) and a fixed outer gear (ring). It also contains a planet carrier to which the planet gears are attached on one side and the input shaft on the other side [147]. Figure 4.8 shows a simplified arrangement of an epicyclic transmission.

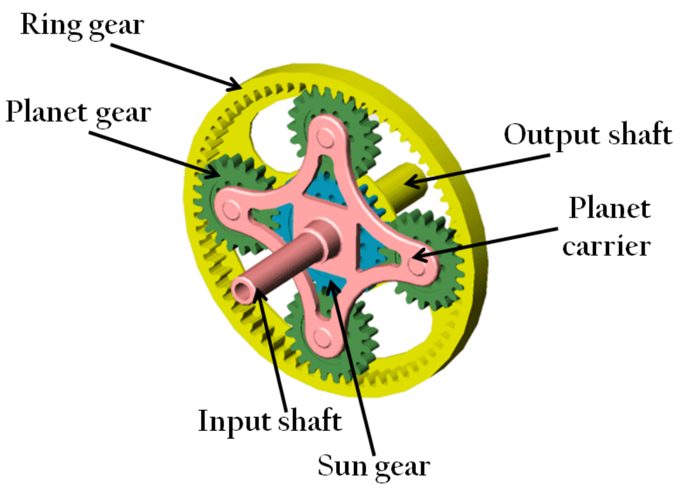

Figure 4.8 Epicyclic transmission system [155]

The disadvantages, however, include complex overall design, production and assembly processes, due to a higher number of rotating elements; complicated manufacturing of internal teeth on the ring gear; difficult servicing caused by the compact and complex design and more difficult condition monitoring (compared to traditional approach) due to a number of elements meshing and rotating together in a small and inaccessible space [156].

Epicyclic gear transmission systems are widely used in helicopters as the last stage of the main rotor gearbox due to their characteristic of relatively high reduction ratios reached at relatively low shaft speeds (hence generating a very high torque) [157]. In a typical helicopter transmissions arrangement the torque is transmitted from the central sun gear through the planets to the planet carrier and from the planet carrier to the main rotor shaft [158].

Regardless of which gear transmission system is used, the gear transmission durability is affected mainly by its gears and rolling element bearings and so these elements are primarily subject to diagnostic assessment [159]. These aspects of machinery usage become of paramount importance in the field of helicopter operations where failure of gears and/or bearings can lead to catastrophic consequences. Despite the differences in design of various gear transmission systems, the main working principles and therefore the main components forming gear transmission system remain the same. This, in turn, supports the use of very similar gear transmission condition monitoring techniques.

4.3 Acceleration transducers

Vibration can be described as a dynamic mechanical phenomenon characterised by periodic osciallatory motion around a reference point [160]. The state of any object in motion can be described by three inter-dependent units: position, velocity and acceleration. As a rule of thumb, in situations requiring measurement of low frequency oscillations (<10 Hz) position and displacement measurements provide good results. Intermediate frequency range events (<1 kHz) are often measured using velocity transducers. In applications with relatively high background noise and frequencies ranging much higher than 1 kHz accelerometers are used to measure the acceleration [160].

Accelerometers represent a family of transducers that provide an output that is proportional to acceleration (which may include vibration and shock) of the surface on which the transducer is mounted. Among many different types of accelerometers, piezoelectric types of transducers represent the most popular class of those sensors [161].

Piezoelectric accelerometer can be modelled as a spring-mass unit, which is used to generate a force that is proportional to the amount of the measured acceleration. At the same time this force is applied to a piezoelectric crystal that produces an electrical charge that is proportional to crystal strain [162]. The measurement frequency band of an accelerometer is limited by its resonant frequency. Therefore it is important to match the requirements of the measurements with the properties of the sensor. Figure 4.9 shows a typical frequency response of a piezoelectric accelerometer. It can be seen that the useful frequency band in which the accelerometer output is meaningful lies below the resonance frequency. The limit for the flat (hence the most reliable) response of the transducer is around 20% of the resonance peak frequency of the accelerometer [163]. Any measurements carried out in the frequency band that coincides with the region of the resonance peak will result in disproportionately amplified, unreliable, acceleration readings.

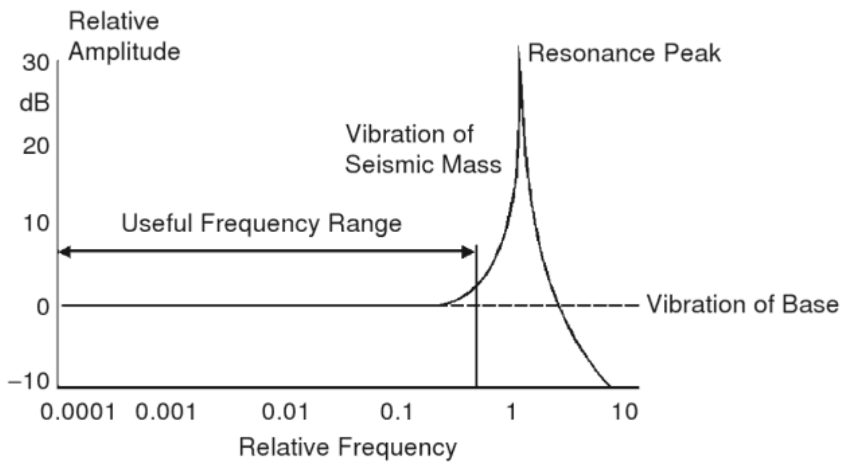

Figure 4.9 Typical frequency response of a piezoelectric accelerometer [164]

4.4 Gear fault datasets

4.4.1 Dataset 1 (SH-60 Sea Hawk test rig)

Dataset 1 was made available for analysis by QinetiQ Ltd. Since there was no description of the data was made available with the vibration data files, all information presented in this section is based on details reported in published articles [165, 166].

The data were generated during the Helicopter Integrated Diagnostic System (HIDS) programme, and the test rig was an SH-60 Sea Hawk helicopter drive train. The goal of the test was to force a gear fault propagation from good working order to a near catastrophic failure. In depth investigation revealed that the component of the drive train that had the potential to deliver the goal in the shortest time was the pinion gear, located in the Intermediate Gearbox (IGB); it had one of the highest bending stresses in the entire SH-60 drive train [166]. Figure 4.10 shows a sketch of the test rig drive train showing the location of the Intermediate Gearbox.

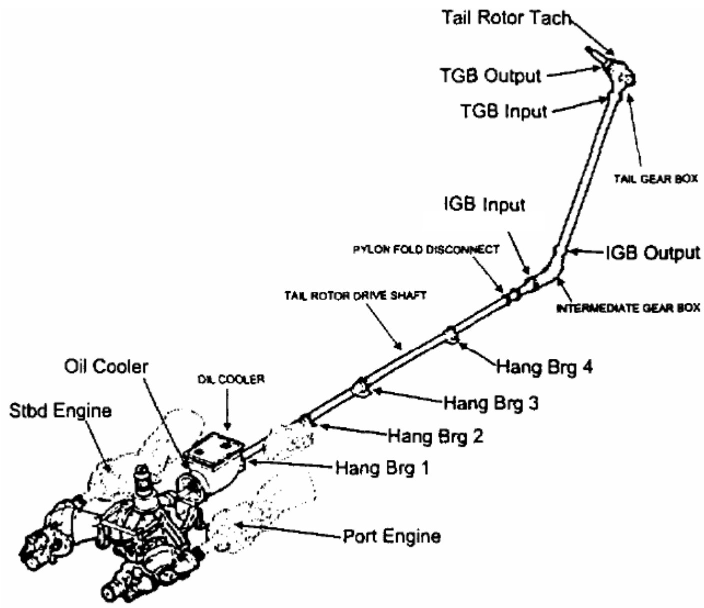

Figure 4.10 Test rig drive train [165]

The objective of the test was to force the crack to propagate along a specific path along the length of the root and down into the web of the gear. In order to achieve this, two small notches were seeded in the gear prior to the test. One notch was located at the root of the tooth, the second near the centre, beneath the point where the load pattern indicated maximum load for a healthy gear. Both notches were 0.1mm wide by 1mm deep by 6.4mm long and they were created using an electrical discharge machine

(EDM). An EDM facilitates precise metal removal using an accurately controlled electrical discharge (spark) that erodes the metal [167].

During the test a constant torque was applied (3,173 Nm which complied with the load ratings of the monitored parts), at a constant speed with manual inspections assessing the condition of the gear carried out approximately every 2 hours. There were a total of 4 inspections carried out after data samples 25, 46, 57 and 74. Each inspection entailed removing the pinion gear from the test rig, removing the lubricant and performing a number of non-destructive tests in order to assess the condition of the gear.

The dataset comprises a total of 86 samples. After recording the last file, the test was stopped due to a severe pinion gear crack. Inspection revealed that the fault originated at the root of a tooth, extended through the gear web and stopped at a bearing support surface. A photograph of the gear taken after the test was terminated is shown in Figure 4.11.

Figure 4.11 A severe gear crack that led to termination of the test [165]

Data files were recorded every 5 minutes and each sample acceleration response contains 30 seconds of raw vibration data. The sampling rate of the system was 100 kHz. The shaft on which the gear was operating was rotating at a speed of 4140 revolutions per minute (RPM) which corresponds to a frequency of 69Hz. The gear had 25 teeth which resulted in a gear mesh frequency of 1725Hz. The gear mesh frequency (GMF) is related to the meshing action of gears and it can be defined as the product of the speed of the given shaft and number of teeth on the gear which is mounted on this shaft [168].

Figure 4.12 shows the amplitude acceleration spectrum collected at sample 1. This figure represents a typical spectrum of the vibration signal recorded on a healthy pair of gears at the beginning of the test. Figure 4.13 shows a magnified view of Figure 4.12 in the region [0 – 12] kHz in order to illustrate the presence of the GMF and its harmonics and the lack of sidebands around those frequencies. Such a spectrum is as expected from a gearbox with a healthy pair of helical gears.

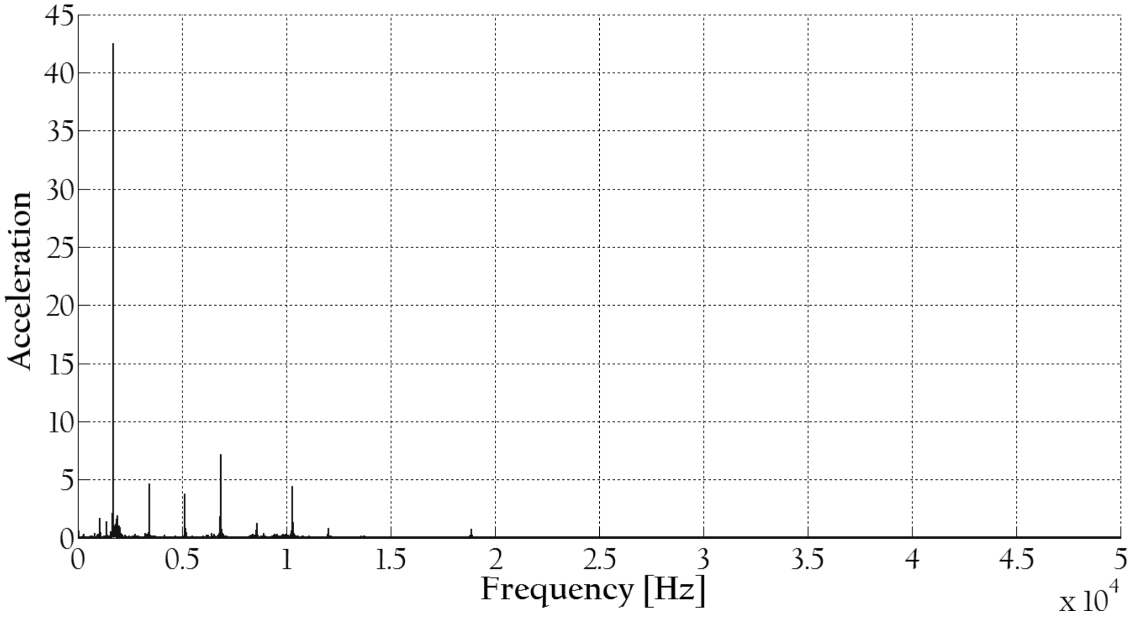

Figure 4.12 Spectrum of sample 1 of Dataset 1

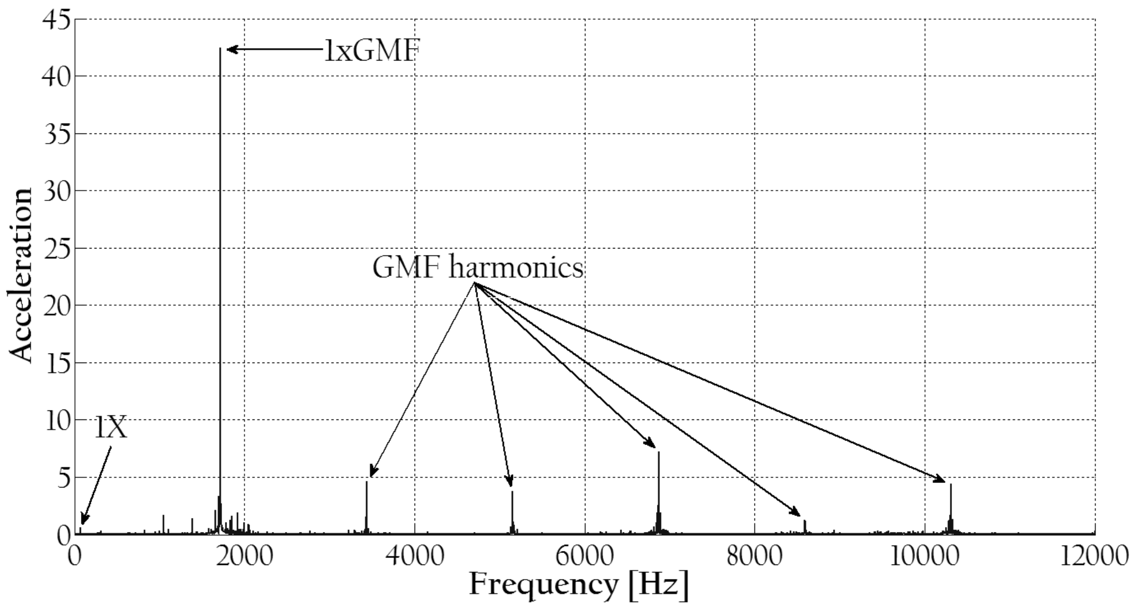

Figure 4.13 Magnified view of Figure 4.12

4.4.2 Dataset 2 (Idefix 701 test rig)

The data was made publicly available on the website of the Laboratory of Signal Analysis and Industrial Processes (LASPI) at the Jean Monnet University in Saint – Etienne, France [169].

The gearbox and the corresponding operating conditions (for example speed and torque) were selected in a way that allowed a spalling fault to develop along the width of the tooth face. At the end of the test a conclusion was drawn that the gear under consideration went from a healthy state to a damaged state.

Table 4.3 shows the result of the once-a-day gear condition inspections.

Table 4.3 Description of the gear condition in each data sample

Test day/ sample number	Tested gear condition
1	Intact
2	Intact
3	Intact
4	Intact
5	Intact
6	Spalling on tooth 1
7	Spalling on tooth 1
8	Spalling on tooth 1 Beginning of spalling on tooth 15
9	Spalling on tooth 1 Spalling progression on tooth 15
10	Spalling on tooth 1 Spalling progression on tooth 15
11	Spalling on tooth 1 Spalling progression on tooth 15
12	Spalling on tooth 1 Spalling across the whole width of tooth 15

The test arrangement comprised two gears: a driven gear with 21 teeth and the test pinion with 20 teeth. The dataset consisted of 12 samples. The test was run for 12 days and the data files were recorded once per day. Each acceleration response sample contains 3 seconds worth of data and the sampling frequency was set to 20 kHz. The speed of the shaft was 1000 RPM (16.67Hz), which resulted in a GMF of approximately 300Hz.

Figure 4.14 shows the amplitude acceleration spectrum collected at sample 1. This figure represents a typical spectrum of the vibration signal from Dataset 2 recorded on a healthy pair of gears at the beginning of the test. Figure 4.15 shows a magnified view of Figure 4.14 in the region [0 – 5.5] kHz in order to illustrate a clear presence of the GMF and its harmonics. In addition, the existence of sidebands around the GMF and its harmonics can be seen (Figure 4.16). This situation usually indicates deterioration of the gear health, but in this case the gears were reported to be in intact condition at the beginning of the test. This might indicate that the sidebands were generated due to inaccurate assembly of the test rig which could have resulted in some degree of misalignment between the shafts or improper meshing of the gears. The former assumption could be further supported by the fact that the amplitude of the fundamental GMF is lower than its harmonics – a known system response in the presence of shafts misalignment or gear eccentricities.

In addition, when comparing spectra from Dataset 1 and Dataset 2, one can see that the spectrum generated from the Dataset 2 vibration record is much noisier and richer in GMF harmonics and shaft speed sidebands. This is due to the fact that the results for Dataset 2 were obtained from a gearbox with spur gears, whereas in Dataset 1 helical gears were used. Helical gears operate in a much quieter and smoother fashion compared to spur gears [170], hence the vibration spectrum contains much less operation-specific components. As mentioned in section 4.1.4, helical gears have higher contact ratios (higher number of teeth meshing at the same time) than spur gears of the same size and each pair of helical teeth slides into full contact before the previous pair is out of mesh, reducing the operational noise [171].

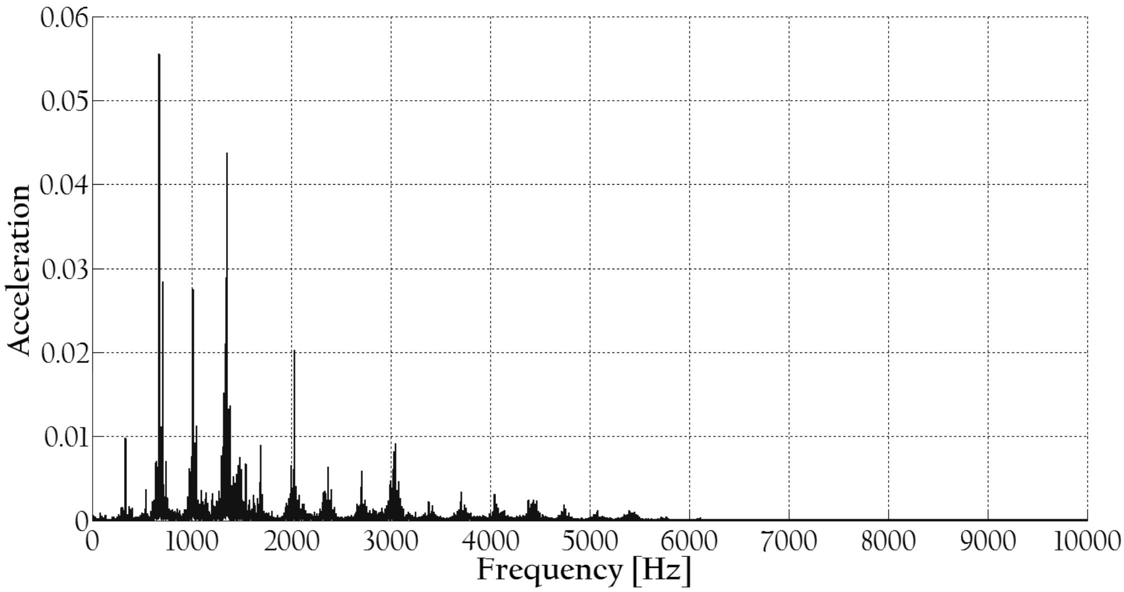

Figure 4.14 Spectrum of sample 1 of Dataset 2

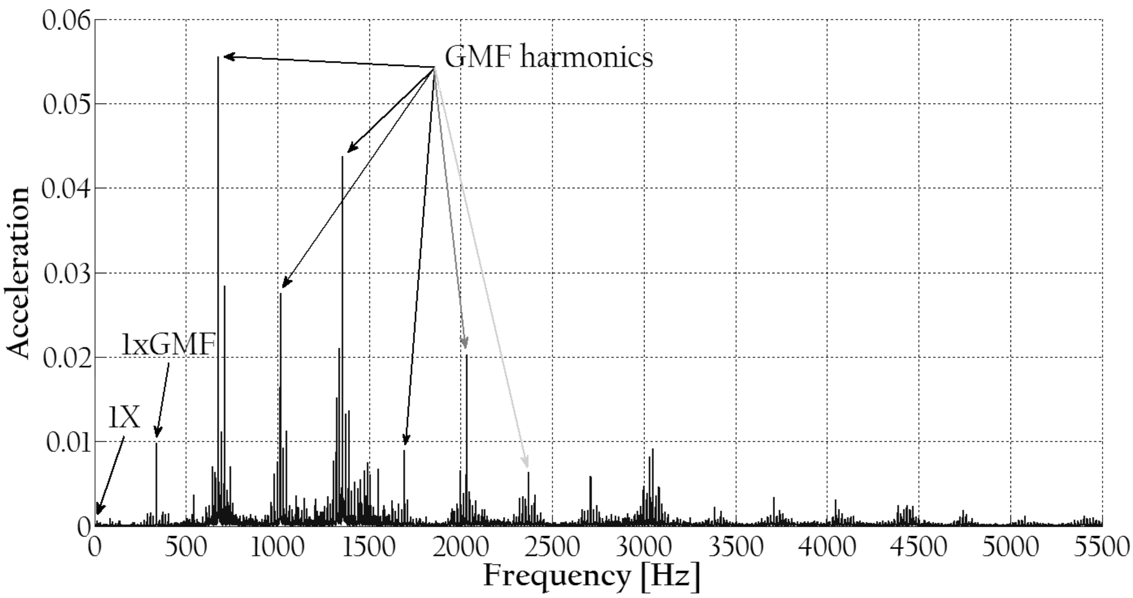

Figure 4.15 Magnified view of Figure 4.14

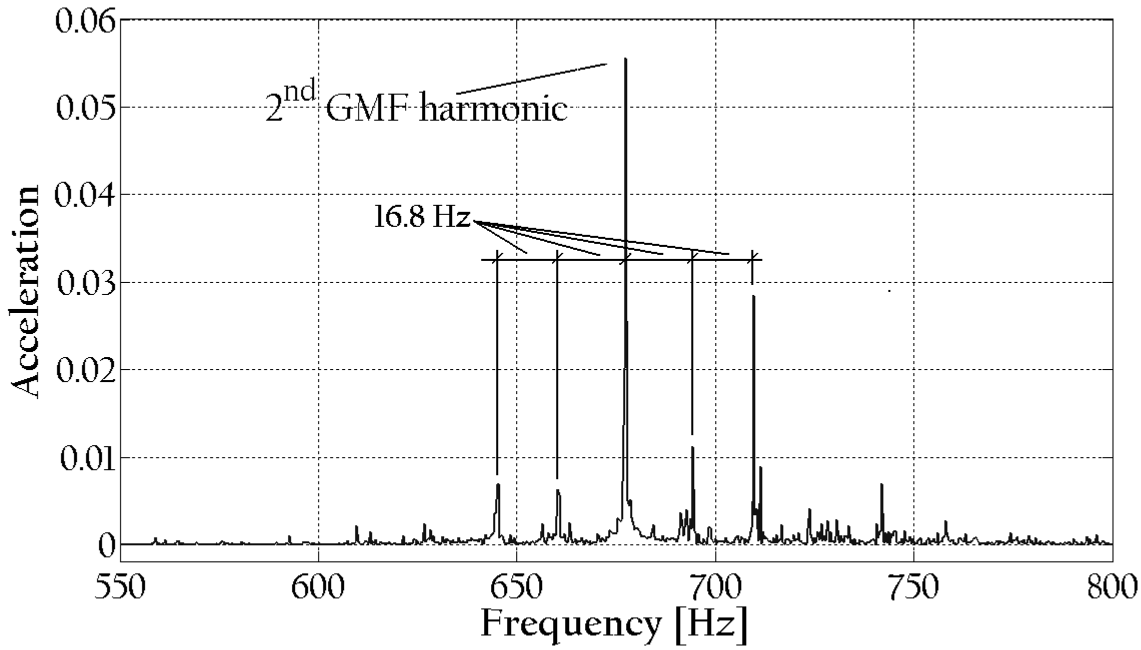

Figure 4.16 Magnified view of Figure 4.15

4.5 Bearing fault dataset

4.5.1 Dataset 3 (Chinook helicopter operational data)

This dataset was made available for analysis by QinetiQ Ltd. The vibration signals were collected by the Chinook Health and Usage Monitoring System and were generated during operations carried out by one of the Chinook fleet helicopters. The documentation that was made available with the dataset stated that the dataset contained a history of a combiner gearbox rolling element bearing outer race defect (typically referred to as Ball Pass Frequency Outer – BPFO [172]) development. The accelerometer was located in a combiner gearbox within the combining transmission module, shown in Figure 4.17.

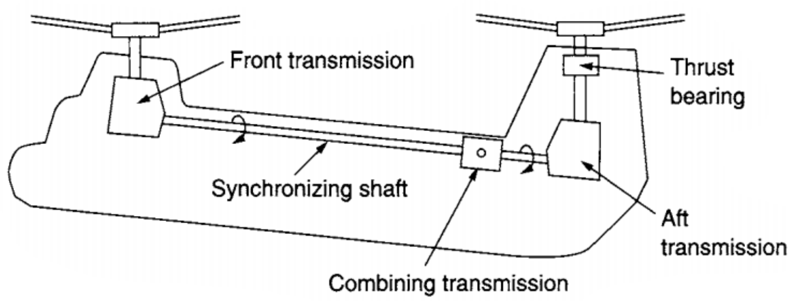

Figure 4.17 Chinook helicopter drive train sketch [173]

The dataset comprises 67 samples but the time frames at which the data samples were collected were not provided with the dataset. Each vibration sample is 0.16 second long and was sampled at the rate of 102400 samples per second.

Figure 4.18 shows the amplitude acceleration spectrum collected at sample 1. It can be observed that the majority of energy in the spectrum is located in the region [0 - 20] kHz. Since the data were collected from a helicopter during routine flight operations, the number of frequency components and the relatively high noise level in the discussed frequency region are as expected.

A diagram of the combining transmission is shown in Figure 4.20. The figure shows the complexity of the monitored structure and the number of different components operating at the same time in a relatively small area adding to the level of the background noise. The exact location of the accelerometer is unknown, however even without this knowledge one can appreciate the large number of different frequency components that are generated by the combining transmission alone, not to mention the influence of other, 'loud' components of the whole drive train.

In order to determine the defect frequency being generated by the outer race bearing failure a standard formula for calculating the theoretical value of the frequency has been used (as per Eq. 4.1 [175]):

$$BPFO = \frac{Nb}{2}(1 - \frac{Bd}{Pd} \cdot \cos\theta) \cdot f_r \tag{4.1}$$

where *Nb* is the number of rolling element balls, *Bd* is the rolling element ball diameter, *Pd* is the bearing pitch diameter, θ is the contact angle between the balls and the races (in degrees as per Figure 4.21), f_r is the shaft rotational frequency. The dimensions of the bearing under consideration and the calculated value of the BPFO are presented in Table 4.4.

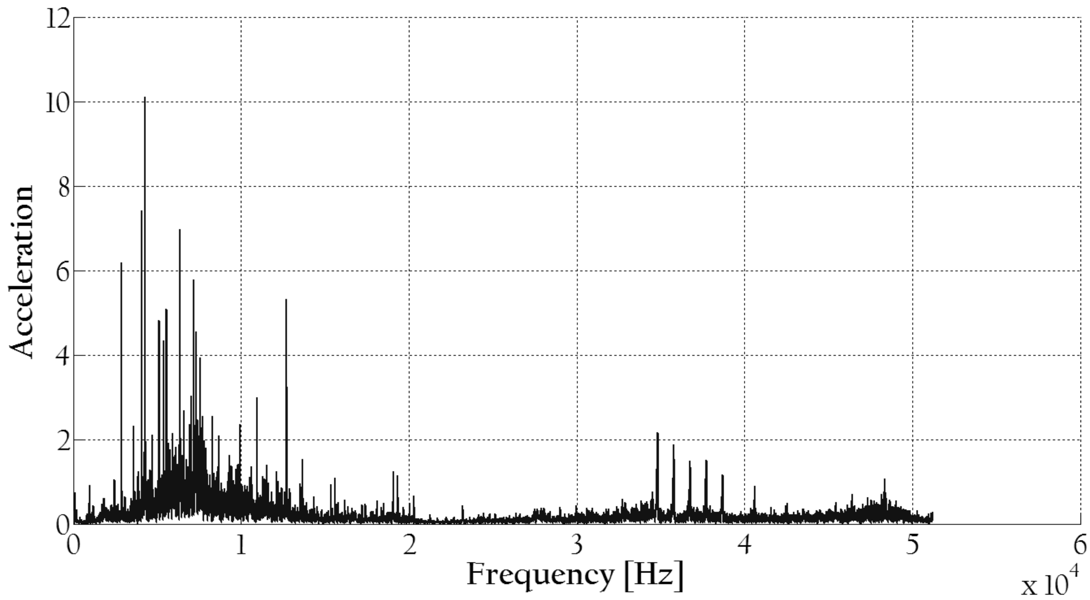

Figure 4.18 Sample spectrum of Dataset 3 (faulty bearing)

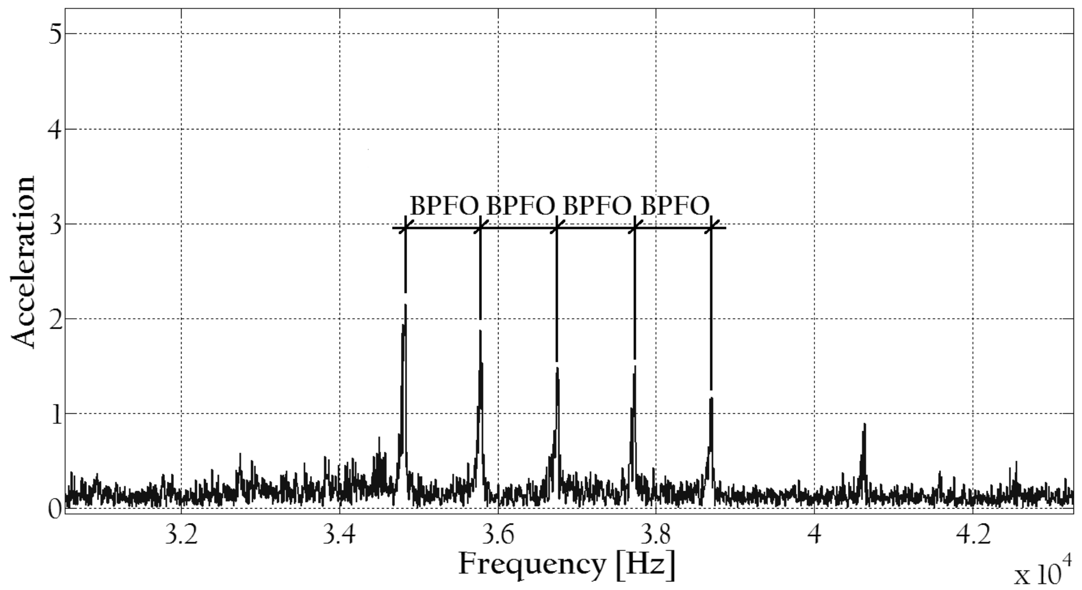

Figure 4.19 Magnified view of Figure 4.18

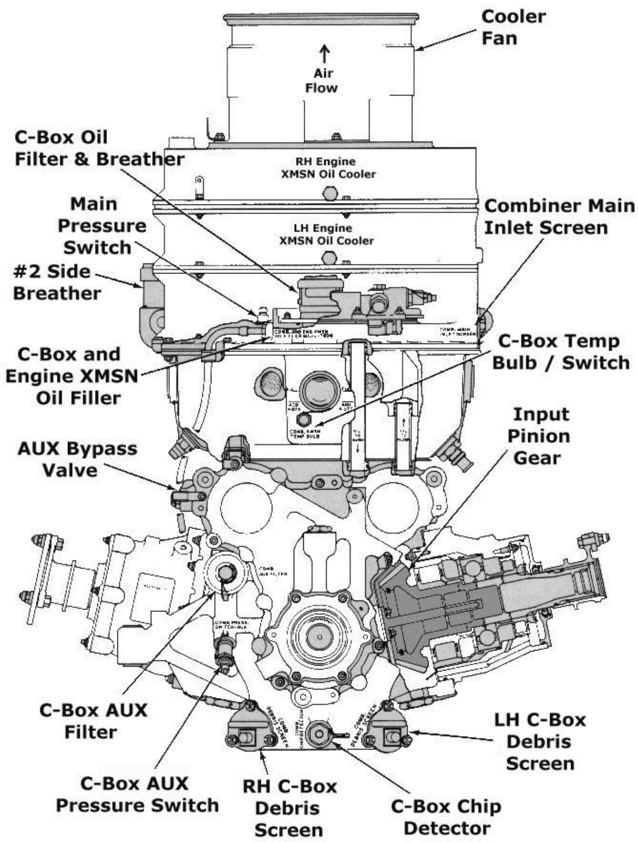

Figure 4.20 Component placement for items installed on the CH-47D Chinook combining transmission [174]

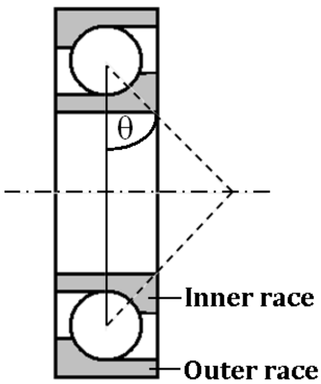

Figure 4.21 Contact angle in rolling element bearing

Table 4.4 Design details and BPFO value of faulty bearing

Nb	12.0000
Bd [cm]	1.0236
Pd [cm]	4.9213
θ [^{o}]	0.0000
f_r [Hz]	204.3843
BPFO [Hz]	971.2124

Based on the information in Table 4.4, the BPFO theoretical value equals 971.2 Hz. It is worth noting that the spectrum from sample 1 of the dataset () already shows signatures of the outer race defect frequency in the upper part of the spectrum ([35-39] kHz). They appear in the form of equally spaced harmonics of the BPFO (shown magnified in Figure 4.19). This shows that the provided dataset contains early samples which indicate that the bearing fault was already present when recording began. The explanation for the presence of the peaks in the upper part of the spectrum is that, as a bearing fault develops, a train of impulses separated by the characteristic bearing defect fault frequency is generated in the whole frequency band. Those impulses become amplified around the resonance frequencies of the system components for example the accelerometer or the bearing housing [176]. At the same time the vibration produced by a damaged bearing may be an order of magnitude smaller than the vibration produced by the meshing of the healthy gears [177]. For this reason when performing bearing diagnostics based on vibration measurements an approach is often incorporated to restrict the analysed frequency range of the spectrum to a small fraction of the bandwidth, around the structure resonance frequencies [178]. Filtering the signal in the appropriate frequency band removes all the redundant frequency components for example gear mesh frequency and its harmonics, shaft rotation frequency and its harmonics and some of machinery background noise. That is why, in order to carry out effective bearing defect diagnosis, the vibration signal was first band-pass filtered in a couple of bands in order to determine the band that enabled the clearest detection of the defect. The filtering band that gave the clearest signatures of the bearing defect was between 20 kHz and 40 kHz, and this filtering band was subsequently used for the analysis of all the data samples.

4.6 Summary

This chapter began with a brief introduction to the most widely used gear types together with their advantages and limitations. This was followed by the characterisation of different types of geared transmission systems as well as the working principles of the piezoelectric accelerometer. This was followed by a description of the three different datasets used throughout this study. Two datasets contained a gear fault and one contained a roller element bearing fault. The description of each dataset was followed by presentation of a typical acceleration amplitude spectrum. In the case of the gear fault datasets, the sample spectra were generated in order to show the initial condition of the gearbox with healthy gear pairs.

The spectrum of Dataset 1 contained only components related to the GMF and some of its harmonics and frequencies related to the rotation of the shaft. Dataset 2 however, in addition to the expected frequencies, contained high energy sidebands around the GMF and its harmonics. Based on the characteristics of the signals in Dataset 2 it needs to be clearly identified, that the sidebands do not appear only in the case of a gear failure since in both datasets the gears were claimed to be in perfect condition at the beginning of the test. Sidebands appear in the signal due to some kind of modulation process, hence they can be caused by a number of different reasons related with the assembly of the test rig or the health of the test rig components. Modulation at the shaft rotation speed can be caused by any periodic event occurring once every shaft revolution. The presence of sidebands does not necessarily indicate deterioration of components – it is the increase in the energy contained within the sidebands that can suggest that the condition of a given element is deteriorating. In addition, Dataset 1 was obtained from a gearbox with a pair of helical gears, in contrast to much noisier spur gears used in Dataset 2. For this reason a reliable gear condition assessment would require observation of any change in the amplitude of the sidebands around the GMF and its harmonics over time and this need to be an automated process in order to perform effective and economically viable condition monitoring.

In the case of the Dataset that contained the bearing fault, a typical spectrum was shown in order to present the characteristic components generated as the bearing outer race fault develops. As explained previously, such features are likely to become visible in the proximity of the resonance frequencies of the system.

Even though the characteristic signatures within vibration signals generated under the condition of a gear or a bearing defect have been well known and documented, there is still a surprisingly high number of circumstances where such events go undetected by HUMS systems [10, 11, 180]. For this reason a new type of indicator is required in some safety critical gear system applications; one that would be capable of quantifying the severity of the potential fault and giving a clear 'GO - NO GO' message. This would make it a useful tool for a quick decision making. The first step that needs to be taken in order to achieve this goal is to examine the performance of the currently most widely used Condition Indicators to try to understand the potential reasons for their inconsistent behaviour.

The next two chapters introduce the existing CIs under investigation and study their performance when applied to the described datasets.

CHAPTER 5

DESCRIPTION OF THE EXISTING CIs

This chapter begins with a brief overview of Health and Usage Monitoring Systems followed by an explanation of the Time Synchronous Averaging (TSA) of vibration signals. Next a definition of the most widely used existing Condition Indicators used in the field of gear systems health monitoring is given together with a comparison of their properties.

Introduction of the CIs is followed by an investigation of each parameter's typical values when applied to a healthy gearbox. Such an evaluation helps to establish the expected baseline values of the normalised CIs (all of the mentioned indicators apart from CI_{RMS}) for a healthy gearbox. This is followed by examination of response of each CI to the introduction and development of a gear fault signature on a simulated sinusoidal signal. This will show the likely responses of each parameter to gear defect and show the potential drawbacks of some approaches. The last part of this section tests the sensitivity of the CIs on a more realistic, simulated case, where a fault develops on a signal that comprises shaft speed components and gear mesh component with associated harmonics. This section also tests the response of the CIs when applied on a raw and residual vibration signal to see if the residual signal provides any advantage over the raw vibration signal. The chapter concludes with a summary.

5.1 HUMS (Health and Usage Monitoring System)

Helicopter condition monitoring systems are very complex arrangements specifically designed to monitor the condition of all the safety-critical components operating in the helicopter. The UK MoD funded the original development work on the key HUMS functions (including transmission vibration monitoring) in the late 1970s and early 1980s and since then the systems have been significantly improved [181]. HUMS monitoring systems are being developed by many companies, among which the main providers include GE Aviation, Goodrich, Honeywell or Altair. There are two major aspects that make HUMS such a popular solution: the first one relates to the criticality and flight safety of the helicopters (Health); the second deals with saving aircraft operation costs (Usage).

The later aspect also helps to efficiently manage the resources related to operating a helicopter. This includes helping to limit the amount of resources spent on an unnecessary servicing of the fleet, or avoiding expenses related to the consequences of a major drive-train failure (for example the costs of the engine overhaul). The proper use of HUMS may also lead to an extended life of the monitored components by collecting information about the degree of general wear of the components during different flight regimes and avoiding those regimes whether possible.

The 'Health' part of HUMS is designed to monitor the condition of the safety-critical components of the drive-train and helps to make maintenance decisions that prevent major failures which, if undetected, in some circumstances could lead to serious consequences, including fatalities [182]. The way the condition monitoring section of HUMS operates is that a number of strategically situated accelerometers receive vibration signals generated by the critical drive train components (mainly gears, bearings and shafts) and send the vibration data to a data acquisition system which records the data during helicopter operations. Apart from recording raw vibration traces, HUMS calculates a number of so called Condition Indicators (CIs) that is signal processing routines, used to characterise the vibration-based condition of the monitored drive train components [183]. CIs are designed to react to various drive-train component faults, for example gear tooth cracking or bearing defects [184].

Each CI outputs a single number that is compared with a pre-defined threshold, based on historical data and the values of the CIs applied to vibrations generated by a healthy component. Threshold values are set in such a way that there is a small probability that CI values of nominal components would exceed them [185]. All data generated by HUMS are downloaded to a ground-based system and automatically examined for fault indication [186]. Depending on the results of the evaluation, the CIs are typically given some kind of ranked class for example 'Good', 'Caution' and 'Exceeded', which is often associated with a characteristic, corresponding colour for example green, amber, red. These classes constitute a clear health indication for the engineers analysing the HUMS output on the ground. Due to the way some CIs are designed, they are not fault-specific in the sense that multiple fault types can affect the same CI, and a single fault can trigger multiple CIs [187].

Condition Indicators have been developed since the advent of HUMS systems more than 25 years ago and the number of existing CIs can be counted in hundreds. However, very few of them have been made available in the public domain. Almost all newly developed parameters are kept secret as they constitute the commercial art of the HUMS supplier and provide the advantage over the competitors. However, among those solutions that are available in public domain, there have been several CIs that over the years of testing have earned a reputation of being the most reliable measures of the gear/bearing faults. This chapter describes the most widely used solutions.

5.2 TSA signal

When dealing with vibration data generated by meshing gears, the standard practice is to create a Time Synchronous Averaged (TSA) signal. As explained by McFadden [188] by using the TSA technique the vibration of a single gear operating in a mechanical system can be extracted from the total vibration of the system. This may enable a defect such as a gear fatigue crack to be detected before any catastrophic failure occurs.

In order to perform the TSA process a second, reference signal is required in addition to the vibration signal recorded by an accelerometer. This signal needs to be synchronised with the rotation of the shaft on which the gear under investigation is mounted to (ideally) produce an easily distinguishable signal (for example an impulse) that is generated on once per shaft revolution basis. This task is usually performed by a tachometer which is set up to generate one impulse at exactly the same angular position of the shaft in every revolution. In such an arrangement the time difference between the consecutive impulses is equal to the length of one full shaft revolution. Based on the time difference between the successive shaft revolutions single gear mesh cycles can be extracted from the complex structure of the whole vibration signal. Consider a single-stage gear transmission system instrumented with one accelerometer (typically mounted on a bearing housing) and a tachometer (Figure 5.1).

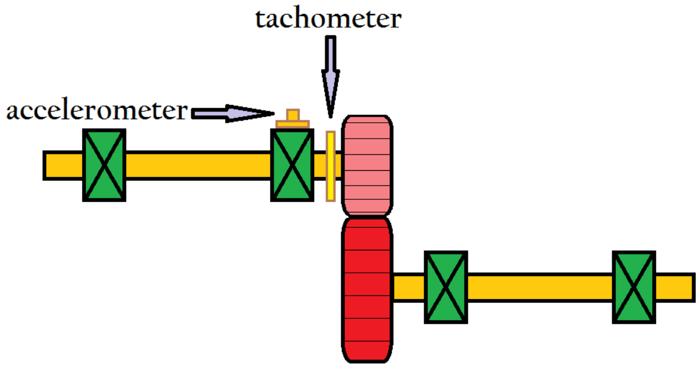

Figure 5.1 Simplified single-stage gear transmission system instrumented with accelerometer and tachometer

Figure 5.2 shows a simplified process of dividing a vibration signal recorded by the accelerometer into a number of single shaft revolution vibration signals. Impulses generated by the tachometer *tacho(t)* are used to divide signal *x(t)* into a number of segment signals, each of them generated during precisely one full revolution of the shaft (denoted as *T* in Figure 5.2). The next step involves adding the segments together. The TSA is created by dividing the sum of the segments by the number of shaft revolutions included in the average calculation as is shown in Figure 5.3. The final product of the entire synchronous averaging exercise is a signal that has a length of one shaft revolution as shown in Figure 5.4. It is worth noting that the input and the output shafts of the gear transmission system are expected to be torsionally rigid, so the time synchronous averaging of the measured signal using the tachometer readings as a reference, should not affect the averaging process.

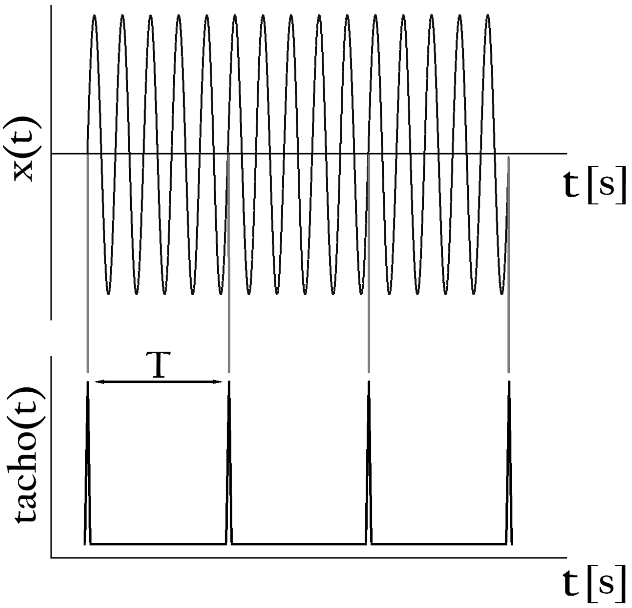

Figure 5.2 Simplified process of dividing accelerometer vibration signal *x(t)* into single shaft revolutions with the use of tachometer signal *tacho(t)*

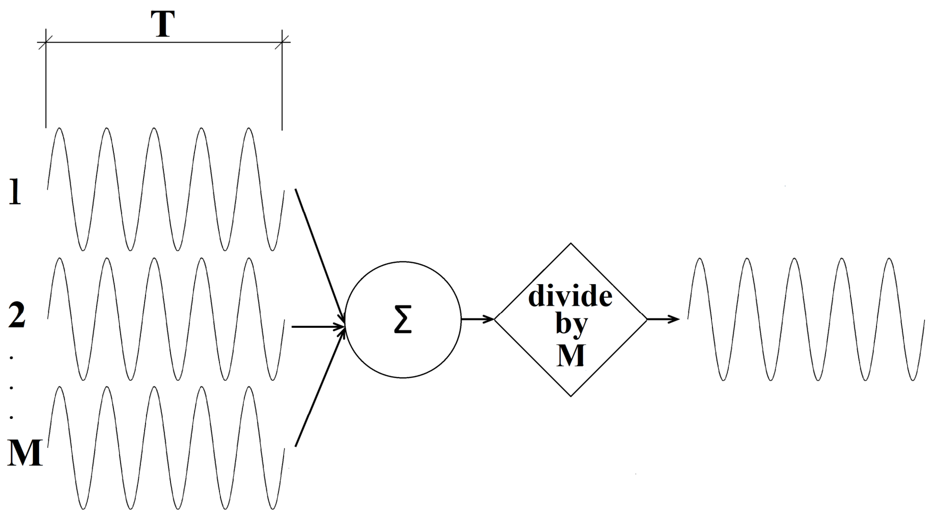

Figure 5.3 Process of creating the TSA from a number of single shaft revolution vibration signals

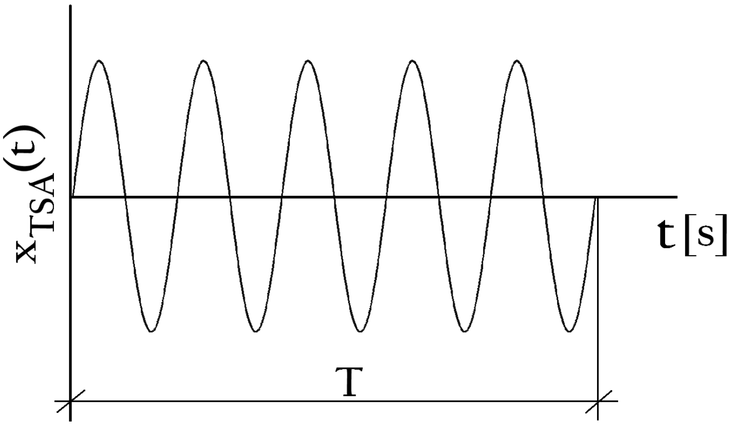

Figure 5.4 Time synchronous averaged vibration signal (T denotes time of one shaft revolution)

The reason for performing the TSA is that, after a high number of waveforms (each having the length of a single shaft revolution) are averaged, all of the vibrations which are not synchronous with the rotation of the given shaft (hence not synchronous with the meshing of the monitored gear pair) tend to be cancelled out, leaving an estimate of the vibration of the gear of interest during one revolution. This technique is particularly useful for complex systems such as gearboxes as it eliminates the vibration from other system elements and thus reduces the problem of complex vibration signal analysis to the study of vibration of a simpler system [189].

When performing the operation of dividing the tachometer signal into a number of single shaft revolution fragments, it is important to realise that the division needs to be extremely accurate in order to create a meaningful, high-quality TSA. The signal should be divided into many once-per-shaft-revolution pieces, each beginning at exactly the same angular position of the shaft. In the current research this is achieved by setting a fixed threshold value on the tachometer output signal. The threshold value is always set to 65% of the maximum amplitude of the entire tachometer signal and the trigger point is the first point above the value of the threshold.

Figure 5.5 shows a typical tachometer output that corresponds to three shaft revolutions. The dashed line represents the value of the threshold which is equal to the 65% of the maximum value present in the signal. All the examined CIs applied to Dataset 1 were calculated on the TSA signal, whereas data in Dataset 2 and Dataset 3 lack the tachometer signal, hence the TSA could not be reliably defined. The influence of the number of once-per-revolution waveforms on the quality of the final TSA was examined by comparing the TSA signals composed of 10, 30, 50, 70 and 100 averages. The results showed that there was virtually no difference between the examined cases.

The reason for this lies in the fact that the data was generated by a test rig and the recorded vibrations had very little background noise that would constitute the part of the signal which is not synchronous with the shaft rotations. Hence, in this case, performing the TSA had very little effect in terms of improving the quality of the data. Since no clear difference could be found, the CIs applied to Dataset 1 were examined on a TSA signal composed of 10 once-per-revolution waveforms, which decreased the computational power required to perform the averaging process. The comparison between TSA signals generated from 10 and 100 once-per-revolution waveforms is shown in Figure 5.6 and the resultant waveform is shown in Figure 5.7.

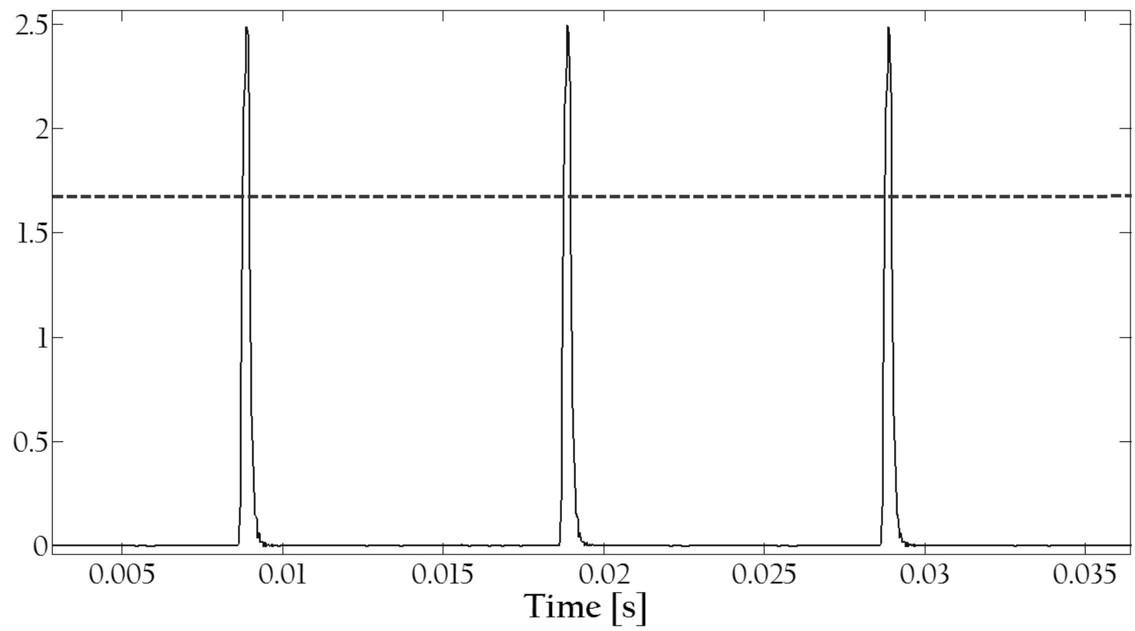

Figure 5.5 Tachometer signal from a shaft rotating at the rate of 100Hz (solid line). Dashed line represents a fixed threshold.

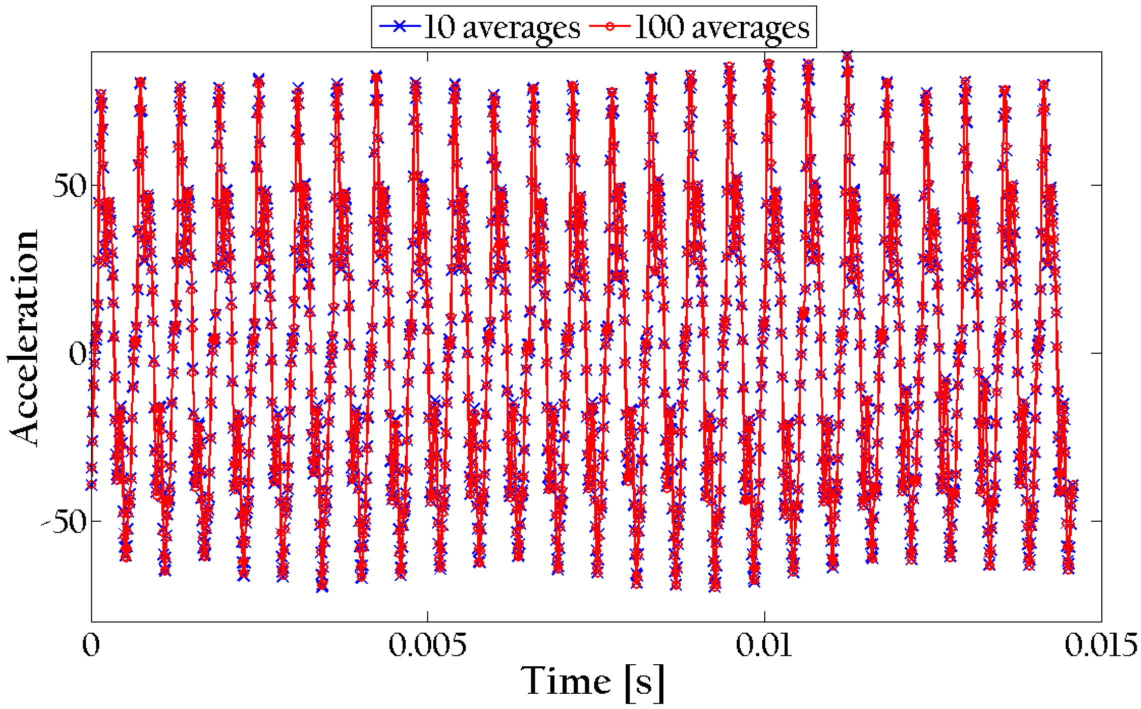

Figure 5.6 TSA signals generated based on 10 and 100 once-per-revolution waveforms

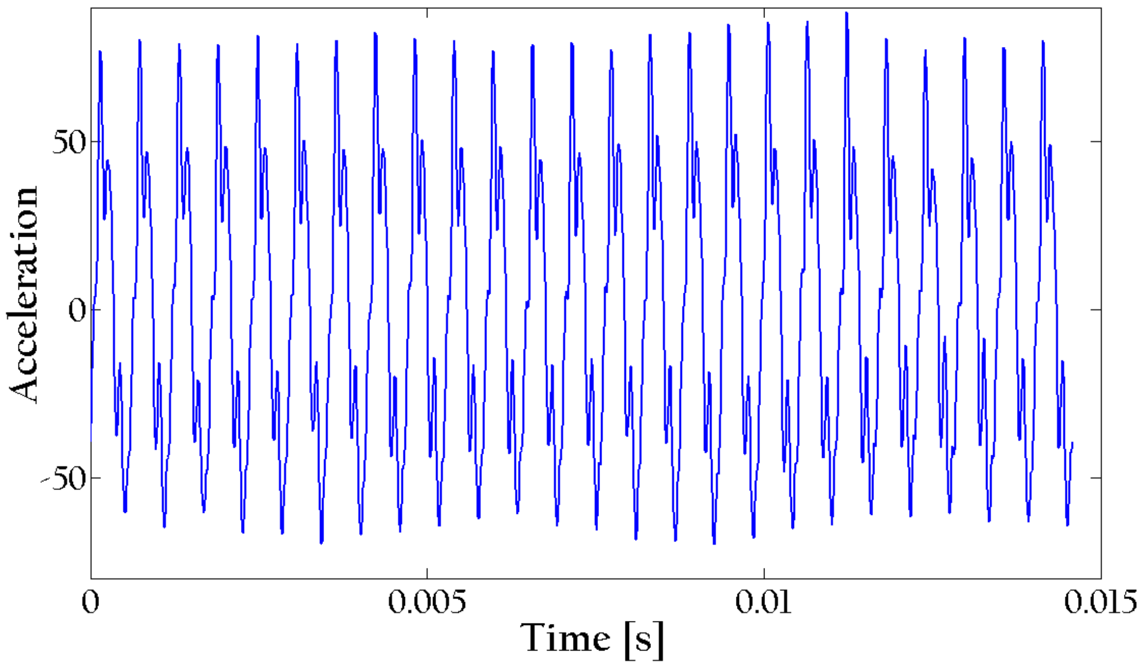

Figure 5.7 TSA signal generated based on 100 once-per-revolution waveforms

5.3 Vibration-based existing CIs

A set of the most widely used vibration-based CIs are outlined in this section. The considered indicators are CI_{RMS}, CI_{CF}, CI_{Ku}, CI_{FM4} and CI_{M6}. All these parameters were already introduced in Section 3.3; however, the explanation of how each CI operates and what features it was designed to detect in a vibration signal is expanded in this section.

5.3.1 CI_{RMS}

CI_{RMS} is based on the Root Mean Square (RMS) parameter values of the vibration response and is defined in Eq. 3.1 Because of the way CI_{RMS} is designed, it is unaffected by isolated peaks in the signal – only a periodic series of high energy events will cause an increase in the overall level of vibration, leading to an increase in the value of CI_{RMS}. As a result, this parameter is not sensitive to an incipient gear tooth failure and starts indicating a fault only after the tooth damage exceed a certain level of severity. Essentially, the value of the CI_{RMS} is a very good descriptor of the overall energy of vibrations generated by the tested gearbox. Its disadvantage, however, is that this parameter is sensitive to load changes within the gearbox. The main usage of this parameter is to monitor the overall vibration level and it should ideally be used in conjunction with other, load independent parameters [53].

5.3.2 CI_{CF}

CI_{CF} is based on the Crest Factor parameter and is defined in Eq. 3.3. CI_{CF} was designed to detect early impulses appearing in the signal, which could indicate an incipient gear fault. As the gear tooth condition deteriorates shortly after developing a fault, the impulsive content within the signal increases, boosting the value of the indicator's nominator. At the same time, the energy within the impulses is sufficient to cause significant changes in the values of CI_{RMS}. This causes the CI_{CF} value to increase. However, as the damage progress the value of CI_{RMS} increases more rapidly than the maximum absolute amplitude present in the signal, which causes the overall CI_{CF} value to decrease. CI_{CF} might therefore be useful in indicating early stages of a gear fault development but as the severity of the fault progress, the CI_{CF} values are likely to decrease [191].

5.3.3 CI_{Ku}

CI_{Ku} is based on the values of the kurtosis parameter and is defined in Eq. 3.4. CI_{Ku} was designed to react to changes in the shape of the signal's amplitude distribution. When the vibration signal contains events which are impulsive in nature, the tails of its amplitude distribution become wider. This makes the overall shape of the amplitude distribution appear sharper, leading to higher kurtosis values [53]. The disadvantage of kurtosis lies in the fact that as the gear fault develops from being localised to more distributed, the variance of the signal (the denominator in kurtosis formula) increases significantly. This in turn causes the kurtosis to decrease in value sometimes below its nominal level.

5.3.4 CI_{FM4}

CI_{FM4} is defined as CI_{Ku} applied to the residual signal. Use of the residual signal, already mentioned in Chapter 3, can be explained as follows. Consider a gearbox with a healthy pair of gears. It is assumed that such a set up would always contain some unavoidable imperfections like slight misalignment or imbalance of the shafts. In such an arrangement the only components present in the spectrum of the vibration signal produced by the gearbox would be frequencies related to the shaft speed, the meshing of the gears and sometimes their harmonic frequencies (Figure 5.8). As a gear tooth fault develops, short duration impacts modulate the vibration signal, which manifests itself in the form of shaft speed sidebands that appear around the GMF and its harmonics (Figure 5.9). This, in turn, changes signal's amplitude distribution [50, 192]. The spacing of the sidebands is equal to the relevant shaft rotation frequency – drive or driven - depending on which shaft the faulty gear is located (Figure 5.10).

Despite this phenomenon being a clear indicator of the gear fault, CI_{Ku} may not respond to it immediately, due to the much stronger GMF and its harmonics which mask the impulsive content of the signal. The development of the CI_{FM4} was based upon this observation. Stewart [30] suggested removing the known spectrum components - that is the GMF and its harmonics together with the shaft rotation frequency and its harmonics - from the original vibration signal, thereby therefore creating a residual signal (Figure 5.11). The advantage of creating the residual signal is that it will only contain information related to gear tooth fault should one occur, [193] hence the kurtosis derived from the residual signal (that is the FM4) is expected to be much more sensitive to the signatures of incipient gear faults than that applied to the raw vibration signal.

Creation of the residual signal in this work was performed manually in the frequency domain. The samples corresponding to the frequencies of interest were removed by setting all the points that comprise a given frequency component equal to the level of the background noise. A visual inspection was then carried out to make sure that no artefacts are left after this filtering process. Although less convenient, this approach was chosen over the use of the digital filters in order to obtain more precise results. An idealised case showing the spectra of raw and residual signals is shown in Figure 5.12.

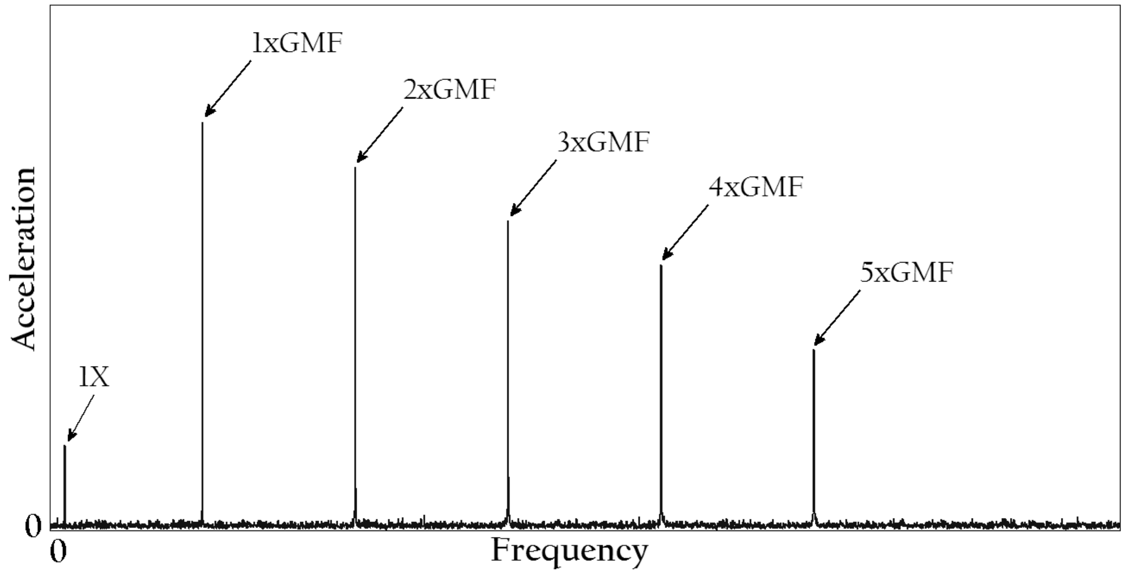

Figure 5.8 Idealised spectrum of a gearbox in healthy condition

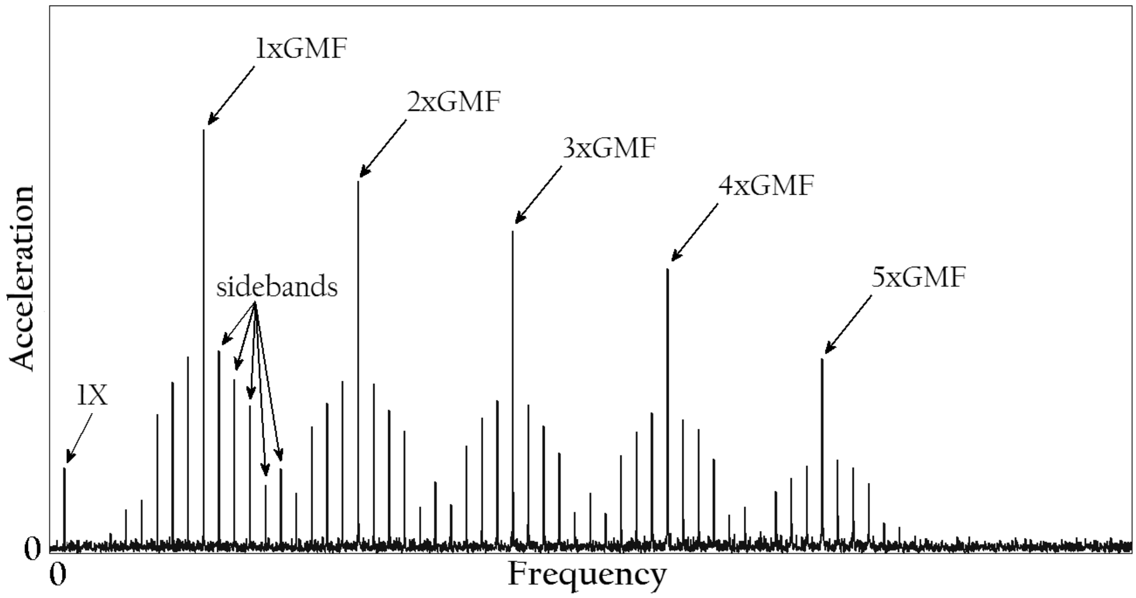

Figure 5.9 Idealised spectrum of a faulty gearbox

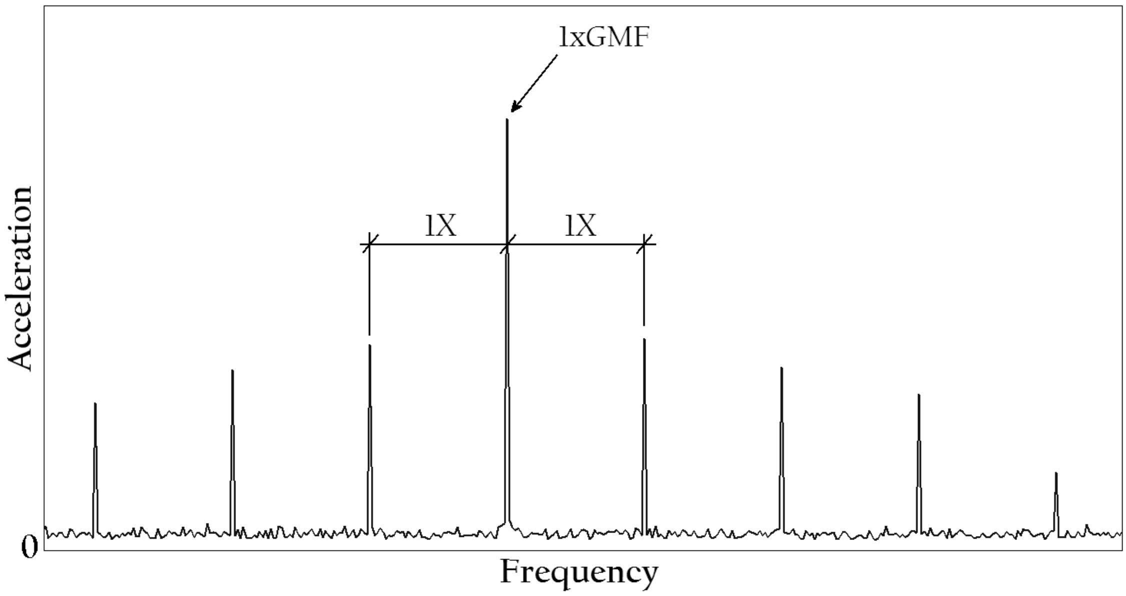

Figure 5.10 Magnified view of Figure 5.9

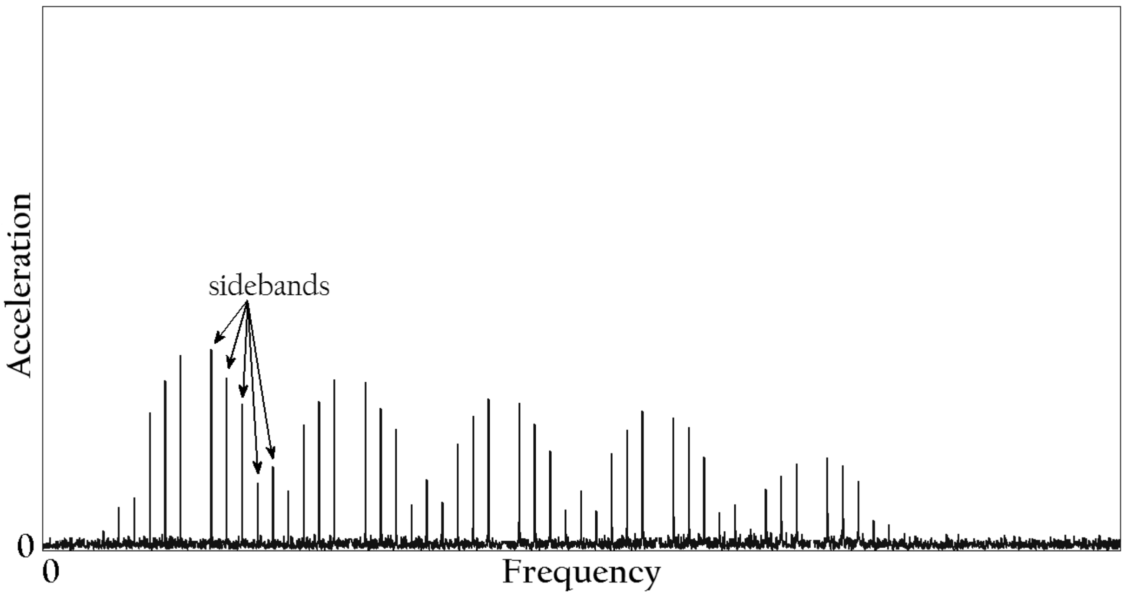

Figure 5.11 Idealised spectrum of a residual signal generated from a faulty gearbox

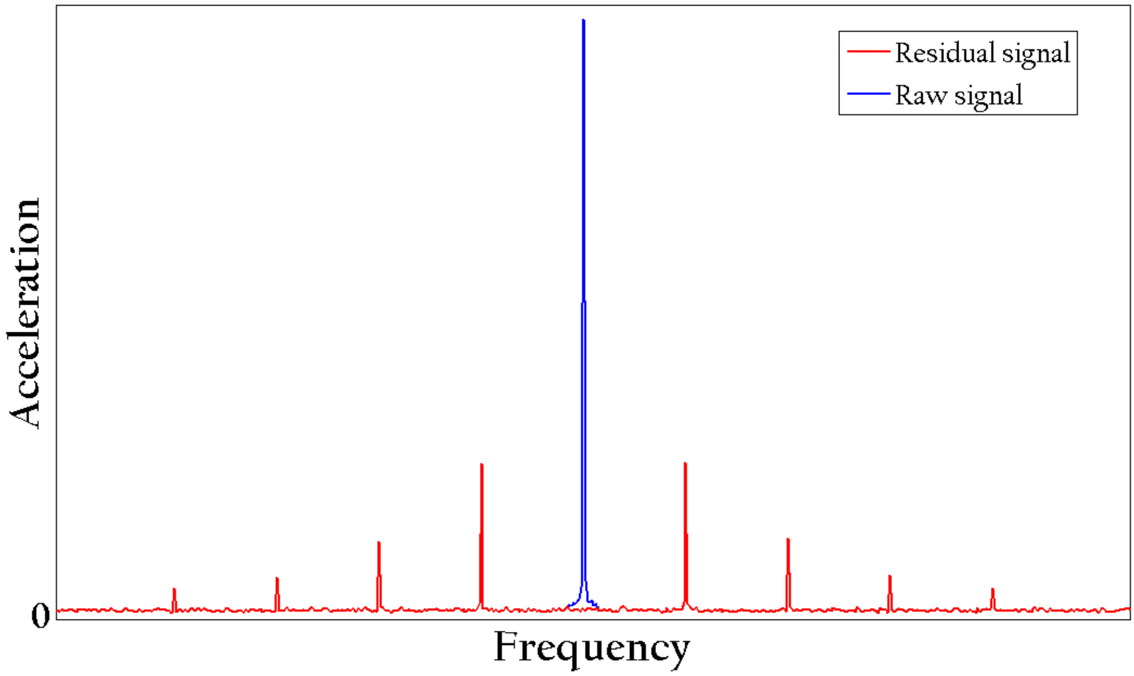

Figure 5.12 Magnified spectra from Figures 5.9 and 5.11 showing raw and residual signal

5.3.5 CI_{M6}

CI_{M6} is defined by the M6 parameter and is the sixth centralised moment of the signal, normalised by the cube of the signal's variance as in Eq. 3.7. Since it is based on the same principle as kurtosis it carries the same properties, however, due to it being a higher statistical moment than kurtosis, it is expected to be even more sensitive to peaks in the signal (as mentioned in Section 3.3).

5.4 CIs default values

In order to determine the default values of the CIs under consideration when applied to a healthy gearbox, the parameters were applied to two random simulated test signals: a 20Hz sinusoid (Signal 1) and a normally distributed random signal with the mean value of 0 and the standard deviation of 0.3271. Signal 2 is shown in Figure 5.13) The first test signal represents the ideal situation of two healthy meshing gears without the influence of any other components of the gearbox. The resultant vibration is simulated by a pure sinusoid, since a nominally perfect gear exhibits a sinusoidal waveform in the time domain, with a dominant peak in the spectrum at the gear mesh frequency [33]. However, in majority of cases such ideal isolation of gear mesh vibration does not occur, as many other gearbox elements affect the frequency content of the signal. These can be caused by imperfect gearbox assembly, slight misalignment of the shafts, imbalance (weight not evenly distributed), eccentricity (bow) of the shafts and gears and ambient noise. Hence the second test signal represents a more realistic residual signal generated by a healthy gearbox. It should be noted that CI_{RMS} is included in this investigation for comparison purposes only, since it is a non-normalised parameter (unlike the other CIs) and its values are dependent on the amplitudes of the signal.

Both random signals were derived using standard Matlab functions to give signals sampled at the rate of 1024 samples per second; both are one second long and their amplitude values are normalised to 1. The results of applying CIs to the two test signals are presented in Table 5.1.

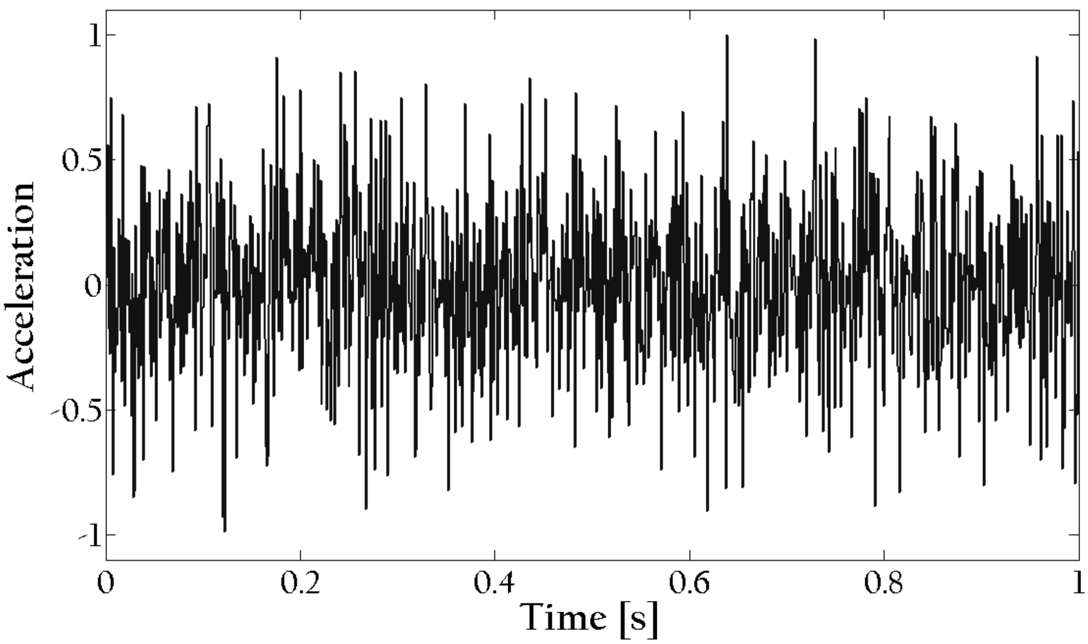

Figure 5.13 Normally distributed simulated test signal

Table 5.1 Values of CIs applied on two test signals

	Signal 1	Signal 2
CI_{RMS}	0.71	1.00
CI_{CF}	1.41	3.73
CI_{Ku}	1.50	2.99
CI_{FM4}	-	2.99
CI_{M6}	2.49	14.39

Table 5.1 shows the expected values of the CIs when applied to a typical gearbox that does not contain a fault. The CI_{FM4} parameter was not applied to Signal 1, as the first step in applying CI_{FM4} entails removing all known sinusoidal content from the signal prior to calculating it. The CI_{FM4} parameter was designed to operate on normally distributed signals and detect deviations from this distribution.

5.5 CIs sensitivity

In order to determine how the advent of an impulsive content within the signal influences the outputs of the CIs, all the considered indicators were applied to three further signals, simulated to represent three different gear health scenarios: no fault, an incipient tooth fault, an advanced tooth fault, as is shown in Table 5.2.

Case 1 represents an idealised signal generated by two healthy meshing gears, Case 2 shows a signal containing signs of a potential tooth fault in its early stages - a localised impulse and Case 3 simulates a severe gear tooth failure represented by a more complex, higher energy event. Comparison of the responses (normalised to the values obtained for case 1) of each CI is graphically presented in Figure 5.14.

CI_{RMS}

The presence of isolated impulses causes a slight increase in the total energy of the signal causing the value of CI_{RMS} to increase. Signal representing an advanced tooth fault contains even more energy causing CI_{RMS} to increase.

CI_{CF}

CI_{CF} reacts quickly to the incipient fault as the peak value of the signal is high, yet CI_{RMS} does not increase dramatically. However, as the fault progresses the increase in the energy content of the signal increases the value of CI_{CF}'s denominator (CI_{RMS}), whlist the value of the numerator (peak value) does not change. This leads to a decrease in CI_{CF}.

CI_{Ku}

CI_{Ku} detects the change between the healthy and the faulty signal, and continues to increase as the fault changes from incipient to more severe.

CI_{M6}

The theory underlying CI_{M6} indicator is the same as the CI_{Ku}, however it was designed to be more sensitive to impulsive content within the signal. As one can see the behaviour of CI_{M6} is similar to CI_{Ku}, however the relative change in the values of CI_{M6} is greater than in the case of CI_{Ku}.

Table 5.2 Typical comparison of CIs values for a 3 types of sinusoidal signals (Cases 1-3)

Case 1 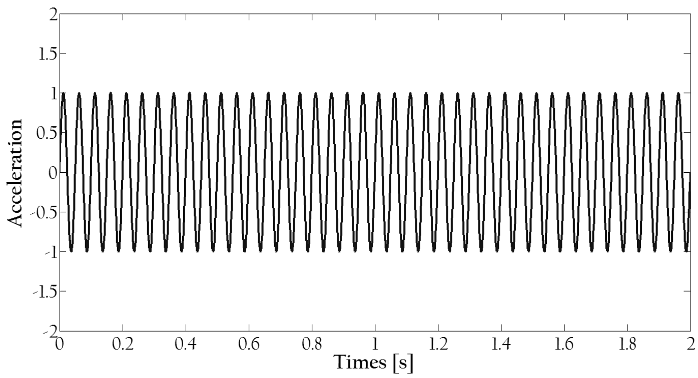	0.71	CI_{RMS}
	1.41	CI_{CF}
	1.50	CI_{Ku}
	2.49	CI_{M6}
Case 2 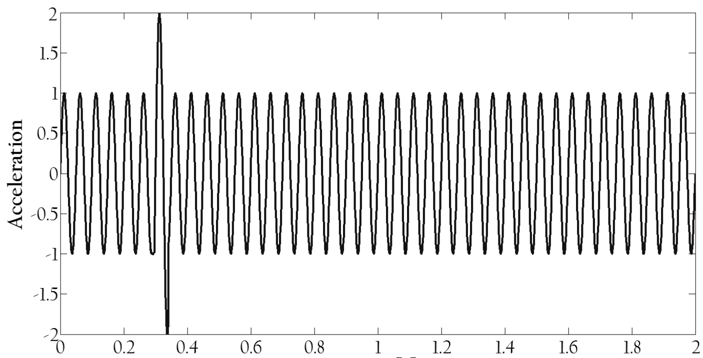	0.74	CI_{RMS}
	2.73	CI_{CF}
	1.77	CI_{Ku}
	5.12	CI_{M6}
Case 3 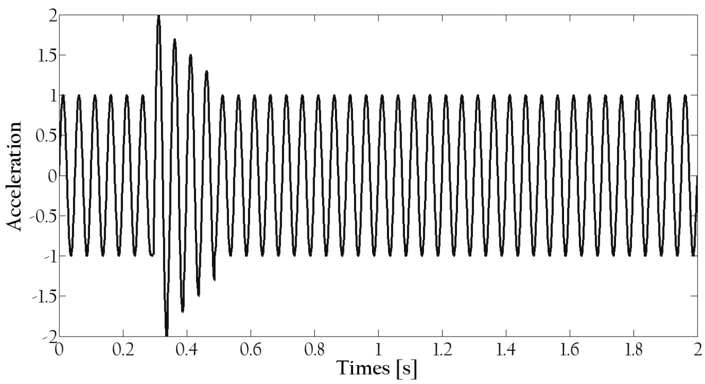	0.76	CI_{RMS}
	2.62	CI_{CF}
	1.85	CI_{Ku}
	5.40	CI_{M6}

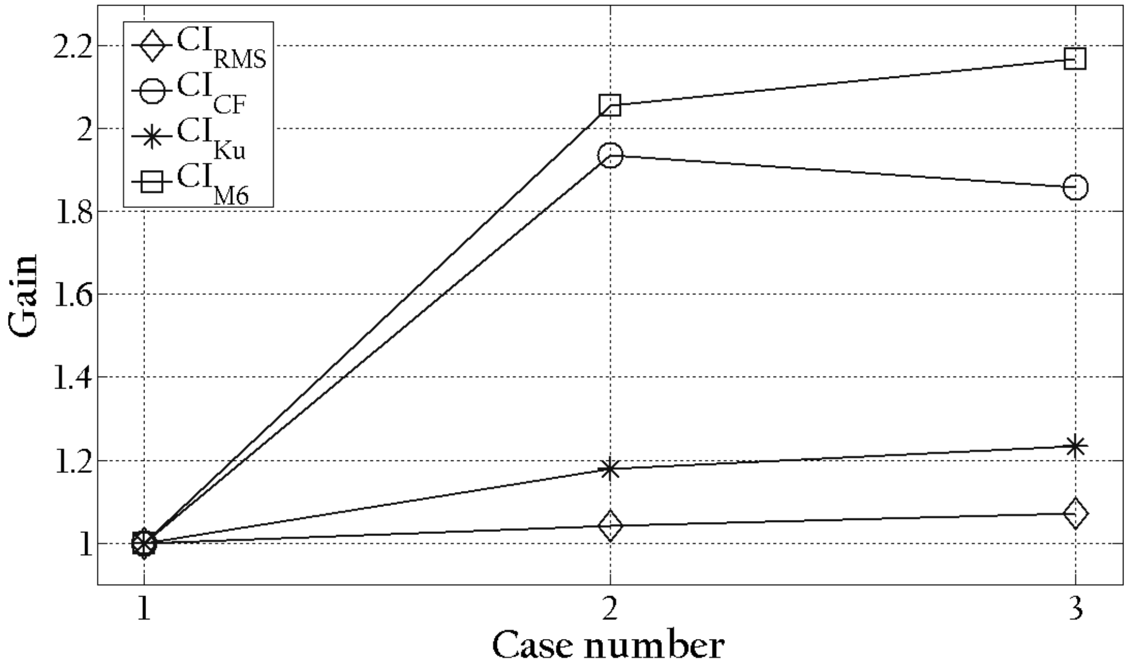

Figure 5.14 Gain of CIs values when applied on test signals from Table **5.2**

5.5.1 CIs sensitivity for geared system

The comparison made in section 5.5 is helpful in understanding the way each parameter reacts to the advent of impulsive content within the sinusoidal signal. However a vibration signal of this shape is very unlikely to appear in field applications due to the high number of additional vibration sources adding to the base frequency components. For this reason the same sensitivity test was carried out on the vibration signals that were shown (in the frequency domain) in Figures 5.8, 5.9 and 5.11. This set of three signals is complemented by a fourth signal, created by removing the GMF and shaft related frequencies from Figure 5.8, thus creating a residual signal from a gearbox in healthy condition presented in Figure 5.13. To avoid confusion with signals from the previous test, signals in this test are referred to as 'Healthy', 'Faulty', 'Residual Faulty' and 'Residual Healthy' respectively. These are shown in the time domain in Figure 5.15 - Figure 5.18. The result of comparison of these signals is presented in two tables. Table 5.3 shows the outcome of applying CI_{CF}, CI_{Ku} and CI_{M6} on the Healthy and Faulty signals. CI_{RMS} has not been included in this comparison, since its outcome is not normalised in any way, making it heavily case dependent (which is not the case for the remaining CIs).

In addition to showing the results of applying CI_{FM4} to Residual Healthy and Residual Faulty signals, Table 5.4 also presents the results of a novel[*] attempt to apply CI_{CF} and CI_{M6} to residual signals.

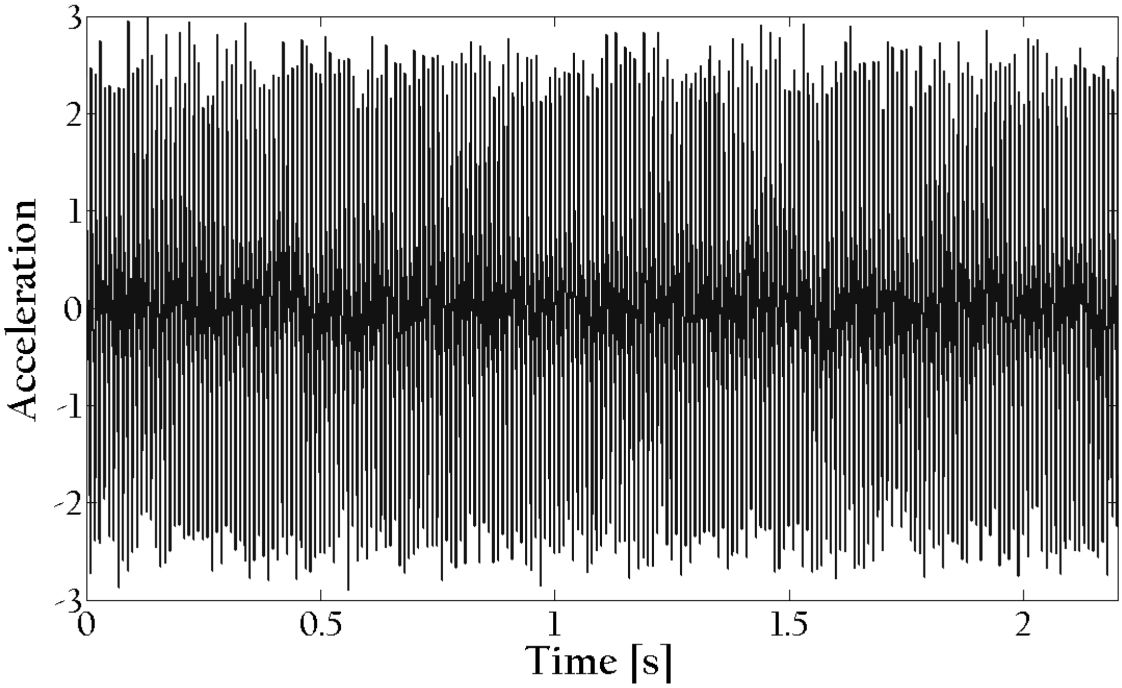

Figure 5.15 Idealised raw vibration signal of a gearbox in healthy condition – 'Healthy'

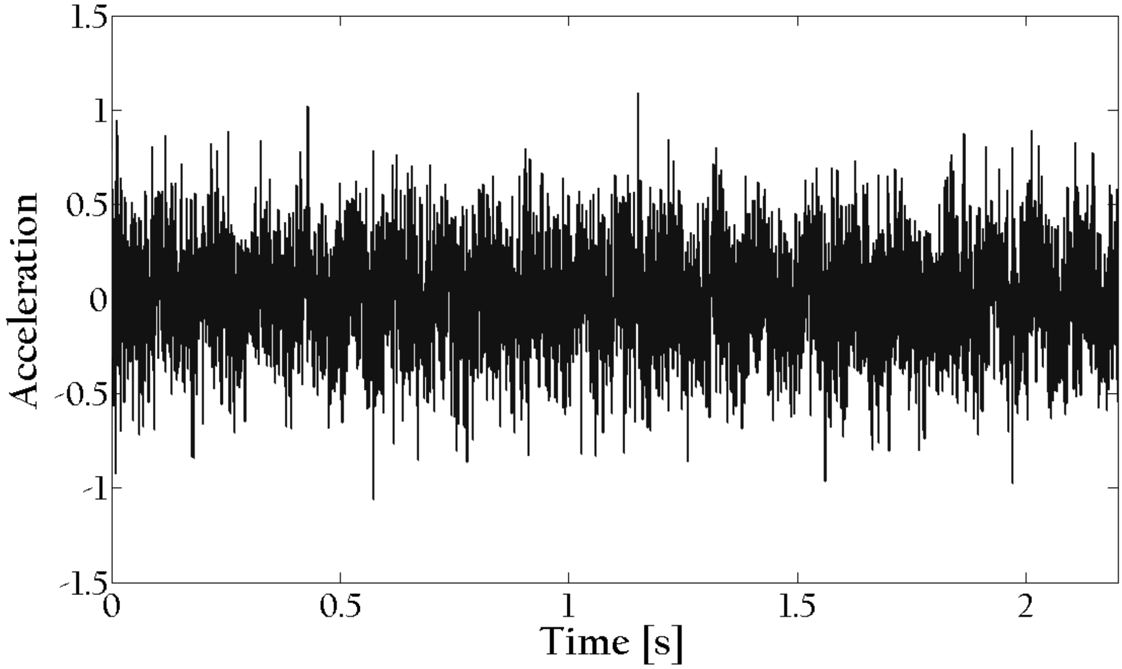

Figure 5.16 Idealised residual vibration signal of a gearbox in healthy condition – 'Residual Healthy'

[*] as far as can be established based on the literature that is available in the public domain

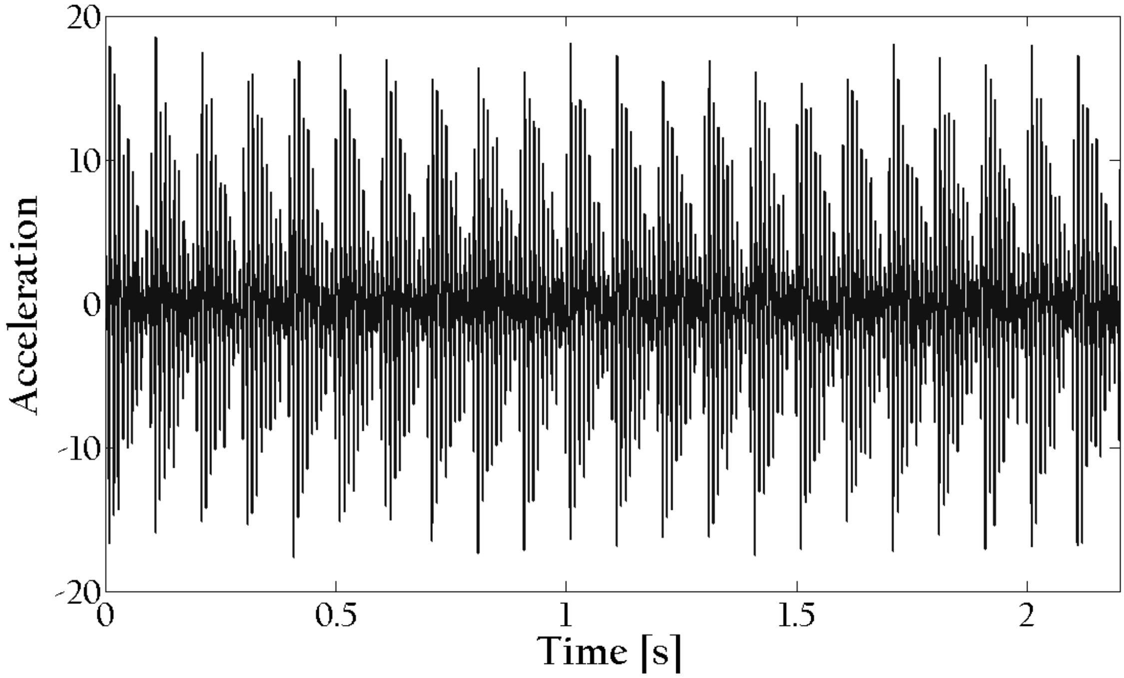

Figure 5.17 Idealised raw vibration signal of a faulty gearbox – 'Faulty'

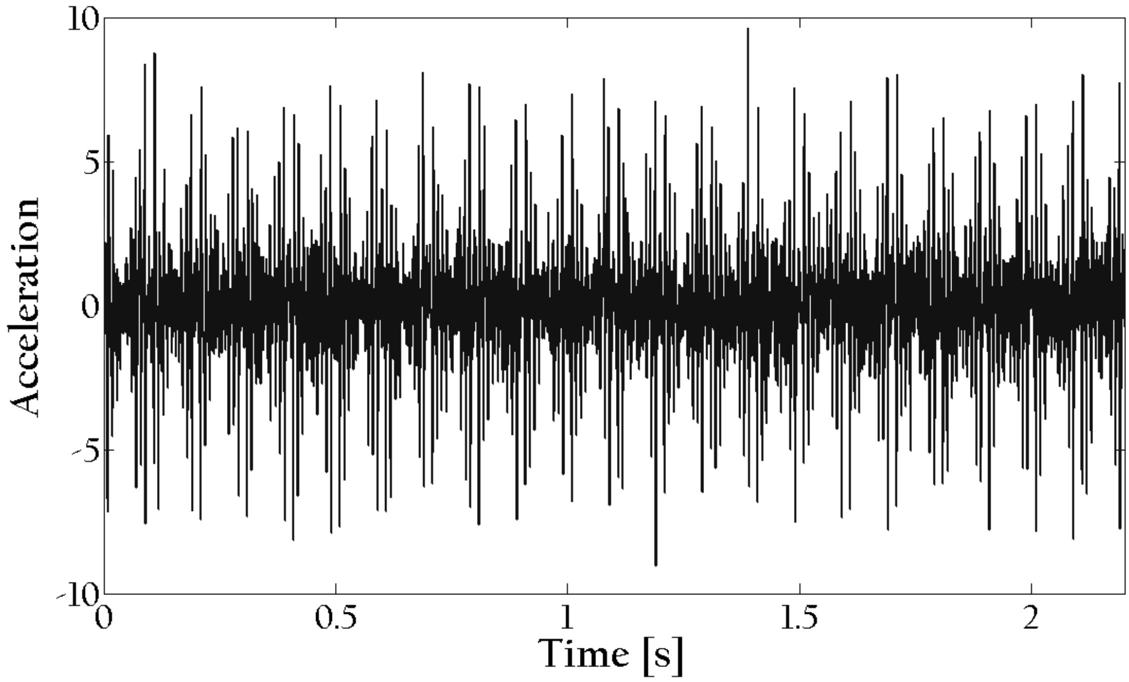

Figure 5.18 Idealised residual vibration signal of a faulty gearbox – 'Residual Faulty'

Table 5.3 Typical comparison of different CIs for Healthy and Faulty signal

	CI_{CF}	CI_{Ku}	CI_{M6}
Healthy	2.37	3.83	17.70
Faulty	3.73	5.80	49.09
Gain	1.57	1.51	2.77

Table 5.4 Typical comparison of different CIs for Residual Healthy and Residual Faulty signal

	CI_{CF}	CI_{FM4}	CI_{M6}
Residual Healthy	3.89	2.99	15.29
Residual Faulty	4.49	8.11	95.05
Gain	1.15	2.71	6.21

The results Table 5.3 show that all three CIs react to the change in gearbox condition with CI_{CF} showing a smaller gain than CI_{Ku} and CI_{M6}. There is a large difference in the gain values between the 4^{th} and 6^{th} signal statistical moments, with the later indicator being 46% more sensitive to the change in gearbox condition. This coincides with the theory, as CI_{M6} was specifically designed to be more sensitive than CI_{Ku} (as explained in section 5.3.5). Comparison of the results presented in Table 5.3 and Table 5.4 clearly indicate that CI_{CF} has smaller gain in the case of the residual signal, whlist the gain of both CI_{Ku} and CI_{M6} have been significantly bigger when compared to the results presented in Table 5.3.

5.6 Summary

After a description of the Health and Usage Monitoring System principles, the concept of the Time Synchronous Averaging technique was presented. This was followed by an introduction of four of the most popular vibration-based Condition Indicators. Defining the parameters by means of mathematical formulae, an explanation of the way in which each CI operates was followed by a derivation of the default parameter values when applied to a vibration signal generated by a healthy pair of gears and examination of their sensitivity to changes within the signal. The sensitivity test showed that CI_{CF} has the smallest value of the gain when detecting a fault compared to CI_{Ku} and CI_{M6}. However, it was also observed that CI_{CF} gave better results when applied to raw data rather than the residual signal whilst the latter signal gave better results for both CI_{Ku}

and CI_{M6}. The novel idea of applying these parameters (apart from CI_{Ku}) on the residual signal led to the generation of some interesting results, discussed in the next chapter, which includes testing the behaviour of CIs on different datasets. This will include examination of each indicator's performance on both: raw and residual signals.

CHAPTER 6

OBSERVATIONS ON EXISTING CIs

This chapter contains a detailed discussion of the results obtained by applying the selected CIs to the available datasets. In order to assess the robustness of the existing CIs described in Chapter 5, all the parameters are applied to the three different, not correlated datasets detailed in Chapter 4. Presentation of the results generated by the CIs is followed by a comparative study assessing the difference in behaviour between the existing CIs in their typical applications (raw TSA signal) against the same CIs, but applied on the residual TSA signal. The results of the comparison for each CI are shown on a single plot for easier analysis. In the case of the bearing fault dataset, the parameters are applied to band-pass filtered vibration signals, as explained in Chapter 4.

6.1 Performance of the existing CIs

6.1.1 CI_{RMS}

Dataset 1

As one can see from Figure 6.1, the mean value of CI_{RMS} stays at a constant level until sample 25, after which the CI values jump suddenly (after the first manual inspection). The output of the parameter does not change radically until sample 45 (the second manual inspection), where it decreases suddenly and continues to decrease until sample 74 (fourth inspection). After that the value jumps up again and presents both rising and falling trends just before the gear detachment took place. Based on the above a conclusion can be made that CI_{RMS} fails to present a meaningful trend indiacting the gear fault progress.

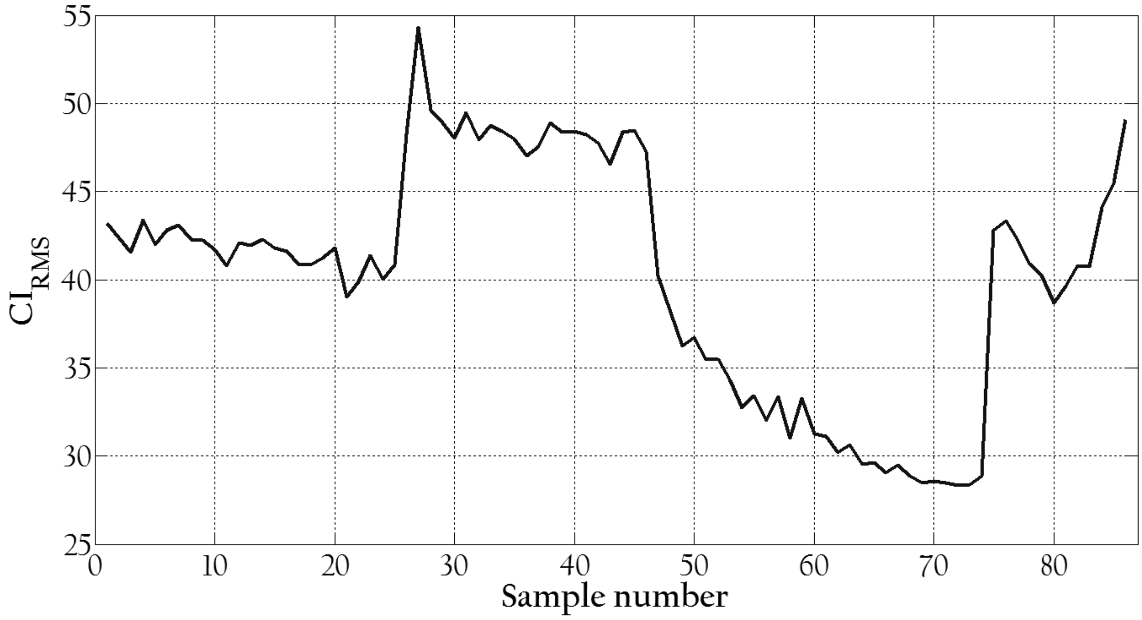

Figure 6.1 Variation of CI_{RMS} for Dataset 1

Dataset 2

The mean value remains approximately constant until sample 10, after which the CI_{RMS} value rises substantially. This increase in the values might be due to the reported deterioration of the gear face condition, which could have led to generatation of some high energy events within the vibration signal exciting the CI_{RMS} output.

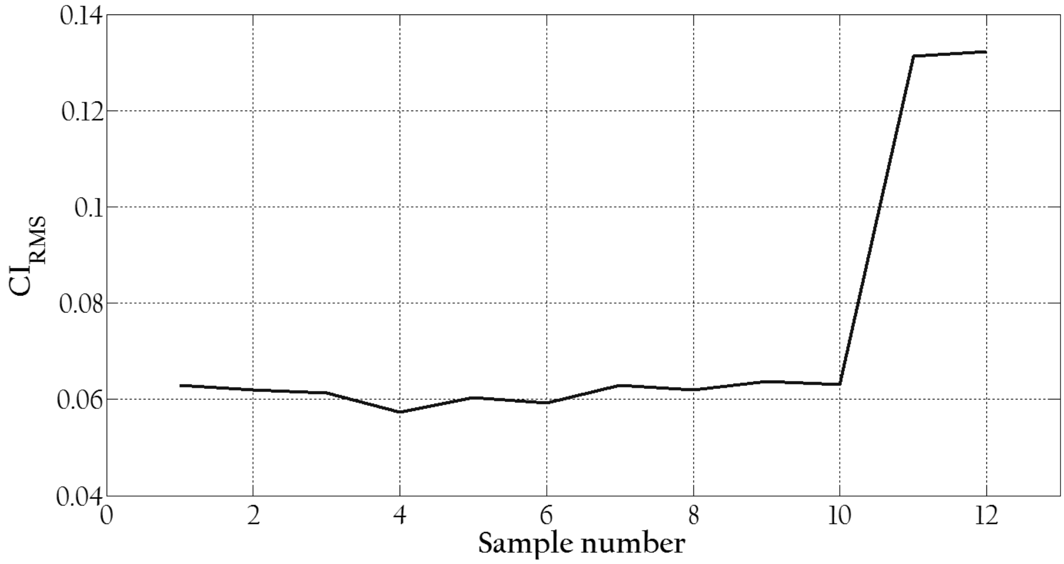

Figure 6.2 Variation of CI_{RMS} for Dataset 2

Dataset 3

The general trend of vibration in the gearbox measured with CI_{RMS} is rising slightly throughout the test. These increasing values for the whole duration of the test could be caused by a slow deterioration of the bearing condition. This theory is supported by the results of a comparison of the level of the BPFO related peaks in the filtered region of the spectra for the first and the last sample in the dataset (Figures 6.4 and 6.5 respectively). The later contains more energy in the fault specific features. The difference is not great, which is consistent with the slight CI_{RMS} increase.

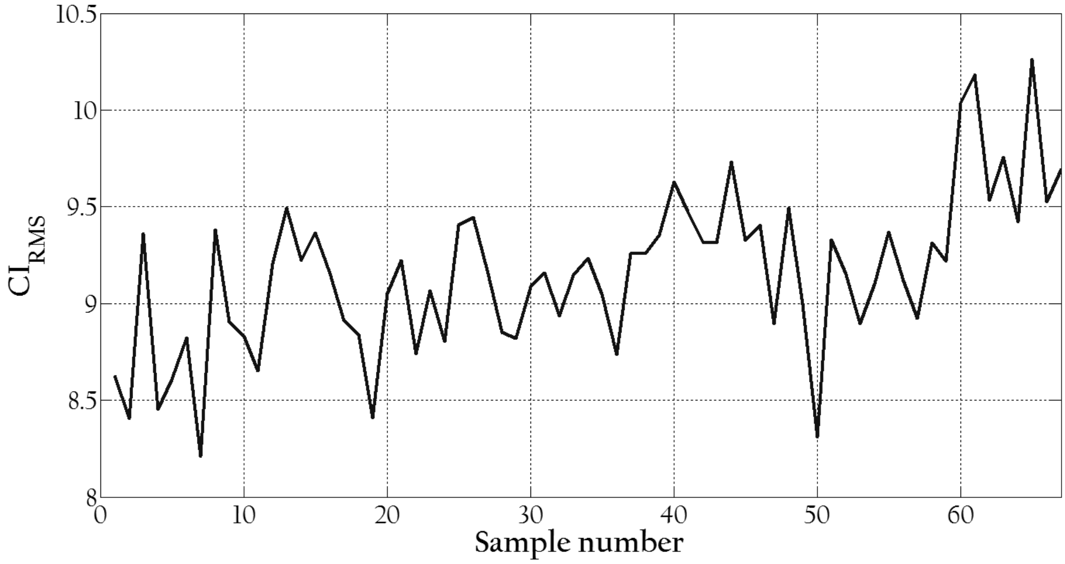

Figure 6.3 Variation of CI_{RMS} for Dataset 3

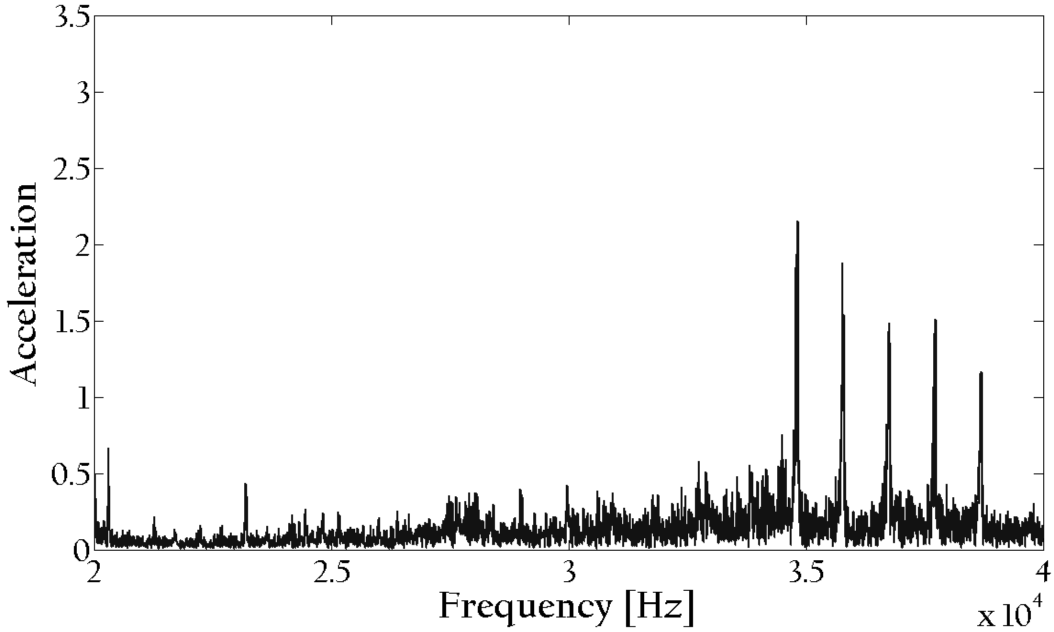

Figure 6.4 Spectrum of sample 1 filtered in the [20 - 40] kHz band

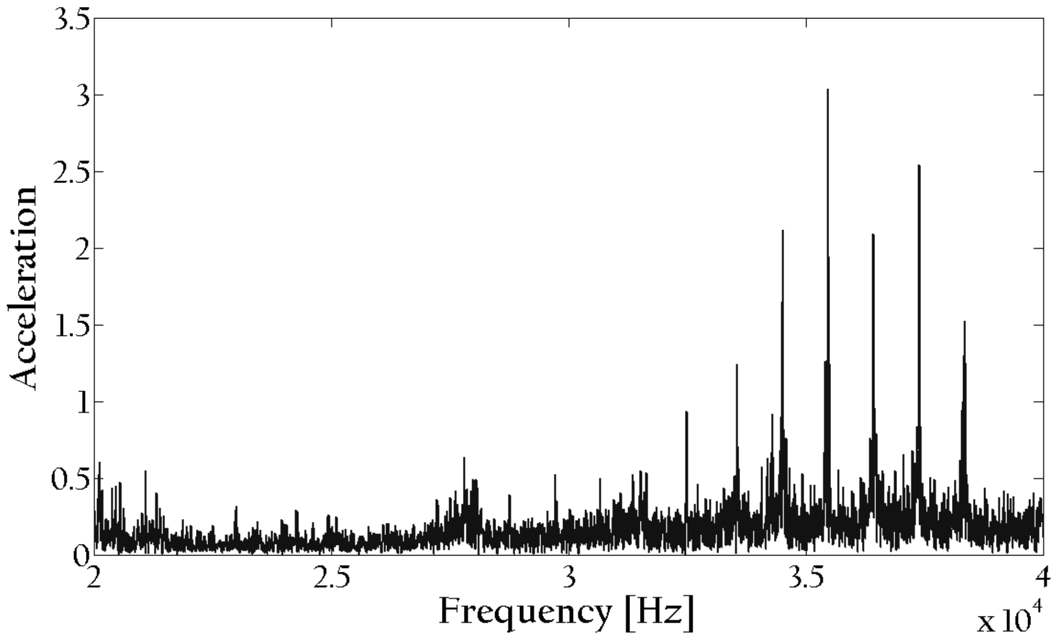

Figure 6.5 Spectrum of sample 67 filtered in the [20 - 40] kHz band

6.1.2 CI_{CF}

Dataset 1

CI_{CF} from Figure 6.6 presents a slowly rising trend that begins at sample 25 and increases until sample 65. However, after that point values of CI_{CF} decrease suddenly and do not start rising until after the fourth manual inspection is carried out.

As outlined in Chapter 5, the performance of CI_{CF} is governed by the ratio of the signal's peak value to signal's CI_{RMS} value. In the early stages of fault initiation the parameter reacts quickly to the appearance of some isolated impulses within the signal. However as the fault progress (impulses are replaced by more complex, high energy events), causing the CI_{CF} values to decrease. As the fault develops it starts to interact with adjacent teeth increasing the overall vibration level, hence heavily increasing the denominator in CI_{CF} formula. It explains the decrease in the parameter output towards the end of the test.

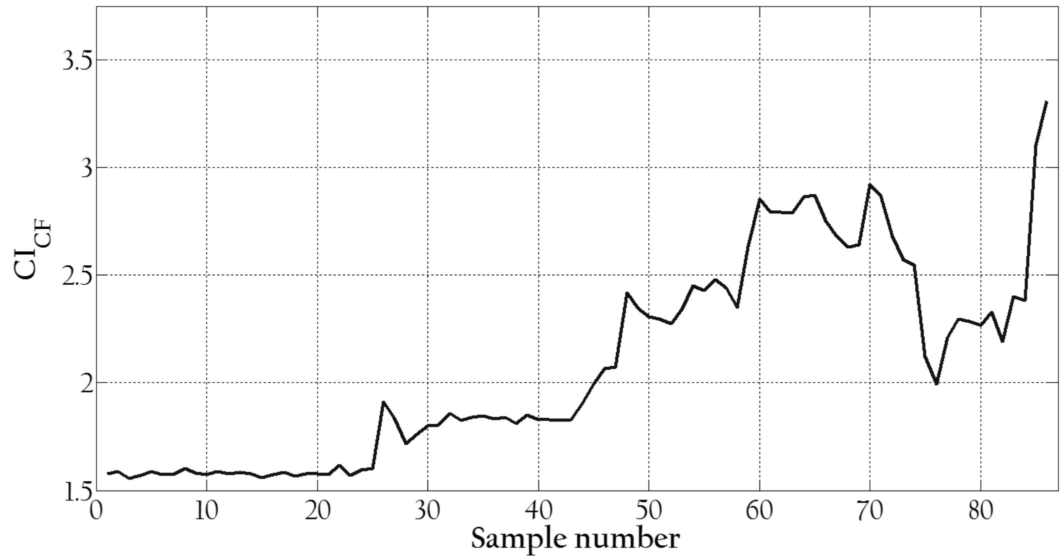

Figure 6.6 Variation of CI_{CF} for Dataset 1

Dataset 2

The output of CI_{CF} oscillates about a constant mean value until sample 9 where an increase is observed. This point is followed by oscillation about a generally rising trend, indicating significant enhancement of impulsive content within the signal.

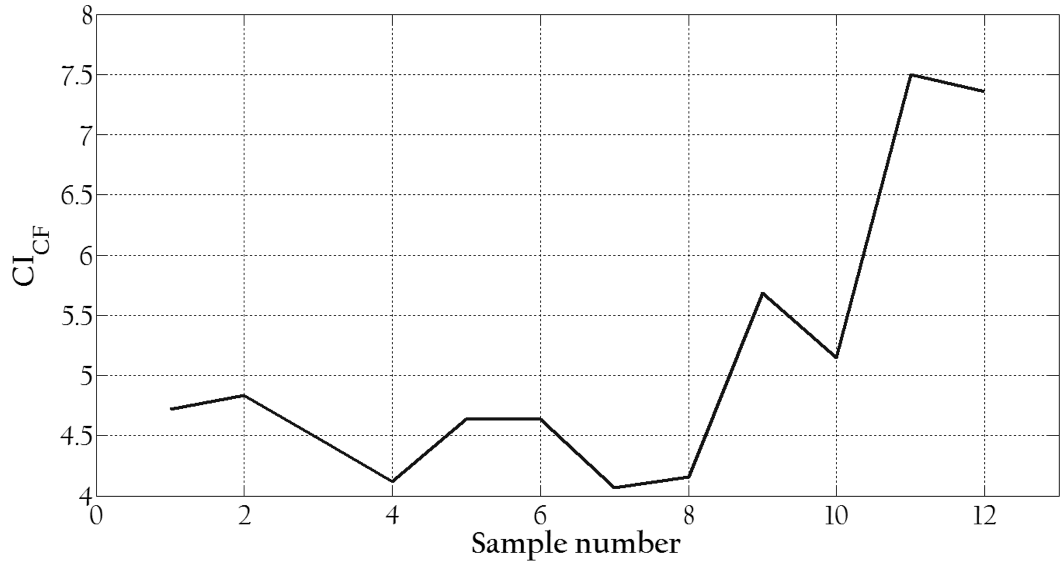

Figure 6.7 Variation of CI_{CF} for Dataset 2

Dataset 3

The CI_{CF} mean value remains constant until sample 59 when a sudden increase is observed. This event could have been driven by deterioration of the bearing outer race condition, which, in turn, would have resulted in isolated peaks being generated during the contact between the rolling element and the damaged outer race surface. The CI_{CF} reached its maximum value at sample 61 after which it generally decreases. This could have been caused by an increase in the energy of the generated events within the signal which, after crossing a certain level, is known to cause the CI_{CF} values to decrease.

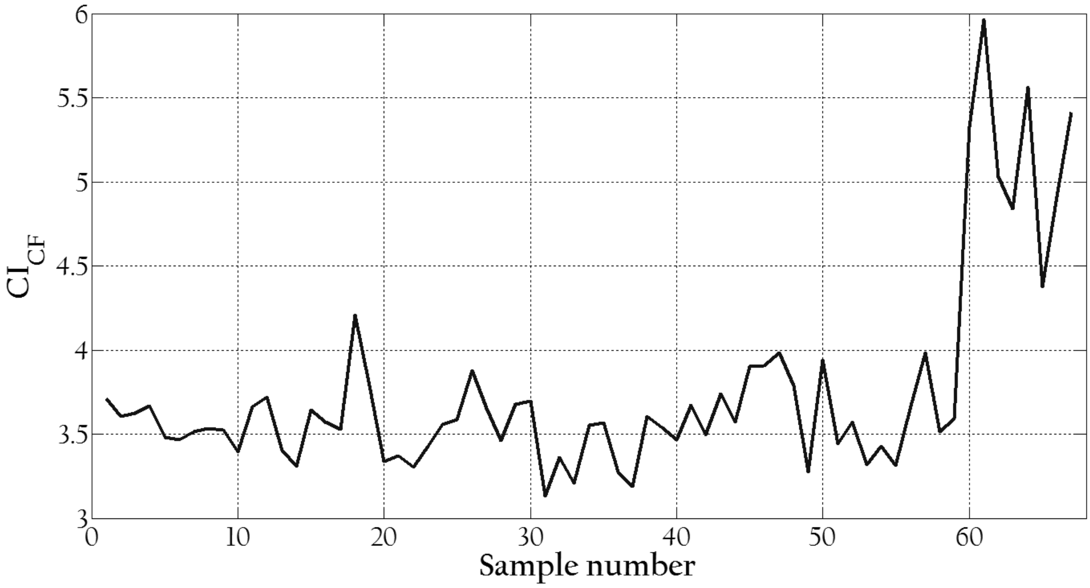

Figure 6.8 Variation of CI_{CF} for Dataset 3

6.1.3 CI_{Ku}

Dataset 1

CI_{Ku} presents a slowly rising trend however the values start to increase late into the test - at sample 46. In addition, the trend is rising only until sample 75 when a significant decrease in the values is seen. This is followed by incerasing trend until sample 84. Only the last three samples in the Dataset cause the CI_{Ku} to indicate a major fault by a large increase in the value.

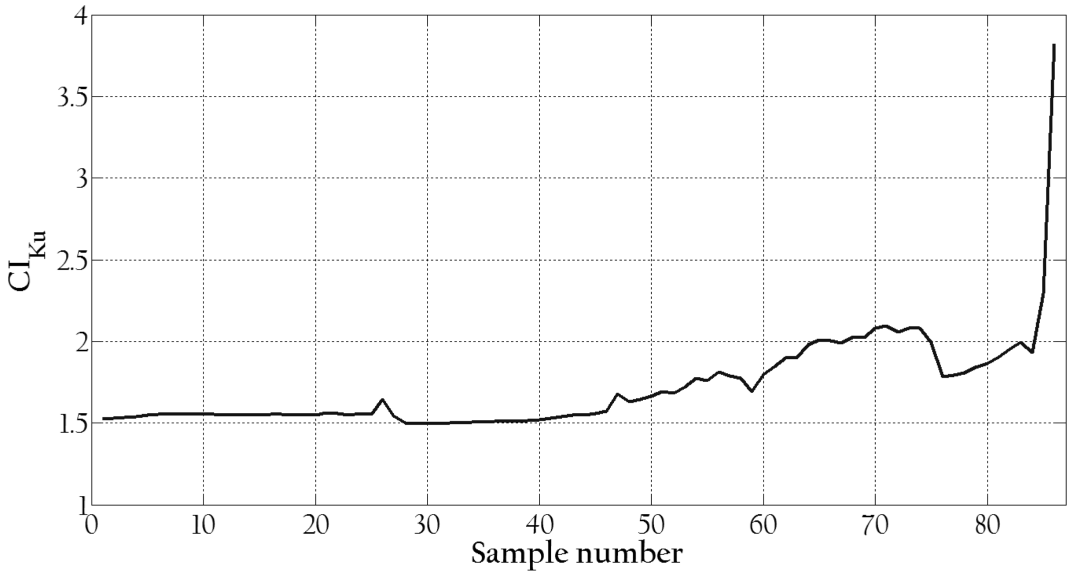

Figure 6.9 Variation of CI_{Ku} for Dataset 1

Dataset 2

The mean value of CI_{Ku} applied on Dataset 2 remains constant until sample 10 after which the parameter values increase substantally. This behaviour is very similar to that of the previously discussed CIs applied on the same dataset.

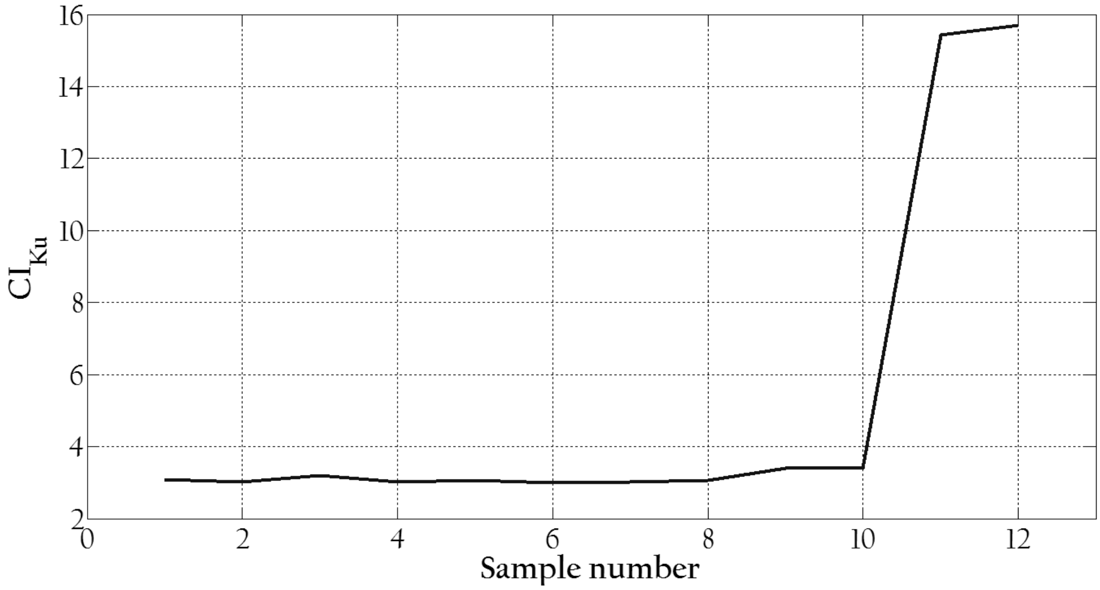

Figure 6.10 Variation of CI_{Ku} for Dataset 2

Dataset 3

The mean value of CI_{Ku}, similar to CI_{CF}, remains constant until sample 59 when a sharp increase is seen. This event could have been caused by an increase in the impulsive content of the signal due to deterioration of the bearing outer race condition. This in turn would have led to widening of the signal amplitude distribution tails making the main part of the distribution appear more sharp. CI_{CF} reached its maximum value at sample 61 after which it decreased slightly, but this decrease does not occur in the case of CI_{Ku}.

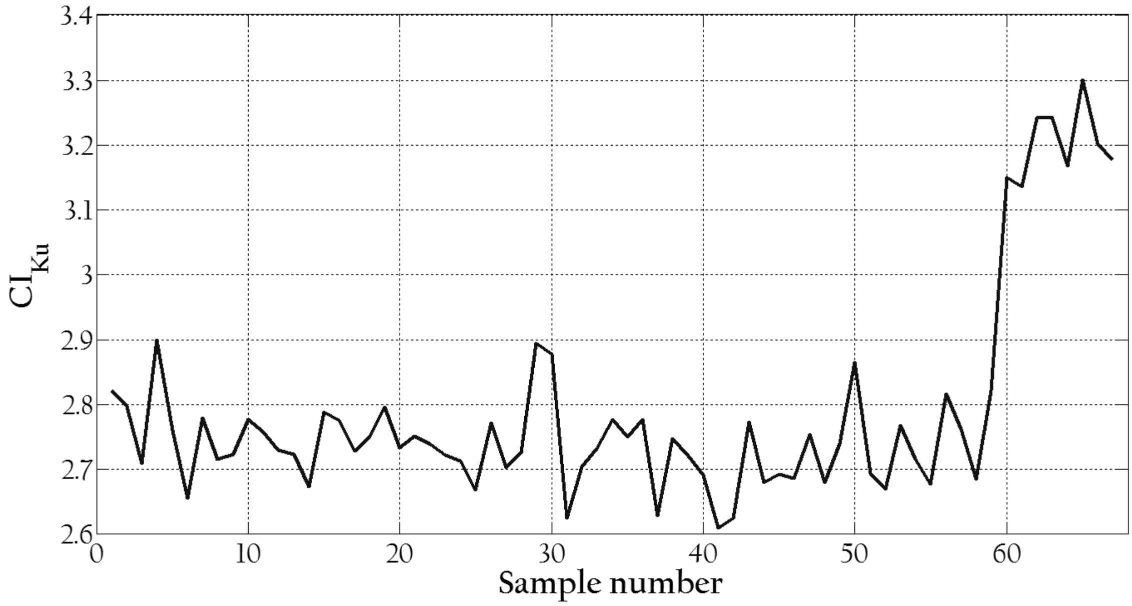

Figure 6.11 Variation of CI_{Ku} for Dataset 3

6.1.4 CI_{M6}

Dataset 1

The behaviour of the CI_{M6} parameter is very similar to that of CI_{Ku}. CI_{M6} presents a constant, slowly rising trend which begins in the late stages of the test **-** sample 46. The trend rises only until sample 75 when a decrease occurs. This event is followed again by a similar increasing trend until the last three samples in the dataset when CI_{M6} indicates a major fault. However, this indication appears too late for a robust gear condition indicator.

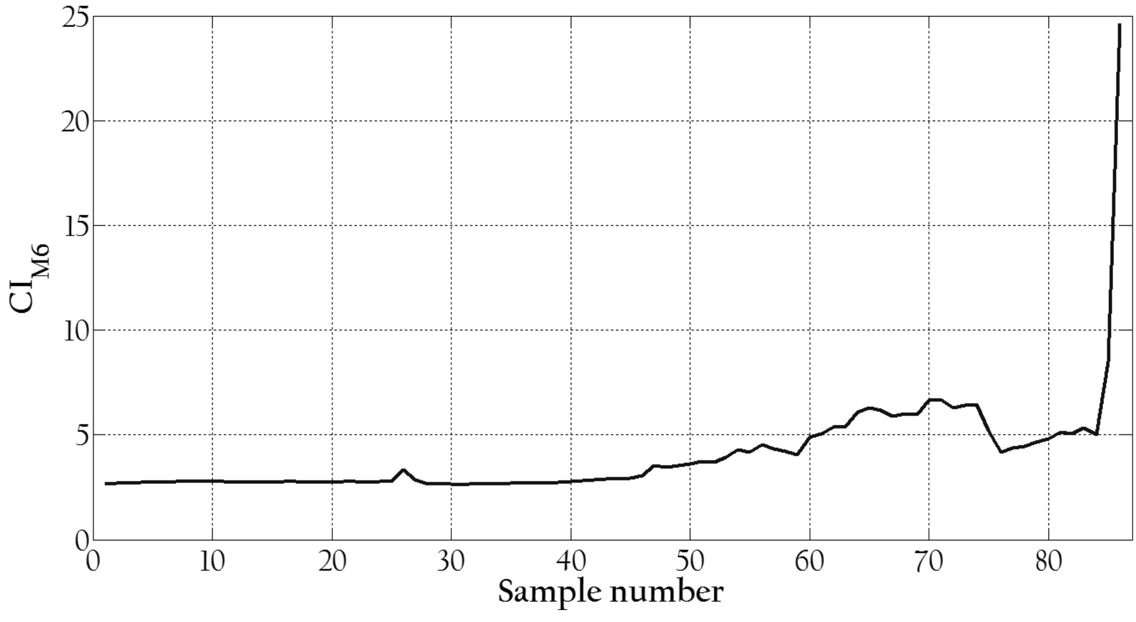

Figure 6.12 Variation of CI_{M6} for Dataset 1

Dataset 2

The behaviour of CI_{M6} is identical to CI_{Ku}. The mean value remains constant until sample 10 when the CI_{M6} values increase substantialy.

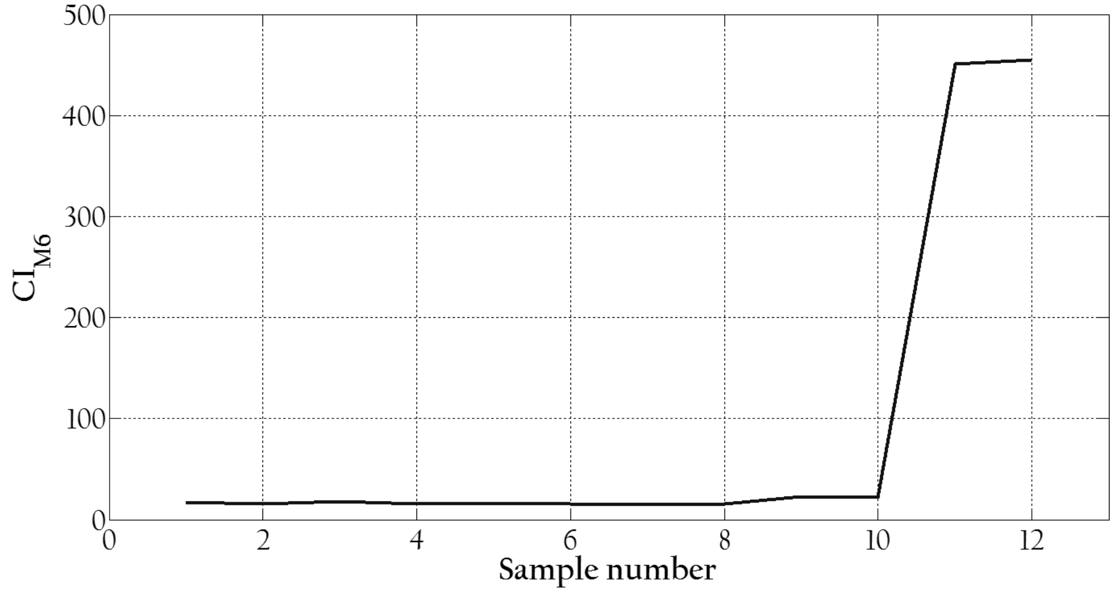

Figure 6.13 Variation of CI_{M6} for Dataset 2

Dataset 3

When applied to the dataset that contained the bearing fault, CI_{M6} behaves in the same way as CI_{Ku} but, because of the way it has been designed, it is more sensitive to the impulsive content within the signal. This means that the difference between the 'healthy' and 'faulty' bearing state is more clearly defined and easier to interpret for a vibration non-specialist.

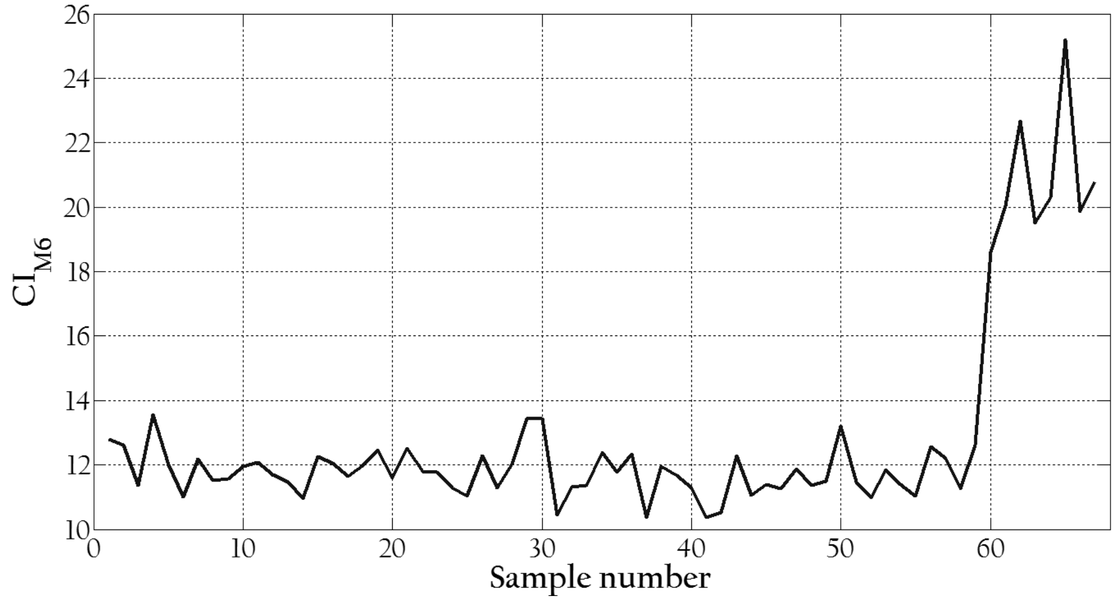

Figure 6.14 Variation of CI_{M6} for Dataset 3

6.2 Modification in the existing CIs

Following the encouraging result of applying CI_{M6} to the simulated residual signal in the previous chapter, an innovative attempt is made to test all the existing CIs on the residual vibration signals as opposed to their typical utilisation on raw vibration signals. The CIs are tested on Datasets 1 and 2, since only they contain a history of a gear fault development. Dataset 3 is band-pass filtered in the high frequency band where the GMF harmonics are at the level of the background noise, so the creation of a residual signal would not have any influence on the results. The results of the comparison are outlined in the following sections.

6.2.1 CI_{RMS}

Dataset 1

Significant increase in the values begins at sample 26 (corresponding with the first response point of the raw signal) and continues until the end of the test, with notable increase in the values after the fourth inspection at sample 74(Figure 6.15). The difference in behaviour between the two implementations of the CI is that CI_{RMS} reacts to any changes in the vibration signal that are not necessarily fault related. However, creation of the residual signal removes the known frequency components (related to gear mesh and shaft rotation) limiting their, otherwise heavy, influence on the overall vibration level of the gearbox. In theory the overall vibration level of the residual signal is driven only by transients that appear in the signal such as for example when a gear fault starts to develop.

Dataset 2

In this case the behaviour of CI_{RMS} is very similar, irrespective of whether it is calculated on the raw or residual signal (Figure 6.16). This could be influenced by the fact that the fault signatures present in the signal were strong enough to dominate the spectrum, so that even without removing the known components the detection of the damage was clear. The difference in the values between the two cases (CI_{RMS} from the raw signal is higher than CI_{RMS} from the residual signal) is as expected, since the majority of the components present in the raw vibration signal were removed in order to construct the residual signal, thus leading to decrease in the overall energy content of the signal.

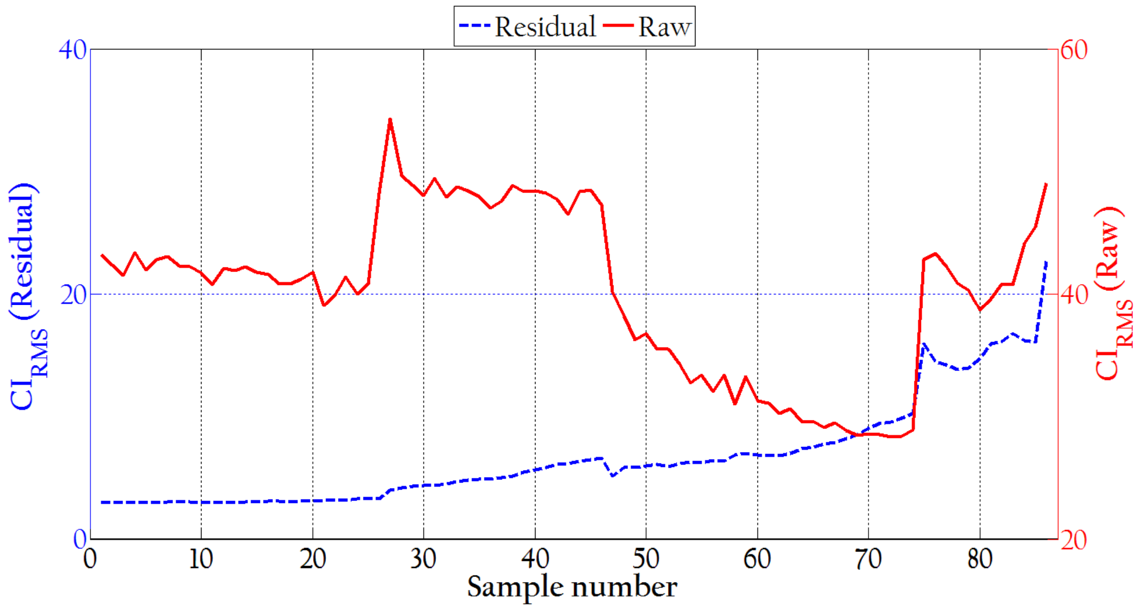

Figure 6.15 Variation of CI_{RMS} for raw (solid line) and residual (dashed line) vibration signal from Dataset 1

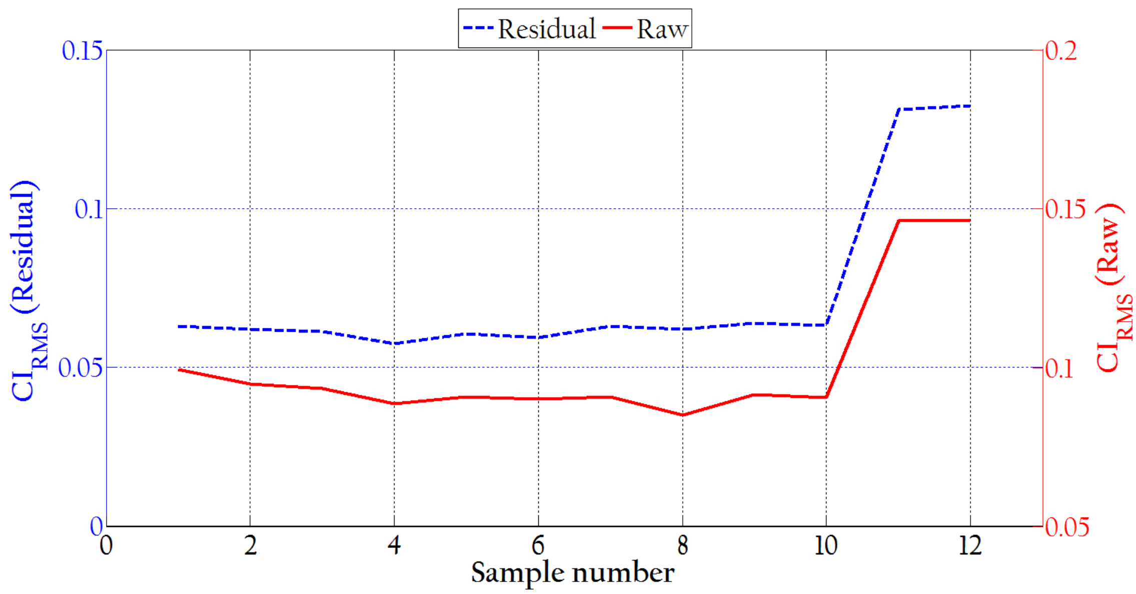

Figure 6.16 Variation of CI_{RMS} for raw (solid line) and residual (dashed line) vibration signal from Dataset 2

6.2.2 CI_{CF}

Dataset 1

An initial increase in the value of the parameter output at sample 18 is followed by a dramatic decrease after sample 25, corresponding with the first inspection. After this point the values rise again until sample 54, when a large decrease in the values initiates a decreasing trend that continues until the end of the test (Figure 6.17). The behaviour of the CI values on both plots is likely to be driven by the same signal behaviour, but occurring at different points in time as explained in section 6.1.2. The performance of CI_{CF} is dependent on the signal's peak-to-CI_{RMS} ratio. In the early stages of a fault progress the parameter reacts quickly to single impulses appearing in the signal. However, as the fault progress, the CI_{CF} values start to decrease. By creating a residual vibration signal the probability of detecting an incipient gear fault becomes greater than in the case of detection performed on the raw vibration signal and a much earlier reaction can be seen in the case of the residual signal in Figure 6.17. As the fault develops and starts to interact with the adjacent teeth the impulsive, short duration, fault-specific features become more widely distributed, last longer and contain more energy. This leads to an increasing overall vibration level of the signal, which, in turn, heavily increases the value of the denominator in the CI_{CF} formula. This explains the decrease in the values for both cases towards the end of the test. Based on these results, it can be stated that CI_{CF} calculated on the residual signal is not capable of presenting a reliable indication of fault progress.

Dataset 2

Until sample 9 both CI_{CF} curves show slight changes in their amplitude values not showing any consistent tendency. Despite the fact that spalling started to develop on tooth 1 at sample 6, no immediate reaction can be seen in either of the CI_{CF} cases. This behaviour continues until sample 9 (spalling on tooth 15) where a slight increase in the value of CI_{CF} calculated on raw vibration signal and a substantial increase in CI_{CF} from the residual vibration signal is observed (Figure 6.18). This point is followed by a slight decrease in the values of both curves. Sample 11 causes a large increase in the values for both cases reflecting a corresponding increase in the impulsive content of the signal.

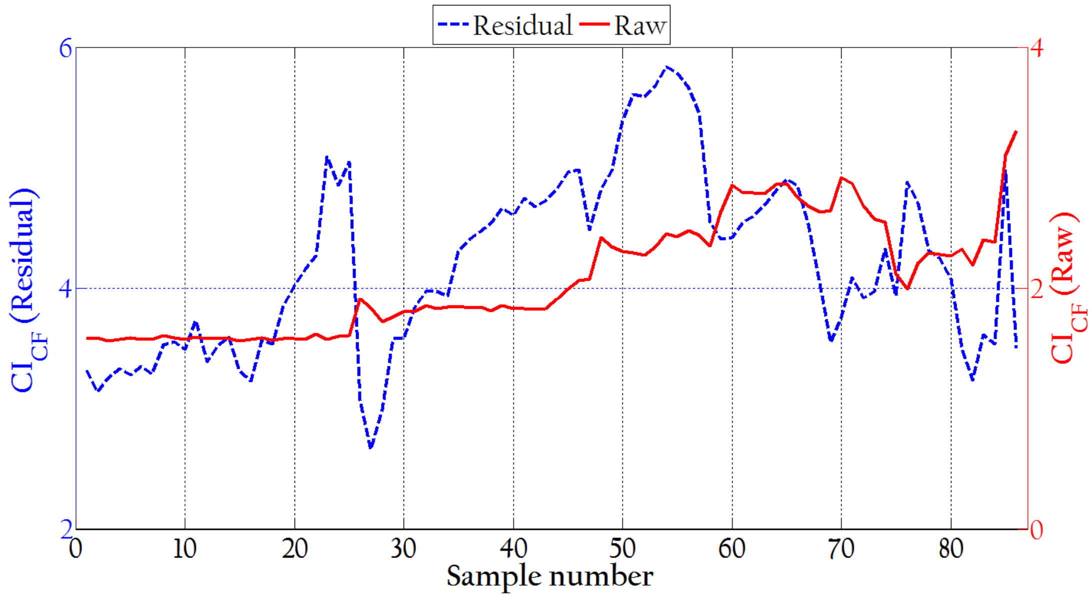

Figure 6.17 Variation of CI_{CF} for raw (solid line) and residual (dashed line) vibration signal from Dataset 1

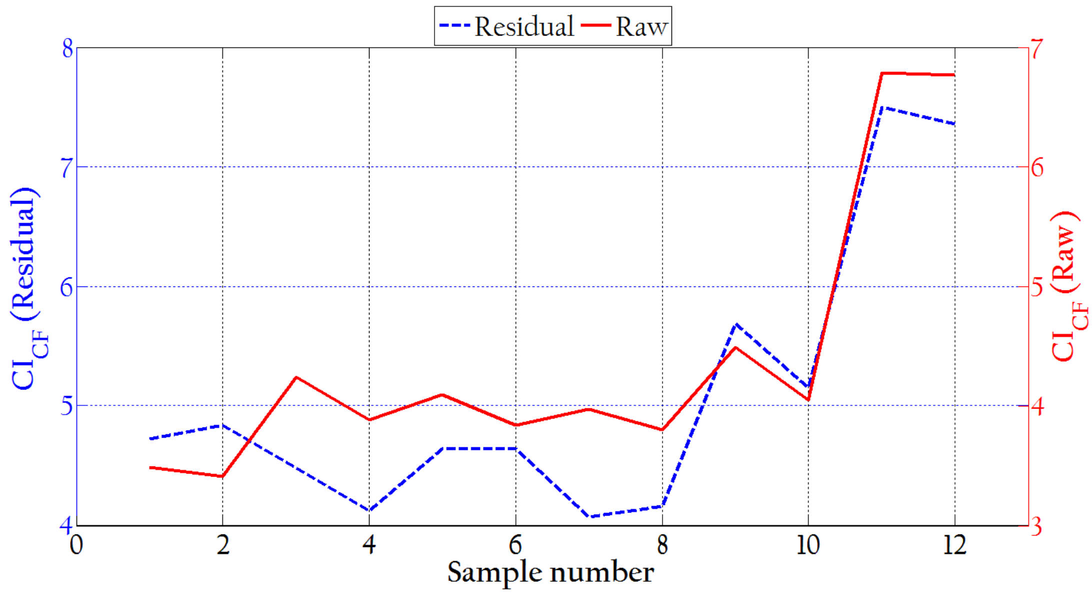

Figure 6.18 Variation of CI_{CF} for raw (solid line) and residual (dashed line) vibration signal from Dataset 2

6.2.3 CI_{Ku}

Dataset 1

CI_{FM4} – that is CI_{Ku} calculated on a residual signal - presents behaviour very similar to that of $CI_{CF.}$ However, it is clear from Figure 6.19 that CI_{Ku} is far more sensitive to the developing fault providing a clearer separation between CI outputs from healthy and faulty gearbox The initial increase in the values starting at sample 18 is followed by a decrease in the values after sample 25 (the first inspection point). This is followed by a further increasing trend which continues until sample 45 (the second inspection point). After this event the values of CI_{FM4} start to oscillate with a generally decreasing trend until the end of the test. Based on the observations, CI_{FM4} is capable of detecting a fault in its early stages. However, as mentioned in Chapter 5, as fault spreads to adjacent teeth the values of CI_{FM4} are very likely to decrease for the same reasons as explained in the case of CI_{CF}.

Dataset 2

The behaviour of both curves is almost identical (Figure 6.20). It is worth noting however that, unlike CI_{RMS} the plots of both CI_{Ku} and CI_{FM4} have very similar values, which shows that these indicators are not amplitude dependant.

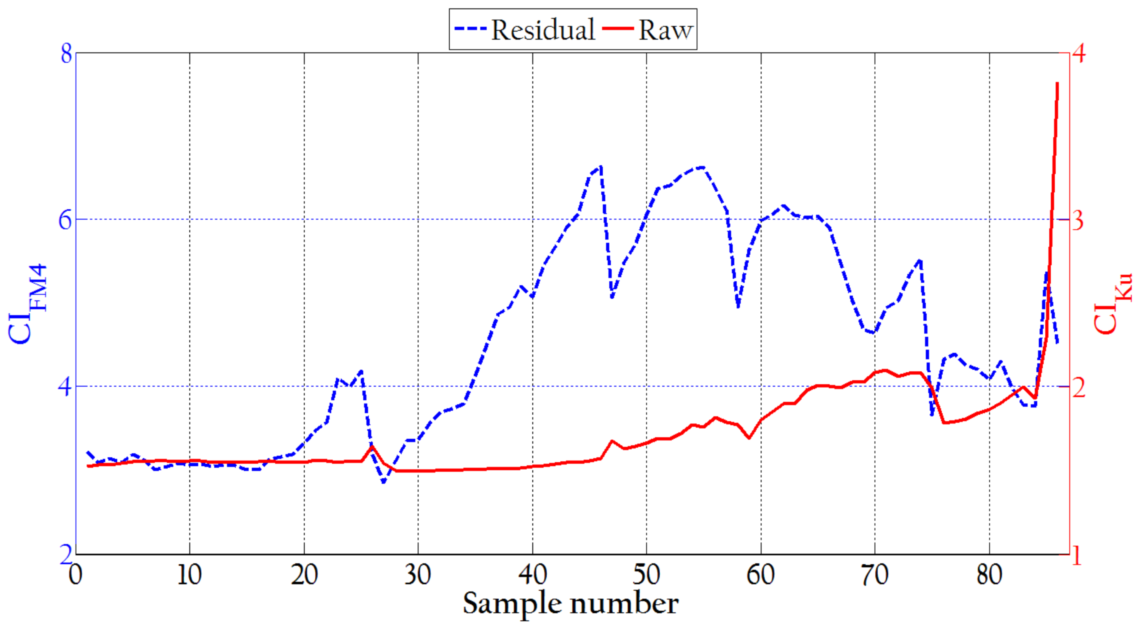

Figure 6.19 Variation of CI_{Ku} and CI_{FM4} for raw (solid line) and residual (dashed line) vibration signal from Dataset 1

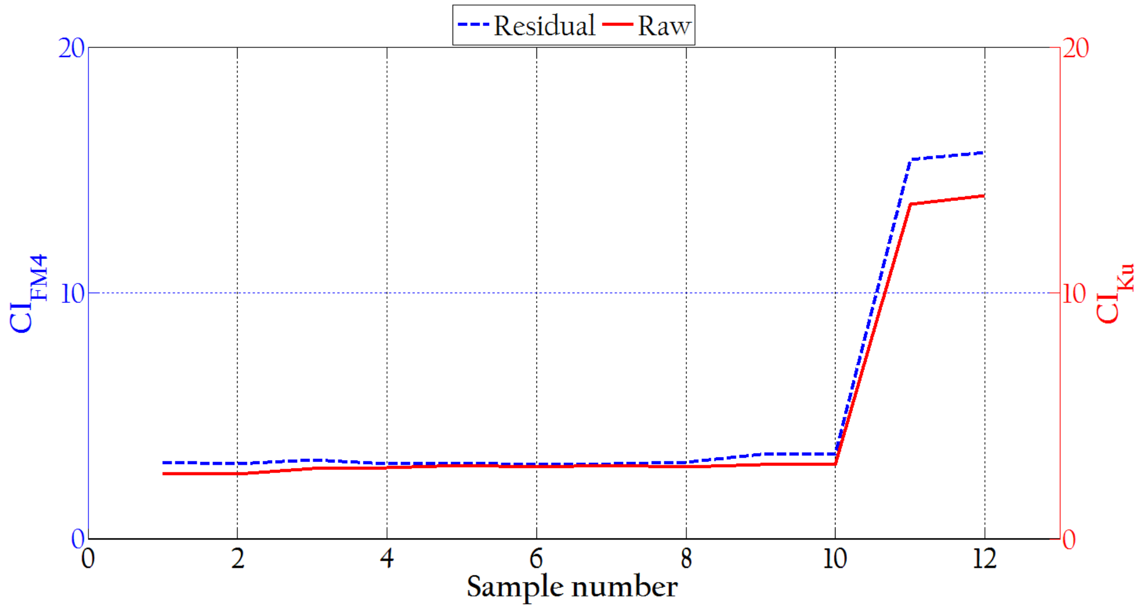

Figure 6.20 Variation of CI_{Ku} and CI_{FM4} for raw (solid line) and residual (dashed line) vibration signal from Dataset 2

6.2.4 CI_{M6}

Dataset 1

The behaviour of CI_{M6} is very similar to CI_{FM4}/CI_{Ku} for both raw and residual vibration signals (Figure 6.21). CI_{M6} calculated on the residual signal behaves much the same way as CI_{FM4} though the falling trend begins slightly later into the test (due to the second oscillatory peak being longer). The initial increase in the values beginning at sample 18 is followed by a decrease in the values after sample 25 (first inspection). After this point the values begin to rise again. After the second inspection the values of CI_{M6} start to oscillate with a decreasing trend which is present until the end of the test. CI_{M6} calculated on the residual signal shows a clear advantage over its application on the raw signal by detecting the fault earlier. However it fails to indicate a gear fault for the whole duration of the test.

Dataset 2

As was the case for CI_{FM4}/CI_{Ku} seen in Figure 6.20, the behaviour of both CI_{M6} curves is almost identical (Figure 6.22). The only significant difference between the trends of two curves appears at samples 11 and 12 which indicates that a gear fault manifests itself more prominently when CI_{Ku} is applied to residual vibration signal.

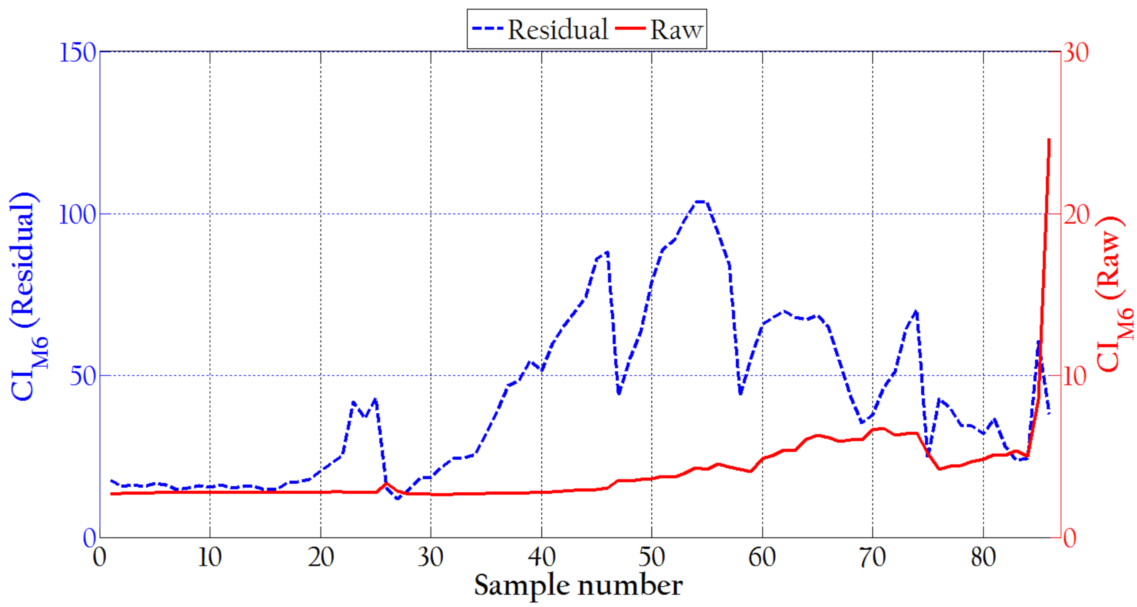

Figure 6.21 Variation of CI_{M6} for raw (solid line) and residual (dashed line) vibration signal from Dataset 1

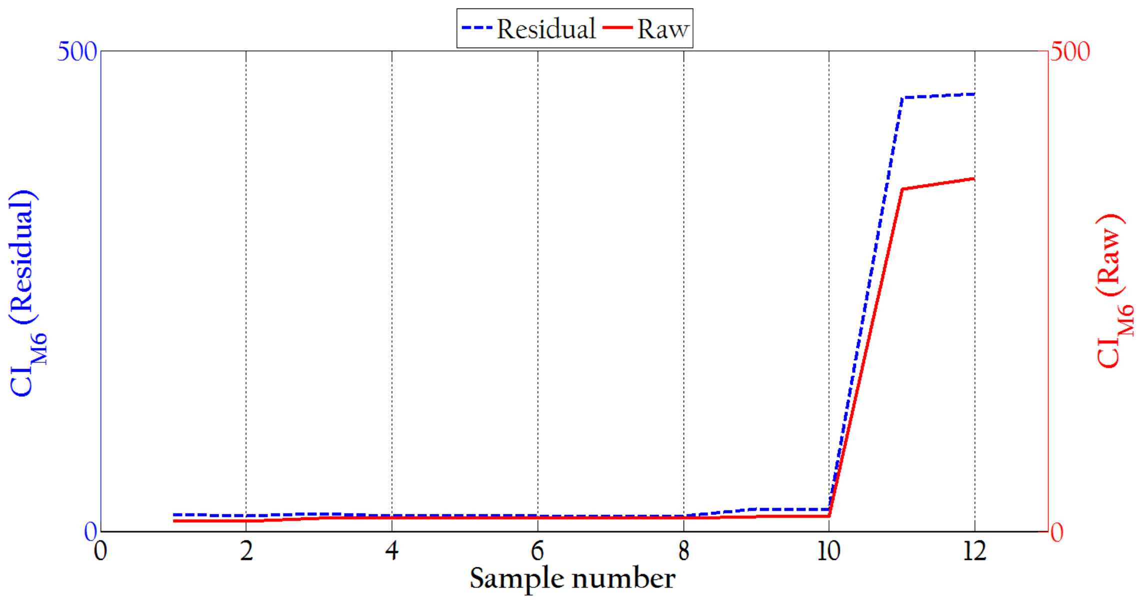

Figure 6.22 Variation of CI_{M6} for raw (solid line) and residual (dashed line) vibration signal from Dataset 2

6.3 Summary

This chapter presented the results obtained when applying the existing CIs to the available datasets. Five different parameters were whilst tested. Section 6.1 examined the performance of the CIs in their typical applications. Section 6.2 attempted to examine the behaviour of the existing CIs under new circumstances by calculating their values on the residual vibration signal. The residual signal was generated only for the datasets containing a gear fault and therefore Section 6.2 described the results based on Datasets 1 and Dataset 2 only. The analysis and explanation of the outcomes led to some important conclusions.

The results showed that CI_{RMS} calculated on the residual vibration signal, provides some advantages compared to CI_{RMS} typically applied on raw vibration data. In Dataset 2 both versions of CI_{RMS} performed in a similar way, however analysis of Dataset 1 revealed a clear improvement when using the residual version of this parameter. Based on the findings from Section 6.2.1, CI_{RMS} calculated on the residual signal will be considered as a newly proposed CI in further study. In the case of the bearing fault, the CI_{RMS} behaved as expected. It was observed to be capable of indicating an outer race bearing fault, by reacting to the increase in the energy of the band-pass filtered signal. This increase is caused by an interaction between the rolling elements and the damaged surface of the outer race.

The behaviour of CI_{CF} applied on Dataset 1 supported the findings from the simulations shown in Section 5.5, which showed that CI_{CF} is a good indicator of gear fault at the early stages of their development process. However, as the fault changes from being localised, spreading to adjacent teeth, the values of CI_{CF} decrease. When applied to a vibration signal containing signatures of an outer race bearing fault, CI_{CF} showed strong detection abilities. Analysis of the behaviour of CI_{CF} suggested that this parameter was capable of detecting the early stages of gear faults, but it was fond to be unreliable over the whole duration of the test. In addition to that it has been shown that CI_{CF} is capable of detecting an outer race bearing fault. Although this detection came much later into the test compared with $CI_{RMS,}$ it was much clearer, probably due to a sudden appearance of an impulsive content in the band pass filtered signal.

The performance of CI_{Ku} applied on Dataset 1 showed that it was relatively late in indicating the advent of the gear fault. Furthermore the values of CI_{Ku} decreased towards the end of the test, a fact which, similarly to $CI_{CF,}$ makes the indicator unreliable for the whole duration of the fault development process. Not withstanding this CI_{Ku} was capable of indicating the outer race bearing fault in Dataset 3.

CI_{FM4} tested on Dataset 1 detect the gear fault at a very early point and during the early stages of the gear fault development process it gave a reliable indication of the advancement of the crack. Although the indication was similar to that of $CI_{CF,}$ applied on the residual signal, the changes in the values during the rising phase were greater, which resulted in a clearer separation between the CI outputs for healthy and faulty conditions. It was also observed that beyond a certain point CI_{FM4} began to decrease. This behaviour is a well documented disadvantage of the technique and takes place when the fault character changes from localised to becoming more spread, involving adjacent teeth [29, 30, 53, 67, 195]. Since this technique gave the best initial results, the general philosophy behind detecting gear fault based on observing changes in the amplitude distribution of a signal will be explored in more detail during the process of improving the existing CIs.

CI_{M6} applied on the raw vibration signal gave approximately identical results to those for $CI_{Ku.}$ However the relative changes in the value were much greater which is consistent with theoretical predictions.

Table 6.1 summarises the findings from this chapter. Some of the presented drawbacks may be acceptable in circumstances when an early fault detection is not of prime importance for example in places that utilise a run-to-failure maintenance approach. For helicopters, however, early detection is of paramount significance and use of a quick, dependable tool for machine condition diagnosis is essential. Testing the behaviour of the existing CIs presented in this chapter clearly revealed the positive and negative properties of each indicator. During the comparison process considerable insight was gained about the reasons for failure of some of the parameters and the properties that allowed some indicators to detect faults at the earliest possible moment. This intelligence constitutes the basis of the development of new, improved Condition Indicators. The next four Chapters introduce the proposed CIs and test their behaviour when applied on the three uncorrelated datasets.

Table 6.1 Comparison of properties of examined CIs

CI	Property type	**Raw signal**	**Residual signal**
CI_{RMS}	Positive	· Early indication of faults compared with residual signal (Dataset 1)	· Continuous fault progression trend · Less sensitive to ambient conditions
	Negative	· Heavily influenced by any (fault and non-fault related) changes in vibration signal	· Later indication of faults (Dataset 1)
CI_{CF}	Positive	· More consistent fault indication compared with residual signal	· Early indication of faults compared with raw signal
	Negative	· Late indication of faults · Values drop as fault becomes more distributed	· Small separation of values between faulty and healthy condition (Dataset 1) · Values drop as fault becomes more distributed
CI_{Ku}/ CI_{FM4}	Positive	· More consistent fault indication compared with residual signal	· Early fault indication compared with raw signal
	Negative	· Late fault indication · Values drop as fault becomes more distributed	· Values drop as fault becomes more distributed
CI_{M6}	Positive	· More consistent fault indication compared with residual signal	· Early fault indication compared with raw signal
	Negative	· Late fault indication · Values drop as fault becomes more distributed	· Values drop as fault becomes more distributed

CHAPTER 7

AMPLITUDE OF SIDEBANDS (ASB) STUDY

7.1 Introduction

Under ideal conditions the only components present in the spectrum of a vibration signal generated by a healthy gearbox would be frequencies related to the shaft speed frequency, the gear mesh frequency (GMF) and perhaps their associated harmonics. As a gear tooth fault develops, the GMF and its harmonics would become modulated at the shaft speed frequency and, as a result, sidebands would start to appear around the GMF and its harmonics. This phenomenon was described by McFadden [50]. McFadden explained that it is widely presumed that an early fatigue crack affects only a small part of the whole gear and that, provided the crack is small enough, there will always be another healthy tooth in contact to carry the load. However, as the crack grows, further deterioration of the gear condition can lead to a situation where only the faulty gear is in contact. McFadden presented two theories about what happens next. The first one suggests that the deflection of the faulty area can cause a relative misalignment of the following teeth on the two gears. As the teeth resume their proper positions an impact is generated (exciting frequencies across a wide frequency band). The second theory implies that, as the healthy tooth goes out of mesh, the faulty gear will be unable to maintain the same load (due to decreased stiffness) leading to a step reduction in tooth contact which will lead to generation of an impact [50]. Even though the exact physical cause is uncertain, the important fact is that the resulting impact is very likely to excite resonances of the gears, shafts, bearings, the machine case, and even the accelerometer itself.

7.2 Proposed CI

Even though McFadden described the effect for the first time in 1989, there are currently no known CIs that take full advantage of the changes that appear within the vibration signal as the phenomenon develops. Hence, a new CI is proposed on this concept which is named: “Amplitude of Sidebands” (CI_{ASB}).

In order to properly calculate CI_{ASB}, the residual vibration signal $x_{TSA}(t)$ needs to be transformed to the frequency domain by means of discrete Fourier transformation (DFT). Applying a DFT to the signal $x_{TSA}(t)$ results in creation of signal *X(f)* from which CI_{ASB} can be mathematically represented as:

$$CI_{ASB} = \sum_{i=0}^{N} \left(\sum_{j=-M}^{M} A_{i,j}(X) \right) \tag{7.1}$$

where *N* is the total number of GMF harmonics in signal *X(f)*, *M* is the total number of sidebands around *i*-th GMF harmonic present in signal *X(f)*, $A_{i,j}(X)$ is the amplitude of the *j*-th sideband around *i*-th GMF harmonic in signal *X(f)* ($A_{0,j}$ representing the fundamental GMF) as shown in Figure 7.1.

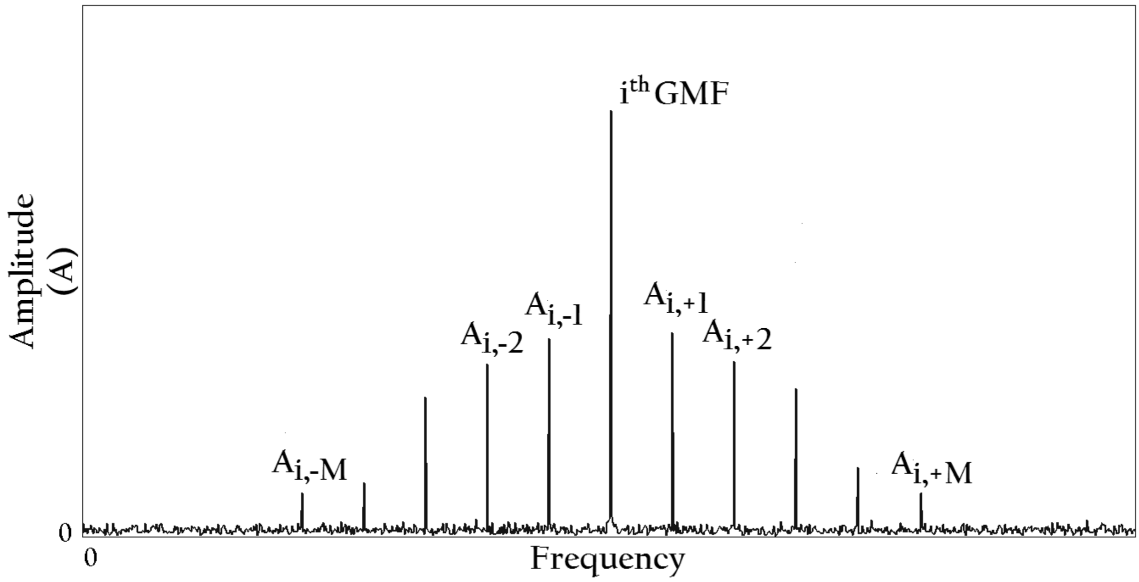

Figure 7.1 Graphical representation of nomenclature used in Eq. (7.1)

The processes that need to be followed in order to calculate CI_{ASB} from a gear train vibration signal begin with computation of the DFT of the gearbox vibration response. This was achieved by means of a Fast Fourier Transform (FFT).

As a gear fault develops, each time the faulty tooth comes into mesh an impact is generated which, in turn, modulates the vibration response. The principle of sideband generation as a result of amplitude modulation is presented in Figure 7.2. The initial signal is a sinusoid with a frequency of 100Hz, and Figure 7.2(a) and Figure 7.2(b) show the signal in the time domain and the frequency domain respectively. The signal in Figure 7.2(c) is constructed by modulating the signal in Figure 7.2(a) by a 10Hz sinusoid of amplitude 1. Note that the maximum amplitude of the resultant signal is equal to 2. This is because the modulating signal has an amplitude of 1 which, when in phase with the original signal, sums doubling the amplitude. Conversely, as the modulating becomes further out of phase, the resultant amplitude decreases to 0. The spectrum in Figure 7.2(d) shows the result of the modulation; two sidebands, each of amplitude equal to 0.5, appear on both sides of the component corresponding to the frequency of the original signal. It is expected that as the gear fault progresses, further sidebands will appear around the GMF and its harmonics, the energy contained in them will increase and the CI_{ASB} values will respond accordingly.

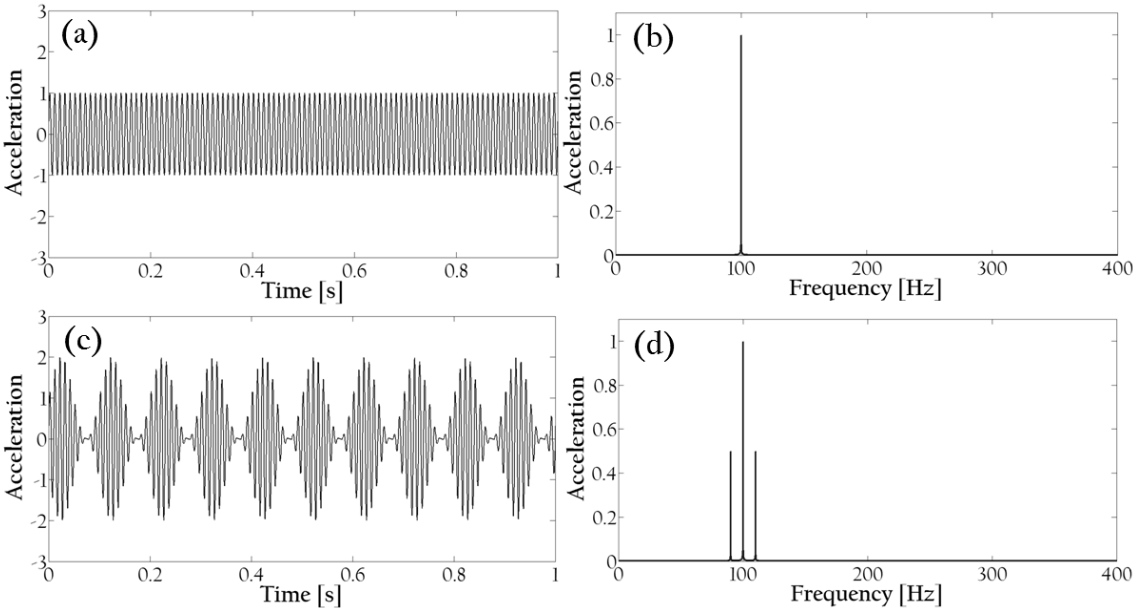

Figure 7.2 Pure sinusoid (a), pure sinusoid spectrum (b), amplitude modulated sinusoid (c), amplitude modulated sinusoid spectrum (d)

7.4 Results

7.4.1 Dataset 1

In order to demonstrate the way CI_{ASB} works a few typical samples from Dataset 1 are examined in the frequency domain. Figures 7.3 - 7.8 depict the process during which the energy contained in the sidebands around the GMF and its harmonics increase as the gear tooth fault develops. One can see that in each consecutive plot (based on chronologically organised data sample numbers), the energy in the GMF sidebands increases, reaching its highest values prior to the gear tooth detachment. It has also been noted that correspondingly the energy contained in the GMF and its harmonics decreases. All the spectra are presented on the same scale, however it is worth mentioning that each spectrum was dominated by the GMF which was greater than the y-axis maximum on all the presented plots. The y-axis was scaled in order to clearly show the sideband energy, regardless of the GMF value.

The spectrum generated from sample 1 is clearly dominated by the GMF and its harmonics with some low energy sidebands around them (Figure 7.3). This situation is as expected, as sample 1 was generated at the beginning of the test and the meshing gears were in a healthy condition. The spectrum of the vibration signal recorded at sample 24 starts to show increased energy in the frequency components that correspond to the GMF sidebands (Figure 7.4). The sidebands become clearly visible in the region around the dominant gear mesh frequency and also between the 2nd and 3rd GMF harmonic. At the same time, the energy contained in the GMF and its harmonics decreased compared to sample 1. Sample 45 shows further increase in the GMF sideband energy content (Figure 7.5), the sidebands becoming visible around every GMF harmonic. By this time a significant decrease in the energy contained in the 4th and 6th GMF harmonic had taken place. Sample 61 shows further progress in terms of increase in the GMF sideband energy. Radical change can be seen particularly around the dominant gear mesh frequency and also in the region between the 2nd and 3rd GMF harmonic and in the sidebands surrounding the 4th GMF harmonic (Figure 7.6). The 2nd GMF harmonic is now virtually invisible in the spectrum. Spectra generated from data samples 78 and 85 show that, apart from the strong dominant GMF, both spectra are dominated by the sidebands and its harmonics (Figures 7.7 and 7.8). The whole area between consecutive GMF harmonics is populated by the sidebands, which also became visible in the higher frequency parts of the spectrum, even beyond 10 kHz. The decrease in the energy of the GMF and its harmonics in the presence of a gear damage has been reported in a number of NASA Technical Reports (for example in [71]). However, no explanation was given regarding potential reasons for this phenomenon.

It is suspected that the decrease in the amplitude of the meshing frequencies might be related to some irregularities in the tooth meshing vibrations and, as a result, migration of the energy to the modulating components (that is the sidebands around the GMF and its harmonics).

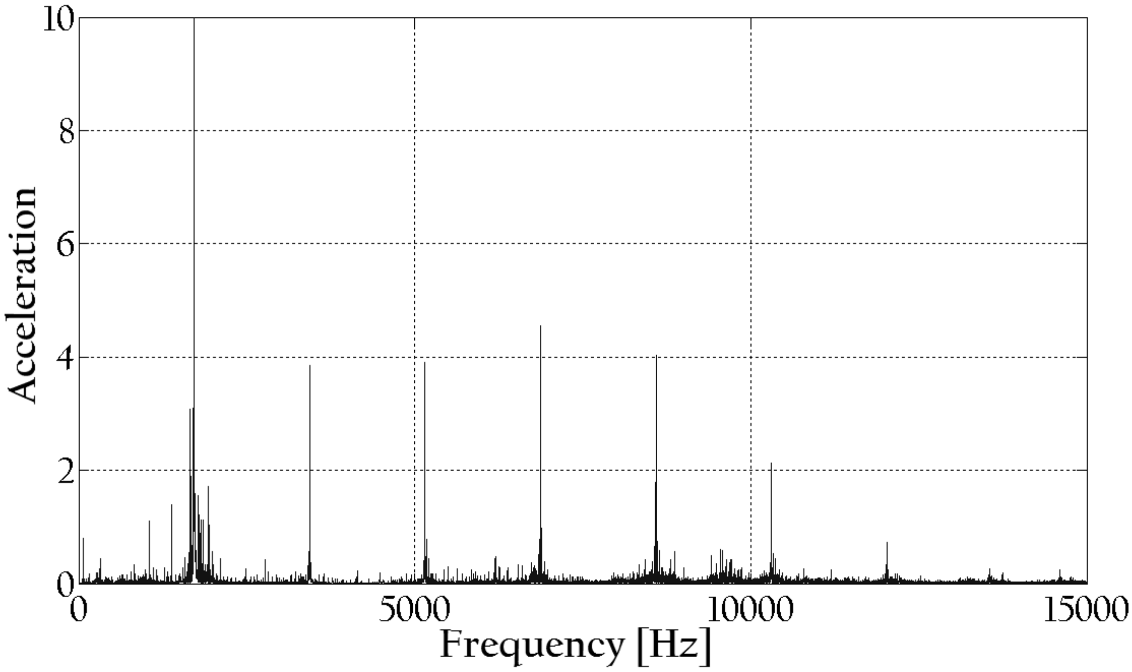

Figure 7.3 Magnified spectrum from sample 1

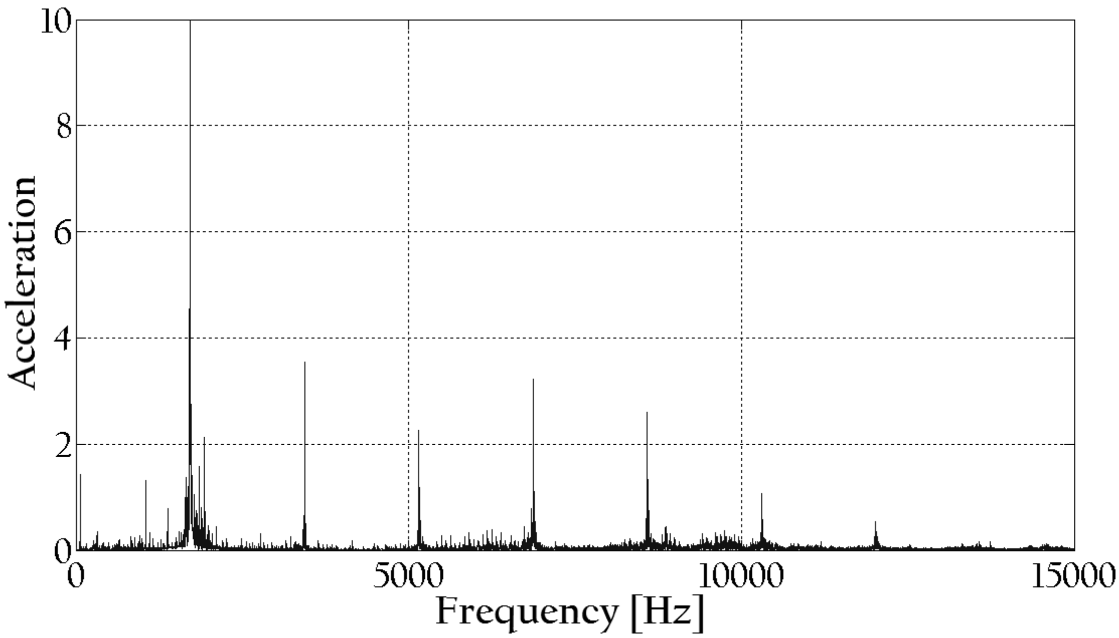

Figure 7.4 Magnified spectrum from sample 24

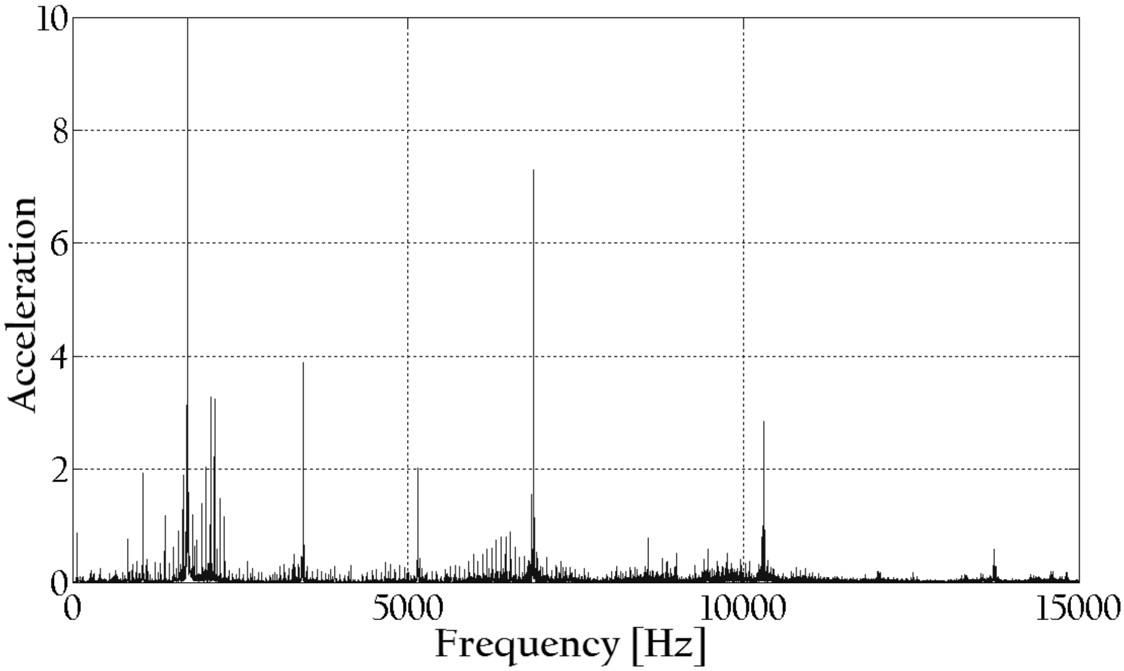

Figure 7.5 Magnified spectrum from sample 45

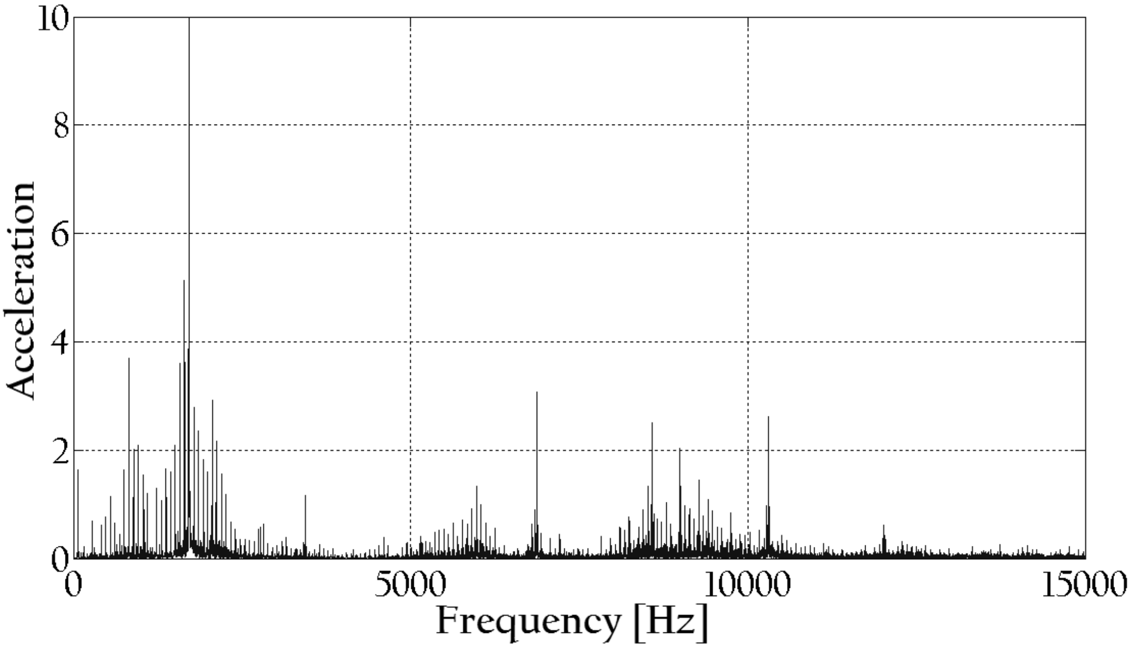

Figure 7.6 Magnified spectrum from sample 61

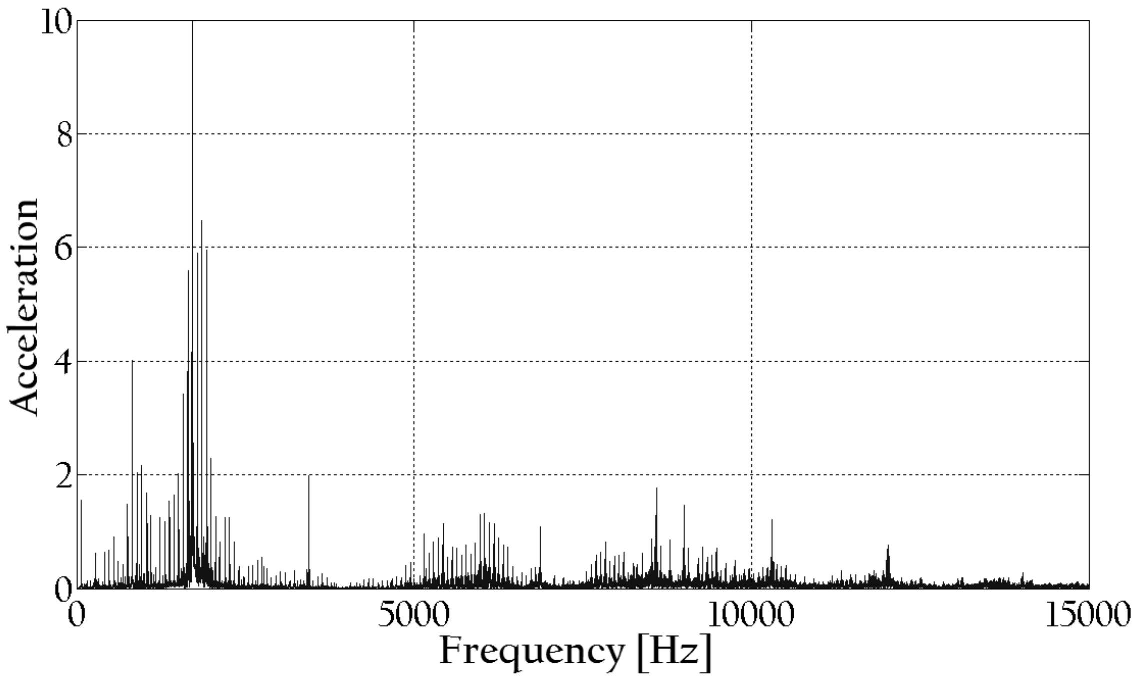

Figure 7.7 Magnified spectrum from sample 78

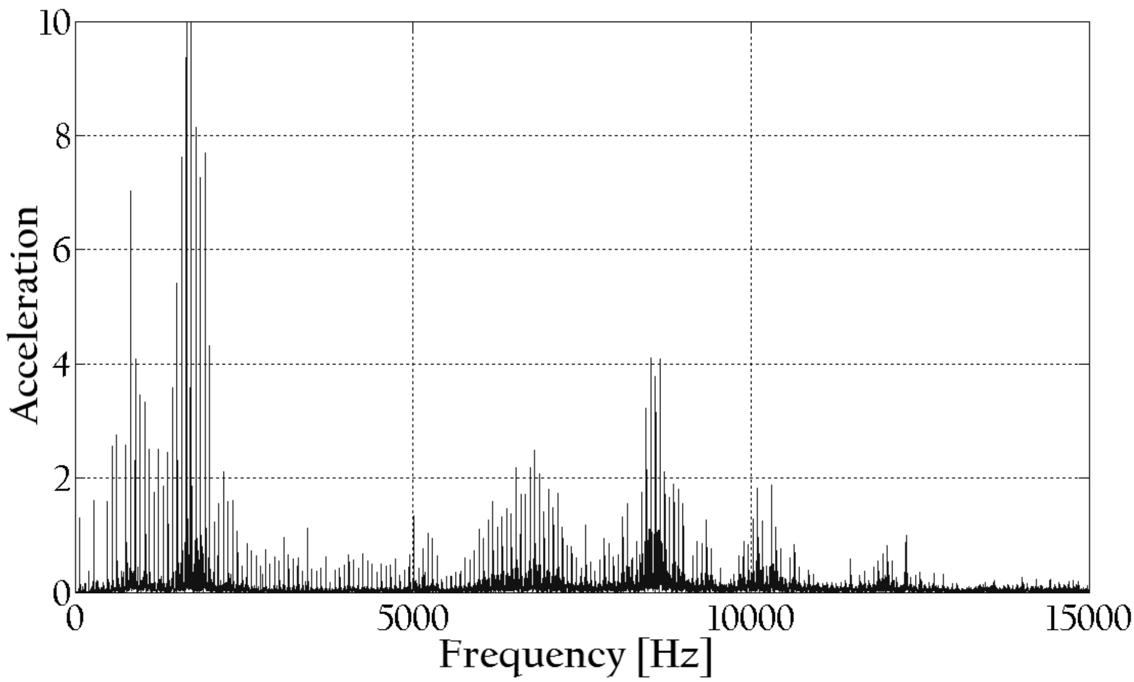

Figure 7.8 Magnified spectrum from sample 85

Comparison of the frequency spectra clearly shows that the appearance of the sidebands around the GMF and its harmonics corresponded with the development of the gear tooth problem. In order to quantify the observed phenomenon CI_{ASB} is applied to Dataset 1. Figure 7.9 shows the obtained result, where a clear rising trend is observed. This starts at sample 28 and continues to rise until the end of the test. In addition to the clear increase in the sideband energy, it has also been noted that the sum of the amplitudes of the GMF and its harmonics (AGMF) decreases as a function of the gear fault development. AGMF is mathematically represented as:

$$AGMF = \sum_{i=0}^{N} AMP_i(X) \tag{7.4}$$

where N is the total number of GMF harmonics in signal $X(f)$, $AMP_i(X)$ is the amplitude of the i-th GMF harmonic (AMP_0 representing the fundamental GMF).

Figure 7.10 supports this observation by showing a generally decreasing trend, which can be used as supporting evidence of a gear degradation process.

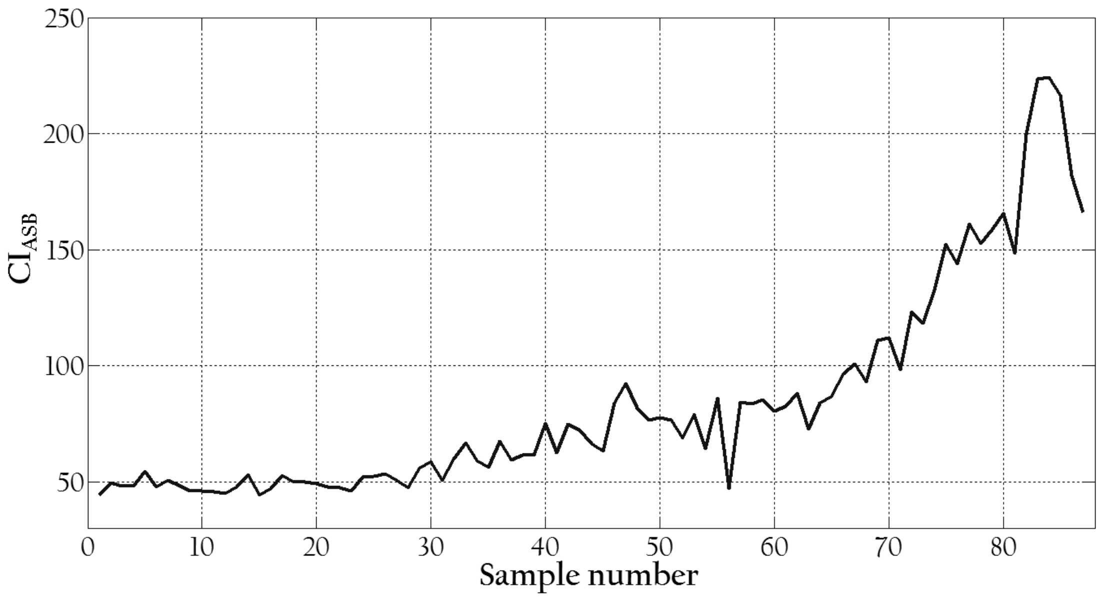

Figure 7.9 Variation of CI_{ASB} on Dataset 1

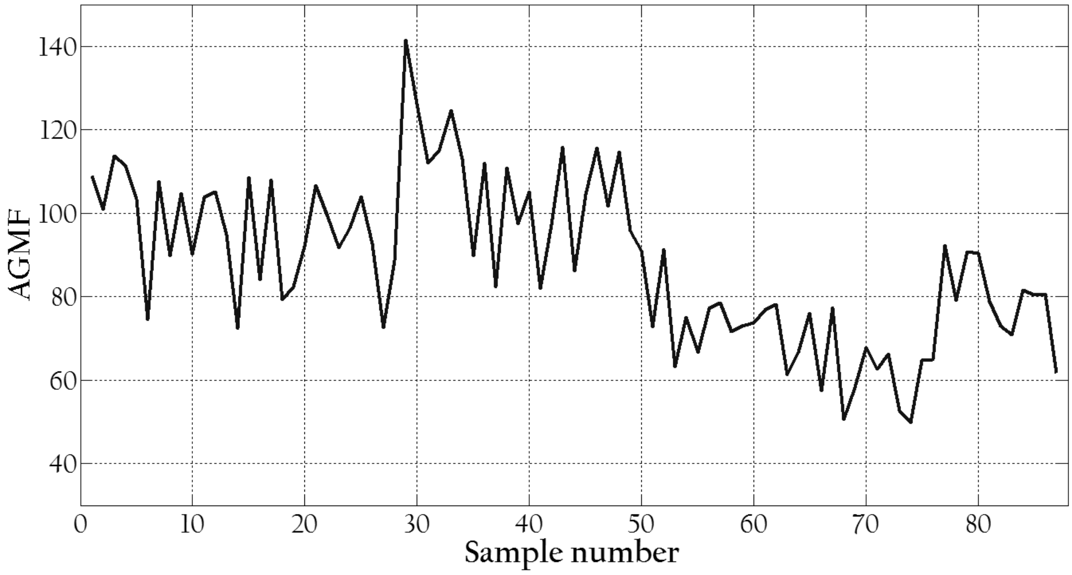

Figure 7.10 Variation of AGMF on Dataset 1

7.4.2 Dataset 2

Dataset 2 contains a lower data density from which to analyse the fault progression history, compared to Dataset 1 - there are fewer vibration samples that were collected throughout the gear deterioration process. Nevertheless, CI_{ASB} was capable of indicating the gear fault equally effectively when compared to the previously tested parameters. Figure 7.11 shows that the level of the energy contained in the GMF sidebands remained constant for the majority of the test and increased substantially for the last two samples. This indicates a rapid deterioration of the gear tooth condition, which resulted in generation of a high sidebands energy around each of the gear mesh frequencies. Conversely the complimentary indicator: AGMF presents a trend that decreases slightly, though not monotonically decreasing. This suggests a deterioration of the gear condition throughout the duration of the test, and not only in the last two samples.

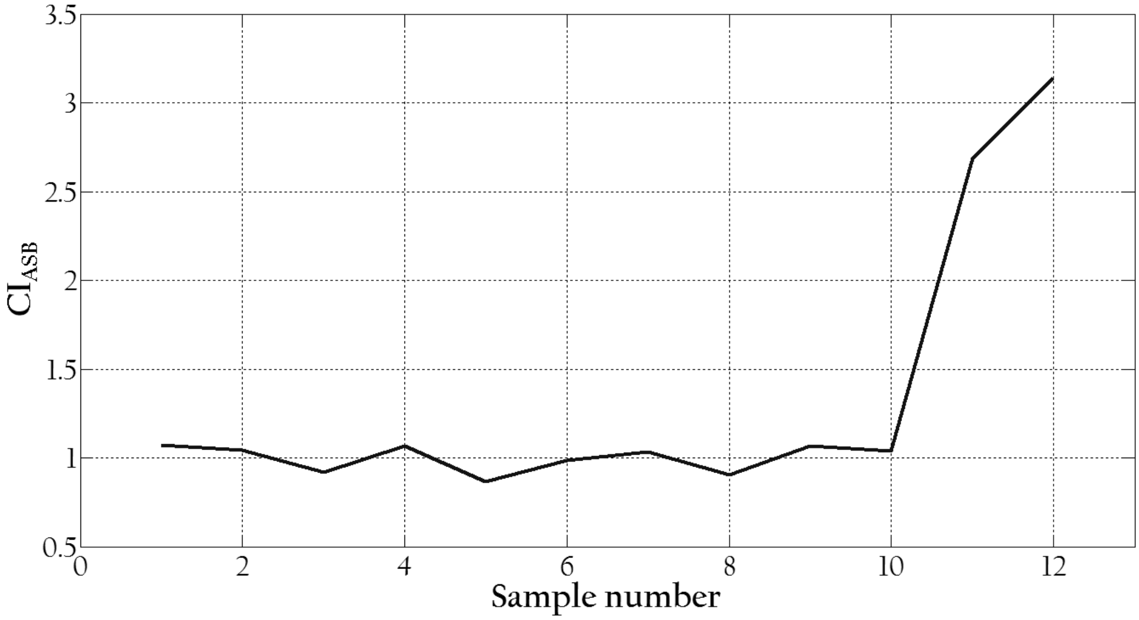

Figure 7.11 Variation of CI_{ASB} on Dataset 2

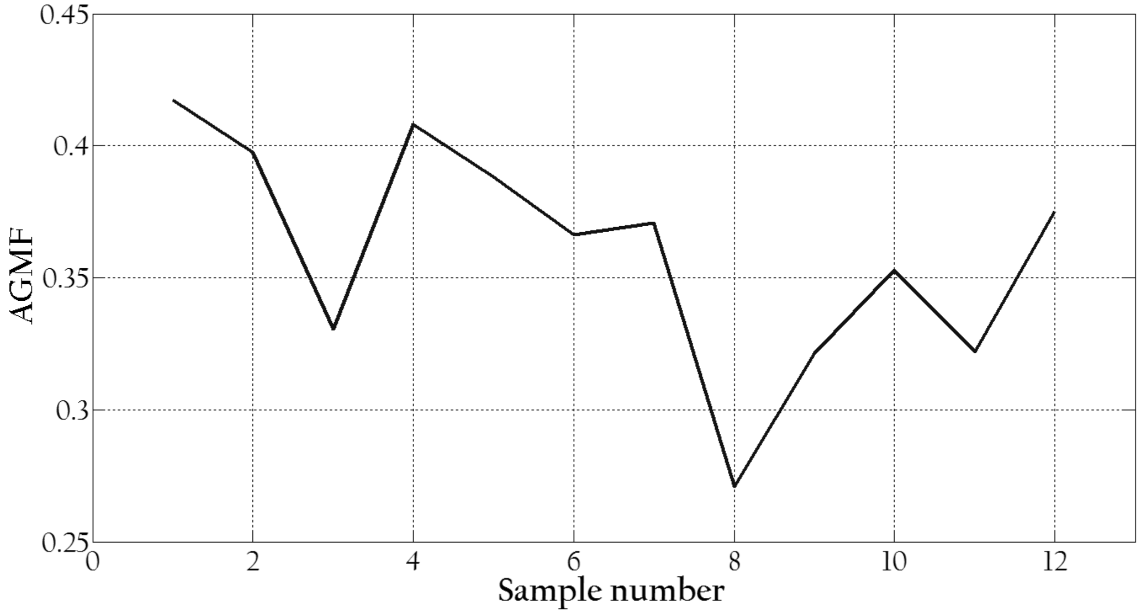

Figure 7.12 Variation of AGMF on Dataset 2

7.5 Improved CI_{ASB}

Combining information about the energy contained within the GMF and its harmonics (Figures 7.10 and 7.12) with information regarding changes taking place in the sidebands around the GMF and its harmonics as the gear fault develops (Figures 7.9 and 7.11) led to a further improved form of CI_{ASB}. The improved CI, called the CI_{ASB*} can be mathematically defined as:

$$CI_{ASB*} = \frac{CI_{ASB}}{AGMF} \tag{7.4}$$

To properly implement the proposed parameter, the CI_{ASB} is first calculated as in Eq. (7.1) and the result is divided by the total energy contained in the GMF and its harmonics. Figures 7.13 and 7.14 show the results of comparison between CI_{ASB} and CI_{ASB*}. In order to assess the relative difference between the two parameters all the curves are presented in a normalised form. The normalisation is performed by dividing the values of a given CI by its value at the start of the test (the healthy state). For Dataset 1 the normalising value is equal to the mean value of the first 17 samples where the gear is known to be in healthy condition, whlist for Dataset 2, the normalising value is the mean value of the CI outputs generated for the first 4 samples. The results show the clear advantage of CI_{ASB*} which has a higher gain compared to $CI_{ASB,}$ and thus a greater gear fault sensitivity.

It should be noted that the decrease in the values of CI_{ASB*} between samples 75 and 82 is due to an increase in the value of AGMF which might have been caused by a severe worsening of the gear condition. Another decrease of AGMF and increase of CI_{ASB} causes CI_{ASB*} to increase its values towards the end of the test.

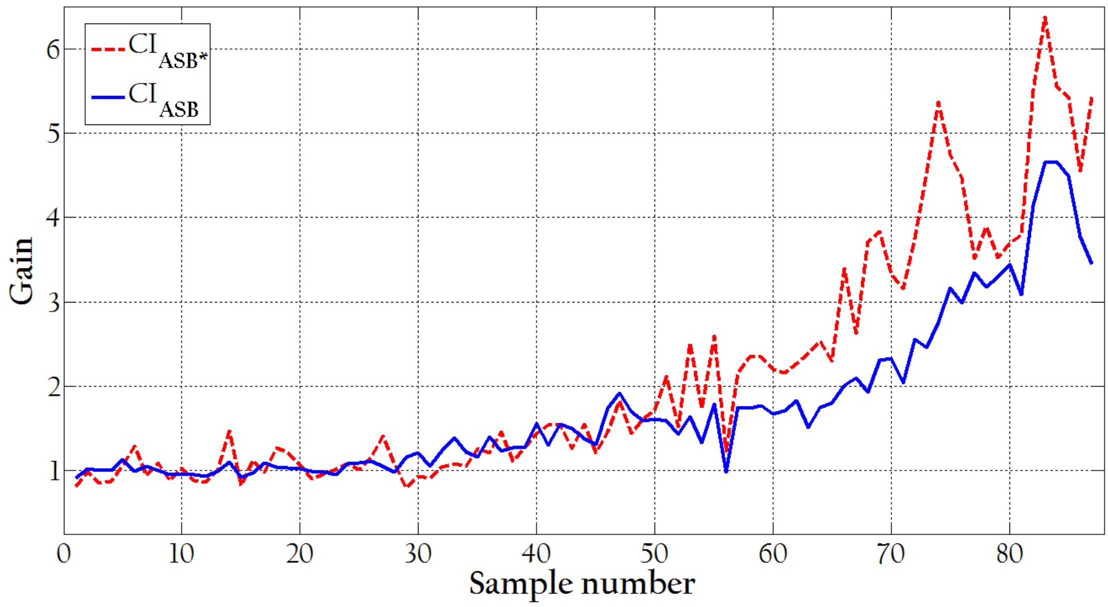

Figure 7.13 Gain of CI_{ASB*} and CI_{ASB} for Dataset 1

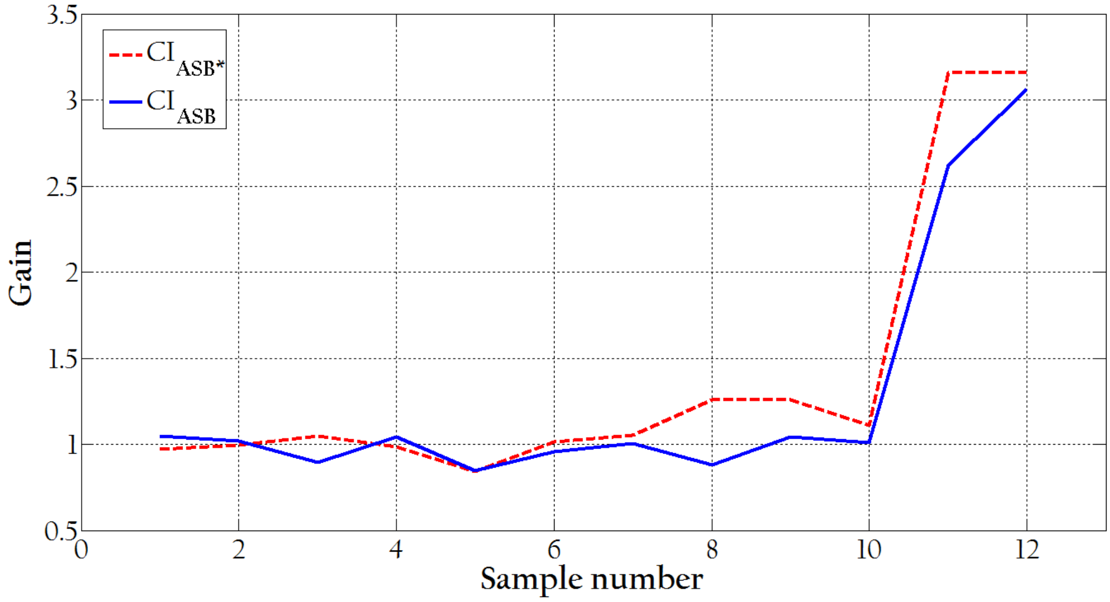

Figure 7.14 Gain of CI_{ASB*} and CI_{ASB} for Dataset 2

7.6 Summary

This chapter proposed a new CI called "Amplitude of Sidebands" (CI_{ASB}) and a further improved version: CI_{ASB*}. The introduction to this chapter stated that the phenomenon that underlines the design of this particular CI, has been reported in the past. However, to date, no indicator has been developed to take full advantage of it. CI_{ASB} can only be used to detect gear faults, since the special features measured by it are not characteristic signs of any bearing defect. As explained in Section 4.5, the standard approach for the diagnosis of bearing faults is to band-pass filter the signal in an appropriate band, usually located in the upper part of the spectrum. The filtering operation removes all the redundant frequency components including gear mesh frequency, shaft speed frequency and their harmonics. The filtering band is selected so that the only expected components above the background noise level are impulses at the characteristic bearing defect fault frequency. For bearing faults no modulation related to the shaft rotation is expected to be present in the vibration signal.

The introduction was followed by a mathematical definition of the new parameter and instructions on its implementation. Explanation of the phenomenon utilised by this technique was followed by analysis of the behaviour of CI_{ASB} when applied to the two datasets that contained a gear fault. In both cases the CI was capable of clearly indicating the development of a gear fault, yet on some occasions the indication started relatively late into the gear fault development process. Nevertheless, once the values began to rise, the increasing trend continued until the end of the test. Therefore CI_{ASB} would best be used in conjunction with other parameters that have the ability to indicate a fault at an earlier stage. The last part of the chapter introduced an improved version of CI_{ASB} which was observed to give results of the same character, but with a higher relative gain between the values obtained for healthy and faulty gearbox.

CHAPTER 8

ROOT MEAN SQUARE (RMS) STUDY

8.1 Introduction

The development of another new CI was inspired by the CI_{RMS} parameter and its ability to indicate the overall vibration level of a machine. This property was studied in Chapter 6. CI_{RMS} was applied to raw and residual vibration signals and the conclusions were that CI_{RMS} applied to a raw vibration signal failed to provide reliable information about the gear fault development in certain circumstances. On the other hand, when applied to the residual signal (CI_{resRMS}) the result was characterised by an early fault detection capability with an increasing trend as a function of the gear health deterioration process. This allowed classifying it as one of the proposed CIs in this study.

This chapter describes the new CI created on the basis of CI_{RMS}, which is called 'normalised RMS' (CI_{nRMS}), it operates on a normalised vibration signal where the amplitude ranges between ± 1. The purpose of the normalisation is to make CI_{nRMS} a dimensionless indicator. The proposed parameter is tested against all 3 available Datasets, followed by a detailed discussion of its behaviour. The chapter ends with a summary of the findings.

8.2 Proposed CI

The proposed CI is based on a "normalised RMS" (CI_{nRMS}) of the residual vibration signal $x_{TSA}(t)$ can be mathematically described as:

$$CI_{nRMS} = 1 - CI_{RMS}(Y) \tag{8.1}$$

where CI_{RMS} is the parameter in Eq. (3.1), Y is defined as $Y = \frac{x_{TSA}}{\max(abs(x_{TSA}))}$, where $\max(abs(x_{TSA}))$ is the maximum absolute value present in the TSA vibration signal.

The steps taken to calculate the value of CI_{nRMS} are as follows:

i. Compute the Time Synchronous Averaged (TSA) signal from the measured vibration signal;
ii. Normalise the TSA by dividing the vibration signal by the maximum absolute value present in the signal;
iii. Calculate CI_{RMS} on the normalised vibration signal;
iv. Subtract the results from 1.

The advent of a gear fault leads to the generation of high energy events within the vibration signal. As the fault develops from being localised to being more widely distributed, the generated signal becomes less impulsive and transforms to a more complex signal that contains high-energy, widely-distributed components. This in turn leads to an increase in the value of CI_{RMS} with decreasing isolation of peaks within the vibration signal.

Since normalisation of the vibration signal always limits the maximum absolute value to ± 1 then, as fault-related events start to appear, the amplitude of the central part of the signal distribution will decrease. This, in turn, leads to a decrease in the value of CI_{RMS} as a function of the gear fault development. Furthermore due to the normalisation of the vibration signal, CI_{RMS} can never reach a value higher than 1 and therefore in order to track fault progress in the natural and typically used form of a rising trend, the value of CI_{nRMS} is subtracted from unity.

8.3 Results

8.3.1 Dataset 1

To illustrate the way CI_{nRMS} operates, Figures 8.1 - 8.3 present the TSA signals generated from Sample 1, 45 and 85 of Dataset 1. It can be clearly seen that the normalisation of the signal causes the general amplitude to decrease with the development of the fault. This, in turn, leads to a decrease of the CI_{RMS} values. The result of applying CI_{nRMS} on samples from Dataset 1 is shown in Figure 8.4 which presents a constantly rising trend as a function of the gear tooth fault progress.

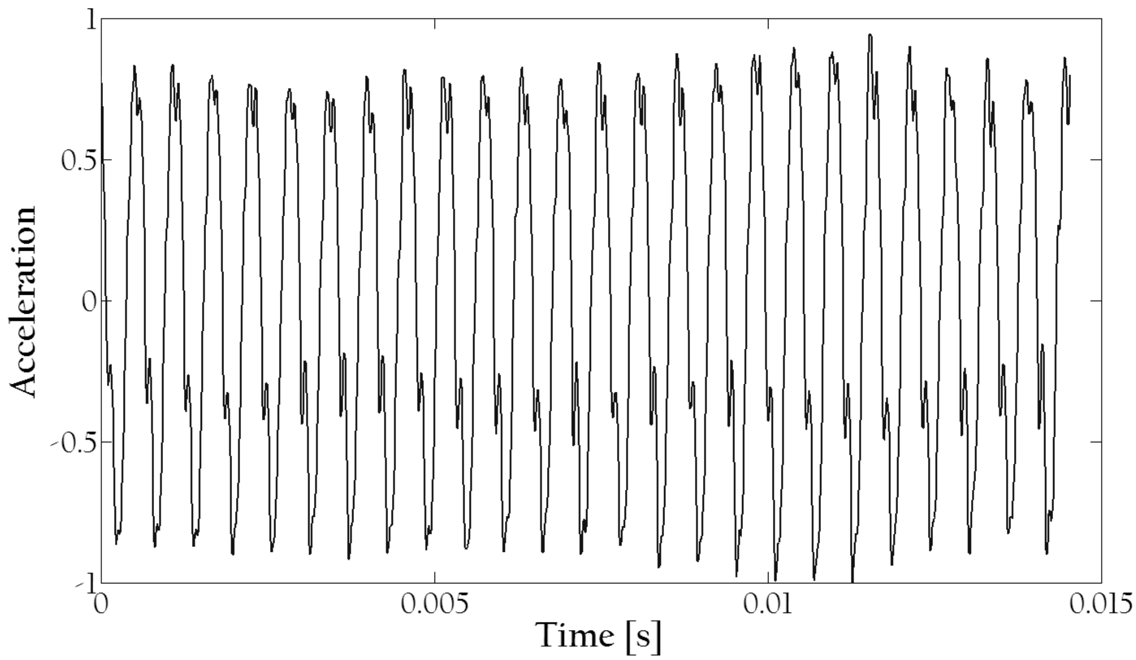

Figure 8.1 Normalised TSA derived from sample 1 (Dataset 1)

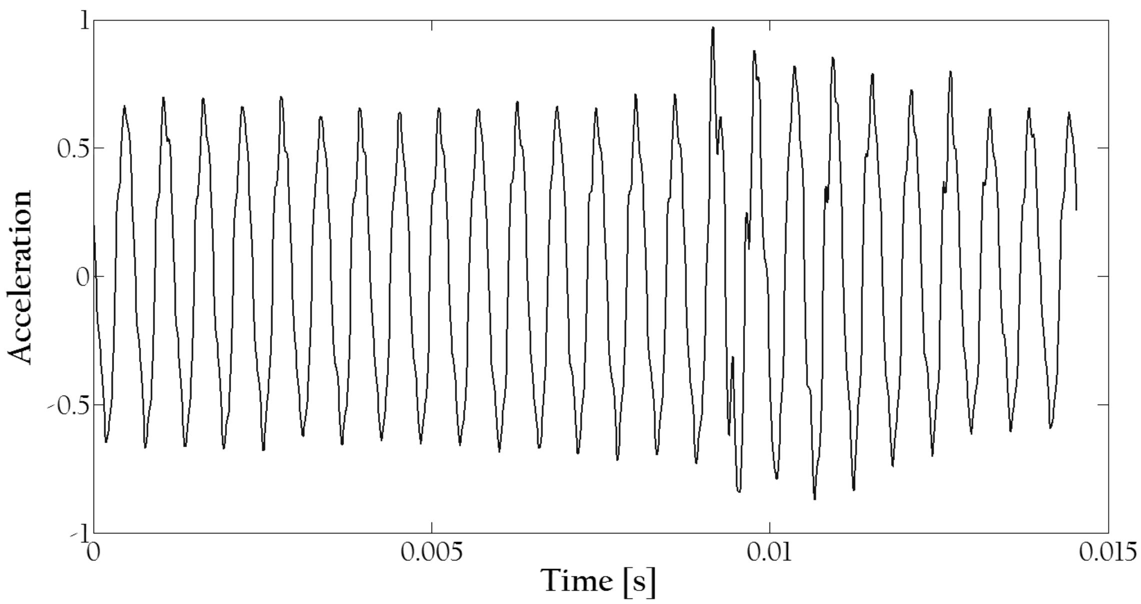

Figure 8.2 Normalised TSA derived from sample 45 (Dataset 1)

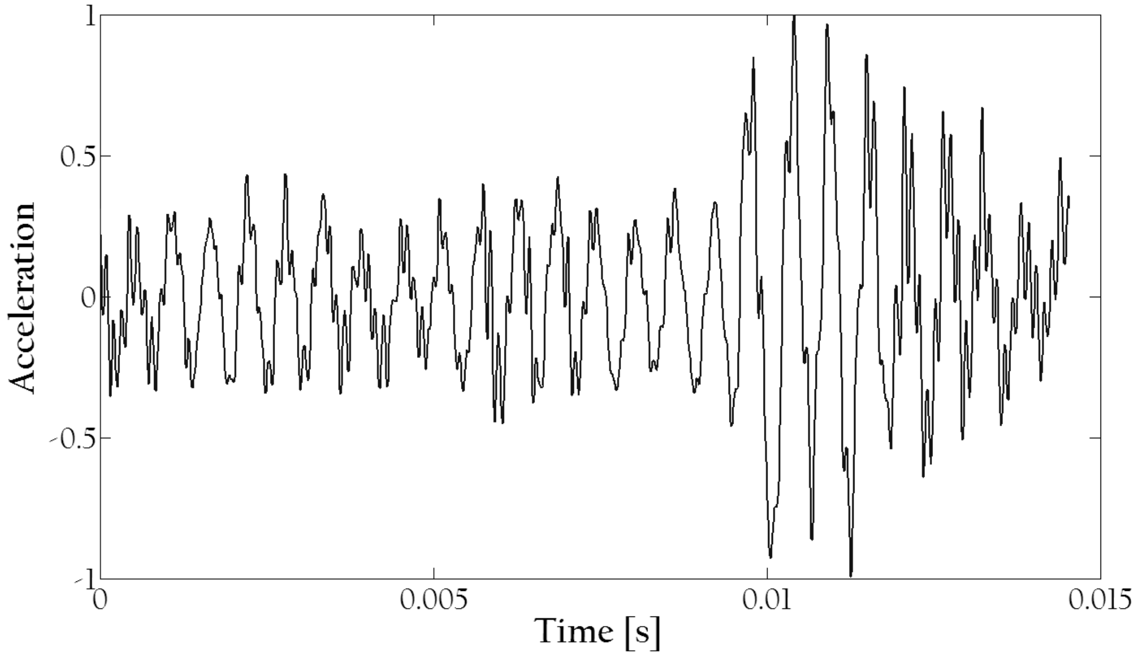

Figure 8.3 Normalised TSA derived from sample 85 (Dataset 1)

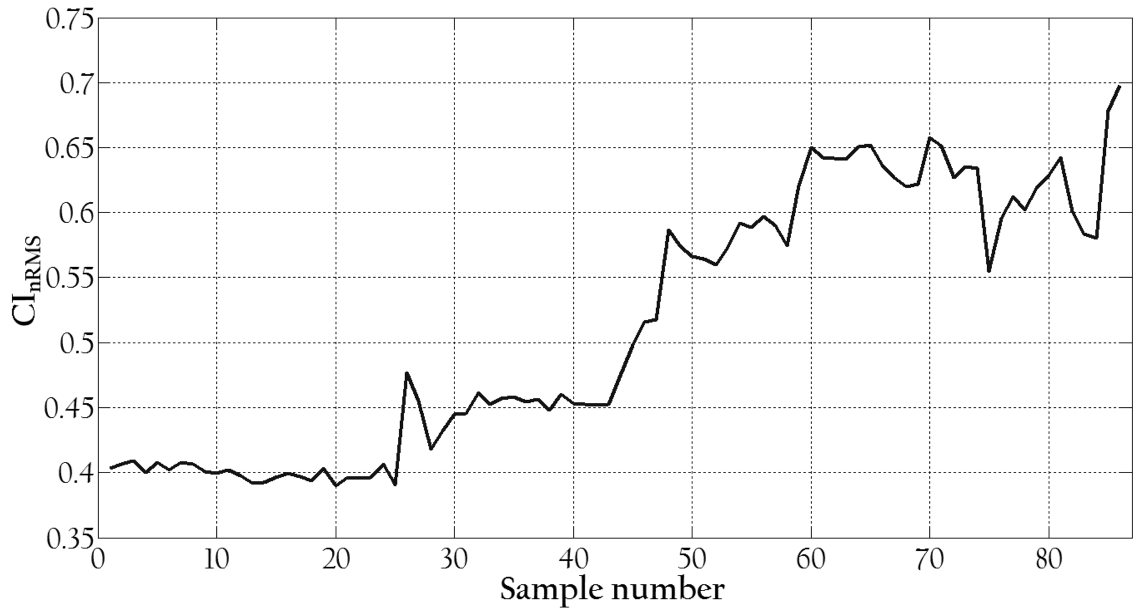

Figure 8.4 Variation of CI_{nRMS} for Dataset 1

Both the proposed CIs based on the CI_{RMS} are able to detect a gear fault early in the process and both increase in value throughout the fault progress. Therefore, in order to assess which of the proposed CI_{RMS}-based parameters (CI_{nRMS} based on a normalised signal or CI_{resRMS} based on a residual signal) is more robust, both metrics are compared by means of their absolute value gain. Both curves are shown in the form of an amplitude gain in order to show the normalised rate of change of the values of both parameters. The gain is calculated by dividing the values of a given CI by the mean of its values during the initial, healthy stage of the test (samples 1-20). The result of the comparison is shown in Figure 8.5. It can be observed that CI_{resRMS} reaches the gain of 7.5. At the same time the maximal gain of CI_{nRMS} is 1.85. Therefore it can be concluded that CI_{resRMS} is more robust of the two proposed CI_{RMS}-based parameters.

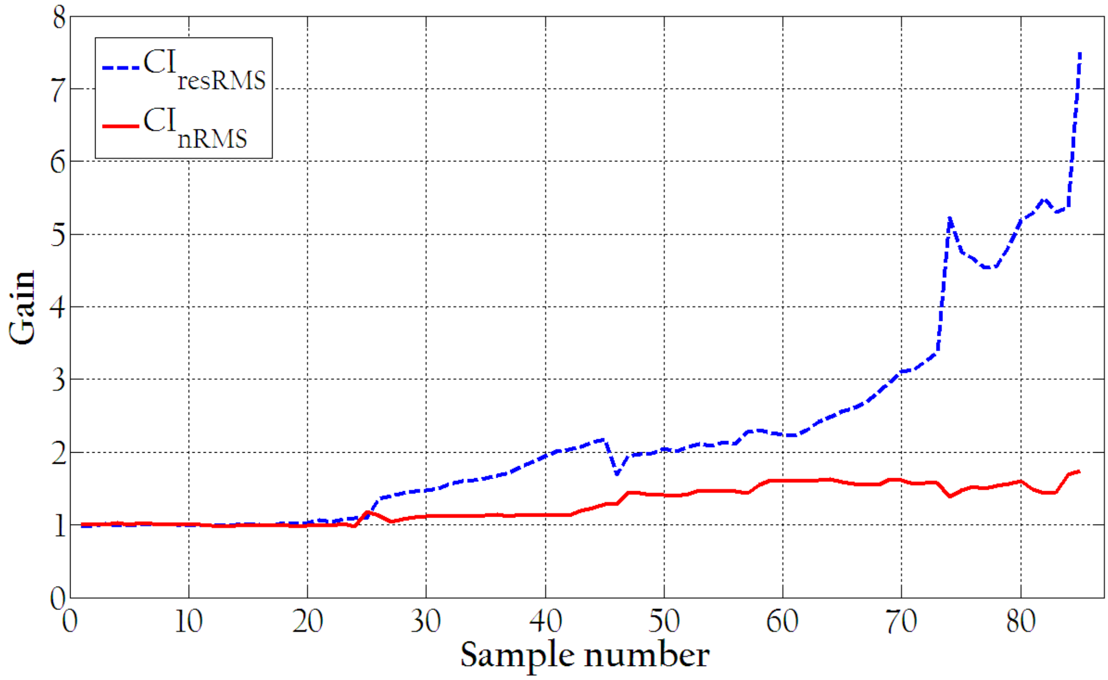

Figure 8.5 Gain of CI_{resRMS} and CI_{nRMS}

8.3.2 Dataset 2

The outcome of applying CI_{nRMS} on Dataset 2 is depicted in Figure 8.6. The values shown in the figure oscillate around a constant mean value until sample 6 after which a clear increase in the parameter's reading can be seen. This shows a big improvement over the previously discussed CIs where most of them were able to indicate a fault only for the last two samples. The behaviour of CI_{nRMS} on this Dataset proves that it is capable of indicating a gear fault in its early stages.

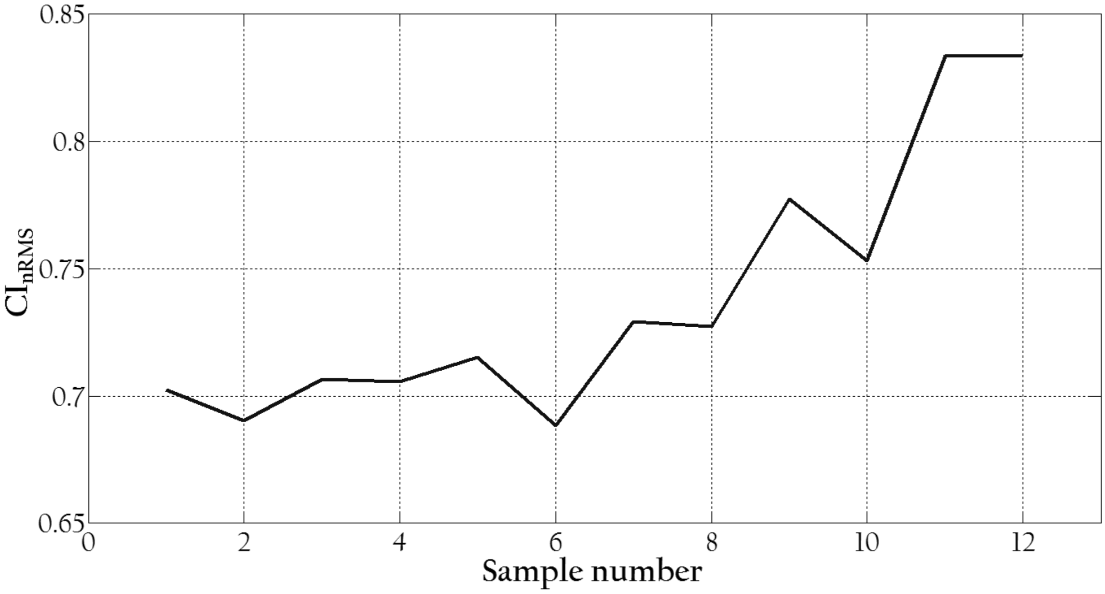

Figure 8.6 Variation of CI_{nRMS} for Dataset 2

8.3.3 Dataset 3

CI_{nRMS} was designed based on observation of the vibration characteristics of gearboxes developing a gear tooth failure. However, further research showed that CI_{nRMS} is also capable of detecting bearing related faults.

The result of applying CI_{nRMS} on the data samples from Dataset 3 is shown in Figure 8.7. CI_{nRMS} indicates the bearing fault with a similar trend to those of the previously discussed, robust CIs: CI_{Ku} and CI_{M6}. The outputs of the parameter oscillate about a constant value until sample 59, when a substantial increase is observed. This suggests that CI_{nRMS} is equally good at indicating a bearing fault compared with the results generated by the existing CIs.

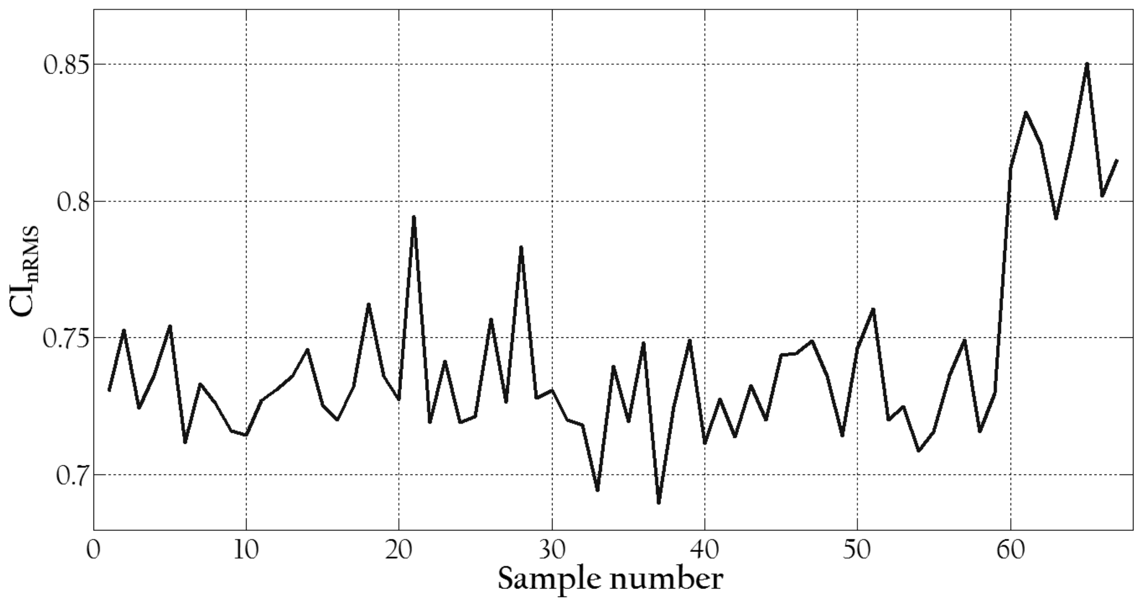

Figure 8.7 Variation of CI_{nRMS} for Dataset 3

8.4 Summary

This chapter proposed a further new CI called "normalised RMS" (CI_{nRMS}). An introduction showing the reasoning behind the development of this parameter was followed by a mathematical definition and instructions for calculation of this CI. The next part of the chapter included an illustration of the way the proposed technique works, based on a series of time-domain plots generated from Dataset 1. This explanation was the basis for analysis of the behaviour of CI_{nRMS} when applied on the same three Datasets that were used to determine the properties of the existing CIs. CI_{nRMS} presented a very consistent ability to detect gear faults and when applied on Dataset 1, it indicated the incipient fault very early, showing great improvement over the traditional CI_{RMS} approach. The fault in Dataset 2 was also successfully indicated by $CI_{nRMS,}$ with a consistently rising trend. In addition, the result from Dataset 3 showed that CI_{nRMS} is also capable of detecting a bearing fault and performed equally well when compared with the existing CIs.

CHAPTER 9

AMPLITUDE OF PROBABILITY DENSITY FUNCTION (APDF) STUDY

9.1 Introduction

All three previously proposed CIs were constructed by modifying of the existing techniques. This chapter introduces a CI based on a new concept that has not been exploited previously.

The results described in the earlier chapters support the assumption that the residual signal generated by a gearbox in a healthy condition is normally distributed. It has also been stated that any deviations from the normal distribution are likely to indicate deterioration of the condition of the meshing gears [195]. In addition to that the distribution of a signal that contains isolated peaks of large amplitude has longer tails which makes the whole distribution appear more peaked (this is what triggers a fault indication in the case of CI_{Ku}) [196], as depicted in Figure 9.1. Figure 9.1(a) shows a simulated normally distributed residual vibration signal generated by a healthy pair of gears: Figure 9.1(b) shows the same vibration signal, but with some impulsive content added to it by a periodic increase of the value, representing a sudden impact within the system simulating a fault in one of the gears. Figure 9.1(c-d) shows histograms of both signals. Both histograms are similar, the main difference appearing, in the tails which are wider in the faulty case due to the impulsive content within the signal. This, in turn, makes the whole distribution appear more sharp compared to the histogram of vibration signal generated by the healthy pair of gears.

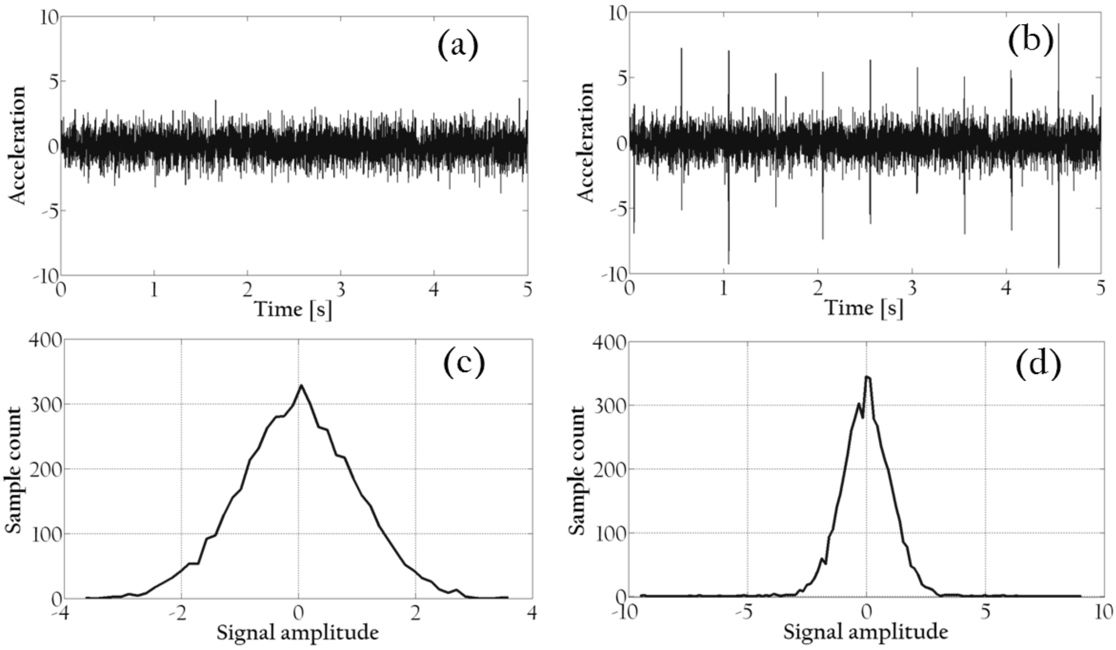

Figure 9.1 Normally distributed signal (a), normally distributed signal with added peaks (b), amplitude distribution of signal a (c) and b (d)

It was shown in Chapter 6 that as the fault changes from being localised to affecting adjacent teeth, the values of CI_{Ku} and CI_{CF} have a tendency to decrease. Therefore a new CI can be constructed which uses the information contained in the distribution of the signal, but in a different way to all the existing solutions. This is based on the idea of generating a normal Probability Density Function (PDF) for each residual vibration signal and recording its maximum value.

The reasoning is that, as a gear fault develops and progresses with time, new components start to appear within the signal and eventually cause a spreading of the amplitude distribution tails, as seen in Figure 9.1. This widening of the tails will always cause the maximum value of the normal PDF curve to decrease, since the area under the PDF curve of a normally distributed signal is always equal to 1.

Figure 9.2 shows two normal PDF curves calculated for the two signals shown in Figure 9.1(a) and Figure 9.1(b). Both PDF curves are defined in the range of $-3\sigma : +3\sigma$, where σ is the standard deviation. It can be seen that, in the case of a vibration response generated by faulty pair of gears, the widening of the distribution tails results in a decrease of the maximum point on the normal PDF curve compared to the corresponding curve for a healthy pair of gears.

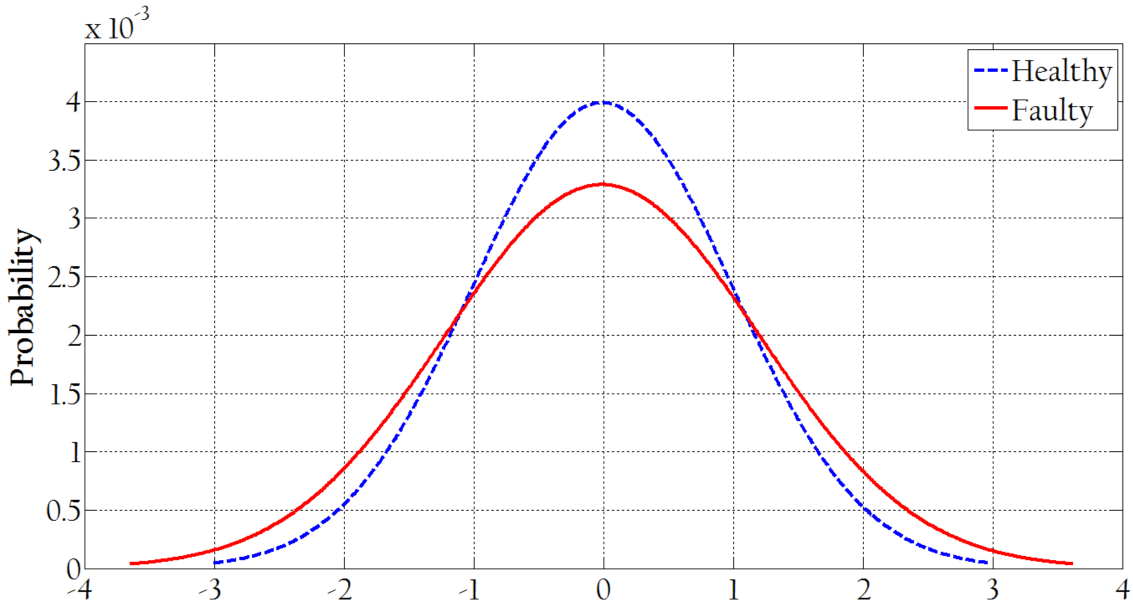

Figure 9.2 Normal PDF curve of signal in Figure 9.1(a) (dashed), of signal in Figure 9.1(b) (solid line)

9.2 Proposed CI

The proposed CI monitors changes in the "Amplitude of normal Probability Density Function" (CI_{APDF}) and for the residual vibration signal $x_{TSA}(t)$ can be mathematically described as:

$$CI_{APDF} = 1 - \max[f(x_{TSA})] \tag{9.1}$$

where $f(x_{TSA})$ is the Normal Probability Density Function given by [197]:

$$f(x_{TSA}) = \frac{1}{\sigma\sqrt{2\pi}} \cdot e^{-\frac{(x_{TSA}-\mu)^2}{2\sigma^2}} \tag{9.2}$$

where σ is the standard deviation of $x_{TSA}(t)$ and μ is the mean value of $x_{TSA}(t)$.

Since, as shown in the previous section, the development of a gear fault causes the maximum value of the normal PDF to decrease, this will result in a decreasing trend for CI_{APDF} as a function of gear fault development. In order to track the fault progress in the form of an increasing trend, the absolute maximum of the normal distribution is subtracted from the unity.

The process steps that need to be followed in order to calculate the value of CI_{APDF} are:

i. Compute the Time Synchronous Averaged (TSA) signal from the measured vibration signal;

ii. Carry out a Discrete Fourier Transform (DFT) on the TSA signal;

iii. Remove all components related to the shaft speed, the GMF and their respective harmonics from the spectrum (thus creating a residual spectrum);

iv. Perform an Inverse DFT on the residual spectrum to generate the residual signal in the time domain.

v. Calculation of normal PDF using Eq. (9.2).

vi. Calculation of the CI_{APDF} using Eq. (9.1).

9.3 Results

9.3.1 Dataset 1

Figure 9.3 presents a comparison of a chronological series of PDF curves generated from sample signals from Dataset 1 for the purpose of calculating the CI_{APDF}. This sequence of the PDF curves from real data support the theoretical assumptions regarding the behaviour of the maximum point of the curve - as the gear fault develops, the tails of the signal's amplitude distribution broaden forcing the value of the central point of the PDF curve to decrease.

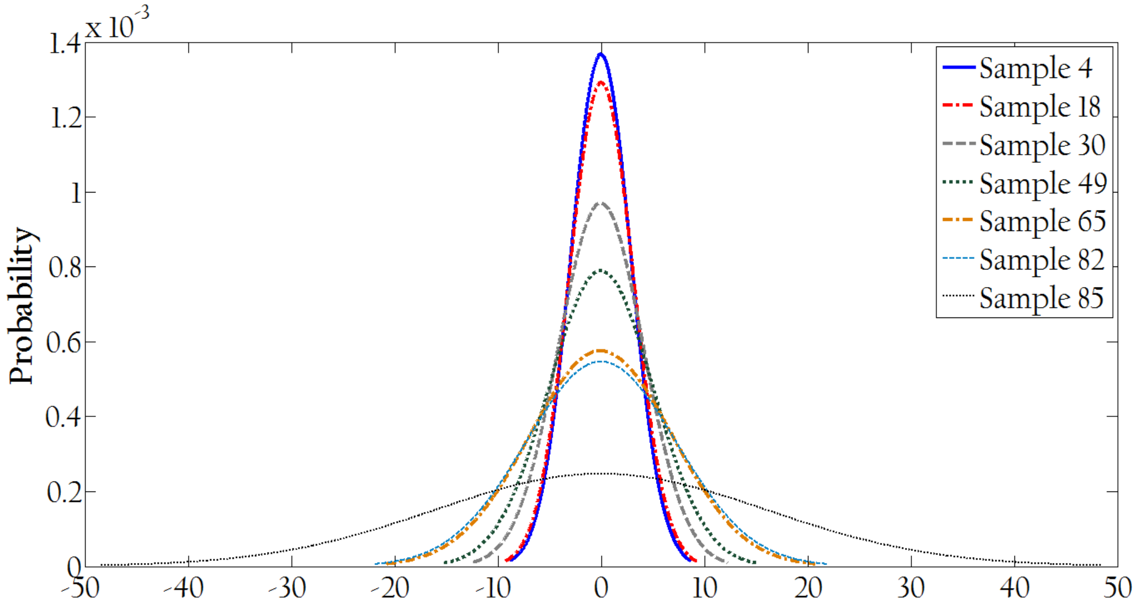

Figure 9.3 Normal PDF curves of Dataset 1 samples as per legend

The result of applying the CI_{APDF} to Dataset 1 is shown in Figure 9.4. The curve shows a continuously rising trend which is correctly indicating the development of the gear fault. The increase in the values begins as early as at sample 20 and continues to rise until the end of the test. This result shows that CI_{APDF} is capable of increasing in value in response to a worsening gear condition.

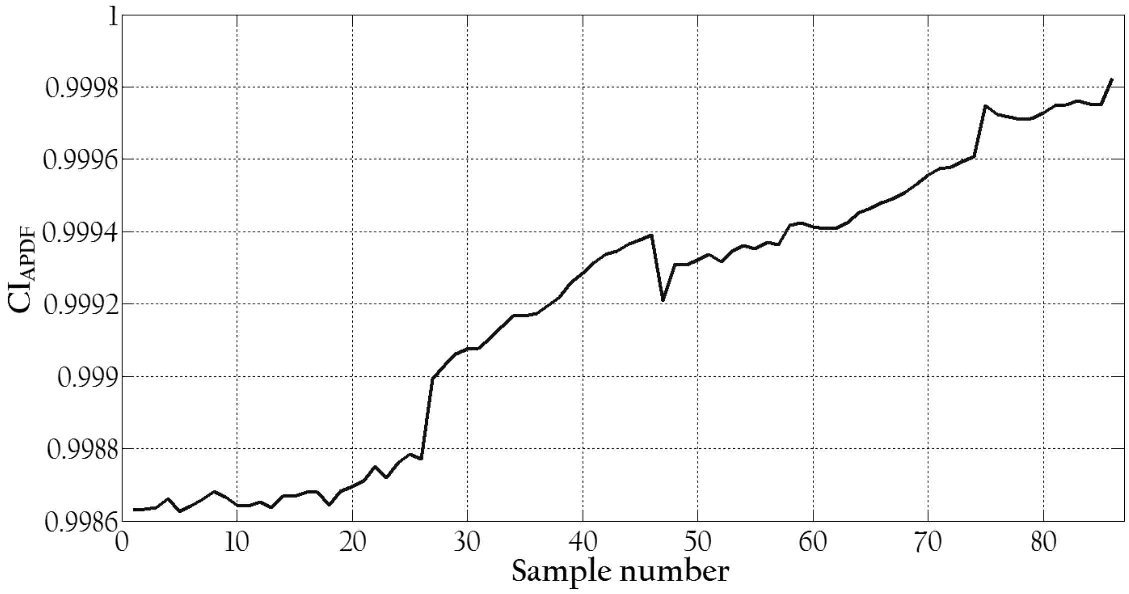

Figure 9.4 Variation of CI_{APDF} for Dataset 1

9.3.2 Dataset 2

The result of applying the CI_{APDF} parameter to vibration signals from Dataset 2 is depicted in Figure 9.5. The first four samples show a slight decrease in value, but from sample 5 the trend is rising, which continues to do until the end of the test. In particular the last two samples show large increase in the CI_{APDF} output consistent with the corresponding results obtained from the previously discussed parameters.

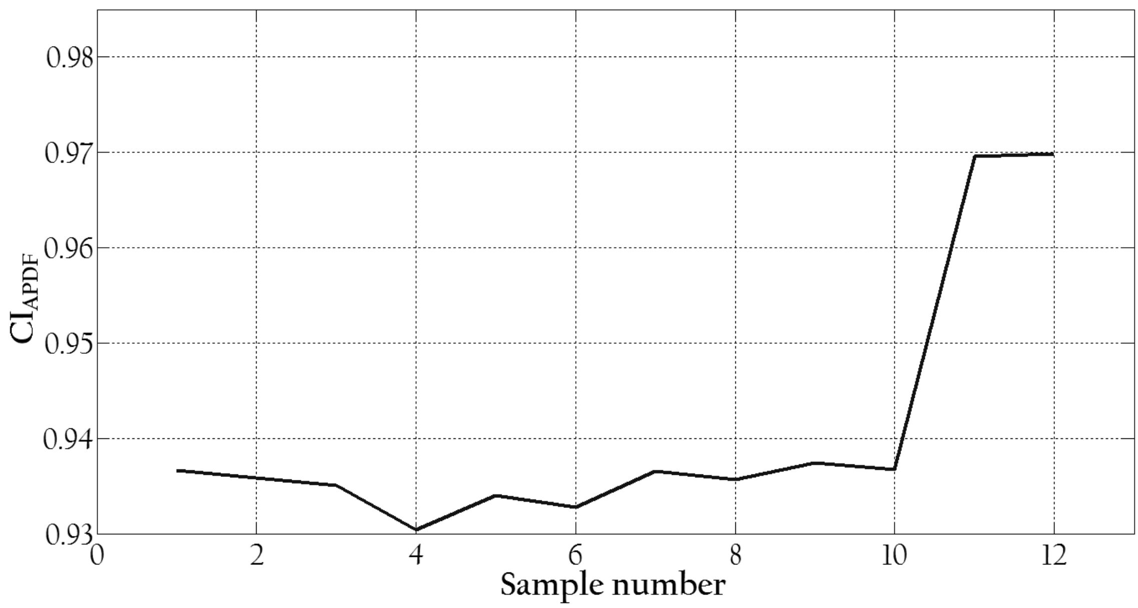

Figure 9.5 Variation of CI_{APDF} for Dataset 2

9.3.3 Dataset 3

The design of CI_{APDF} focused on the influence of the peaks generated by a faulty gear tooth on the amplitude distribution function. However, further research showed that CI_{APDF} is similarly capable of detecting a bearing fault based on the same principle. Figure 9.6 shows the result of applying CI_{APDF} to vibration data from Dataset 3. It can be seen that although the overall trend of the condition indicator is rising for the whole duration of the test, the changes are rather subtle. The reason lies in the character of the vibration signals recorded by the accelerometer. Figures 9.7 and 9.8 show two time domain signals generated from samples 1 and 62 respectively. The difference between the response to the two samples recorded by some of the previously discussed CIs was large, yet CI_{APDF} did not produce such a contrast. The reason for this can be explained by comparison of both figures. One can see that even though the signal in Figure 9.8 contains more higher-amplitude events, their amplitude is nor particularly high. Thus the influence of the impulses on the standard deviation of the signal – used to calculate the PDF - is small and, as a result both standard deviation values are similar, and the difference between the PDF curves of both signals becomes almost insignificant. This is evident from the scale of the y-axis in Figure 9.6 and the high variance of the trend.

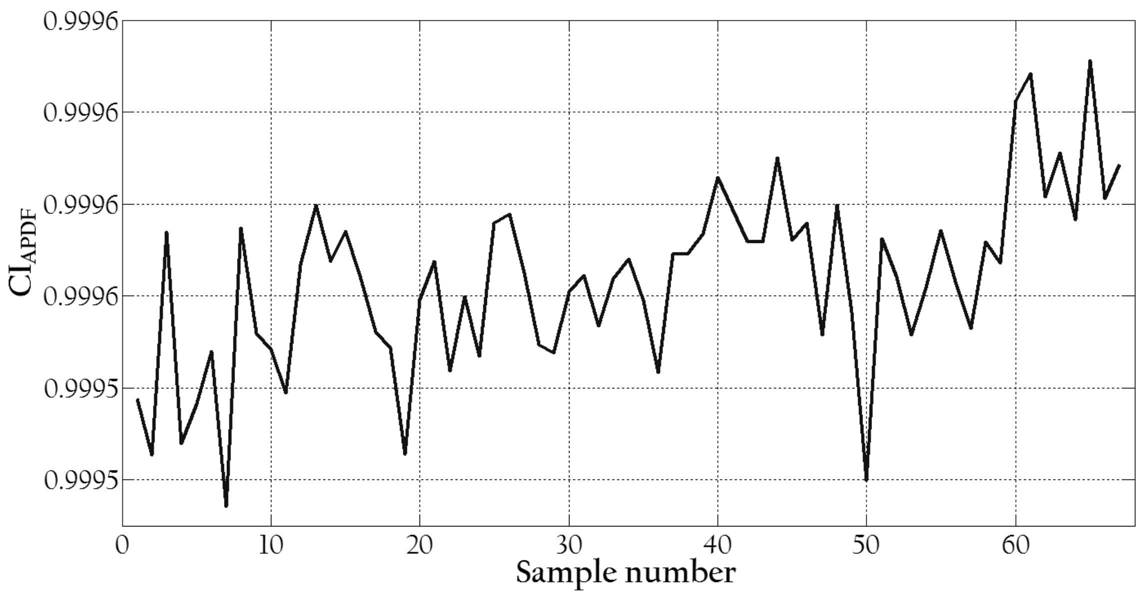

Figure 9.6 Variation of CI_{APDF} for Dataset 3

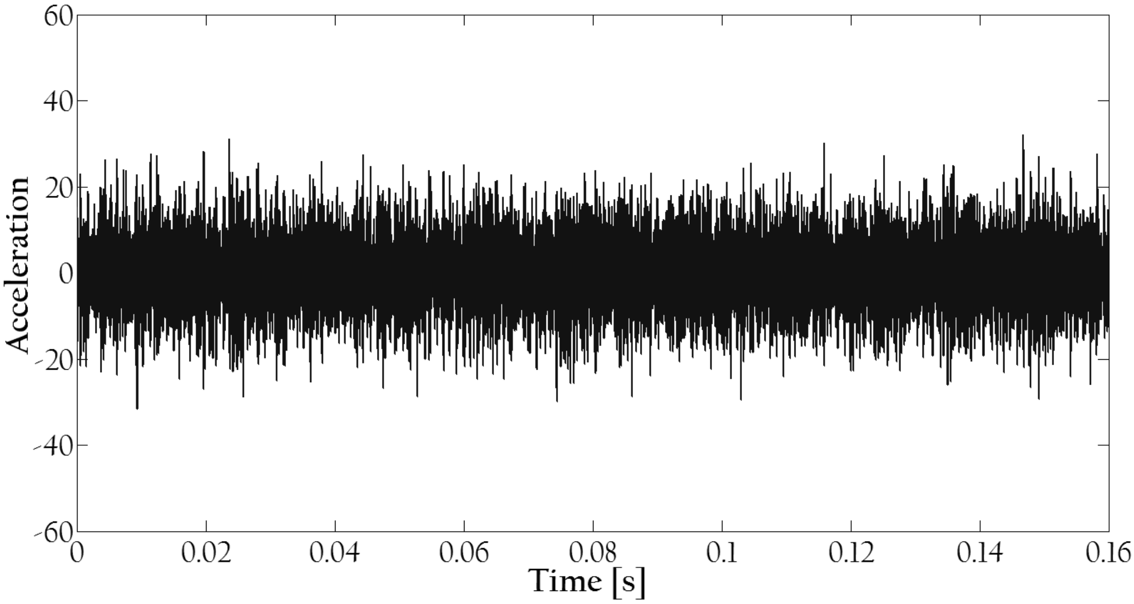

Figure 9.7 Vibration signal from sample 1 in Dataset 3

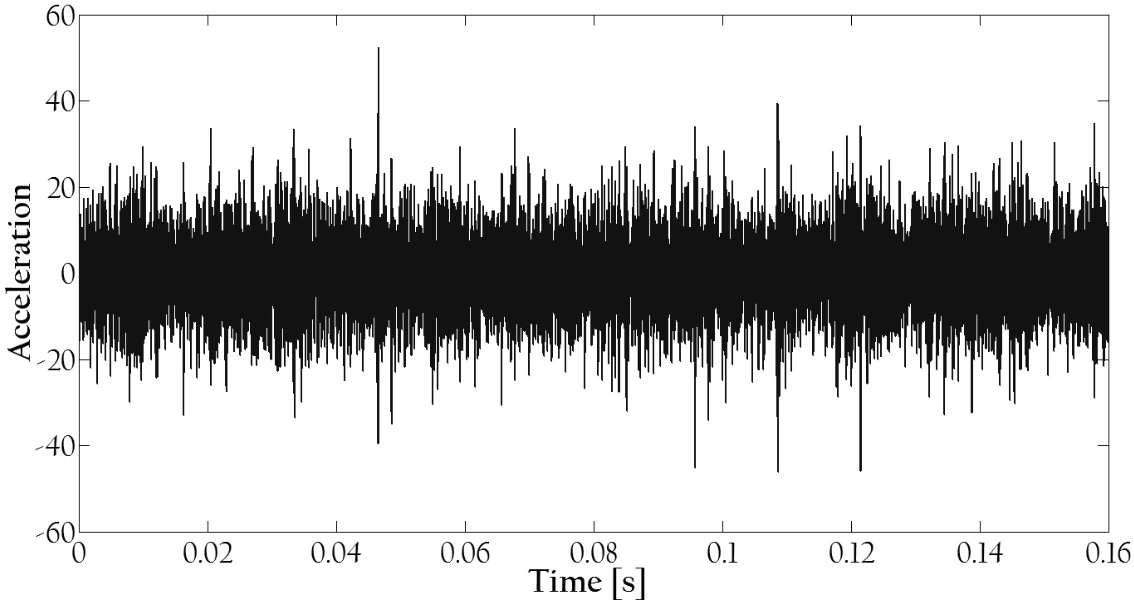

Figure 9.8 Vibration signal from sample 62 in Dataset 3

9.4 Summary

This Chapter introduced a new CI called "Amplitude of normal Probability Density Function" (CI_{APDF}). The Chapter began with an introduction explaining the concept behind the development of this parameter, followed by a mathematical definition and instructions for the proper computation of the parameter value. This was followed by an explanation of how the proposed technique responds to a gear fault based on a series of PDF curves generated from a number of chronologically arranged samples from Dataset 1. Presentation of the working principles of the CI was followed by testing of CI_{APDF} on the available datasets. Changes in the maximum point of the normal Probability Density Function curve of a given sample was demonstrated to be a robust indication of gear and bearing faults. The results obtained for Dataset 1 gave a very consistent and convincing indication of the gear fault progress. The indicator did not suffer from any transient decrease and first indicated the fault shortly after the degradation process began. The values of CI_{APDF} in Dataset 3 showed less-steep, yet consistently rising trend. The outcome of applying CI_{APDF} to the available datasets showed that it is not only capable of detecting an incipient gear tooth fault, but also can be used as a bearing fault indicator.

CHAPTER 10

DEVIATION FROM NORMAL DISTRIBUTION (DND) STUDY

10.1 Introduction

Chapter 9 introduced the CI_{APDF} where change in the value of the maximum point of a normal Probability Density Function curve was used as a tool for assessing the condition of a monitored gearbox. This chapter introduces another CI, which works on a similar basis. However, instead of measuring the peak of the normal PDF curve, it measures the deviation of the actual signal from a theoretically-simulated normally distributed signal. The technique used to determine the degree of deviation from a normal distribution is the Normal Probability Plot (NPP). The NPP is a type of Quantile-Quantile plot (QQ plot), which compares the quantiles of the observed population with the quantiles of a theoretical population [199]. In the case of the NPP, the values observed from the distribution of the measured vibration signal are compared with the same number of samples from a corresponding was normally distributed dataset. If the distribution under consideration is normal then the majority of points on the NPP would fall on a straight line. Regular deviations from linearity, however, indicate non-normality [200]. Deterioration of a gear condition will usually result in some impulsive events appearing in the residual signal, which would otherwise be normally distributed for the healthy case. Those impulses increase the variance of the signal, and lead to deviation from the normal distribution. The gradient of the NPP is related to the amplitude of the normal PDF curve such that signals with a smaller range of amplitudes result in a higher gradient, and the larger the amplitude range, the smaller the gradient will be. Typical NPPs generated from a vibration signal from a healthy and damaged pair of meshing gears are shown in Figures 10.1 and 10.2 respectively.

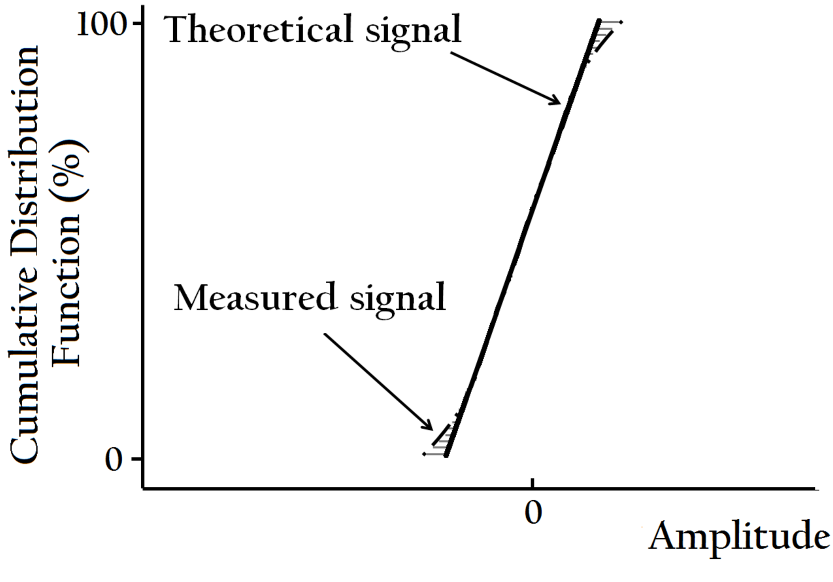

Figure 10.1 NPP of vibration signal generated by a healthy pair of gears

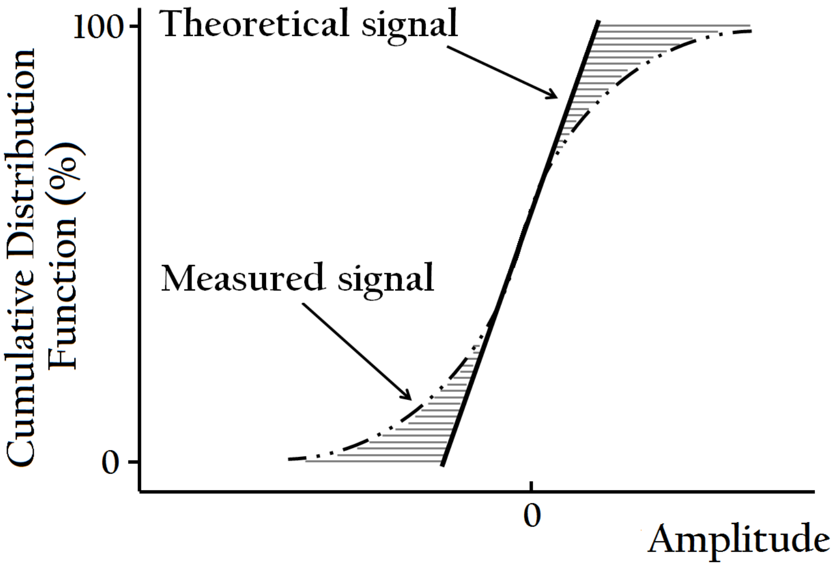

Figure 10.2 NPP of vibration signal generated by a faulty pair of gears

10.2 Proposed CI

It is expected that the difference between the two lines on the NPP will be very small for a healthy gear condition (normally distributed residual vibration signal) and increase in the presence of a fault as the residual vibration signal deviates from a normal distribution. Hence the value of the proposed indicator is calculated as the normalised cumulative summation of the absolute difference between the two lines at every data point (shown as shaded area in Figures 10.1 and 10.2). Normalisation is performed by dividing the cumulative sum by the number of data points used in the summation. For this reason, the proposed CI is called “Deviation from Normal Distribution” (CI_{DND}) and can be mathematically represented as:

$$CI_{DND} = \frac{\sum_{i=1}^{N} \left| P_{a,i} - P_{t,i} \right|}{N} \tag{10.1}$$

where N is the number of data points in the signal, $P_{a,i}$ is the value of the actual curve at the i-th data point, $P_{t,i}$ is the value of the theoretical curve at the i-th data point. The theoretical distribution is derived from the actual signal’s mean and the standard deviation values. Once the residual signal is derived the NPP can be generated and the area between the two curves calculated using Eq. 10.1.

10.3 Results

10.3.1 Dataset 1

In order to demonstrate CI_{DND} a few typical NPPs from Dataset 1 are examined. Figures 10.3 - 10.9 present a comparison of some chronologically arranged NPPs generated from sample signals from the Dataset.

The normal probability plot of sample 1 shows two curves in near-perfect alignment which supports the assumption that the residual signal of a healthy gear has a normal amplitude distribution. The dashed line is hardly visible indicating that the vibration of the healthy gearbox is normally distributed (Figure 10.3). This situation persists until sample 18 when a small deviation can be observed between the top ends of the two curves (Figure 10.4). By sample 24 both tails of the tested distribution deviate from the normal line. As in most cases, the deviation begins at the tails of the distribution corresponding to changes in the distribution outliers (Figure 10.5). The NPP of sample 45 shows a much larger deviation compared to the previous cases as the gradient at the tails of the cumulative distribution curve decreases (Figure 10.6). Samples 61 and 78 show further deviation from the normal distribution (Figures 10.7 and 10.8) with a reduction in the gradient over the entire distribution, and the probability plot calculated on sample 85 (last recorded sample before the end of the test) show a large reduction in both the gradient and the deviation of the tails from a normal distribution (Figure 10.9).

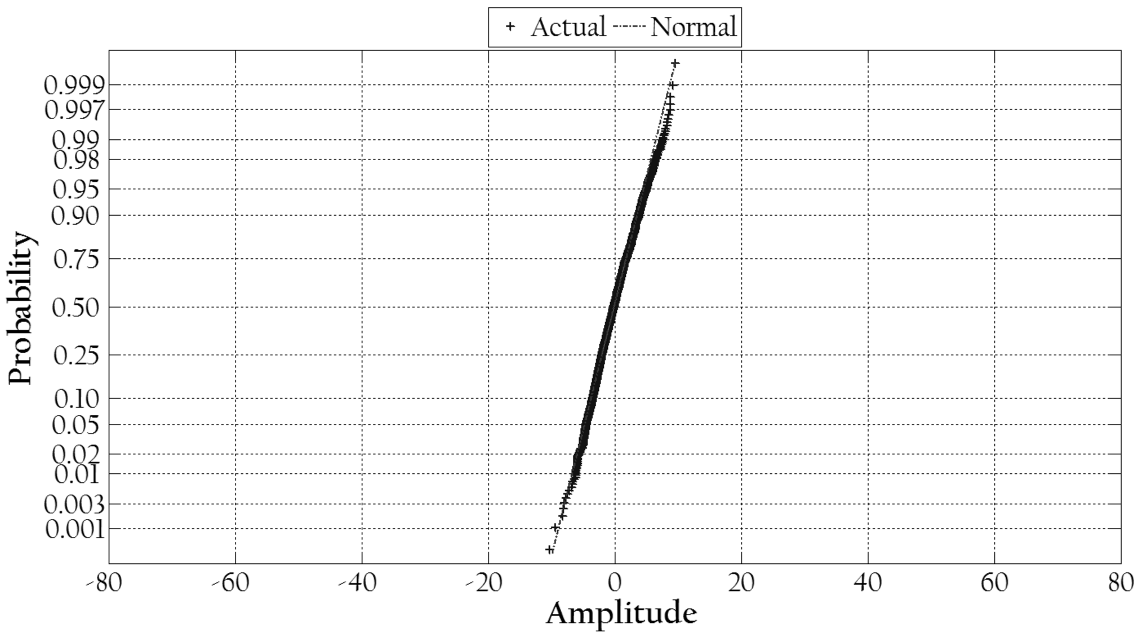

Figure 10.3 NPP of sample 1 in Dataset 1

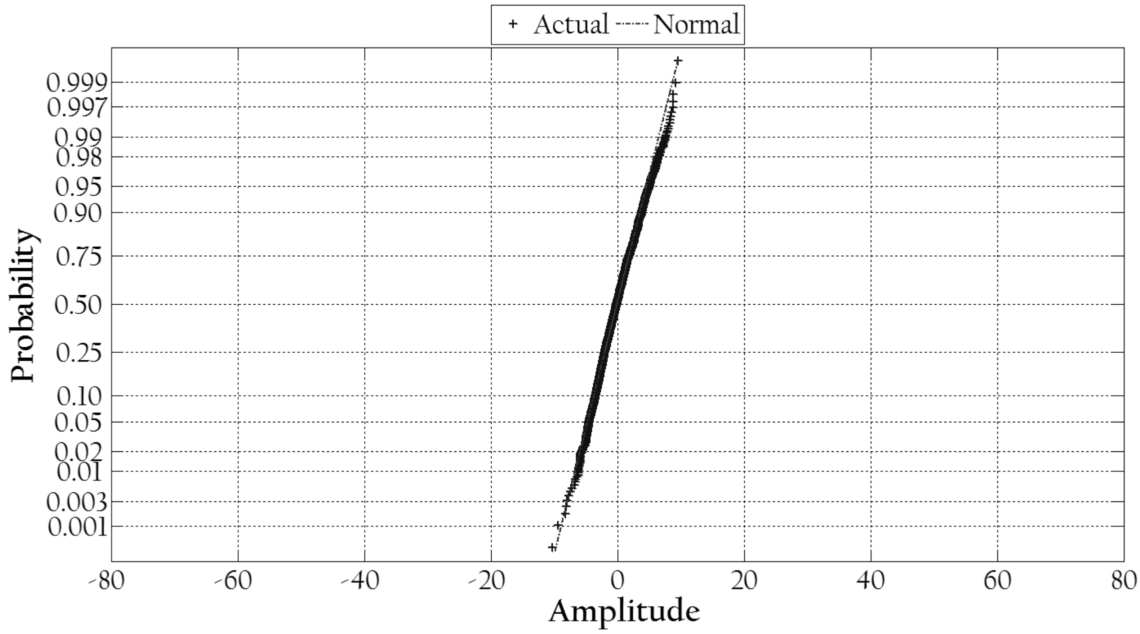

Figure 10.4 NPP of sample 18 in Dataset 1

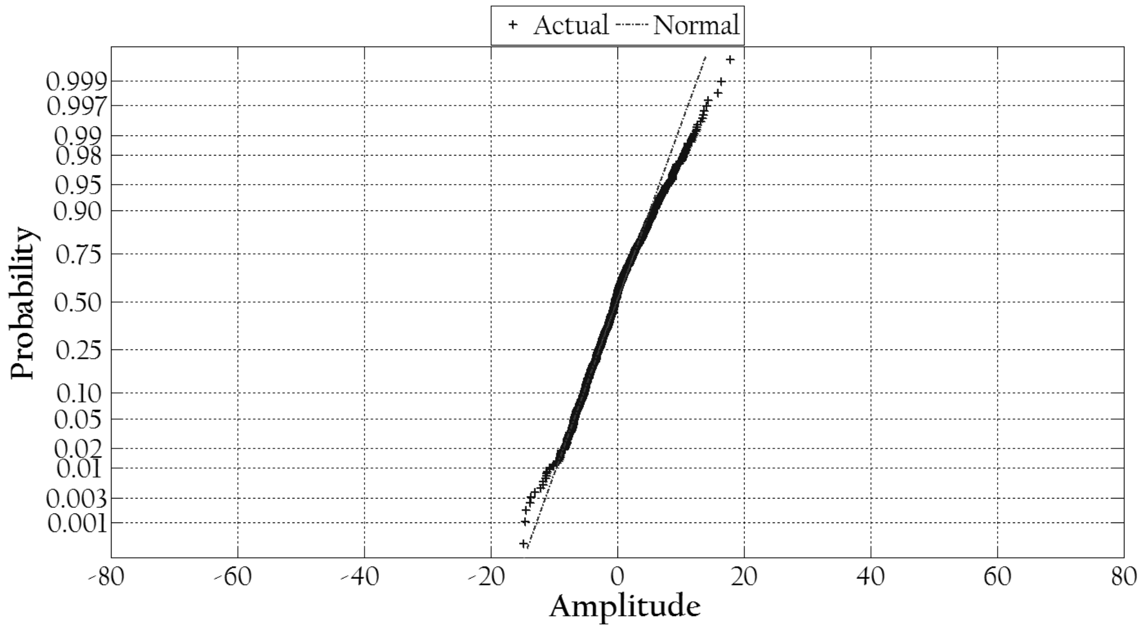

Figure 10.5 NPP of sample 24 in Dataset 1

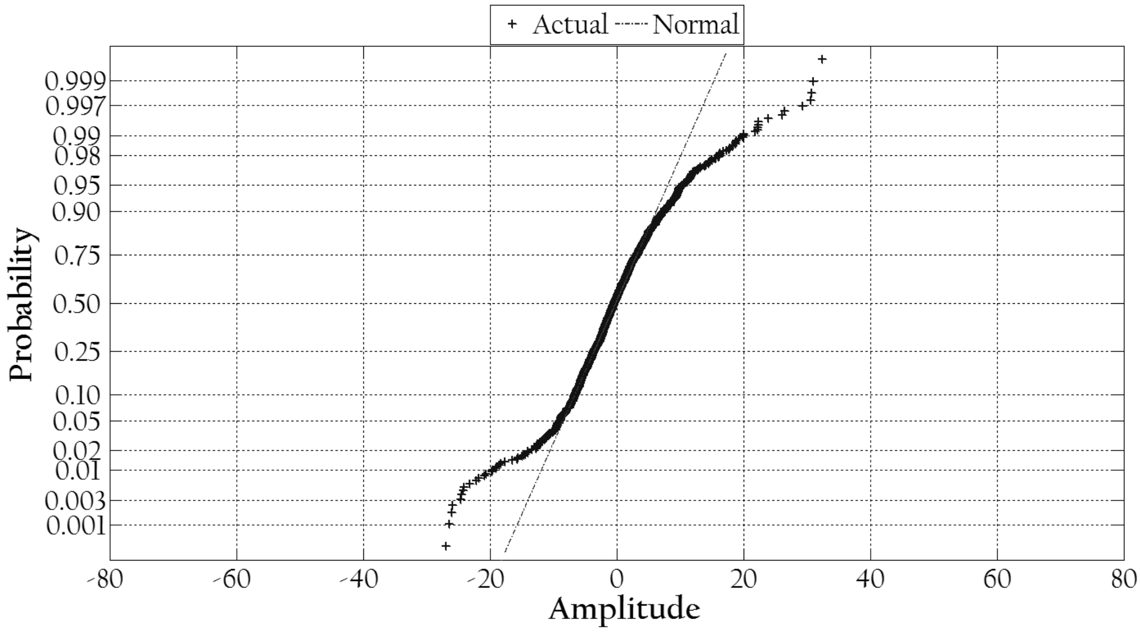

Figure 10.6 NPP of sample 45 in Dataset 1

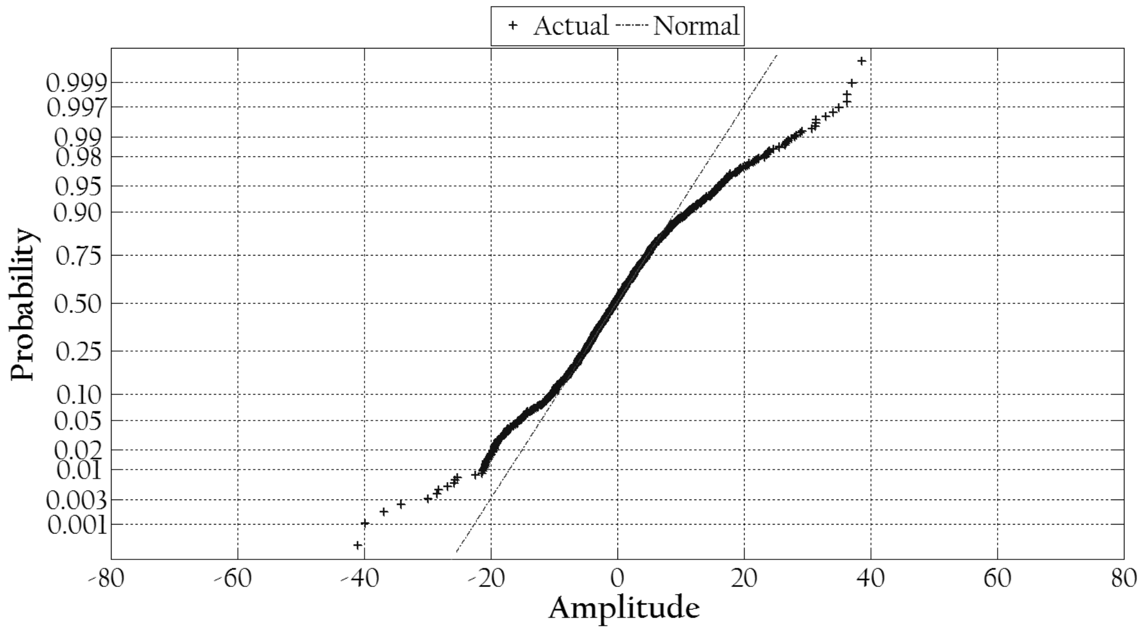

Figure 10.7 NPP of sample 61 in Dataset 1

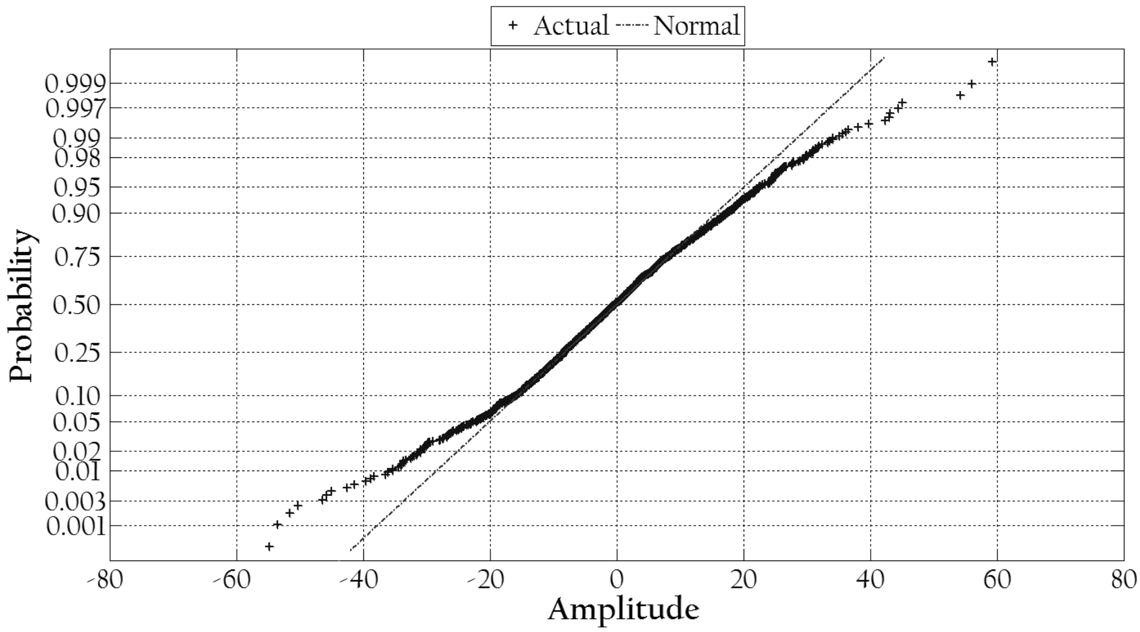

Figure 10.8 NPP of sample 78 in Dataset 1

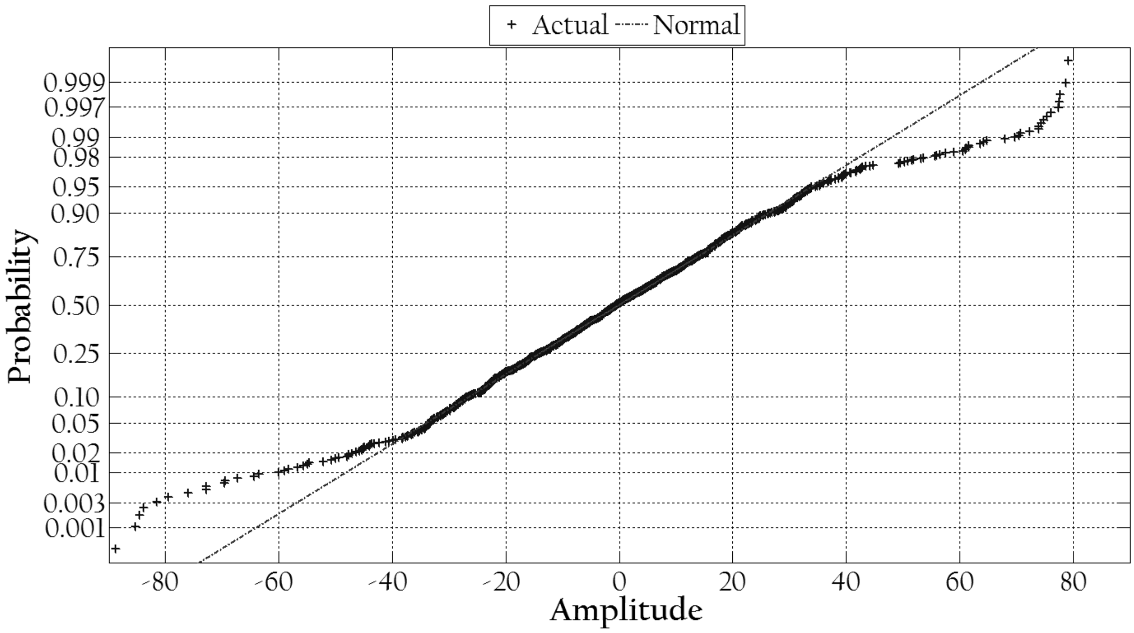

Figure 10.9 NPP of sample 85 in Dataset 1

Based on the comparison between the figures shown above it is apparent that, except for the early stages of the test where the gears are healthy, the distribution of the residual vibration signal from a faulty pair of gears is not normally distributed. The amount of deviation from the normal distribution is dependent on the condition of the gear tooth. The more severe the damage becomes, the bigger deviation can be observed on the NPP curve, hence the bigger the area between the two curves (increase in CI_{DND} value).

In order to quantify this observation, CI_{DND} has been applied on all 85 samples and the obtained result can be seen in Figure 10.10. As one can see, the global trend of CI_{DND} is rising for the entire duration of the gear health deterioration process. In addition to that the increase in the values begins very early in the test (sample 18).

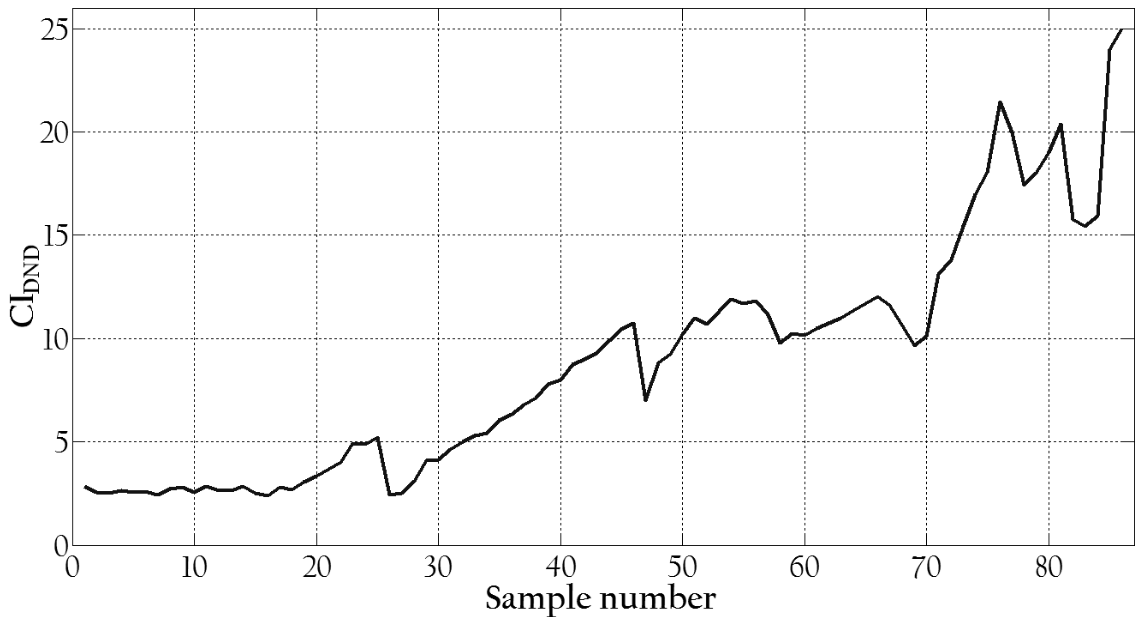

Figure 10.10 Variation of CI_{DND} for Dataset 1

10.3.2 Dataset 2

The result of applying CI_{DND} on Dataset 2 is presented in Figure 10.11. The values of the condition indicator show slightly decreasing trend right until sample 8 when an increase is seen. The increase in the CI_{DND} values for the last two samples is very clear indicating a large deterioration of the gear condition, however the rising trend from sample 8 provides an early indication of the fault.

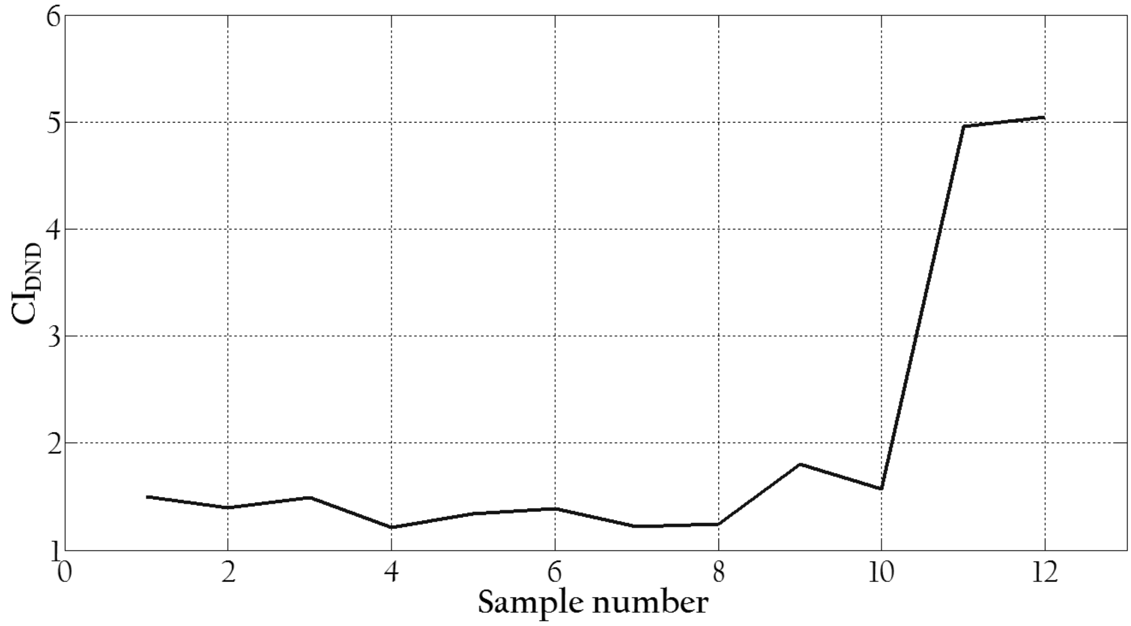

Figure 10.11 Variation of CI_{DND} for Dataset 2

10.3.3 Dataset 3

Although the CI_{DND} was primarily designed to detect gear faults, based on the assumption that the residual vibration signal of a healthy gear pair has a normal amplitude distribution, the parameter was found to be capable of detecting a bearing fault equally well, when compared to the existing CIs.

Figure 10.12 shows the effect of applying CI_{DND} to Dataset 3. The values of CI_{DND} oscillate around a constant value until sample 59 when a substantial step increase in the parameter's output takes place. This is likely to have been caused by an increase in the outliers of the signals amplitude distribution, as a result of a deterioration of the bearing outer race condition. This result from a bearing fault suggests that the approach behind the CI_{DND} is suitable not only for detecting gear defects in the very early stages of the fault development process, but also proves capable of detecting bearing outer race defects.

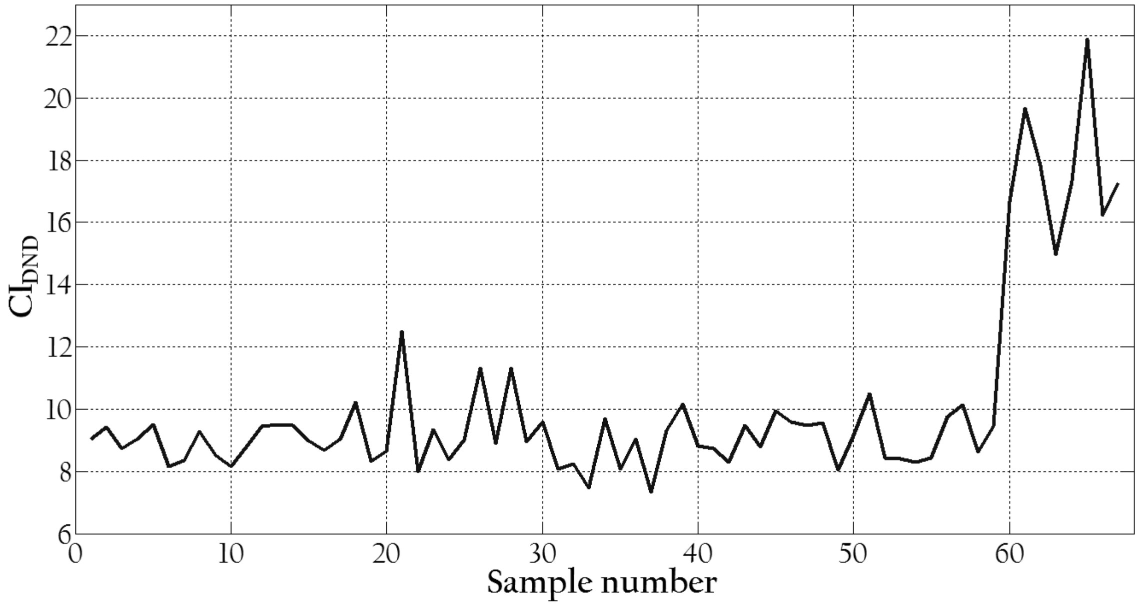

Figure 10.12 Variation of CI_{DND} for Dataset 3

10.4 Summary

This Chapter introduced a fifth new CI. The CI is called “Deviation from Normal Distribution“(CI_{DND}) and works in a similar way to that utilised by CI_{FM4} that is it detects the degree of deviation from the residual signal’s normal distribution. The introduction to the Chapter discussed the concept of the proposed CI, followed by a mathematical definition and instructions for the appropriate computation of the parameter values. The technique was then tested on the same three Datasets that were used to assess the robustness of the existing CIs. In both gear fault cases CI_{DND} demonstrated a strong ability to indicate gear faults. In the case of the bearing outer race fault, CI_{DND} presented similar efficiency the fault indication when compared with the existing CIs. The results of the analysis of Dataset 3 showed a clear reaction of the indicator to deterioration of the bearing outer race. Based on the results it can be stated that CI_{DND} is capable of properly indicating not only gear related faults, but also faults developing in the outer race of a bearing.

The next chapter introduces the concept of integrating a data fusion model with the output of each of the proposed CIs and examines the behaviour of such a scheme when applied to the three datasets. In addition, sensitivity of the proposed data-fusion model is tested by comparing the model’s output when applied to both the existing CIs and the proposed new CIs.

CHAPTER 11

DATA FUSION

Section 3.4 outlined a number of advantages of fusing the data coming from multiple information sources. Suc data fusion processing can take place on a number of different levels and this chapter examines three different approaches and tests their properties on the 3 Datasets available in this study.

11.1 Feature fusion level

Extracting features (Condition Indicator values) from a vibration signal and simply combining the information obtained from each feature is the principle behind feature fusion level. In order to perform a successful fusion of the information provided by all the newly proposed CIs, a common fault criterion has to be established and the values of all the CIs have to be combined to create one, robust indication of fault development.

The process of designing a feature level data fusion model involved testing a number of different model configurations. In-depth analysis of the results and proper implementation of suggested improvements, led to selection of the three most consistent approaches. These are described in the following subsections.

11.1.1 Data fusion model v1

Description

Figure 11.13 contains a flowchart that explains the first of the described data fusion approaches. The step at the top of the diagram involves extracting the *i*-th vibration signal sample and calculating a set of proposed CIs, that is CI_{ASB*}, CI_{nRMS}, CI_{resRMS}, CI_{APDF} and CI_{DND} for that sample. Each of the calculated CI values is tested against the first condition of the model, which examines if the current value of the CI exceeds the value of the same CI calculated in the preceding loop iteration. If none of the CIs satisfy the first condition, then the loop proceeds to the next iteration and the value of the Cumulative Condition Indicator of the data fusion model v1 (CCI v1), which constitutes the output of the loop, remains constant. However, if the value of any of the CIs satisfies the first condition, then the algorithm proceeds to the next step which involves adding the values of all the CIs that satisfy the first statement. The newly calculated value constitutes the current value of the CCI v1. After the summation process the second condition of the model compares the current CCI v1 value with the value that has been generated in the preceding loop iteration. If the current CCI v1 value is lower than the value of CCI v1 generated in any of the preceding loop iterations, then

CCI v1 retains its value from the previous cycle. If, however, the current CCI v1 value is higher than the CCI v1 value from the previous cycle, then the current value is stored.

The first condition is set up to ignore CI values in the case when its trend is falling. The reason for the second statement is that if the values of the CCI v1 do not exceed the values recorded to that point this indicates that the condition of the monitored component has not deteriorated, and the final CCI v1 values should remain at the same level. On the other hand, if CCI v1 exceeds the previous value this corresponds to the condition of the monitored component deteriorating and the output value of the CI should increase.

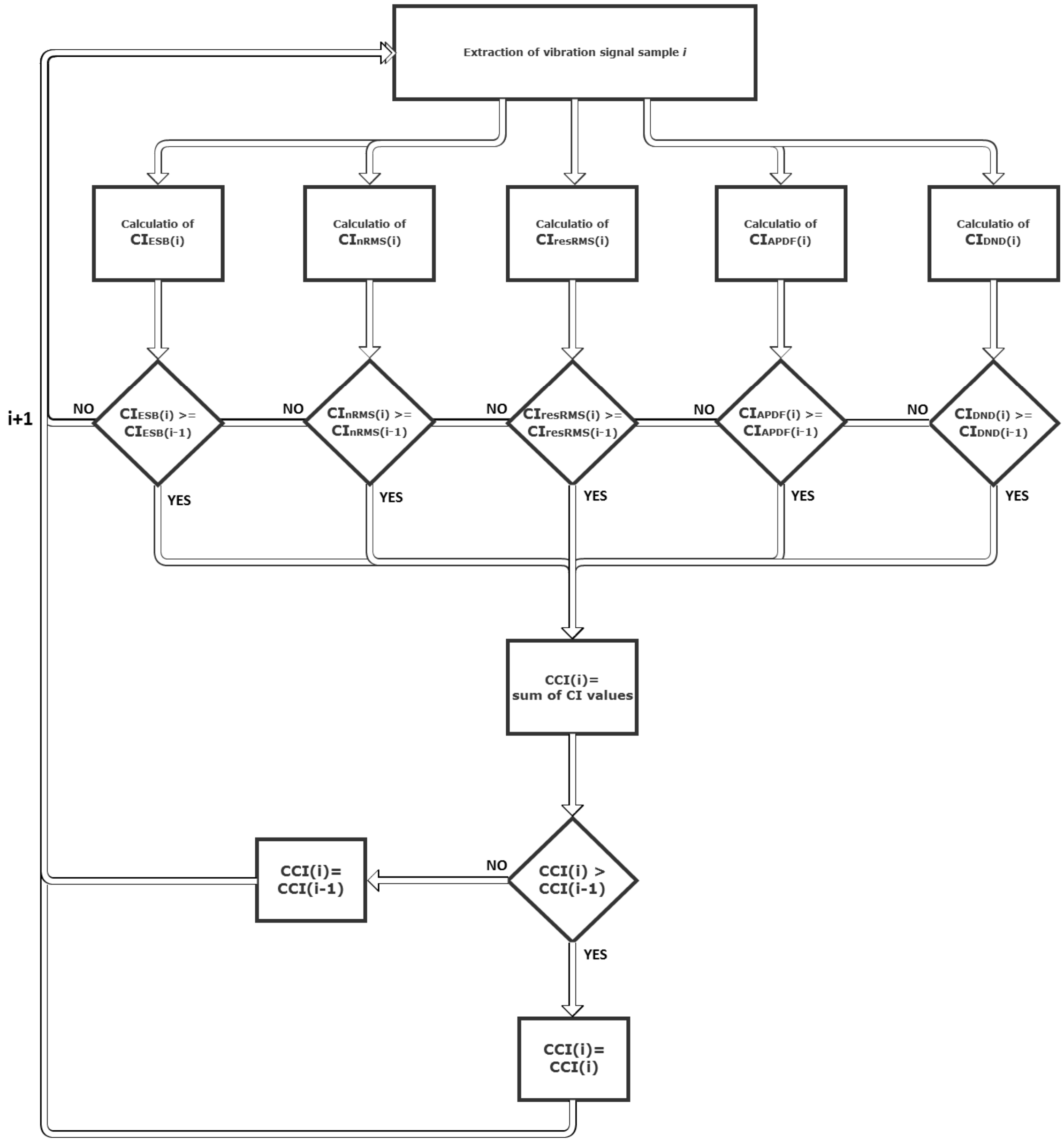

Figure 11.13 Data fusion model v1

Results

Dataset 1

Figure 11.14 shows the result generated by applying CCI v1 to Dataset 1. The values start to increase from the beginning of the test. Between samples 12 and 18 the values remain constant which indicates that one of the two model conditions was not satisfied. After that the trend rises again and continues to do so until the end of the test.

Dataset 2

The CCI v1 values remain constant until sample 6 when the reaction from the model begins to indicate a fault. Sequentially the values of the parameter rise monotonically, with two steps in the trend, until the end of the test(Figure 11.15).

Dataset 3

The shape of the curve in Figure 11.16, obtained from CCI v1 applied to Dataset 3, shows an almost linearly rising trend for the entire test.

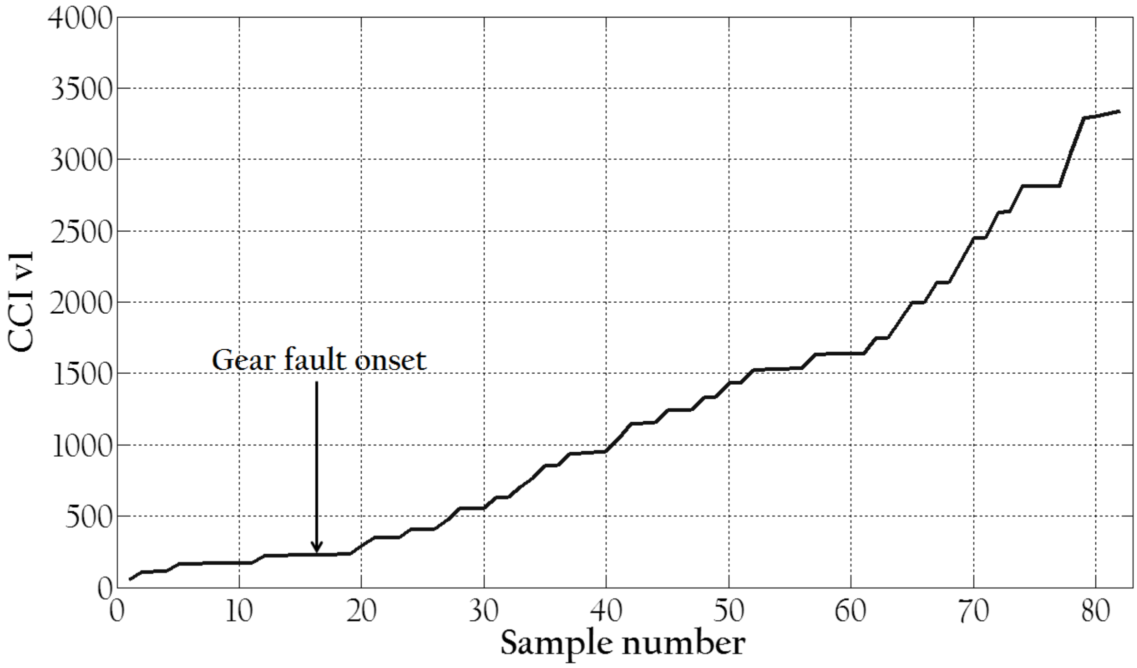

Figure 11.14 Variation of data fusion model v1 for Dataset 1

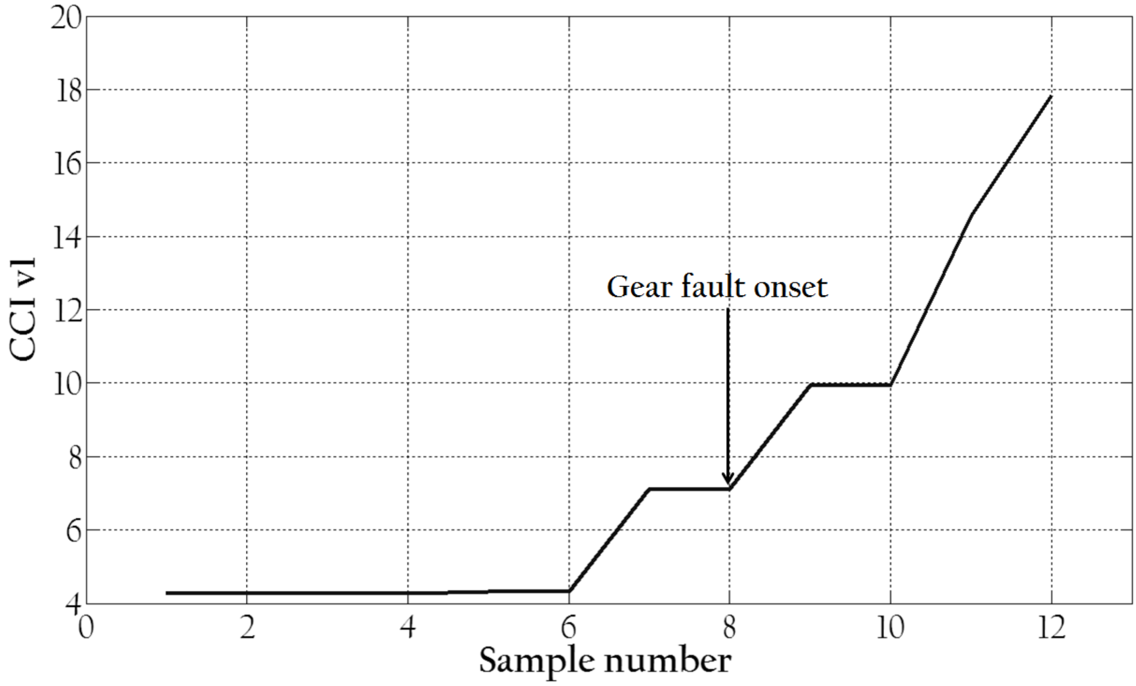

Figure 11.15 Variation of data fusion model v1 for Dataset 2

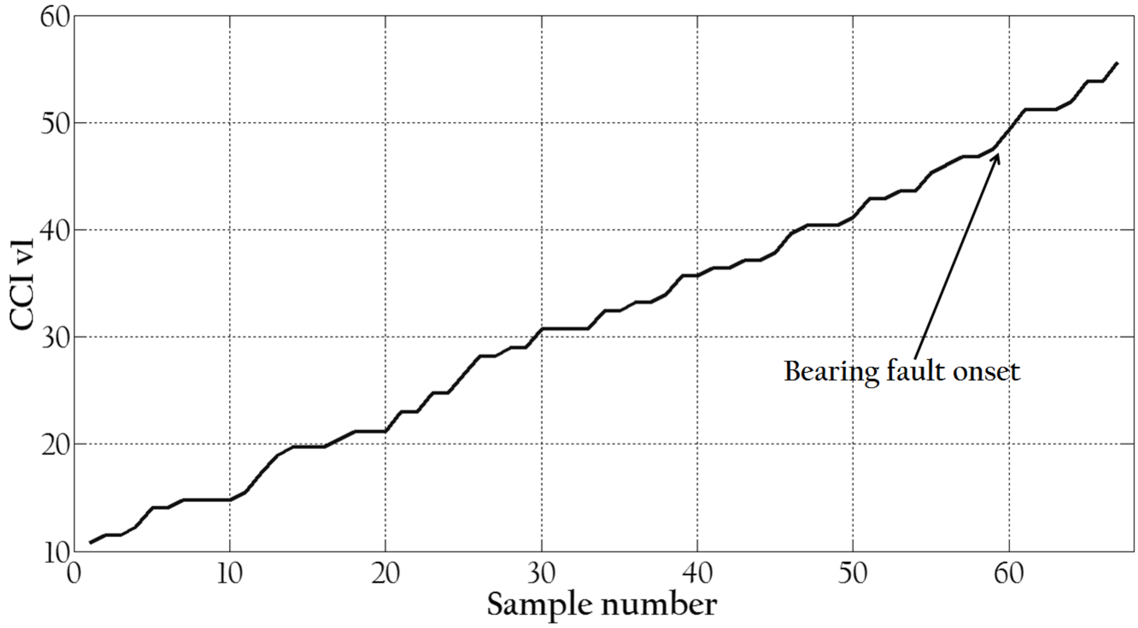

Figure 11.16 Variation of data fusion model v1 for Dataset 3

Observations

The results of CCI v1 obtained for Dataset 3 expose the weakness of the data fusion model v1: it responds to non-significant, single-sample increases in the CI value, which would have not been considered a fault indication when analysed manually. For all the datasets, the values of CCI v1 start to increase too early; increase in value from the beginning of the test and are too sensitive to any increase in the value of the CIs.

Such a data fusion model would lead to a very high number of false alarms and it would be impossible to distinguish between a fault indication and random, small, insignificant value variations of the proposed CIs. Some improvements need to be incorporated in order to make CCI responsive to the actual indication of a gear fault whlist decreasing its sensitivity to single-sample increases in the values.

11.1.2 Data fusion model v2

Description

The structure of the algorithm used in an improved data fusion model v2 is similar to the previously described approach; however, the conditioning statements are differently designed (Figure 11.17). The first step in the diagram involves extracting the *i*-th vibration signal sample and calculating the proposed CIs, that is CI_{ASB*}, CI_{nRMS}, CI_{resRMS}, CI_{APDF} and CI_{DND} for that sample signal. Each of the calculated CI values is tested against the first condition of the model which comprises two elements. The first element determines if the value of the current CI is larger than the value of the previous sample and is smaller than the value of the next sample (trend not falling and no single sample, short impulses). The second element checks if the value of current CI is greater than or equal to the standard deviation of the CI values calculated for the whole dataset. If none of the CIs satisfy the first condition, then the loop proceeds to the next iteration and the value of the Cumulative Condition Indicator of the data fusion model v2 (CCI v2) remains constant. However, if any of the CIs satisfies the first condition, the values of those CIs are summed, and the result constitutes the current value of CCI v2. After the summation process the algorithm moves to the second condition: if the current value of CCI v2 is lower than the CCI v2 values recorded in any of the preceding loop iterations, then CCI v2 retains its value from the previous cycle. On the other hand, if the current CCI v2 value is higher than the CCI v2 values recorded in the preceding loop iterations, then the current value is retained.

The first element of the first statement is included to avoid taking into account CI values generated during a falling trend and, also, to decrease the significance of impulsive events that are very short in time (one sample increase followed by immediate decrease). The second part of the first condition is designed to prevent the model reacting to random increases in the CI values. In the current form it reacts only to substantial changes – higher than the standard deviation of the CI values calculated for the whole duration of the test. The reason for the second statement, just as for the model

CCI v1, is that if the current value of CCI v2 does not exceed the values recorded to that point (that is, the condition of the monitored component has not deteriorated further), then the final CCI v2 value should remain at the same level. If, however, CCI v2 exceeds values recorded since the beginning of the test (representing a deteriorating condition of the monitored gear), then the output should increase.

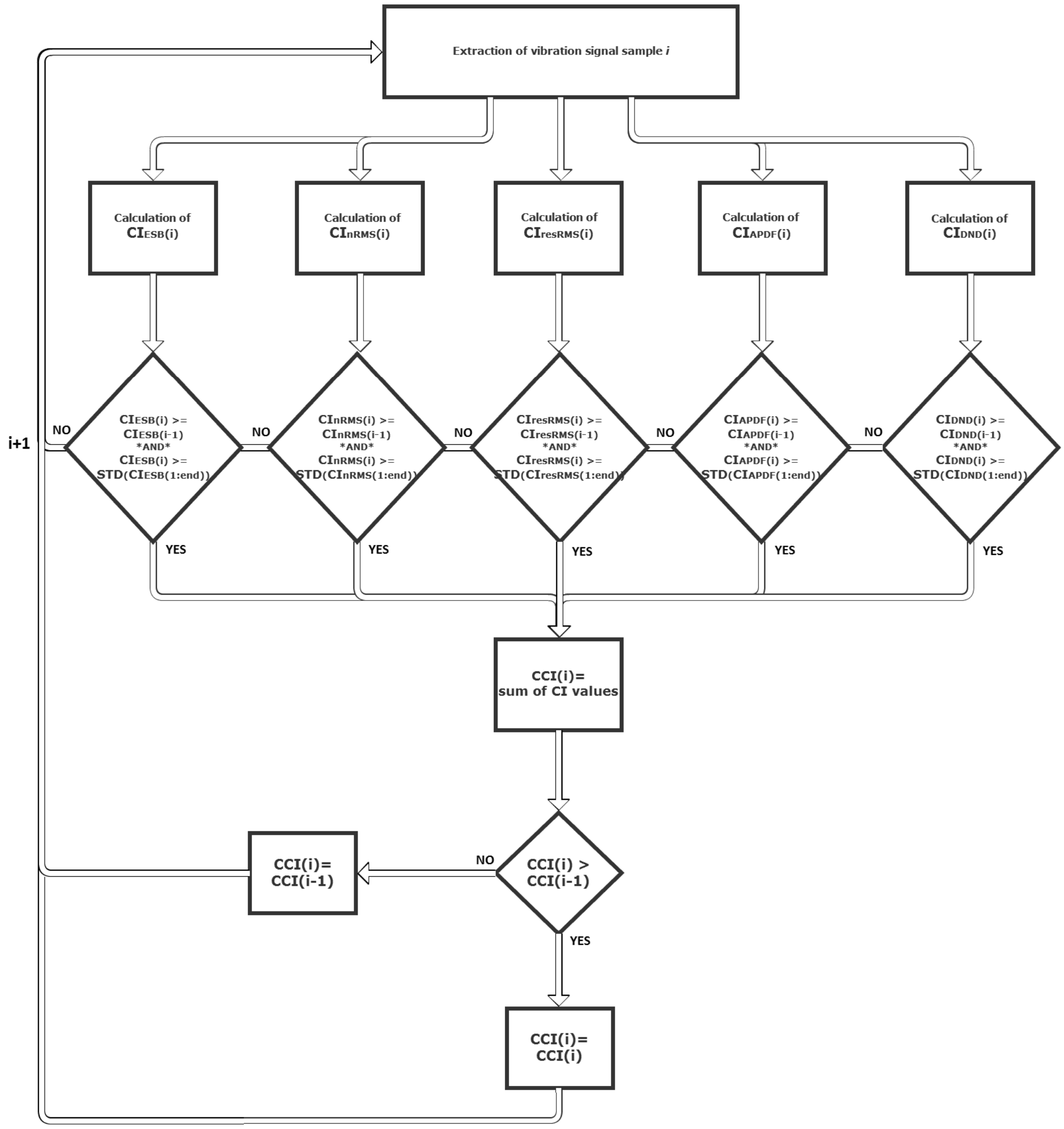

Figure 11.17 Data fusion model v2

Results

Dataset 1

Figure 11.18 depicts the result of applying CCI v2 to Dataset 1. The values of CCI v2 remain constant until sample 20. After this point an increase in the values is observed. This rising tendency continues until sample 42. For the next 21 samples the values of CCI v2 remain constant. This is followed by increases in the CCI v2 values until sample 78 after which they remain constant until the end of the test.

Dataset 2

The CCI v2 values remain constant until sample 10 when CCI v2 records a large increase in output value which is retained in the last sample of the test (Figure 11.19).

Dataset 3

The CCI v2 shows a small increase in the value at sample 4, after which it remains constant until sample 20. At this point a substantial increase in the output occurs, but the CCI v2 value does not change for the next 39 samples when (at sample 59) an increase in the value takes place again and the rising tendency continues until the end of the test (Figure 11.20).

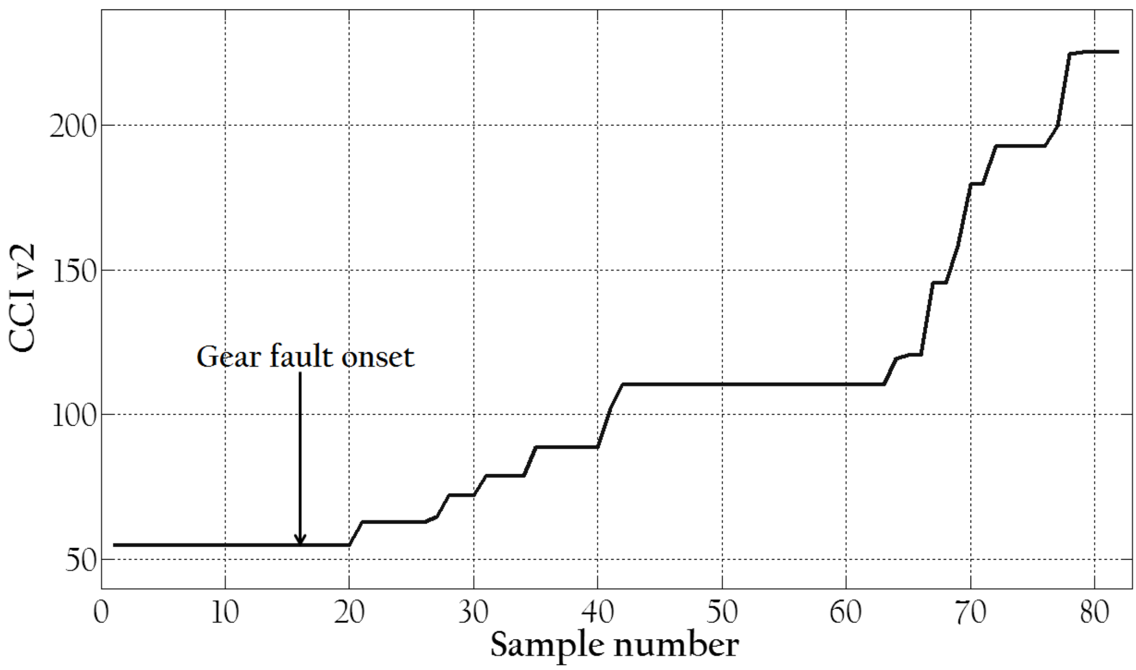

Figure 11.18 Variation of data fusion model v2 for Dataset 1

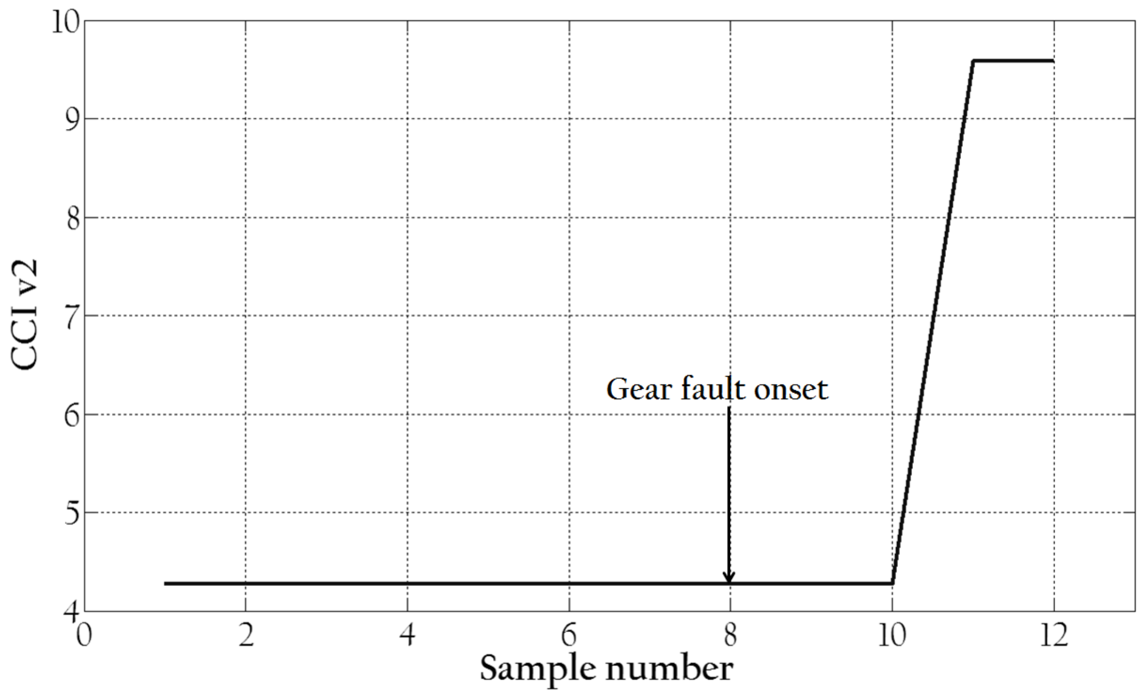

Figure 11.19 Variation of data fusion model v2 for Dataset 2

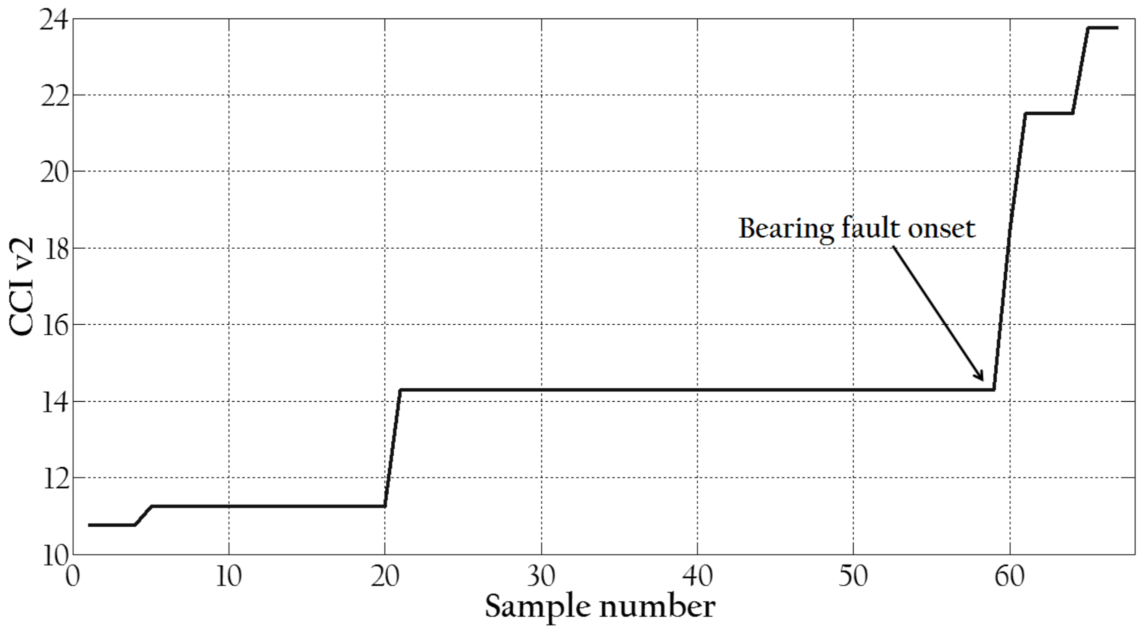

Figure 11.20 Variation of data fusion model v2 for Dataset 3

Observations

The data fusion model v2 constitutes a clear improvement over the model v1. Eliminating the influence of the transient increases combined with the condition testing if the CI value is greater than the standard deviation calculated over all the measurements in the test proves very efficient at eliminating the influence of random peaks in the values of the CIs. This increases the reliability of the results generated by CCI v2 compared with that of model CCI v1.

However the condition related to the comparison of the current CI values with a standard deviation of the given CI over all the measurements in the test requires *a priori* knowledge about the future values of the proposed indicators. Such an arrangement could find utilisation in situations where the health of the monitored components is not of critical safety and the analysis can be performed some time after recording the first sample - for instance analysis of vibration signals recorded after a whole day of measurements, when the CIs values are recoded relatively often, for example every twenty minutes. On the other hand, this technique cannot be used in environments where a reliable real-time condition monitoring is of paramount importance, for example in a helicopter on-board condition monitoring system.

Another observation is that the final value of CCI should not be composed of the actual CI values, since they operate on different value ranges; CI_{APDF} and CI_{nRMS} are always normalised to 1, whereas CI_{DND} and CI_{ASB} reach higher values. Such an arrangement inevitably leads to situations where the input of CI_{APDF} and CI_{nRMS} measurements with a strong increasing trend, could be dominated by the CIs that output larger values: CI_{DND} and CI_{ASB}. Normalisation of the CIs to unity would also require some prior knowledge about the maximum value that will be generated by the monitored machine over entire length of the measurement.

Consequently an upgraded model needs to be developed that: a) will not make use of the actual CIs values when constructing the CCI and b) will not require any *a priori* knowledge about the values of parameters under consideration.

11.2 Decision fusion level

The observations made in the previous sections suggested an approach that entails fusing the decisions based on each CI output rather than fusing their raw output values. This, in turn, constitutes a change of data fusion approach, from a feature level fusion to a decision level fusion. The results of implementing such improvements are described below.

11.2.1 Data fusion model v3

Description

Figure 11.21 shows a flowchart that explains the data fusion model v3. Instead of two-step condition structure of model v1 and v2, model v3 contains only one condition. The whole philosophy incorporated in this model is based on comparison of the values of each proposed CI against a threshold value defined by a running standard deviation of the signal. The running standard deviation is calculated separately for each indicator and it is updated after each iteration of the loop. It is derived from the history of the CI values from sample 1 until the current loop iteration. The initial value of the threshold is equal to the first calculated value of each CIs. Such an implementation is self-tuning and does not require any input from the operator who, in the case of a fixed threshold value system, would have to input the values manually based on the history of each monitored system alone. The threshold value can be calculated as per Eq. 11.2:

$$threshold = x_1 + \sqrt{\frac{1}{N-1}\sum_{i=1}^{N}\left(x_i - \overline{x}_{1:i}\right)^2} \tag{11.2}$$

where N is the number of the data points measured until given point in time, x_i is the value of a CI at the *i*-th data point, $\overline{x}_{1:i}$ is the mean value of all the data points measured until given point in time.

The first step of the model, identical to that of previous versions, involves calculation of value of the proposed CIs, that is CI_{ASB}, CI_{nRMS}, CI_{resRMS}, CI_{APDF} and CI_{DND} for vibration sample *i*. Each of the calculated CI values is tested against the first condition: if the value of the current CI is larger than the value of the threshold, then a flag is set (from 0 to 1). The value of CCI is dependent on the number of flags raised when checking the condition. Each CI crossing the threshold value contributes a value of 1 to the final value of CCI. If none of the indicators satisfy the condition, then the initial value of CCI will be zero. In addition to the threshold condition, the safety rule, that does not allow any transient insignificant peaks to be counted as events, is retained in the model, but is improved in model v3 - the previous implementation of this safety statement required that $x_{i-1} < x_i < x_{i+1}$. This arrangement took into account only those samples that were generated during the rising trend of the curve. In the case of model v3 the statement is slightly altered – for a sample to be counted as a real indication, the current value of the CI has to be above the threshold AND the value of sample *i-1* has to be larger than the threshold value at sample *i-1*. In some cases this may lead to one sample lag in detecting a fault, but it significantly decreases the number of false alarms.

The statement used in model v3 guarantees that the final result is easy to interpret. It counts the number of CIs that raised a flag thus making the contribution of each parameter equal.

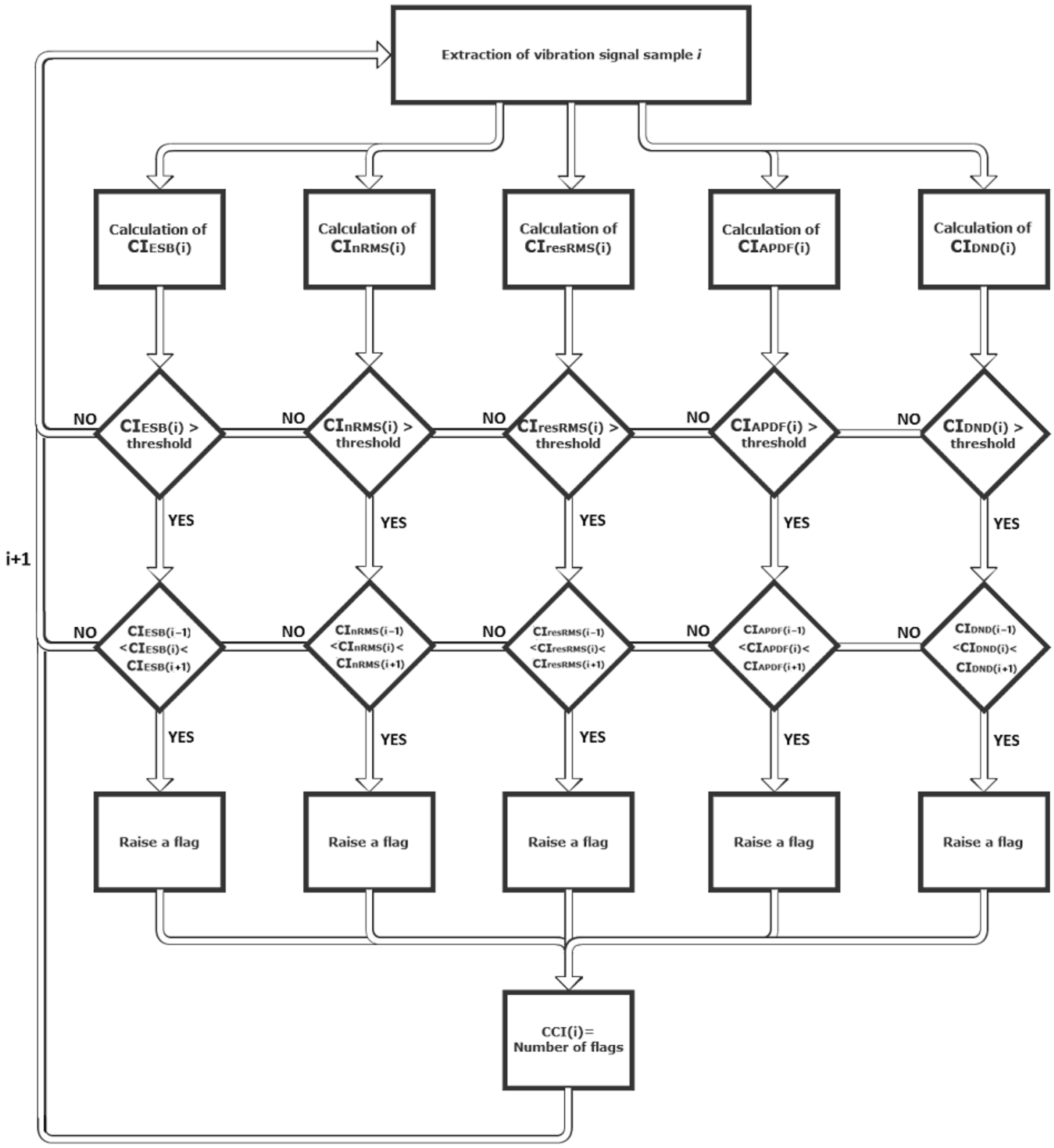

Figure 11.21 Data fusion model v3

The final improvement in the model design is based on the binary threshold-crossing approach shown in Figure 11.22. As long as the CI value is lower than the threshold value, the condition output is 0. Once the value of the CI crosses the threshold the output changes to 1.

In the case of gear condition monitoring (Datasets 1 and 2), five different CIs are proposed, which correspond to the six different colours on the proposed colour map (Figure 11.23). The green colour indicates a situation where none of the CIs crossed the threshold. The more flags raised, the 'warmer' the colour becomes. In the case of bearing condition monitoring (Dataset 3) three CIs are proposed (CI_{nRMS}, CI_{APDF} and CI_{DND}), and therefore the colour map is divided into four levels as shown in Figure 11.24.

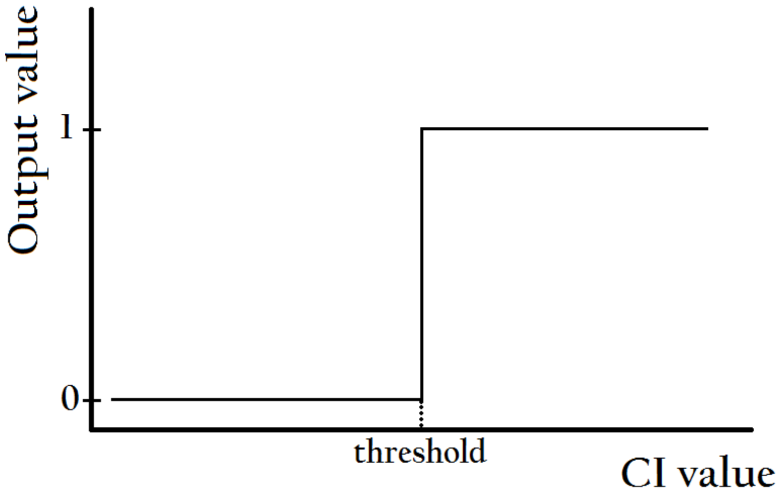

Figure 11.22 Binary threshold-crossing condition

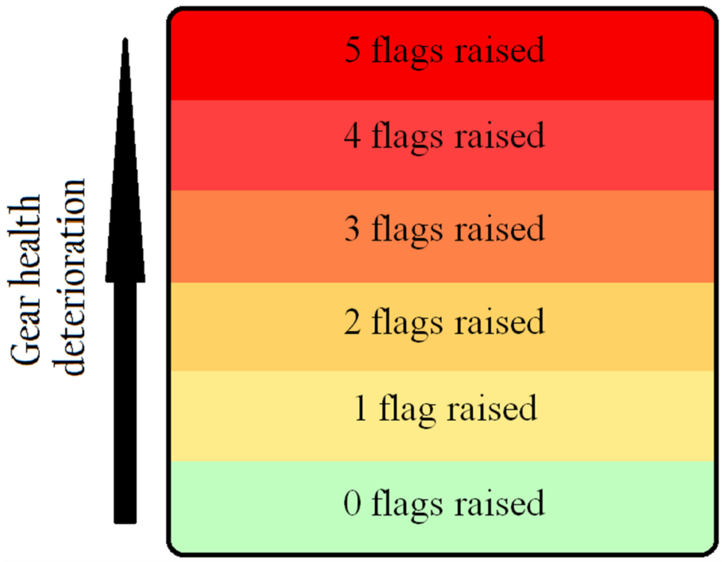

Figure 11.23 Colour map designed to indicate gear health deterioration

Figure 11.24 Colour map designed to indicate bearing health deterioration

Results

The result for each Dataset is presented similarly. Firstly a set of plots is drawn showing the relationship between the output of each of the proposed CIs and the curve created by plotting the change in the threshold values with time. This set of plots is followed by a further plot showing the Cumulative Condition Indicator for the data fusion model 3 (CCI), plotted with the accompanying colour map

Dataset 1

The CI_{nRMS} value does not cross the threshold until sample 22 when a transient peak occurs, after which it remains above the threshold until the end of the test (Figure 11.25). Although CI_{resRMS} first crosses the threshold between sample 6 and 9 it remains very close to the threshold value until sample 22 when a significant increase occurs corresponding with the transient peak in the CI_{nRMS} trend. Following this the CI_{resRMS} follows a generally rising trend, remaining above the threshold until the end of the test (Figure 11.26). The CI_{APDF} curve crosses the threshold line very early at sample 2 and marginally tracks the threshold line until sample 14 after which rises throughout the remainder of the test (Figure 11.27). CI_{ASB} crosses the threshold line at sample 19 and approximately follows the trend line until sample 26. The CI value then remains above the threshold with a slight decrease at sample 51 (Figure 11.28). Figure 11.29 shows that CI_{DND} begins a rising trend, crossing the threshold line at sample 14. The trend features four transient decreases, one of which falls below the threshold line.

Figure 11.30 shows the final shape of CCI. It is seen that, in the first 14 samples two CIs respond to changes in the signal by setting flags (those are CI_{resRMS} and CI_{APDF}). However, after sample 10 the CCI decreases to green zone twice. After sample 14 a sudden increase in the CCI level takes place, which results in the fourth level being reached at sample 20. This is followed by a decrease at sample 23, when all the CIs, apart from CI_{resRMS} and CI_{APDF}, decrease to just below the threshold level. At sample 28 the CCI reaches the red zone indicating that all of the proposed CIs have crossed the threshold level.

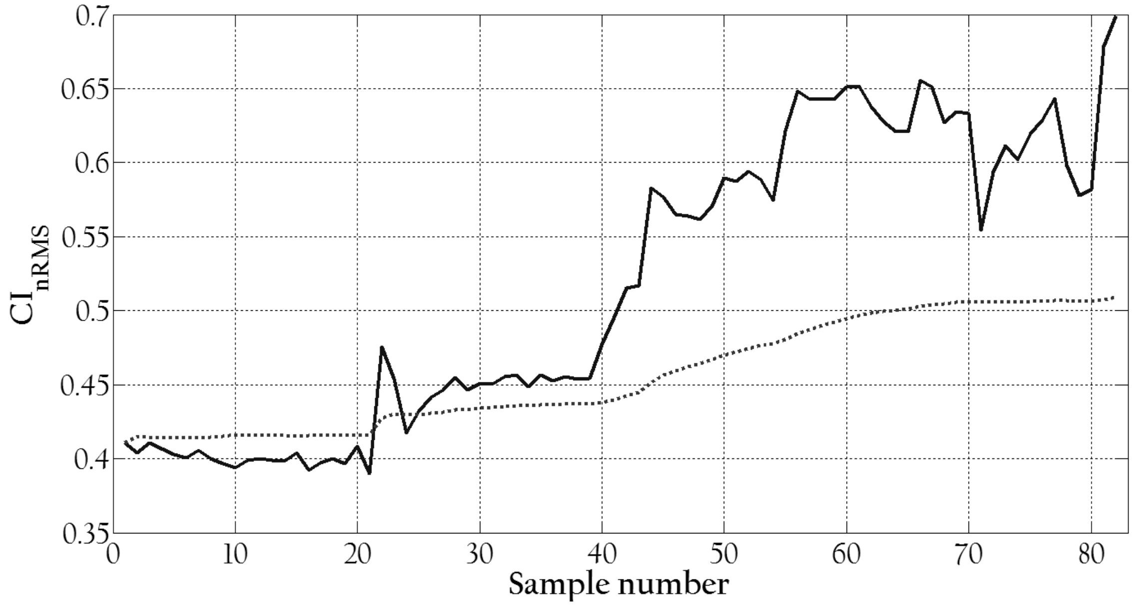

Figure 11.25 Variation of CI_{nRMS} (solid line) and threshold (dotted line) for Dataset 1

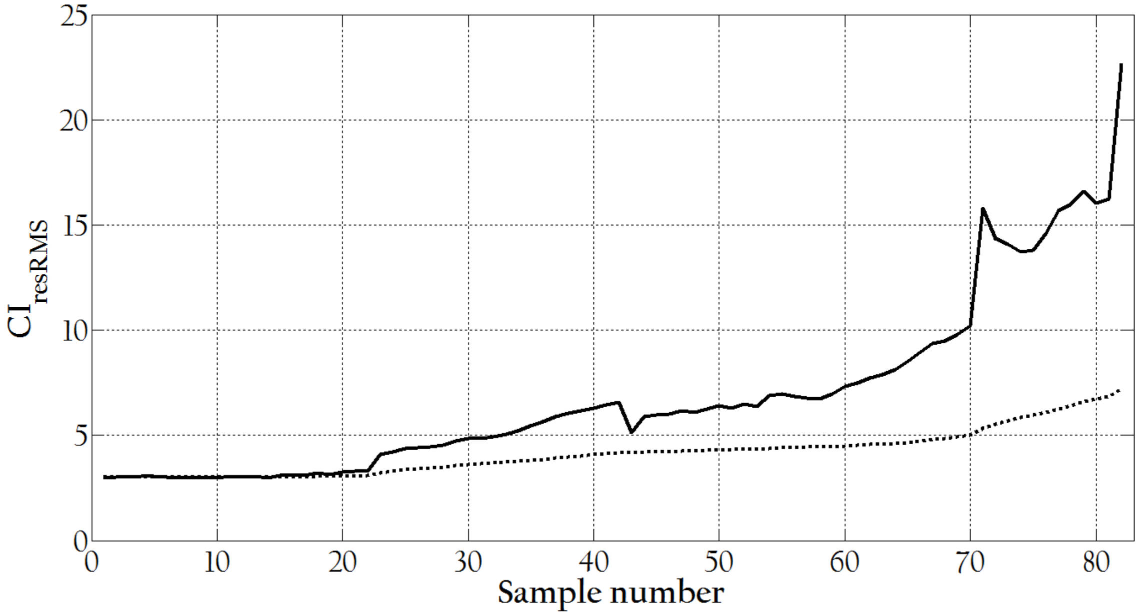

Figure 11.26 Variation of CI_{resRMS} (solid line) and threshold (dotted line) for Dataset 1

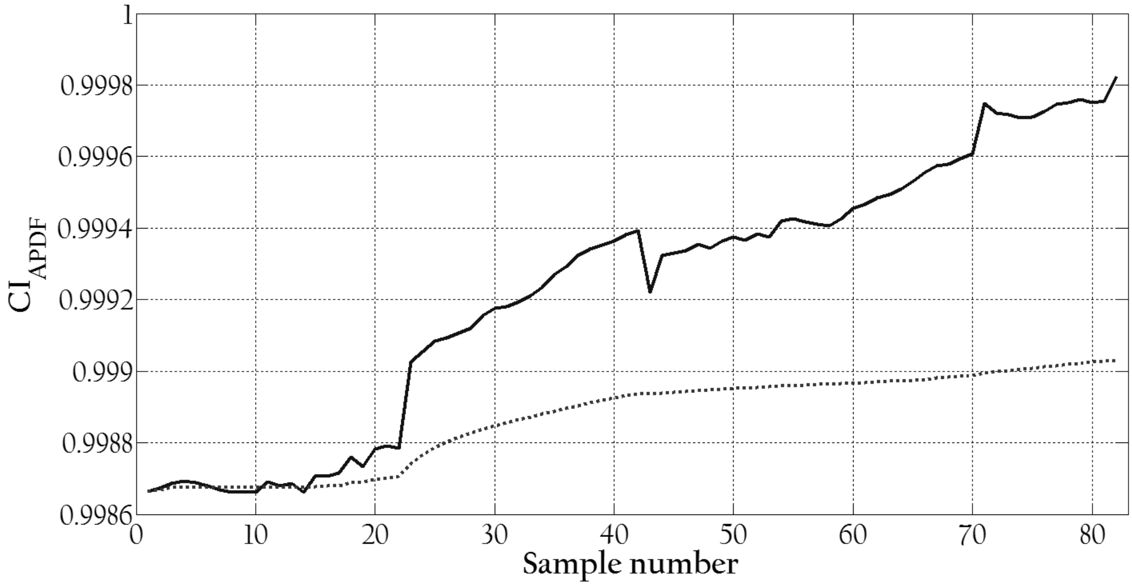

Figure 11.27 Variation of CI_{APDF} (solid line) and threshold (dotted line) for Dataset 1

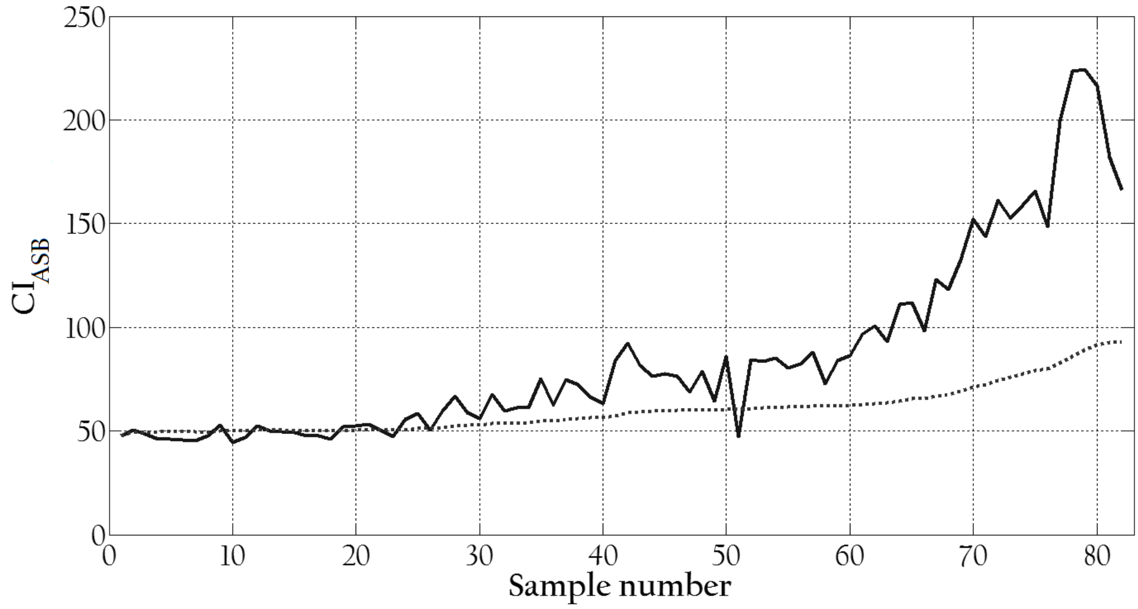

Figure 11.28 Variation of CI_{ASB} (solid line) and threshold (dotted line) for Dataset 1

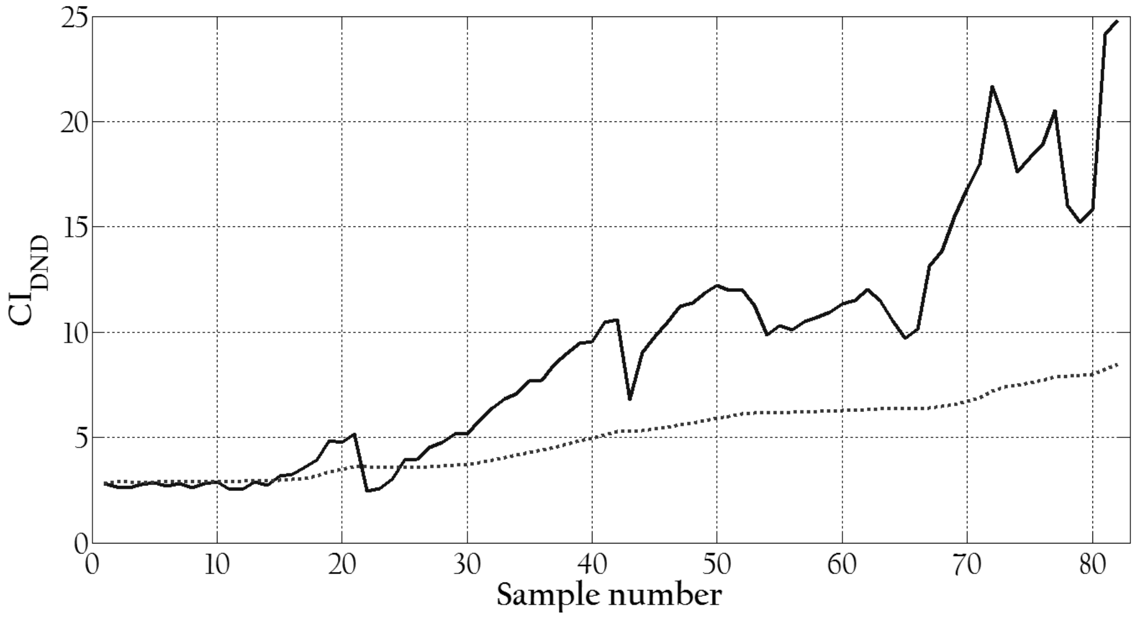

Figure 11.29 Variation of CI_{DND} (solid line) and threshold (dotted line) for Dataset 1

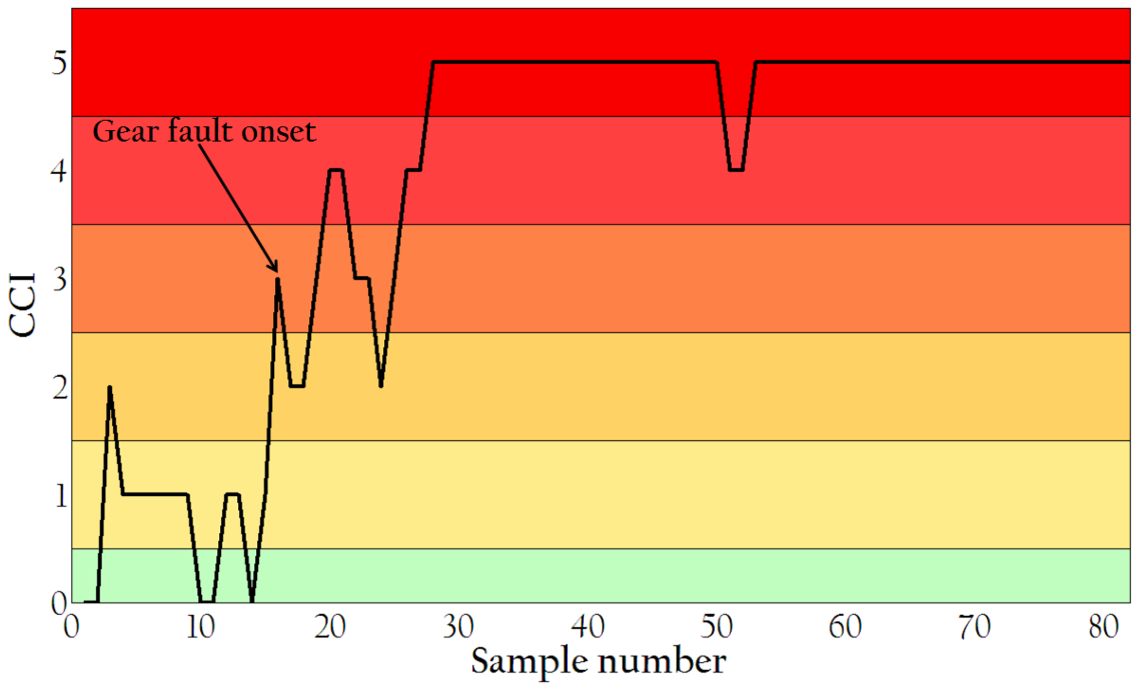

Figure 11.30 Variation of data fusion model v3 for Dataset 1

Dataset 2

CI_{nRMS} curve crosses the threshold for the first time at sample 5, but this is a single-sample event and is therefore not counted as a fault indication. The true alarm level crossing takes place at sample 7 and continues until the end of the test (Figure 11.31). CI_{resRMS}, CI_{APDF} and CI_{ASB} curves stay below the threshold value until sample 11 and 12 (Figures 11.32 - 11.34). CI_{DND} crosses the threshold value at sample 9, for just one sample hence it is treated as a false indication. The real gear damage detection starts at sample 11(Figure 11.35). The CCI curve indicates no fault until sample 7 after which the first, early indication of the fault arises. The CCI remains at level 1 until sample 12 when all of the flags are raised entering the red zone of the colour map (Figure 11.36).

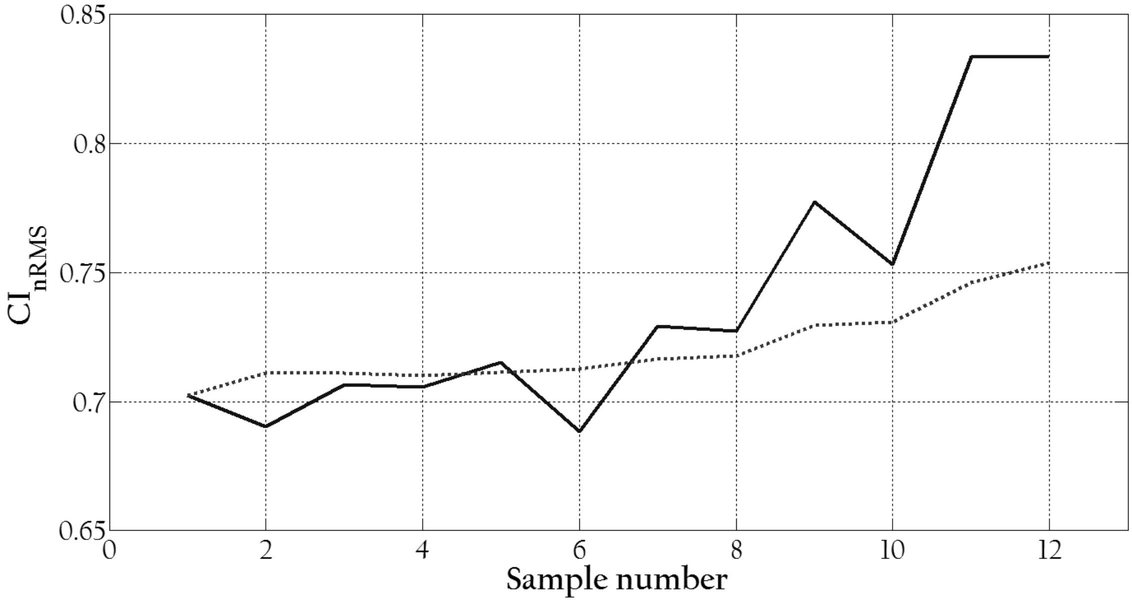

Figure 11.31 Variation of CI_{nRMS} (solid line) and threshold (dotted line) for Dataset 2

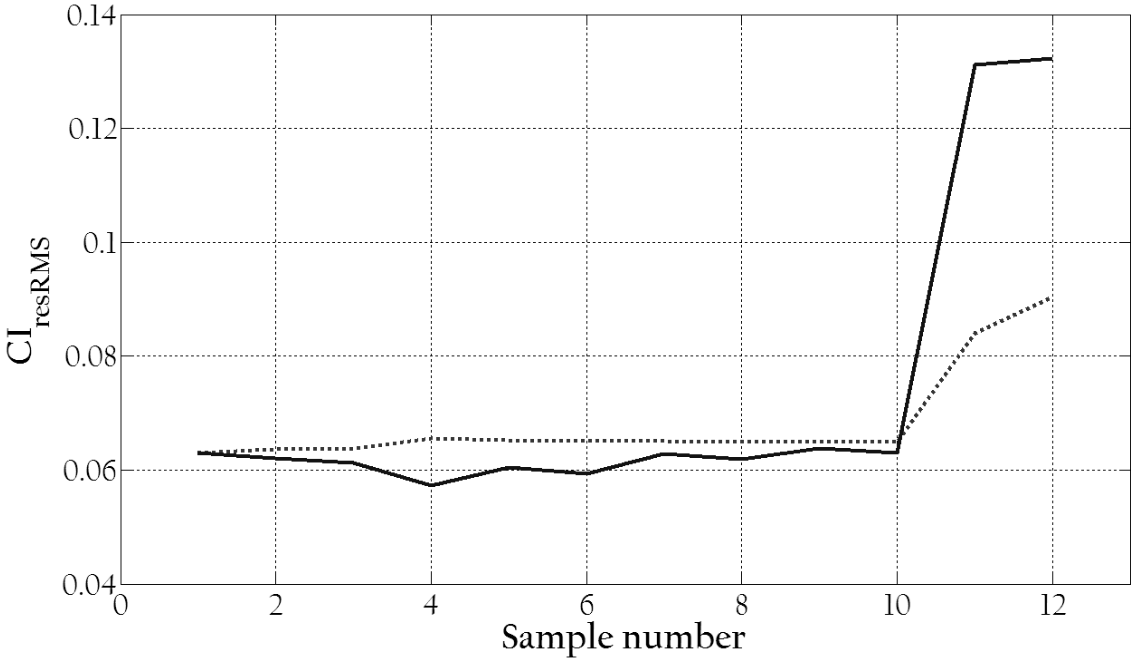

Figure 11.32 Variation of CI_{resRMS} (solid line) and threshold (dotted line) for Dataset 2

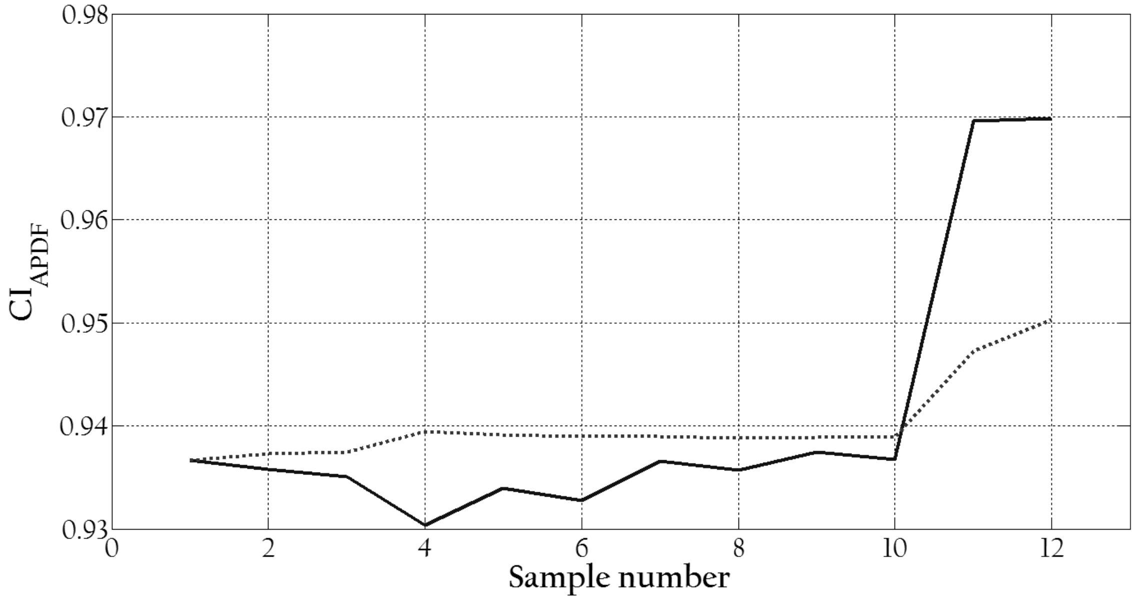

Figure 11.33 Variation of CI_{APDF} (solid line) and threshold (dotted line) for Dataset 2

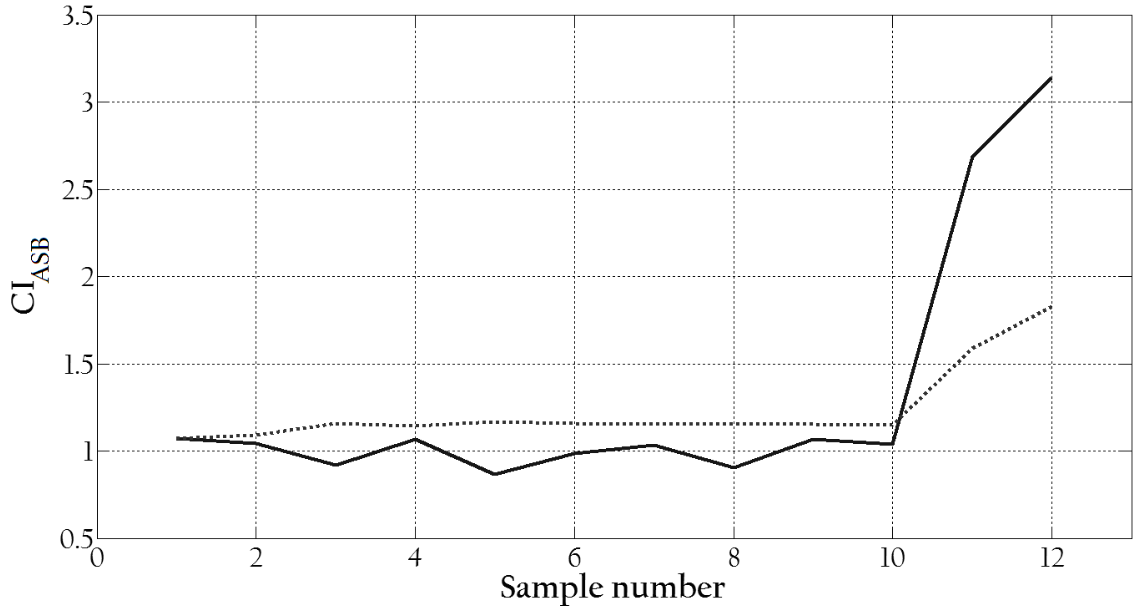

Figure 11.34 Variation of CI_{ASB} (solid line) and threshold (dotted line) for Dataset 2

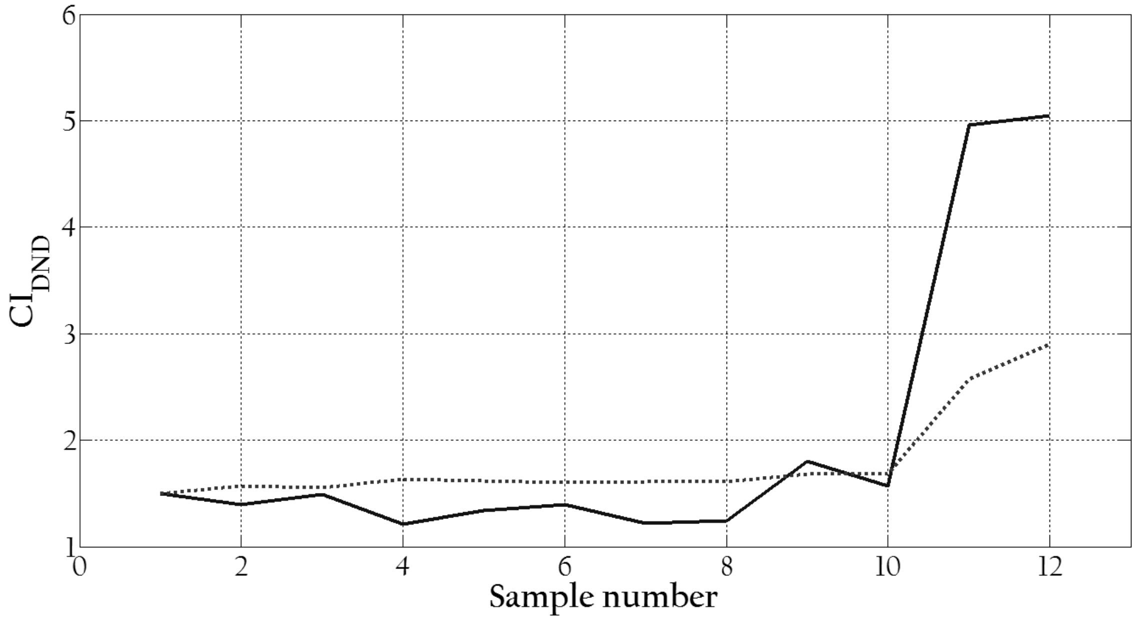

Figure 11.35 Variation of CI_{DND} (solid line) and threshold (dotted line) for Dataset 2

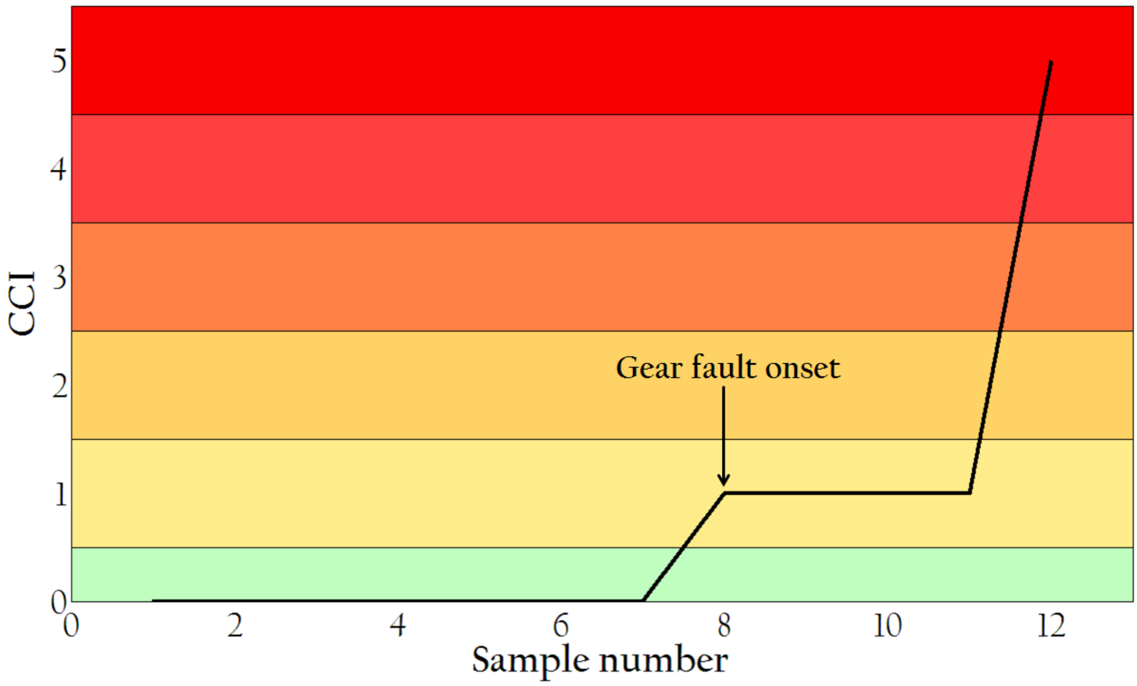

Figure 11.36 Variation of data fusion model v3 for Dataset 2

Dataset 3

It is notable that in Figure 11.37, CI_{nRMS} crosses the threshold numerous times in the region between sample 1 and 59 but each of these are single-sample crossings that are not counted by model v3. The first fault indication appears at sample 60 after which the CCI remains above the threshold until the end of the test. CI_{APDF} curve is also very active, indicating a potential fault as it crosses the threshold line many times. Several of these are multi-sample crossings, for example at samples 13, 26 and 47. The longest period above the threshold occurs towards the end of the test, starting at sample 58 and continuing until the end of the test (Figure 11.38). CI_{DND} records several single-sample threshold crossings, but the real indication begins at sample 60 and lasts until the end of the test (Figure 11.39). For the first 60 samples the CCI oscillates between 0 and 1 due to the activity of CI_{APDF}. This makes the indicator enter the Zone 1, but does not go above that until sample 61 when the indication moves to the red zone where it stays for the rest of the test (all three indicators set a flag) (Figure 11.40).

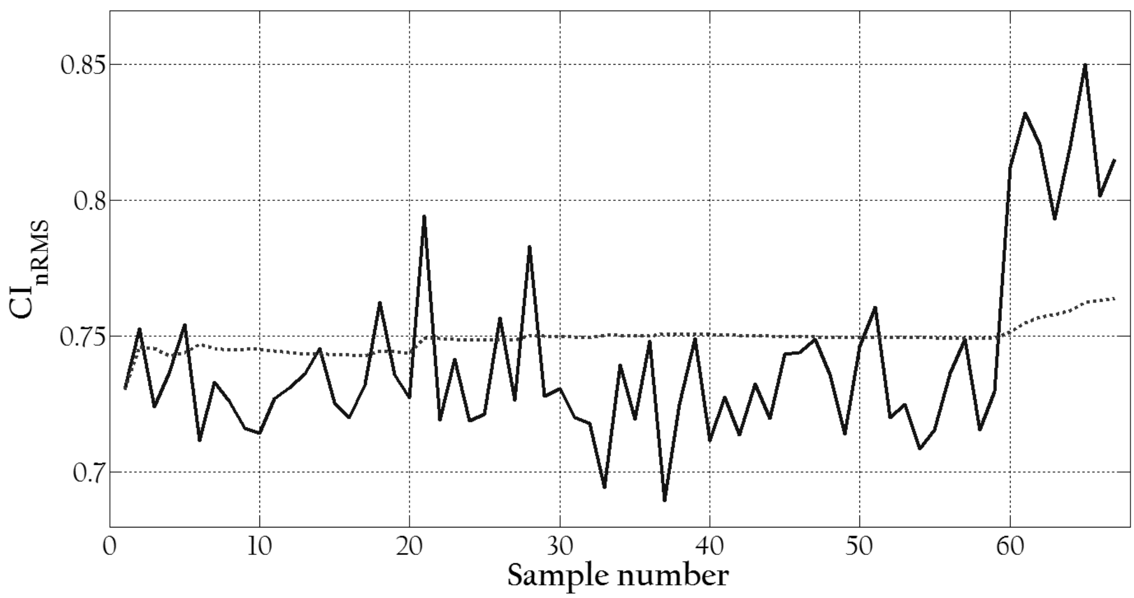

Figure 11.37 Variation of CI_{nRMS} (solid line) and threshold (dotted line) for Dataset 3

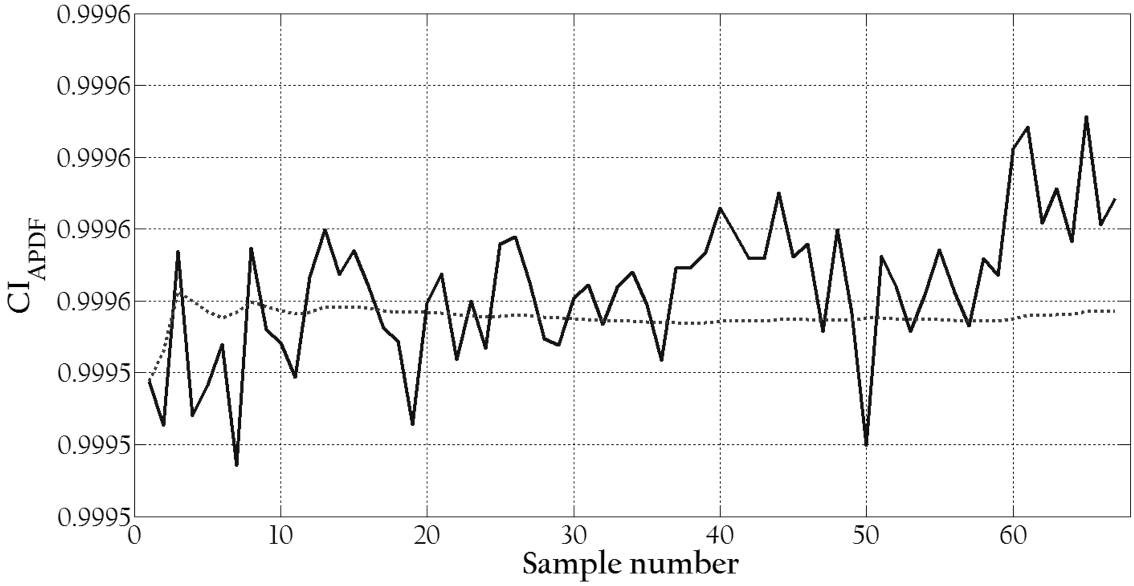

Figure 11.38 Variation of CI_{APDF} (solid line) and threshold (dotted line) for Dataset 3

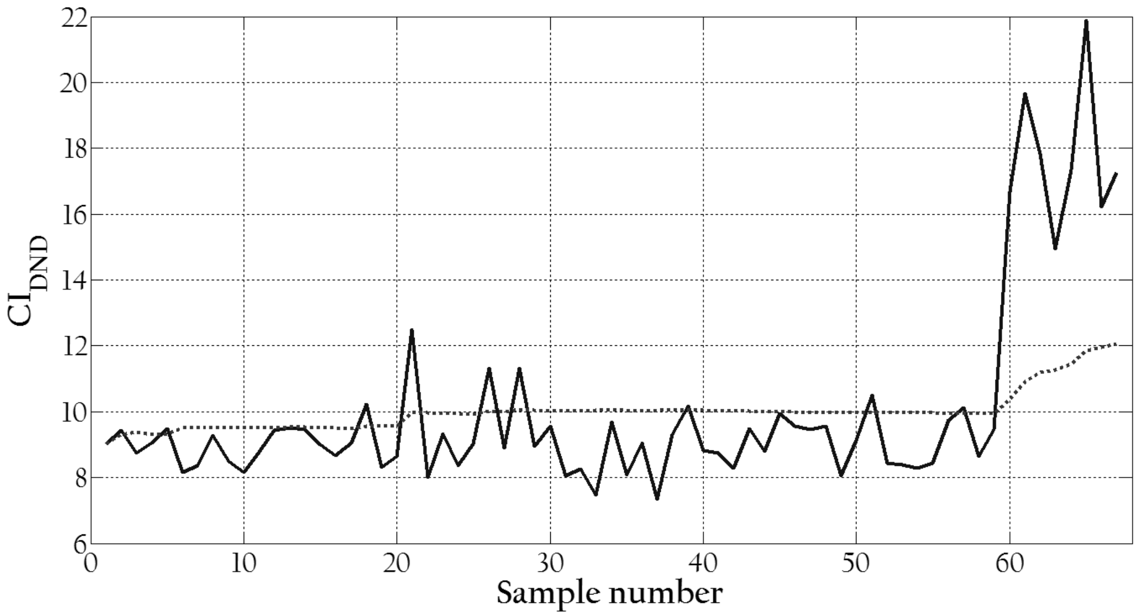

Figure 11.39 Variation of CI_{DND} (solid line) and threshold (dotted line) for Dataset 3

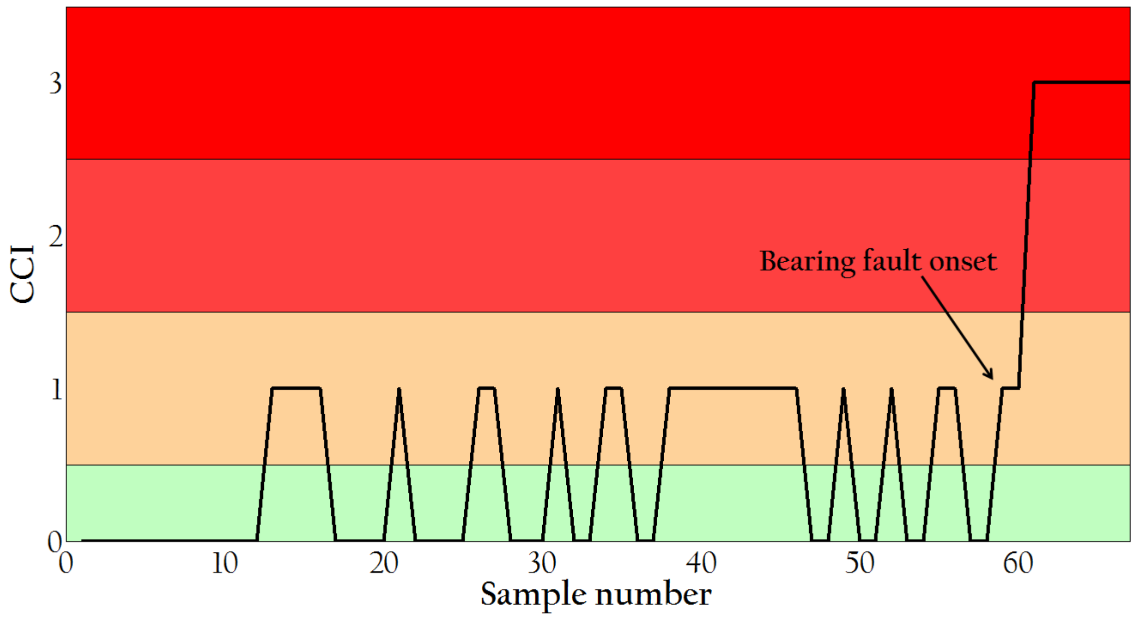

Figure 11.40 Variation of data fusion model v3 for Dataset 3

Observations

The third implementation of the data fusion model is clearly giving the most stable and reliable indications of gear or bearing faults. For Dataset 1 the indicator began to increase early in the test and reached the red zone shortly after that. The results for Dataset 2 show the clear advantage of data fusion model v3. The values remained in the green zone until sample 8 (one sample earlier than model v2). In the case of bearing damage, CI_{APDF} is prone to indicating damage over the whole duration of the test. However, the final result of the CCI reacts to that hyper-activity in a stable way, entering only the Zone 1 region of the colour map. It is not until the end of the tests that the CCI starts to indicate more severe damage, which is in agreement with the results indicated by each of the CIs alone.

11.2.2 Data fusion model v3 sensitivity

In order to assess the robustness of the data fusion model v3 the results discussed in the last section are compared against the outcome of applying model v3 to the same data using the existing CIs (described in Chapter 5). This comparison is essential in order to assess if model v3 is both robust and sensitive enough to react to the changes in the behaviour of the input CIs. If the output of the model based on the existing techniques has a continuously rising trend that does not decrease its value towards the end of the test, it will mean that the data fusion model v3 is not sufficiently agile to dependably reflect the current state of each parameter; it will be liable to mask the clear disadvantages of the existing solutions that become apparent in certain circumstances (which were discussed in Chapter 6). This, in turn, could mean that model v3 may not give reliable results on every occasion. The comparison is carried out on a single dataset for each failure type: Dataset 1 which contained the most vibration samples for a gear fault and Dataset 3 for a bearing fault.

Dataset 1

The result of applying the data fusion model v3 using the two different sets of CIs to Dataset 1 is presented in Figures 11.41 and 11.42. The comparison shows the clear advantage of model v3 applied with the new set of CIs. The shape of the curve in Figure 11.41 shows an inconsistent gear fault indication. Although it reaches the highest level at sample 17 it has a large gap where only one flag is indicating the fault (samples 22-28). Perhaps more most important in this comparison is the characteristic decrease in the CCI value towards the end of the test (beyond sample 63). This decrease is the main disadvantage of the CI_{CF}, CI_{FM4} and CI_{M6} parameters and this comparison showed that the data fusion model v3 appropriately reflects the actual behaviour of the existing CIs. The CCI in Figure 11.42 on the other hand predominantly indicates the red level, when all four CI warning flags are set.

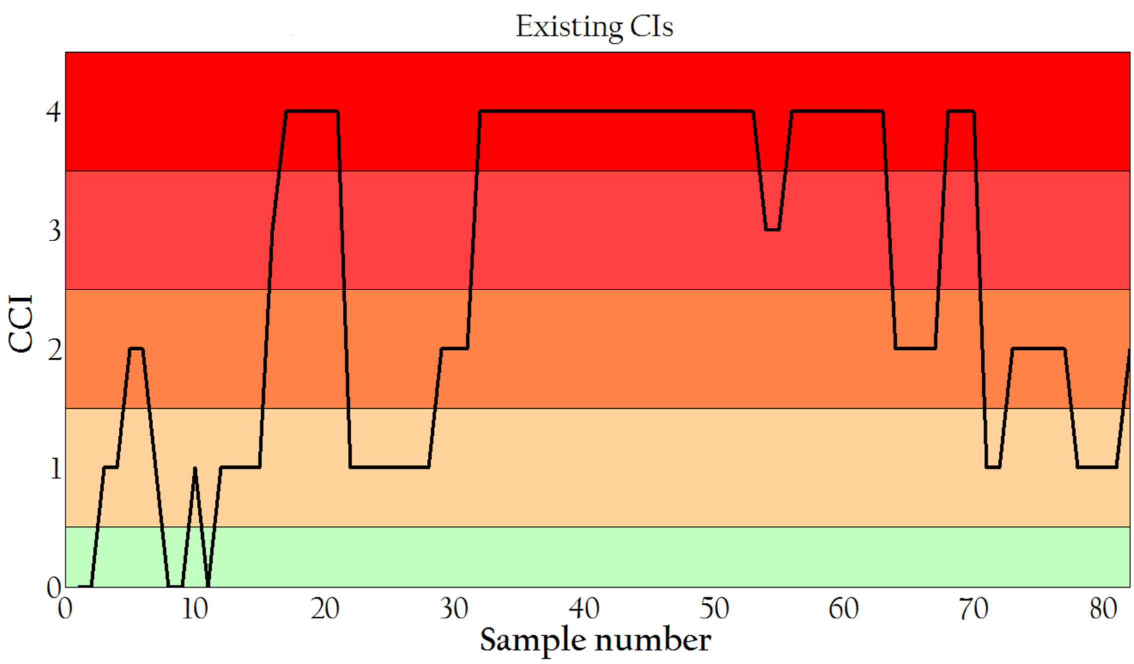

Figure 11.41 Variation of data fusion model v3 on existing CIs for Dataset 1

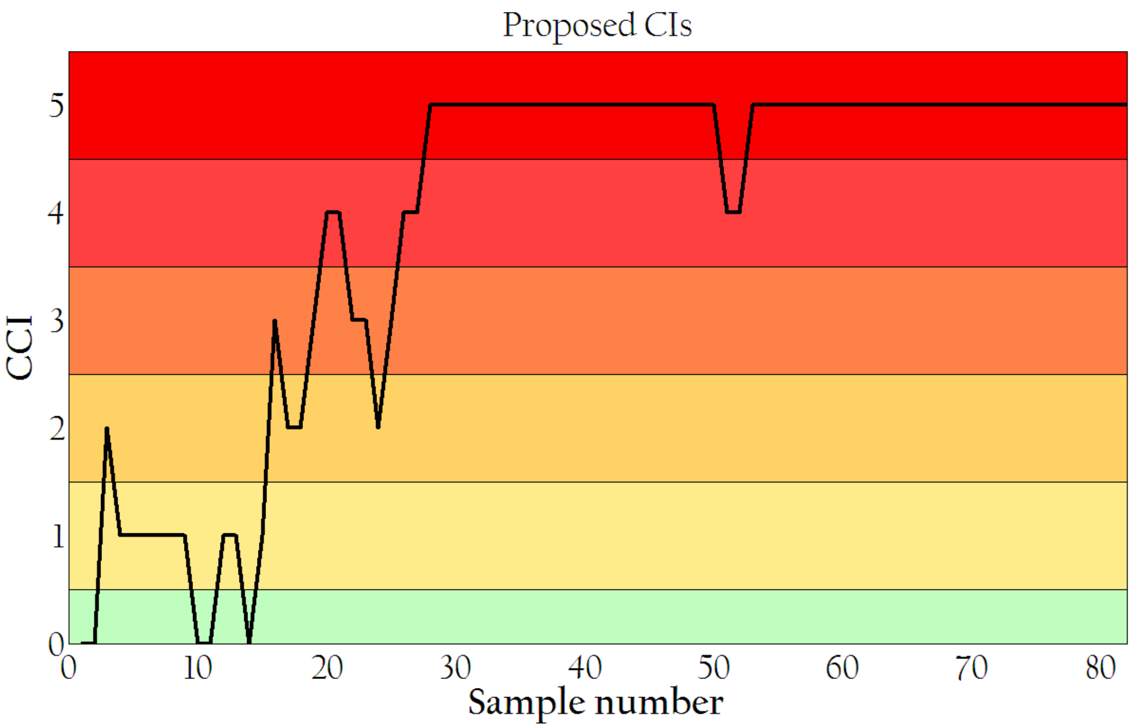

Figure 11.42 Variation of data fusion model v3 on proposed CIs for Dataset 1

Dataset 3

The results of applying the data fusion model v3 using both the existing and the new proposed CIs are shown in Figures 11.43 and 11.44 respectively. The individual results obtained directly from the existing and the proposed CIs are very similar when applied on Dataset 3. Consequently, the outcome of the data fusion model v3 is identical, even though only three parameters are used in Figure 11.44 (CI_{ASB} and CI_{resRMS} are designed to indicate gear faults only). The conclusion from the comparison is that model v3 does not introduce any false information into the final outcome and neither does it lose any information during the fusion process. Since individual results are similar for all the parameters under investigation, the final shape of both CCIs should also be similar.

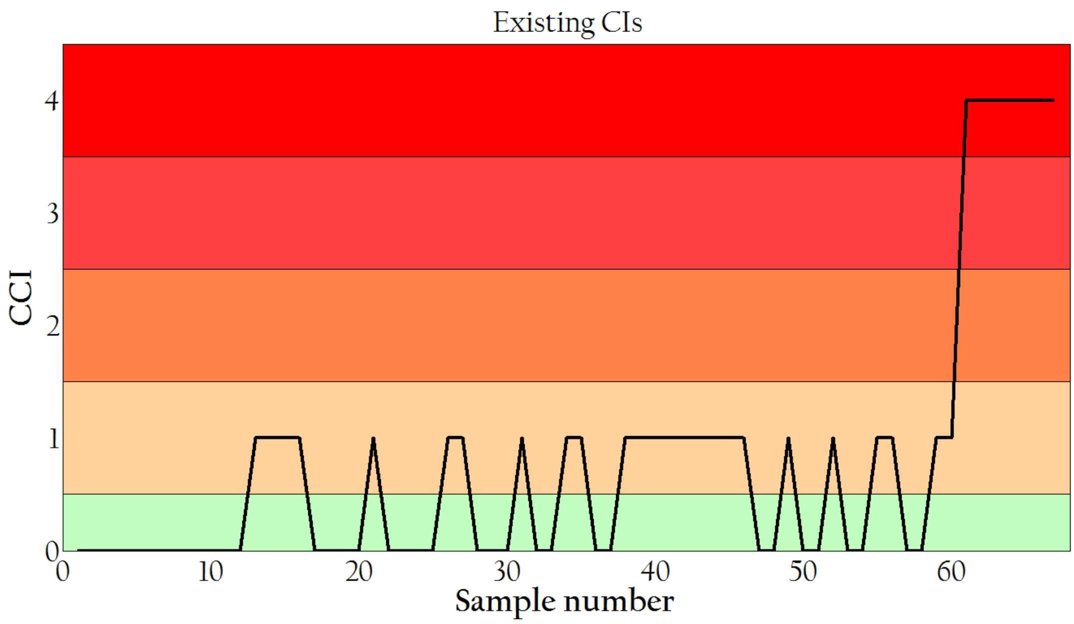

Figure 11.43 Variation of data fusion model v3 on existing CIs for Dataset 3

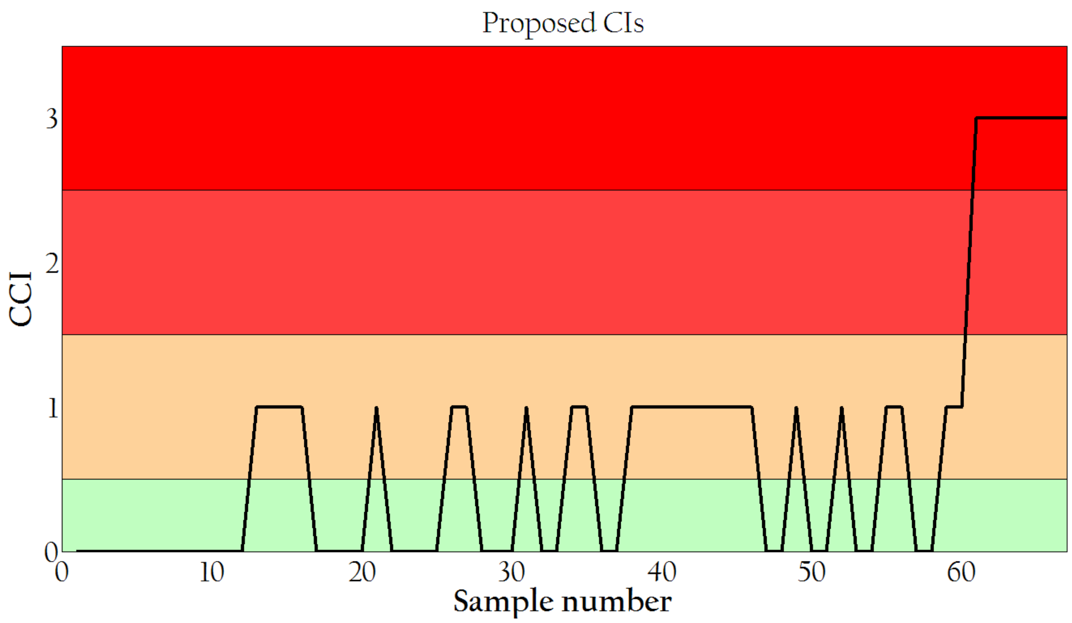

Figure 11.44 Variation of data fusion model v3 on proposed CIs for Dataset 3

Observations

Comparison of the results generated by the data fusion model v3 applied to the existing and the proposed CIs, shows the clear advantage of the model when used in conjunction with the proposed indicators. The comparison revealed that the data fusion model v3 is sensitive enough to transmit the undesired behaviour of the existing CIs. This in turn suggests that the model is unlikely to introduce any artificial components into the final output. It is also apparent that the data fusion model v3, applied with the proposed CIs, has a lower rate of false indication and is less likely (compared to the existing parameters) to return to the green (safe) zone after an initial fault indication has occurred.

11.3 Summary

This chapter presented the results of applying different approaches to the data fusion process. Observations and improvements were made after each model was tested, in order to achieve a model that is capable of reliably fusing the information provided by the proposed CIs and, thereby, providing a dependable gear or bearing condition indication, based on the input information. By fusing information from many sources, the model not only indicates a gear or a bearing fault with higher confidence than each CI alone, but also decreases the likelihood of false alarms generated during the analysis. Three different data fusion models were tested on the three datasets. Each subchapter was arranged in the same way, first describing the model (along with a flowchart depicting the approach), followed by analysis of the results of implementing the data fusion model on the Datasets. Each investigation was followed by a set of observations.

Investigation of the properties of the data fusion model v1 revealed that it was too sensitive to any changes in the CI values and, hence did not truly represent the actual condition of either the gear or the bearing under examination.

Data fusion model v2 was modified based on the conclusions from model v1 and, despite being a clear improvement over model v1, it utilised on approach that could not be used in the field of the helicopter condition monitoring. Using *a priori* knowledge about the condition of a given component is not acceptable when instantaneous, in-flight, real-time indications are required. This led to the solution that the output of the data fusion model should not be based on the actual values of the CIs, but should accept a standardised input form.

The data fusion model v3 was the last and most reliable version built based on observations made in the previous implementations. The results of applying model v3 on all three datasets gave reliable and convincing indications reducing the false alarm rate compared with the previous model versions. Introducing a standardised output and presenting it on a colour map gave a simple-to-analyse, robust gear or bearing fault indication.

The last Section examined the sensitivity of model v3 to any changes occurring within the CI readings. The examination was carried out by applying the model using the existing CIs, which were known to improperly indicate the faults. The data fusion model v3 appropriately reflected the drawbacks of the existing CIs and correctly responded to the changes in the input parameters. This showed that model v3 is unlikely to produce any indications that are not consistent with information provided by each individual input parameter.

CHAPTER 12

CONCLUSIONS AND FUTURE WORK

12.1 Overview

Condition monitoring of gears and bearings is a very well established domain in the field of machinery condition monitoring. Over the past decades many different techniques have emerged that enabled detection of faults with a high precision and presented the results in a very detailed format. Those techniques vary from the pioneering approaches performing signal analysis in the time or the frequency domain, through to the time-frequency domain analysis and wavelet analysis to some more recent concepts like the neural networks and fuzzy logic. Each technique has its own advantages, however almost all of them require a high degree of experience and expert knowledge in order to interpret the results correctly. This, in turn, is not acceptable when a quick 'GO, NO-GO' type of indication is required in order to inform about the safety of the mechanical system operation – as in the case of a helicopter for example. On the other hand, time domain analysis gives the opportunity to design signal processing routines that output a single number which has been 'engineered' to reflect the actual condition of the monitored component. Such an indication can be easily understood by a non-specialist, such as a helicopter mechanic. Many such algorithms – called Condition Indictors – have been designed to date, the most widely used being Crest Factor, Kurtosis, FM4 and M6. Even though, in general they are capable of properly indicating a gear or a bearing fault, there have been several instances where they failed to do so. This inability to properly indicate a fault in some critical circumstances could cost millions of pounds worth of damage and may even lead to some fatalities. Consequently research into a new means of performing a quick and robust condition assessment of the flight critical safety components is an ongoing process fuelled by the constant demand for increased reliability of safety-critical, machines like helicopters.

12.2 Achieved objectives

Review of the most widely used helicopter drive train CIs and examination of their performance using experimental data.

A comprehensive review of the existing Condition Indicators has been carried out and five of the most widely described techniques used in the field of the gear and/or bearing condition monitoring have been selected for further testing. The existing CIs that have been reviewed are: CI_{RMS}, CI_{CF}, CI_{Ku}, CI_{FM4} and CI_{M6}. The performance of the selected parameters has been examined by applying them to three experimental datasets, each containing acceleration response vibration signals. Two of the datasets were generated from two different test rigs which contained a gear-related fault. The third dataset was obtained from a helicopter main rotor gearbox which developed a bearing fault.

Defining new improved CIs based on a performance assessment of the existing methods.

Based on the conclusions drawn from analysis of the performance of the existing CIs, a set of five new Condition Indicators have been proposed. These are: CI_{ASB}, CI_{nRMS}, CI_{resRMS}, CI_{APDF} and CI_{DND}. Observation and analysis the characteristics of the existing techniques suggested means of improving the limitations of the existing solutions, whilst retaining their robust properties. The reasoning behind the design of every CI has been documented in detail together with the processes that need to be followed in order to properly implement each parameter.

Presentation of the advantages of the proposed CIs over the existing CIs.

Both the existing and the proposed new CIs have been applied to the same set of non-correlated datasets, in order to give an unbiased and meaningful comparison. The results were presented in the form of standardised plots showing the reaction of each parameter to the progressively deteriorating gear (2 datasets) or bearing (1 dataset) condition. The advantages of the proposed techniques have been discussed and differences in their response explained.

Definition of a data fusion approach to improve the application of the proposed CIs.

A data fusion approach has been defined employing decision level fusion, where decisions made by a number of CIs (based on a threshold crossing criterion) are combined to create a more reliable and robust gear or bearing condition indicator. Three different data fusion models were tested and the most reliable of them was used to further demonstrate its practical use as a 'GO, NO-GO' type of tool for gear fault detection. In addition, the sensitivity of the data fusion model was examined using both the existing and the proposed CIs. The results showed that the model responded correctly to any change in the actual reading from each indicator, thus assuring that the final design would not produce any decisions that are not consistent with the information provided by each individual data fusion component.

12.3 Overall conclusions

The analysis of the results obtained by comparing the existing and the proposed Condition Indicators showed that the later presents a much higher level of robustness when indicating the advent and progress of an incipient gear fault. They were also observed to be equally dependable in signaling a fault developing within a bearing (compared with the existing CIs), giving them the potential to be used as a multi-purpose detection tool. The proposed CIs design was based on the limitations of existing techniques and the reason for their improved robustness has been explained in detail. The data fusion model showed that combining information from a number of different CIs derived from the same vibration signal has a great potential to increase the dependability and precision of the fault indications made, whlist minimising their false alarm levels rate.

12.4 Future work

i. In order to further increase confidence in the reliability of the proposed CIs, they should be applied to vibration response signals generated by a number of laboratory gearboxes, both simple and complex. It is important that further tests of the techniques are performed on test rigs that allow controlled fault generation under variable test conditions.

ii. The proposed CIs and the data fusion model should be tested on data generated by a machine operating in the field to evaluate the practical use in the industrial environment.

iii. A commercial application of the proposed techniques of the new CI's requires the development of dedicated software, capable of applying the CIs and the data fusion model on vibration signals. The software should be integrated with a data acquisition system and appropriate sensors.

iv. At present, the data fusion model used for decision making is based on the proposed CIs related to vibration analysis. The decision making process could potentially further improved if other sources of information are incorporated in the data fusion model. This could be achieved perhaps by investigating information contained in other condition monitoring techniques operating in different domains such as acoustic emission and oil debris analysis, for example.

REFERENCES

[1] McGowen, S.S. *Helicopters: an illustrated history of their impact (Weapons and warfare series)*, ABC-CLIO, 2005.

[2] De, D.K. *Public System Management*, New Age International, 2007.

[3] Padfield, G.D. Helicopter flight dynamics: the theory and application of flying qualities and simulation modelling, John Wiley and Sons, 2007.

[4] Harris, F.D., Kasper, E.F., Iseler, L.E. *U.S. Civil Rotorcraft Accidents, 1963 Through 1997*, Ames Research Center, NASA/TM-2000-209597, 2000

[5] John Burt Associates Limited/BOMEL Limited. *UK offshore public transport helicopter safety record (1976 – 2002)*, 2004, http://www.hse.gov.uk/research/misc/helicoptersafety.pdf, accessed on the 05.05.2011.

[6] Gavaghan, H. *The price of helicopter safety*, New Scientist magazine, 112(1536): 23-25, 1986.

[7] Samuel, P.D., Pines, D.J *Constrained adaptive lifting and the CAL4 metric for helicopter transmission diagnostics*, Journal of Sound and Vibration, 319: 698-718, 2009.

[8] McColl, J. *Overview of Transmissions HUM Performance in North Sea Helicopter Operations*, Institution of Mechanical Engineers Seminar S553, November 1997.

[9] Dempsey, P.J., Lewicki, D.G., Lee, D. *Investigation of Current Methods to Identify Helicopter Gear Health*, Ames Research Center, NASA/TM-2007-214664, 2007.

[10] Conversation with Dr. Duncan Shepherd, Capability Group Leader at the Advanced Diagnostics and Prognostics team within the Air Vehicle Concepts and Structures group in QinetiQ Ltd.

[11] Air Accidents Investigation Branch (AAIB) - Initial Report 2, AAIB Ref: EW/C2009/04/01, 2009.

[12] Butcher, J., Jeffrey, P. *A view from the coal face : UK research student perceptions of successful and unsuccessful collaborative projects*, Research Policy, 36: 1239-1250, 2007.

[13] Engineering Doctorate at The University of Manchester website, http://www.engd.manchester.ac.uk/ accessed on the 03.03.2011.

[14] Kerr, C.I., Ivey, P.C. *The Engineering Doctorate model of consultant / researcher / innovator / entrepreneur for new product development – a gas turbine instrumentation case study*, Technovation, 36: 95-102, 2003.

[15] Evatt, M.A.C., Brodhurst, E.K. *Sharing Experience in Engineering Design (SEED 2002)*, John Wiley and Sons, 2002.

[16] Al-Dossarya, S., Hamzahb, R.I.R., Mba, D. *Observations of changes in acoustic emission waveform for varying seeded defect sizes in a rolling element bearing*

[17] http://renewablelubricants.com/images/four_ball_test.gif accessed on the 03.03.2011.

[18] Samuel, P.D., Conroy, J.K., Pines, D.J. *Planetary Transmission Diagnostics*, Ames Research Center, NASA/TM-2004-213068, 2004.

[19] McFadden, P.D. *A Technique For Calculating The Time Domain Averages Of The Vibration Of The Individual Planet Gears And The Sun Gear In An Epicyclic Gearbox*, Journal of Sound and Vibration, 144(1): 163-172, 1991.

[20] QinetiQ website, www.qinetiq.com accessed on the 03.03.2011.

[21] FAME website, https://fame.bvdep.com accessed on the 03.03.2011.

[22] Talon® picture, http://www.robotliving.com/wp-content/uploads/picture-11.jpg accessed on the 03.03.2011.

[23] Information about Talon®, http://www.qinetiq.com/home/products/talon_robot.html accessed on the 03.03.2011.

[24] Information about Talon®, http://www.army-guide.com/eng/article/article_1393.html accessed on the 03.03.2011.

[25] Information about Talon®, http://www.militaryaerospace.com/index/display/mae-defense-executive-article-display/2289000582/articles/military-aerospace-electronics/executive-watch-2/2010/5/army-to_buy_talon.html accessed on the 03.03.2011.

[26] Information about Corlan™, http://www.qinetiq.com/home/products/corlan_wireless_corrosion.html accessed on the 03.03.2011.

[27] Information about X-Net®, http://www.qinetiq.com/home/newsroom/news_releases_homepage/2008/3rd_quarter/invetors__awards.html accessed on the 03.03.2011.

[28] Information about X-Net®, http://www.qinetiq.com/home/newsroom/news_releases_homepage/2006/4th_quarter/xnet_idiq.html accessed on the 03.03.2011.

[29] Samuel, P.D., Pines D.J. *A review of vibration-based techniques for helicopter transmission diagnostics*, Journal of Sound and Vibration, 282: 475 – 508, 2005.

[30] Stewart, R.M. *Some Useful Data Analysis Techniques For Gearbox Diagnostics*, Proceedings of Meeting on Applications of Time Series Analysis, 18: 18.1-18.19, 1977.

[31] Peng, Z., Kessissoglou, N. *An integrated approach to fault diagnosis of machinery using wear debris and vibration analysis*, Wear, 255: 1221-1232, 2003.

[32] Peng, Z. *An integrated intelligence system for wear debris analysis*, Wear, 252: 730-743, 2002.

[33] Crocker, M.J. *Handbook of acoustics*, Wiley-IEEE, 1998.

[34] Niu, G., Yang B.-S. *Intelligent condition monitoring and prognostic system based on data-fusion strategy*, Expert Systems with Applications, 37(12): 8831-8840, 2010.

[35] Ahn, H.S., Yoon, E.S., Sohn, D.G., Kwon, O.K., Shin, K.S., Nam, C.H. *Practical contaminant analysis of lubricating oil in a steam-turbine generator*, Tribology International, 29(2): 161-168, 1996.

[36] Herguth, W.R., Nadeau, G. *Applications of Scanning Electron Microscopy and Energy Dispersive Spectroscopy (SEM/EDS) To Practical Tribology Problems*, Herguth Laboratories Inc., http://www.herguth.com/technical/sem.pdf, accessed on the 21.12.2008.

[37] Sugimura, J., Takesue, M., Yamamoto, Y. *Wear debris analysis for condition monitoring of gears*, Tribology Series, 34: 431-442, 1998.

[38] Ebersbach, S., Peng, Z., Kessissoglou, N.J. *The investigation of the condition and faults of a spur gearbox using vibration and wear debris analysis techniques*, Wear, 260: 16-24, 2006.

[39] Dempsey, P.J. *Integrating oil debris and vibration measurements for intelligent machine health monitoring*, Ames Research Center, NASA/TM-2003-211307, 2003.

[40] Chambers, K.W., Arneson, M.C. *An online ferromagnetic wear debris sensor for machinery condition monitoring and failure detection*, Wear, 128: 325-337, 1988.

[41] Atkin, M.L., Doyle, E.D. *The condition monitoring of heavily loaded spur gears*, Wear, 88: 115-124, 1983.

[42] Miller, J.L., Kitalievich, D. *In-Line Oil Debris Monitor for Aircraft Engine Condition Assessment*, IEEE Aerospace Conference Proceedings, p. 49-56, 2000.

[43] Han, L., Hong, W., Wang, S. *The key points of inductive wear debris sensor*, Proceedings of International Conference on Fluid Power and Mechatronics, p. 809-815, 2011.

[44] Tucker, J.E., Reintjes, J., Duncan, M.D., McClelland, T.L., Tankersley, L.L., Schultz, A., Lu, C., Howard, P.L., Sebok, T., Holloway, C., Fockler, S. *LASERNET FINES Optical Oil Debris Monitor*, Naval Research Laboratory, Washington, D.C., Laser physics section http://www.dtic.mil/cgi-bin/GetTRDoc?Location=U2&doc=GetTRDoc.pdf&AD=ADA347453 accessed on the 10.11.2008.

[45] Randall, R.B. *Vibration-based Condition Monitoring: Industrial, Aerospace and Automotive Applications*, John Wiley and Sons, 2011.

[46] Yardley, E.D. *The use of ferrography and spectrographic oil analysis to monitor the performances of three 90kW gearboxes*, Wear 56: 213-226, 1979.

[47] Advanced technology in failure prevention: proceedings of the 43rd Meeing of the Mechanical Failures Prevention Group, Mechanical Failures Prevention Group, Cambridge University Press, 1991.

[48] Norton, M.P., Karczub, D.G. *Fundamentals of noise and vibration analysis for engineers*, Cambridge University Press, 2003

[49] Nikolaou, N.G., Antoniadis, I.A. *Rolling element bearing fault diagnosis using wavelet packets*, Non-Destructive Testing and Evaluation (NDT&E) International, 35(3): 197-205, 2002.

[50] McFadden, P.D. *Low frequency vibration generated by gear tooth impacts*, Non-Destructive Testing (NDT) International, 18(5): 279-282, 1985.

[51] Girdhar, P., Scheffer, C. *Practical machinery vibration analysis and predictive maintenance*, Elsevier, 2004.

[52] Bently, D.E., Hatch, C.T. *Fundamentals of Rotating Machinery Diagnostics*, Bently Pressurized Bearing Press, 2002.

[53] Vecer, P., Kreidl, M., Smid, R. *Condition Indicators for Gearbox Condition Monitoring Systems*, Acta Polytechnika, 45(6): 35-43, 2005.

[54] Moore, D.S. *The basic practice of statistics*, Palgrave Macmillan, 2009.

[55] Zakrajsek, J.J., Handschuh R.F., Decker, H.J. *Application of Fault Detection Techniques to Spiral Bevel Gear Fatigue Data*, Ames Research Center, NASA/TM-106467, 1994.

[56] Smith, S.W. *The Scientist and Engineer's Guide to Digital Signal Processing*, California Technical Publications, 1997.

[57] Hartmann, W.M. *Signals, sound and sensation*, Springer, 1997.

[58] Friedman, A. *What Is The "Crest Factor" And Why Is It Used?*, DLI Engineering Corporation, http://www.dliengineering.com/downloads/crest%20factor.pdf accessed on the 17.12.2008.

[59] Gray, R.M., Davisson, L.D. *An introduction to statistical signal processing*, Cambridge University Press, 2004.

[60] Miller, M.B., *Mathematics and Statistics for Financial Risk Management*, John Wiley and Sons, 2012.

[61] Lebold, M., McClintic, K., Campbell, R., Byington, C., Maynard, K. *Review of Vibration Analysis Methods for Gearbox Diagnostics and Prognostics*, Proceedings of the 54th Meeting of the Society for Machinery Failure Prevention Technology, p. 623-645, 2000.

[62] Decker, H.J. *Gear Crack Detection Using Tooth Analysis*, Ames Research Center, NASA/TM-2002-211491, 2002.

[63] Taylor, J.I. *The Gear Analysis Handbook. A Practical Guide For Solving Vibration Problems in Gears*, VCI, 2000.

[64] Liu, B., Riemenschneider, S., Xu, Y. *Gearbox fault diagnosis using empirical mode decomposition and Hilbert spectrum*, Mechanical Systems and Signal Processing, 20: 718-734, 2006.

[65] Al-Najjar, B. *Accuracy, effectiveness and improvement of vibration-based maintenance in paper mills: case studies*, Journal of Sound and Vibration, 229(2): 389-410, 2000.

[66] Choi, S., Li, C.J. *Estimation of Gear Tooth Transverse Crack Size from Vibration by Fusing Selected Gear Condition Indices*, Measurement Science and Technology, 17: 2395-2400, 2006.

[67] Hochmann, D., Bechhoefer, E. *Gear Tooth Crack Signals and their Detection via the FM4 Measure in Application for Helicopter HUMS (Health Usage and Management System)* Proceedings of the Aerospace Conference, 7: 3313 – 3326, 2003.

[68] Rao, V.B. *Kurtosis as a Metric in the Assessment of Gear Damage*, Shock and Vibration Digest, 31(6): 443-448, 1999.

[69] Blechertas, V., Bayoumi, A., Goodman, N., Shah, R., Shin, Y-J. *CBM Fundamental Research at the University of South Carolina: A Systematic Approach to U.S. Army Rotorcraft CBM and the Resulting Tangible Benefits*, Presented at the American Helicopter Society Technical Specialists' Meeting on Condition Based Maintenance, 2009

[70] Wang, L., Gao, R.X. *Condition Monitoring and Control for Intelligent Manufacturing*, Springer, 2006.

[71] Zakrajsek, J.J., Townsend, D.P., Decker, H.J. *An Analysis of Gear Fault Detection Methods as Applied to Pitting Fatigue Failure Data*, Ames Research Center, NASA/TM 92-C-035, 1993.

[72] Dempsey, P.J., Zakrajsek J.J. *Minimizing Load Effects on NA4 Gear Vibration Diagnostic Parameter*, Ames Research Center, NASA/TM 2001-210671, 2001.

[73] Nachtsheim, P.R. *Detecting tooth Damage in Geared Drive Trains*, Ames Research Center, NASA/TM 1997-112207, 1997

[74] Decker, H.J., Lewicki D.G. *Spiral Bevel Pinion Crack Detection in a Helicopter Gearbox,* Ames Research Center, NASA/TM 2003-212327, 2003.

[75] Choy, F.K., Huang, S., Zakrajsek, J.J., Handschuh, R.F. *Vibration Signature Analysis of a Faulted Gear Transmission System*, Ames Research Center, NASA/TM 106623, 1994.

[76] Zakrajsek, J.J., Lewicki, D.G. *Detecting Gear Tooth Fatigue Cracks in Advance of Complete Fracture*, Ames Research Center, NASA/TM 107145, 1996.

[77] Decker, H.J. *Crack Detection of Aerospace Quality Spur Gears*, Ames Research Center, NASA/TM 2002-211492, 2002.

[78] Wu, S., Zuo, M.J., Parey A. *Simulation of spur gear dynamics and estimation of fault growth*, Journal of Sound and Vibration, 317: 608 – 624, 2008.

[79] O'Shea, P., Sadik, A.Z., Hussain, Z.M. *Digital Signal Processing: An Introduction with MATLAB and Applications*, Springer, 2011.

[80] Pryor, A.H., Mosher, M., Lewicki D.G. *The Application of Time-Frequency Methods to HUMS*, Presented at the American Helicopter Society's 57th Annual Forum, 2001.

[81] Djurovic, I., Rubezic, V. *Multiple STFT-based approach for chaos detecting in oscillatory circuits*, Signal Processing, 87(7): 1772-1780, 2007.

[82] Wang, W.J., McFadden, P. D. *Early detection of gear failure by vibration analysis I: calculation of the time-frequency distribution*, Mechanical Systems and Signal Processing, 7(3): 193-203, 1993.

[83] Staszewski, W. J., Tomlinson, G. R. *Local tooth fault detection in gearboxes using a moving window procedure*, Mechanical Systems and Signal Processing, 11(3): 331-350, 1997.

[84] Williams W.J., Zalubas, E.J. *Helicopter transmission fault detection via time-frequency, scale and spectral methods*, Mechanical Systems and Signal Processing, 14(4): 545-559, 2000.

[85] Loughlin, P., Cakrak, F., Cohen, L. *Conditional moments analysis of transient with application to helicopter fault data*, Mechanical Systems and Signal Processing, 14(4): 511-522, 2000.

[86] Bartelmus, W., Zimroz, R. *Vibration condition monitoring of planetary gearbox under varying external load*, Mechanical Systems and Signal Processing, 23(1): 246-257, 2009.

[87] Chen, V.C., Ling, H. *Time-frequency transforms for radar imaging and signal analysis*, Artech House, 2002.

[88] Lu, F.-S., Yang, C.-Y., Lin, P.-L. *An Improved Wigner Distribution Based Algorithm for Signal Identification*, Proceedings of International Symposium on Underwater Technology, p. 39-45, 2004.

[89] Chen, V. *The Micro-Doppler Effect in Radar*, Artech House, 2011

[90] Pachori, R.B., Sircar, P. *A new technique to reduce cross terms in the Wigner distribution*, Digital Signal Processing, 17(2): 466-474, 2007.

[91] Baydar, N., Ball, A. *A Comparative Study of Acoustic and Vibration Signals in Detection of Gear Failures Using Wigner-Ville Distribution*, Mechanical Systems and Signal Processing, 15(6): 1091-1107, 2001.

[92] Staszewski, W.J., Worden, K., Tomlinson, G.R. *Time-frequency analysis in gearbox fault detection using the Wigner-Ville distribution and pattern recognition*, Mechanical Systems and Signal Processing, 11(5): 673-692, 1997.

[93] Neild, S.A., McFadden, P.D., Williams, M.S. *A review of time-frequency methods for structural vibration analysis*, Engineering Structures, 25(6): 713-728, 2003.

[94] Zu, S., Ye, L. *Identification of Damage Using Lamb Waves: From Fundamentals to Applications*, Springer 2009.

[95] Wang, W.J., McFadden, P.D. *Application of Wavelets to Gearbox Vibration Signals for Fault Detection*, Journal of Sound and Vibration, 192: 927-939, 1996.

[96] Sung, C.K., Tai, H.M., Chen, C.W. *Locating defects of a gear system by the technique of wavelet transform*, Mechanism and Machine Theory, 35(8): 1169-1182, 2000.

[97] Belsak, A., Flasker, J. *Wavelet Analysis For Gear Crack Identification*, Engineering Failure Analysis, 16(6): 1983-1990, 2009.

[98] Lopez, J.E., Tenney, R.R., Deckert, J.C. *Fault Detection and Identification Using Real-Time Wavelet Feature Extraction*, Proceedings of the Institute of Electrical and Electronic Engineers (IEEE)-Signal Processing International Symposium on Time-Frequency and Time-Scale Analysis, p.217-220, 1994.

[99] Dalpiaz, G., Rivola, A., Rubini, R. *Effectiveness and sensitivity of vibration processing techniques for local fault detection in gears*, Mechanical Systems and Signal Processing, 14(3): 387 – 412, 2000.

[100] Lin, J., Qu, L. *Feature extraction based on Morlet wavelet and its application for mechanical fault diagnosis*, Journal of Sound and Vibration, 234: 135-148, 2000.

[101] Begg, R., Palaniswami, M. *Computational intelligence for movement sciences: neural networks and other emerging techniques,* Idea Group Inc., 2006

[102] Gao, R.X., Yan, R. *Wavelets: Theory and Applications for Manufacturing*, Springer, 2010

[103] Omar, F.K., Gaouda, A.M. *Dynamic wavelet-based tool for gearbox diagnosis*, Mechanical Systems and Signal Processing, 26: 190-204, 2012.

[104] Chatfield, C. *The analysis of time series. An introduction*, Chapman & Hall, 1989.

[105] Salas, J.D. *Applied modeling of hydrologic time series*, Water Resources Publication, 1980.

[106] Shadbolt, J. *Neural networks and the financial markets: predicting, combining, and portfolio optimisation*, Springer, 2002.

[107] Rofe, S. *Signal processing methods for gearbox fault detection*, Technical Report DSTO-TR-0476, Australian Department of Defence: Defence Science and Technology Organisation, 1997.

[108] Rantala, S., Suoranta, R. *Enhanced vibration monitoring using parametric modelling techniques*, IEEE 8th Instrumentation and Measurement Technology Conference, p. 2-5, 1991.

[109] Wang, W., Wong, A.K. *A Model-Based Gear Diagnostic Technique*, Technical Report DSTO-TR-1079, Australian Department of Defence: Defence Science and Technology Organisation, 2000.

[110] Wang, W., Wong, A.K. *Some New Signal Processing Approaches For Gear Fault Diagnosis*, Proceedings of the 5th International Symposium on Signal Processing and its Applications, p. 587-590, 1999.

[111] Lee, J., Wang, B. *Computer-aided maintenance: methodologies and practices*, Springer, 1999

[112] Tavner, P.J., *Condition monitoring of rotating electrical machines*, IET, 2008.

[113] Williams, J.H., Davies, A., Drake, P.R., Condition-based maintenance and machine diagnostics, Springer 1994.

[114] http://www.reliabilityweb.com/articles/shock_pulse.pdf accessed on the 04.12.2012

[115] Shi, L., Randall, R.B., Antoni, J. *Rolling element bearing fault detection using improved envelope analysis*, Vibrations in Rotating Machinery, John Wiley and Sons, 2004.

[116] Nikolaou, N.G., Antoniadis, I.A. *Demodulation of vibration signals generated by defects in rolling element bearings using complex shifted Morlet wavelets*, Mechanical Systems and Signal Processing, 16(4): 677-694, 2002

[117] Antoni, J., Randall, R.B. *The spectral kurtosis: application to the vibratory surveillance and diagnostics of rotating machines*, Mechanical Systems and Signal Processing, 20(2): 308-331, 2006

[118] Esteban, J., Starr, A., Willetts, R., Hannah, P., Bryanston-Cross, P. *A Review of data fusion models and architectures: towards engineering guidelines*, Neural Computing & Applications, 14: 273-281, 2005.

[119] Hall, D.L., Llinas, J. *An introduction to multisensor data fusion*, Proceedings of the IEEE, 85: 6-23, 1997.

[120] Niu, G., Yang, B.-S., Pecht, M. *Development of an optimized condition-based maintenance system by data fusion and reliability-centred maintenance*, Reliability Engineering and System Safety, 95: 786-796, 2010.

[121] Chang, W.Y., Abu-Amara, H., Sanford, J. *Transforming Enterprise Cloud Services*, Springer, 2010.

[122] Shahbazian, E., Rogova, G., Valin, P. *Data fusion for situation monitoring, incident detection, alert and response management*, NATO science series: Computer and Systems Sciences 198, IOS Press, 2005.

[123] Worden, K., Bullough, W.A., Haywood, J. *Smart technologies*, World Scientific, 2003.

[124] Hyder, A.K., Shahbazian, E., Waltz, E. *Multisensor fusion*, Springer, 2002.

[125] O'Gorman, L. *What is Pattern Recognition?*, International Association for Pattern Recognition newsletter, Vol. 25, 2003.

[126] Ince, A.N., Topuz, E., Panayirci, E. *Principles of integrated maritime surveillance systems*, Springer, 1999.

[127] Halloun, I.A. *Modelling theory in science education*, Springer, 2004.

[128] Hall, D.L. *Mathematical Techniques in Multisensor Data Fusion*, Artech House Inc., 2004.

[129] Bishop, C.M. *Neural Networks for Pattern Recognition*, Oxford University Press, 1995.

[130] Roos, J., Costa, R.J. *Scientific Computing in Electrical Engineering (SCEE) 2008*, Springer, 2010

[131] Liu, D., Fei, S., Hou, Z., Zhang, H., Sun, C. *Advances in Neural Networks*, Proceedings of 4th International Symposium on Neutral Networks, 2: 352-361, 2007.

[132] Westphal, C., Blaxton, T. *Data Mining Solutions. Methods and Tools for Solving Real-World Problems*, John Wiley and Sons, 1998.

[133] Aldenderfer, M.S., Blashfield, R.K. *Quantitative Applications in the Social Sciences*, Sage Publications, 1984.

[134] Jain, A.K., Murty, M.N., Flynn, P.J. *Data clustering: A review*, , ACM Computing Surveys, 31: 265-323, 1999.

[135] Azzam, H., Cook, J., Knight, P., Wakefield, N. *FUMS™ Fusion For Improved Aircraft MAAAP*, IEEE Aerospace Conference, p. 3782-3796, 2005.

[136] Akerkan, R., Sajja, P. *Knowledge-Based Systems*, Jones & Bartlett Learning, 2009.

[137] McDonald, J.R., Burt, G., Moyes, A. *Knowledge based systems for condition monitoring*, Proceedings of United Kingdom Automatic Control Council (UKACC) International Conference on Control, 2:1424-1429, 1996.

[138] Klein, L.A. *Sensor and data fusion: a tool for information assessment and decision making*, SPIE Press, 2004.

[139] Ma, J., Chen, S., Xu, Y. *Fuzzy logic from the viewpoint of machine intelligence*, Fuzzy Sets and Systems, 157(5): 628 – 634, 2006.

[140] Bahandari, V.B. *Design Of Machine Elements 3E*, Tata McGraw-Hill Education, 2010.

[141] http://static.ddmcdn.com/gif/gear-worm.jpg accessed on the 06.03.2012

[142] http://2.imimg.com/data2/XK/KD/MY-150305/spiralbevel-gear-250x250.jpg accessed on the 14.02.2012.

[143] http://img.tradeindia.com/fp/1/573/814.jpg accessed on the 14.02.2012

[144] Rao, J.S., *The Theory Of Machines Through Solved Problems*, New Age International, 2007.

[145] http://static.ddmcdn.com/gif/gear-spur.jpg accessed on the 24.02.2012

[146] Pope, J.E. *Rules of thumb for mechanical engineers: a manual of quick, accurate solutions to everyday mechanical engineering problems*, Gulf Professional Publishing, 1997.

[147] Maitra, G.M. *Handbook of gear design*, 2nd edition, Tata McGraw-Hill Education, 2001.

[148] http://static.ddmcdn.com/gif/gear-helical1.jpg accessed on the 24.02.2012.

[149] Els, J., Hornveld, M., Kiewet, J., Kotze, R., Sololo, A. *FCS Applied Engineering Technology L4*, Pearson Education South Africa, 2009.

[150] Erjavec, J. *Automotive technology: a systems approach, volume 2*, Cengage Learning, 4th Edition, 2005.

[151] Kirkpatrick, L.D., Francis, G.E. *Physics: A World View*, Cengage Learning, 2006.

[152] Engström, S. *Trends and development in wind power technology*, Elforsk report 10:79, 2010, accessed on the 15.07.2011.

[153] Manwell, J.F., McGowan, J.G., Rogers, A.L. *Wind Energy Explained: Theory, Design and Application*, John Wiley and Sons, 2nd Edition, 2010.

[154] Bartelmus, W. *Condition monitoring of open cast mining machinery*, Oficyna Wydawnicza Politechniki Wroclawskiej, 2006.

[155] http://www.mathworks.de/help/toolbox/physmod/drive/planetary.gif accessed on the 04.01.2012

[156] Grote, K.-H., Antonsson, E.K. *Springer Handbook of Mechanical Engineering, Volume 10*, Springer, 2009.

[157] Samuel, P.D., Conroy, J.K., Pines, D.J. *Planetary Transmission Diagnostics*, NASA/CR-2004-213068, Ames Research Centre, 2004

[158] Belanger, P., Berry, A., Pasco, Y., Robin, O., St-Amant, Y., Rajan, S. *Multi-harmonic active structural acoustic control of a helicopter main transmission noise using a principal component analysis*, Applied Acoustics, 70(1): 153-164, 2009.

[159] Bartelmus, W. *Computer-aided multistage gearbox diagnostic inference by computer simulation*, Oficyna Wydawnicza Politechniki Wroclawskiej, 2002.

[160] Fraden, J. *Handbook of Modern Sensors: Physics, Designs, and Applications*, Springer, 2010

[161] Wilson, J.S. *Sensor technology handbook, Volume 1*, Newnes, 2005

[162] Merhav, S. *Aerospace sensor systems and applications,* Springer, 1996

[163] Silvus, Jr., Howard, S. *Electronically tunable resonant accelerometer*, US Patent nr. 4197478

[164] Wilson, J.S. *Test and measurement*, Newnes, 2009

[165] Hess, A.J., Hardman, B., Neubert, C. *SH-60 Helicopter Integrated Diagnostic System (HIDS). Program Experience and Results of Seeded Fault Testing*, Proceedings of IEEE Aerospace Conference, 2: 473-491, 1999.

[166] Hardmann, W. *Mechanical and Propulsion Systems Diagnostics: U.S. Navy Strategy and Demonstration*, Journal of Minerals, Metals and Materials Society, 56(3): 21-27, 2004.

[167] Brown, J.A. Modern manufacturing processes, Industrial Press Inc. 1991.

[168] Guan, Y.H., Lim, T.C., Shepard, W.S.Jr. *Experimental study on active vibration control of a gearbox system*, Journal of Sound and Vibration, 282: 713-733, 2005.

[169] Laboratory of Signal Analysis and Industrial Processes (LASPI) at the Jean Monnet University in Saint – Etienne, France website: http://www.laspi.fr/vibrabase/ accessed on the 22.03.2011.

[170] Mobley, R.K. *Plant engineer's handbook*, Butterworth-Heinemann, 2001.

[171] Bowen, R. *How to Rebuild and Modify Your Manual Transmission*, MotorBooks International, 2005.

[172] Randall, R.B., Antoni, J. *Rolling element bearing diagnostics*, Mechanical Systems and Signal Processing, 25(2): 485 – 520, 2011.

[173] Watkinson, J. *Art of the helicopter*, Butterworth-Heinemann, 2004.

[174] Chinook Helicopter dedicated website http://www.chinook-helicopter.com/standards/areas/cbox.html accessed on the 07.07.2011.

[175] Tandon, N. *A comparison of some vibration parameters for the condition monitoring of rolling element bearings*, Measurement, 12: 285-289, 1994.

[176] Sheen, Y.-T. *An envelope analysis based on the resonance modes of the mechanical system for the bearing defect diagnosis*, Measurement, 43: 912-934, 2010.

[177] Ben-Daya, M., Duffuaa, S.O., Raouf, A. Maintenance, modeling, and optimization, Springer, 2000.

[178] McFadden, P.D., Smith, J.D. *Vibration monitoring of rolling element bearings by the high-frequency resonance technique – a review*, Tribology International, 17(1): 3-10, 1984.

[179] J. Lee, H. Qiu, G. Yu, J. Lin, and Rexnord Technical Services (2007). 'Bearing Data Set', IMS, University of Cincinnati. NASA Ames Prognostics Data Repository, [http://ti.arc.nasa.gov/project/prognostic-data-repository], NASA Ames, Moffett Field, CA. Accessed on the 31.03.2011.

[180] Opinions on HUMS by system users http://www.pprune.org/archive/index.php/t-101272.html accessed on the 7.07.2011.

[181] Larder, B.D. *Helicopter HUMS – the evolutions of a system*, IMechE Seminar Publications, Vol. 9, 1996.

[182] Moir, I., Seabridge, A. *Aircraft systems: mechanical, electrical and avionics subsystems integration*, John Wiley and Sons, 2008.

[183] Bechhoefer, E., Bernhard, A.P.F. *Setting HUMS condition indicator thresholds by modelling aircraft and torque band variance*, Aerospace Conference, Proceedings 2004 IEEE 6-13, p. 3590 – 3595, 2004

[184] Boakes, S. *Definitive HUMS*, GE Aviation Technical papers, http://www.geaviationsystems.com/About/Technical-Papers/Literature/Definitive-HUMS.pdf, accessed on the 03.03.2011

[185] He, D., Bechhoefer, E. *Development and validation of Bearing Diagnostic and Prognostic Tools using HUMS Condition Indicators*, IEEE Aerospace Conference, p. 1-8, 2008

[186] Knight, P., Cook, J., Azzam, H. *Intelligent management of helicopter health and usage management systems data*, Journal of Aerospace Engineering, 219(6): 507-524, 2005.

[187] Goodman, N., Bayoumi, A. *Fault Class Identification through Applied Data Mining of AH-64 Condition Indicators*, presented at the American Helicopter Society 66th Annual Forum, 11-13.05.2010.

[188] McFadden, P.D. *Determining the location of a fatigue crack in a gear from the phase of the change in the meshing vibration*, Mechanical Systems and Signal Processing, 2: 403 – 409, 1988.

[189] McFadden, P.D. *Examination of a technique for the early detection of failure in gears by signal processing of the time domain average of the meshing vibraiton*, Mechanical Systems and Signal Processing 1: 173 – 183, 1987.

[190] Hartmann, W.M. *Signals, sound and sensation*, Springer, 1997.

[191] Kiral, Z., Karagülle, H. *Vibration analysis of rolling element bearings with various defects under the action of an unbalanced force*, Mechanical Systems and Signal Processing, 20: 1967-1991, 2006.

[192] Combet, F., Gelman, L. *Novel adaptation of the demodulation technology for gear damage detection to variable amplitudes of mesh harmonics*, Mechanical Systems and Signal Processing, 25: 839-845, 2011.

[193] Endo, H., Randall, R.B. *Enhancement of autoregressive model based gear tooth fault detection technique by the use of minimum entropy deconvolution filter*, Mechanical Systems and Signal Processing, 21: 906-919, 2007.

[194] Hochmann, D., Bechhoefer, E. *Gear Tooth Crack Signals and their Detection via the FM4 Measure in Application for Helicopter HUMS (Health Usage and Management System)*, IEEE Proceedings of Aerospace Conference, 7: 3313-3326, 2003.

[195] Zakrajsek, J.J. *An Investigation of Gear Mesh Failure Prediction Techniques*, Ames Research Center, NASA/TM 89-C-005, 1989.

[196] McFadden, P.D., Smith, J.D. *A signal processing technique for detecting local defects in a gear from the signal average of the vibration*, Proceedings of the Institution of Mechanical Engineers, 199(C4): 287-292, 1985.

[197] Johnson, R.A., Bhattacharyya, G.K. *Statistics: Principles and methods*, John Wiley and Sons, 6^{th} Edition, 2009.

[198] Lutfiyya, L.A. *The essentials of probability*, Research and Education Associated, 1991.

[199] Jobson, J.D. *Applied Multivariate Data Analysis: Regression and Experimental Design*, Springer, 4^{th} Edition, 1991.

[200] Larose, D.T. *Data Mining methods and models*, John Wiley and Sons, 2006.